Reconstitution des évènements climatiques extrêmes (crues et tempêtes) au cours de l'Holocène dans le Golfe d'Aigues-Mortes (Sud de la France)

Pierre Sabatier

UNIVERSITE MONTPELLIER II
SCIENCES ET TECHNIQUES DU LANGUEDOC

T H E S E

pour obtenir le grade de

DOCTEUR DE L'UNIVERSITE MONTPELLIER II

Discipline : Sciences de la Terre et de l'Univers
Ecole Doctorale : SIBAGHE (Systèmes Intégrés en Biologie, Agronomie, Géosciences, Hydrosciences, Environnement)

présentée et soutenue publiquement par

Pierre SABATIER

Le 30 septembre 2009

Reconstitution des évènements climatiques extrêmes (crues et tempêtes) au cours de l'Holocène dans le Golfe d'Aigues-Mortes (Sud de la France)

JURY

Serge Berné	**Professeur, IMAGES**	**Examinateur**
Christophe Colin	**Professeur, IDES**	**Invité**
Michel Condomines	**Professeur, GM**	**Directeur de Thèse**
Laurent Dezileau	**Maître de Conférences, GM**	**Directeur de Thèse**
Jean-Claude Duplessy	**Directeur de Recherche, LSCE**	**Examinateur**
Olivier Radakovitch	**Maître de Conférences, CEREGE**	**Rapporteur**
Bernadette Tessier	**Directrice de Recherche, M2C**	**Rapporteur**

UNIVERSITE MONTPELLIER II
SCIENCES ET TECHNIQUES DU LANGUEDOC

T H E S E

pour obtenir le grade de

DOCTEUR DE L'UNIVERSITE MONTPELLIER II

Discipline : Sciences de la Terre et de l'Univers
Ecole Doctorale : SIBAGHE (Systèmes Intégrés en Biologie, Agronomie, Géosciences, Hydrosciences, Environnement)

présentée et soutenue publiquement par

Pierre SABATIER

Le 30 septembre 2009

Reconstitution des évènements climatiques extrêmes (crues et tempêtes) au cours de l'Holocène dans le Golfe d'Aigues-Mortes (Sud de la France)

JURY

Serge Berné	**Professeur, IMAGES**	**Examinateur**
Christophe Colin	**Professeur, IDES**	**Invité**
Michel Condomines	**Professeur, GM**	**Directeur de Thèse**
Laurent Dezileau	**Maître de Conférences, GM**	**Directeur de Thèse**
Jean-Claude Duplessy	**Directeur de Recherche, LSCE**	**Examinateur**
Olivier Radakovitch	**Maître de Conférences, CEREGE**	**Rapporteur**
Bernadette Tessier	**Directrice de Recherche, M2C**	**Rapporteur**

Remerciements

Enfin… ça y est !!! J'en suis aux remerciements près de 8 ans après ma première inscription à la fac de sciences de Montpellier. Mais en réalité cette aventure a commencé bien avant dixit mon père durant mon mariage lors de sa présentation quelque peu orientée : « son intérêt pour la géologie a débuté à l'âge de deux ans quand, avachit dans l'herbe, il découvrit son premier caillou qu'il essaya de manger !». Depuis bien qu'ayant arrêté de dévorer mon outil de travail la passion est restée et j'espère vous le montrer à la lecture de cette thèse…

Je tiens d'abord à remercier les rapporteurs de cette thèse, Bernadette Tessier et Olivier Radakovitch pour prendre le temps de lire ce manuscrit durant leurs vacances d'été. Merci également à Jean-Claude Duplessy, Serge Berné et Christophe Colin pour l'intérêt que vous montrez pour ce travail en acceptant de l'examiner.

Mes pensées vont ensuite à mes directeurs de thèse : Laurent Dezileau et Michel Condomines. Un grand merci à Laurent à qui je dois l'intérêt pour la paléoclimatologie et ce depuis son premier cours en licence. Je souhaite également le remercier chaleureusement pour sa disponibilité, son optimisme et son enthousiasme à toute épreuve, même à celle de la boue puante des lagunes. Merci à Michel pour m'avoir transmis une partie de sa rigueur scientifique et de ses immenses compétences, j'en profite pour m'excuser de mes mails bourrés de fautes qui le hérissaient.

Je tiens ensuite à remercier quatre personnes qui ont grandement contribué à ce travail de thèse à savoir Philippe Blanchemanche, Louis Briqueu, Christophe Colin et Frédérique Bouchette auprès desquels j'ai énormément appris.

Un grand merci également à Raphaël Certain, Olivier Raynal, Johanna Lofi et Pierre Ferrer avec qui j'ai eu de fréquents et enrichissants échanges concernant nos travaux. Merci aussi à Guiseppe Siani et Ilhem Bentaleb pour leurs idées enrichissantes et leur disponibilité. Et à Uli von Grafenstein, sans lequel ce travail n'aurait probablement pas été le même, merci capitaine !

Je veux aussi remercier pour nos collaborations Frédérique Carcaillet : pour nos immersions lagunaires mensuelles et qui gardait le sourire malgré l'hiver et ses eaux frôlant les 5°C !!!! Merci également à Serge Muller pour son enthousiasme polliniste à l'égard de nos archives. Ces collaborations, bien que non abouties à l'heure actuelle donneront dans le futur, à n'en pas douter, d'intéressantes découvertes.

Je tiens également à remercier toutes les personnes avec qui j'ai travaillé au cours de ces trois années :
Christophe Jorda, Jean-François Berger, Claude Vella, Lucie Chabal, Gaël Piquès ainsi que Coraline, Julien, Laurie et toute l'équipe du musée archéologique de Lattes pour nous avoir si souvent accueilli dans une ambiance très conviviale.
Philippe Martinez, Jacques Giraudeau, Michel Cremer, Joël Saint-Paul pour nous avoir permi d'utiliser leurs instruments à Bordeaux, ainsi qu'à Bruno Malaizé, Samuel Toucane et Julien Bourget pour leur accueil chaleureux.

Bruno Joly, Didier Swingedouw et Christophe Cassou de Toulouse, pour votre aide dans la compréhension des phénomènes météorologiques actuels, bien que je n'ai pas eu l'occasion de vous rencontrer.
Jean-Louis Reyss et Michel Fontugne pour leurs discussions enrichissantes sur les aspects chronologiques, ainsi qu'aux personnes du LIDES que je n'ai pas encore citées, comme Florent Tournier, pour m'avoir reçu dans leur laboratoire, je vous rejoins bientôt…
A l'EID Montpellier pour l'utilisation de leurs photos aériennes et à l'IFRMER Palavas pour le stockage de nos carottes.
Christelle Reynès et Nicolas Pujol pour leur aide précieuse quant à l'utilisation de méthode statistique que je maîtrise mal.
A Jean-Luc Seidel et Luc Neppel d'Hydrosciences Montpellier.
Et à Marc Desmet pour avoir cru en ce projet.
Puis tous les chercheurs de Géosciences de Montpellier qui ont participé de près ou de loin à ce travail avec Michel Séranne, Yann Leredde, Marc Jolivet, Nicolas Arnaud, Aurélien Gay, Yves Lagabrielle et Marc Daignière pour son implication auprès des doctorants.
Un grand merci à tous les étudiants qui ont travaillé avec nous durant ces années et même avant cela, à savoir Stéphanie Bordelais, Michaël Barbier, Jérôme Castaings, Estelle, Anis, Romain, et la team EG08.
Et enfin à Nathalie pour ses corrections orthographiques plus que nécessaires, comme vous le savez tous !

Faisant partie d'une UMR je tiens à remercier chaleureusement les secrétaires de Géosciences Montpellier Céline Fabrégat, Nathalie Mouly, Marie-France Roch et Bernadette Marie, toujours présentes et qui ont facilité bon nombre de mes démarches, ainsi qu'Anne Delplanque pour sa patience lors de mes multiples impressions de poster. Merci également à tout le service informatique : Josiane, Tan, Jérôme et Fabrice pour leurs interventions.

L'enseignement a fait partie intégrante de ce travail de thèse. Durant mes trois années de monitorat à l'Université Montpellier 2, je tiens donc à remercier son directeur Henri de la Boisse mais aussi toutes les personnes avec lesquelles j'ai enseigné comme Suzanne Raynaud, et Jean-Emmanuel Hurtrez.
Ensuite, vu que j'en suis à l'enseignement, je souhaiterais largement remercier les professeurs de géologie qui m'ont le plus marqué et donné envie de m'impliquer à fond dans mes études à savoir : Philippe Laurent, Jean-Marie Dautria, Jean-Marc Luck, André Leyrloup et Michel Lopez, cela va être dur quand dans deux ou trois ans la grande majorité d'entre eux sera partis à la retraite !!!

Ensuite, évidement j'aimerais remercier tous « mes potes de galère », ceux avec lesquels j'ai passé tant de week end à la fac ; mais heureusement aussi de très très bons moments en dehors. Tout d'abord un grand merci à mes « collocs » de bureau, Rémi puis Philou pour n'avoir jamais compris ce que je faisais dans la boue. Cependant la bonne ambiance du bureau 13 est une valeur sûre! Et puis à Bruno et Flo avec qui je suis embarqué depuis le M2 et même avant. Courage les gars vous y êtes presque, idem pour Lyd et Karen : plus que quelques mois, vous tenez le bon bout ! Puis à El Colombiano Vollador, Eric, Fabien, Lara, Linda, Magalie, Marion, Marion, Mickaël, Mickaël, Mrs Bling Bling, Mrs Joke, Nans, Nicolas, Ricardo, Thomas, Véronique, Vincent…

Et puis parce que cette fin de thèse signe également la fin de ma vie de près de 27 ans à Montpellier, je voudrais remercier tous mes collègues montpelliérains de la première heure

avec qui on a passé des moments inoubliables, à savoir : Adrien, Alix, Bobee, Chab, Clément, Corneille, Fai, John, Juliette, Karot, Lucille, Msi, Neaj, Nico, Ryan, Seb, Vinz…

Enfin à ma famille Blandine, Marina, Noah, Raoul, Natacha, ma Mère, ma Grand-mère pour leurs encouragements et à mon Père qui m'a transmis la passion pour la recherche et m'a si bien coatcher tout au long de mes études.

Et parce que l'on garde le meilleur pour la fin : à ma femme et future mère de mes enfants (ça ne tardera pas trop promis !) pour sa tendresse, sa compréhension, son aide et son soutien sans faille dans les moments difficiles ! Femme parfaite ce n'est pas pour rien que je t'ai épousé !!!!

Table des matières

1. Introduction et problématique

Il est maintenant clairement établi que notre planète se réchauffe depuis l'époque préindustrielle (IPCC, 2007). Cependant le changement climatique affecte la Terre avec une intensité variable selon les régions, ainsi la Méditerranéenne apparaît comme une des zones les plus vulnérables sur notre planète (Giorgi, 2006). Les simulations climatiques à l'échelle régionale sont fréquemment utilisées afin de prédire les changements de température ainsi que les variations des phénomènes extrêmes (précipitations et cyclones). Gibelin et Déqué (2003) prédisent, à l'aide du modèle ARPEGE, un réchauffement global et une augmentation des sècheresses durant toutes les saisons sauf en hiver dans la partie Nord Ouest de la Méditerranée. De plus, Lionello et Giorgi (2007) mettent en évidence une réduction de l'activité des cyclones dans les futurs scénarios induisant un bilan négatif de précipitation dans le Sud et l'Est de la Méditerranée, et une augmentation dans la partie Nord en lien avec le renforcement des vents d'Ouest. La régionalisation du changement climatique et l'étude de la modification éventuelle des événements extrêmes constituent des objectifs de recherche majeurs à travers des programmes nationaux gérés par l'Institut National des Sciences de l'Univers (ECLIPSE, GICC, PNEDC, PATOM…) mais aussi internationaux (Programme mondial de recherche sur le Climat, Programme international Géosphère-Biosphère). De plus, l'intérêt croissant de l'Union Européenne et de la France envers les pays Méditerranéens, dans un contexte de bouleversement climatique sans précédent, fait de cette zone et de ce domaine de recherche une problématique majeure à l'échelle des Sciences de la Terre.

Les effets de ce changement climatique sur les évènements climatiques extrêmes sont difficiles à estimer car ils présentent une variabilité plus grande que la moyenne et sont par conséquent plus difficiles à identifier à l'aide de données instrumentales couvrant de courtes périodes temporelles (Webster *et al.*, 2005; Emanuel 2006a; Landsea *et al.*, 2006). La reconstitution de la fréquence et de l'intensité des paléotempêtes en domaine côtier, est d'autant plus nécessaire que les concentrations en ressources et en population dans cette zone n'ont cessé de croître durant les dernières dizaines d'années (Pielke et Landsea 1999; Turner *et al.*, 2006; Lionello *et al.*, 2006). L'action de l'homme sur son milieu, le développement de nos sociétés et l'accroissement des richesses susceptibles d'être détruites, démultiplient l'impact destructeur des épisodes climatiques intenses. Toutefois, la question des phénomènes

extrêmes reste entière : sont-ils liés au réchauffement planétaire ou bien appartiennent ils à la variabilité naturelle du climat?

Dans cette thèse nous nous focalisons sur les événements extrêmes (principalement les tempêtes) qui affectent le Golfe du Lion situé dans la partie Nord Ouest de la Mer Méditerranée. La problématique des risques naturels (crues, tempêtes) dans cette région est tout à fait d'actualité au regard notamment des dernières grandes crues catastrophiques du Languedoc-Roussillon (1994, 1999, 2002…). Les enjeux des inondations sont considérables. Les impacts sociaux et économiques directs en font, pour la France, le risque le plus dommageable. L'événement de crue de Septembre 2002 causa la mort de 23 personnes et des dégâts estimés à un milliard d'euros. De plus, les fortes houles, bien qu'exceptionnelles, ont des conséquences irréversibles sur l'érosion et la submersion du littoral. Au cours de la tempête de 1982, des vents supérieurs à 180 km/h sur le littoral languedocien (categorie 2 sur l'échelle de Saffir–Simpson) ont ainsi créé des surcôtes atteignant 1,5 m NGF et levant une houle dévastatrice, rompant par endroits les cordons dunaires et causant la mort de 15 personnes ainsi que des pertes économiques estimées à 400 millions d'euros. Ces tempêtes de secteur Sud ont aussi un effet aggravant sur les crues car elles perturbent l'écoulement des fleuves vers la mer. Les archives communales de la région conservées depuis le 15ème siècle révèlent de nombreuses périodes où l'activité hydrologique a été perturbée, en particulier durant le Petit Age Glaciaire (Blanchemanche, 2009). Cependant sur des intervalles de temps plus longs, la fréquence de ces événements est difficile à estimer à partir des enregistrements instrumentaux et historiques qui ne sont respectivement valables que sur des périodes de l'ordre du siècle à quelques siècles. Dans ce contexte, la prise en compte des données géologiques offre l'unique opportunité pour reconstituer un enregistrement à long terme des événements extrêmes, permettant ainsi d'accéder à l'évolution de l'activité des tempêtes en relation avec les changements climatiques passés.

Le littoral du Golfe du Lion est caractérisé par de nombreux systèmes lagunaires qui résultent de l'interaction entre un processus de régularisation du trait de côte, par migration de barrières sableuses dues au transfert de sédiment par l'hydrodynamique littoral, et par un lent remplissage de ces zones par des apports fluviaux et marins (Certain *et al.*, 2004). Cette étude se concentre sur le complexe lagunaire palavasien et plus particulièrement sur l'étang de Pierre Blanche dont la bordure Sud est formée par un cordon littoral sableux très faiblement anthropisé. Ainsi cette étude a pour but d'identifier les événements extrêmes de tempêtes

ayant affecté le bassin Nord Ouest Méditerranéen et d'estimer leur récurrence au cours de l'Holocène en lien avec les changements climatiques passés. Ce travail entre dans le cadre du projet ECLICA « Evènements CLImatiques CAtastrophiques (crues et tempêtes) au cours de l'Holocène et leurs impacts sur l'environnement et les sociétés humaines » (ACI FNS « Aléas et changements globaux, 2003, coordinateur L. Dezileau). Notre recherche s'est organisée autour de quatre objectifs principaux qui définissent les chapitres de cette thèse (i) caractériser des sources par une approche sédimentologique (granulométrie, minéraux argileux), géochimique (éléments majeurs et traces) et faunistique afin d'identifier les phénomènes brefs de fortes amplitudes, (ii) établir un cadre chronologique (^{210}Pb, ^{137}Cs, ^{14}C et chroniques historiques), (iii) comprendre l'évolution paléoenvironnementale du système lagunaire étudié, et (iv) reconstituer les événements extrêmes au cours de l'Holocène afin de comprendre leurs liens avec les variations climatiques passées.

2. Présentation générale

2.1 La Méditerranée, changements climatiques et événements extrêmes

Le changement climatique affecte la Terre dans sa globalité, néanmoins ce réchauffement n'affecte pas toutes les régions avec la même intensité. De plus certaines zones sont plus vulnérables que d'autres à ces changements, c'est dans ce cadre que Giorgi (2006) définit un Index Régional du Changement Climatique (RCCI) basé essentiellement sur les variables de température et de précipitation. Cet index permet de mettre en évidence certaines régions comme étant des « Hot-Spot » du changement climatique dans lesquelles apparaissent au premier rang l'Europe du Nord et surtout la région Méditerranéenne (*Figure 2.1*).

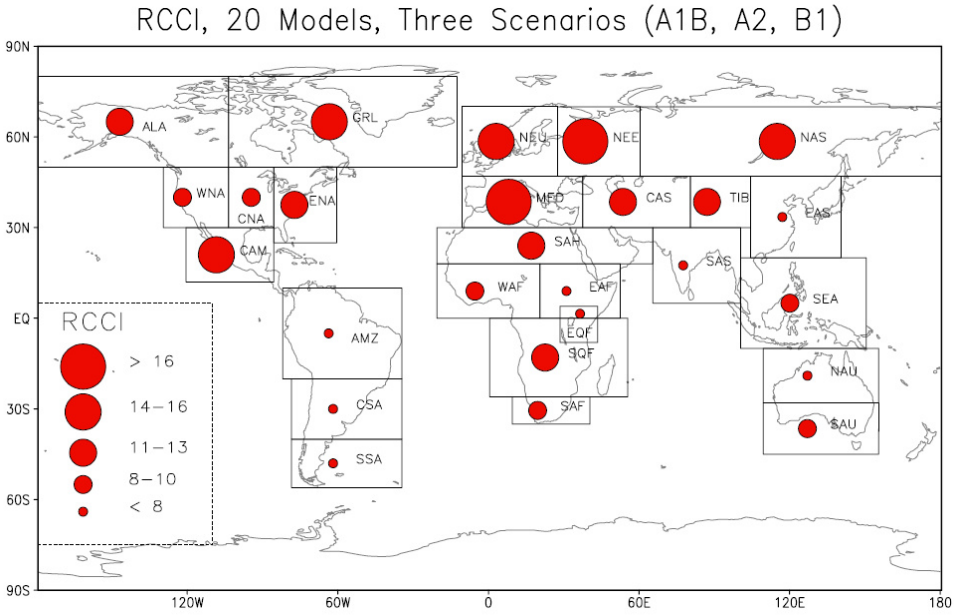

Figure 2.1 : Index Régional du Changement Climatique (RCCI) à travers 26 régions du monde calculé à partir de 20 Models Climatiques Globaux couplant l'Atmosphère et l'Océan (AOGCM) à partir de 3 scénarii d'émission (IPCC, 2000). D'après Giorgi, (2006).

2.1.1 Les simulations

Les dernières simulations à l'aide de Modèle Climatiques à l'échelle Régionale couplant l'Océan et l'Atmosphère (AORCM), réalisées par Somot *et al.*, (2008) selon le scénario A2

(IPCC, 2000) prévoit un important réchauffement de la région Méditerranéenne d'ici la fin du 21ème siècle. Cette augmentation des températures s'observe au cours de toutes les saisons avec cependant des valeurs maximales l'été, dans les parties Nord et Nord-Ouest de la Méditerranée, pouvant atteindre des valeurs supérieures à 5°C. De plus, Somot *et al.*, (2008) prévoient une diminution des précipitations pouvant atteindre 30% dans le Sud de l'Europe durant l'été. Ces résultats sont en accord avec ceux de Giorgi et Lionello, (2008) présentant une synthèse des différentes projections à l'échelle régionale tant pour l'augmentation de température (4-5°C avec le scénario A1B) que pour la diminution des précipitations entre 25 et 35% selon les région durant l'été (*Figure 2.2*).

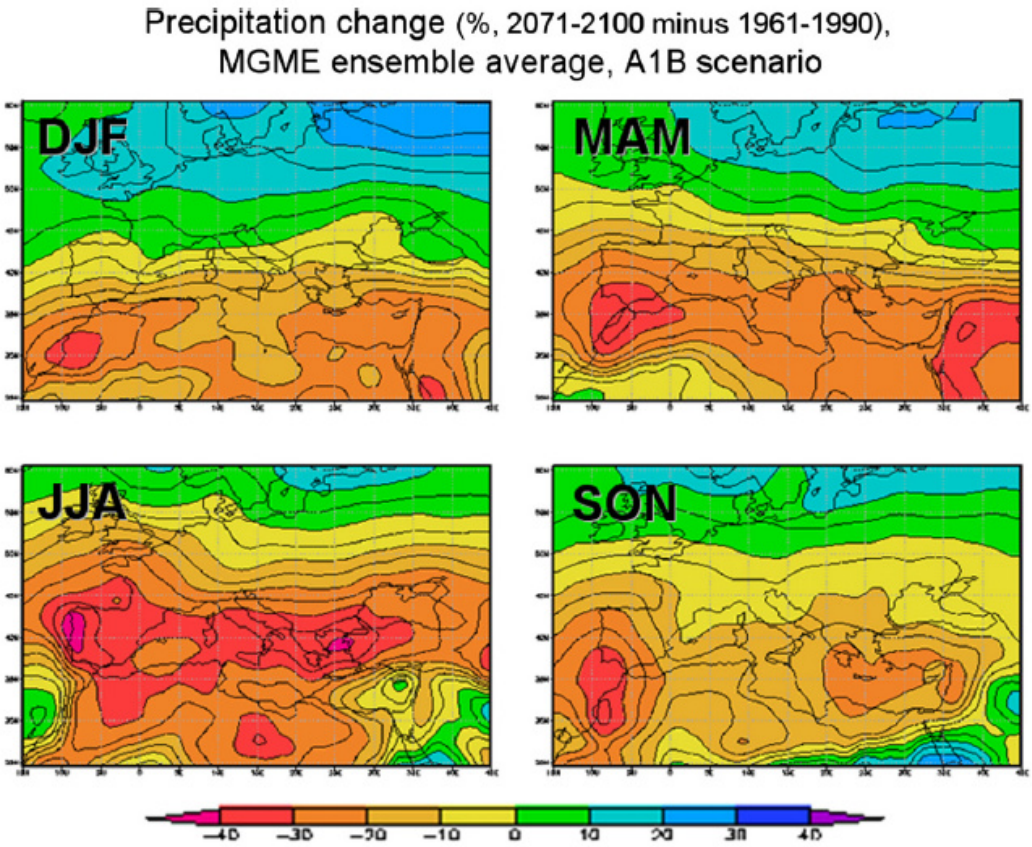

Figure 2.2 : Simulations des changements moyens des précipitations obtenues à partir de l'ensemble MGME (Multi Global Model Ensemble), entre les périodes 1961–1990 et 2071–2100 avec le scénario A1B, pour les quatre saisons. Les unités sont exprimées en % par rapport à la valeur de 1961–1990, d'après Giorgi et Lionello, (2008).

Nous pouvons remarquer certaines exceptions comme par exemple une légère augmentation des précipitations durant l'hiver dans la région des Alpes et dans le Sud de la France.

Cependant cette forte diminution des précipitations moyennes durant l'été n'est pas liée à une diminution de l'intensité des événements mais plutôt à leurs fréquences (Giorgi et Lionello, 2008). Certains modèles prévoient même une augmentation de l'intensité des événements de précipitations (Goubanova et Li, 2007). D'autre part Lionello et Giorgi, (2007) montrent (à l'aide de modèles climatiques régionaux) une augmentation de l'activité des cyclones dans la partie Nord Ouest de la Méditerranée associée à une diminution dans la partie Est, qu'ils imputent aux changements de l'intensité et de la position des vents d'Ouest. Ces modélisations montrent des tendances en accord avec la diminution des précipitations simulée à l'échelle de la Méditerranée (*Figure 2.2*).

2.1.2 Observations et tendances au cours des derniers siècles

L'évolution de la température de l'air près de la surface durant l'hiver (DJF) depuis 500 ans présente une tendance générale au réchauffement qui débute à partir de 1890 avec une augmentation d'environ 0.8°C au cours du dernier siècle (*Figure 2.3*, d'après Luterbacher *et al.*, 2004 ; Mitchell et Jones, 2005). Bien que la variabilité de la température est importante, nous observons quelques anomalies significatives surtout au cours du 17ème siècle. La décennie la plus chaude est 1993-2002 alors que la plus froide est 1680-1689.

Le phénomène frappant dans la reconstitution des précipitations hivernales (DJF) depuis 500 ans, est la forte diminution des pluies depuis les années 1960 qui semble n'avoir aucun précédent au cours des 5 derniers siècles. La décennie la plus sèche est 1986-1995 avec une diminution de 15 mm, alors que la plus humide est 1961-1970 avec une augmentation de 5 mm par rapport à la période (1961-1990). D'autres études indiquent une tendance générale à la diminution des précipitations durant l'hiver, particulièrement dans la partie Nord du bassin Méditerranéen (Trigo *et al.*, 2000 ; Alpert *et al.*, 2002 ; Xoplaki *et al.*, 2004).

Les autres phénomènes extrêmes affectant le climat dans cette région sont les cyclones et les tempêtes. Les cyclones Méditerranéens sont généralement caractérisés par un cycle de vie court et une taille plus faible que les cyclones extratropicaux développés en Atlantique. Comprendre l'évolution des cyclones dans cette région est primordial, car ils engendrent beaucoup de phénomènes extrêmes comme les précipitations intenses, les vents violents, les vagues, les surcotes et les glissements de terrain. Pour tous ces phénomènes, la géographie à l'échelle régionale joue un rôle important, elle détermine les effets des cyclones sur l'environnement (Lionello *et al.*, 2006). Les événements pluvieux les plus intenses ont lieu

quand la trajectoire d'un cyclone est telle qu'il produit des convergences locales d'air humide Méditerranéen pouvant être accentués par la topographie (Trigo *et al.*, 2000 ; Jansá *et al.*, 2001). Dans la Méditerranée de l'Ouest Jansá *et al.*, (2001) ont démontré que dans plus de 90% des cas de fortes précipitations il y avait un centre cyclonique à proximité (c'est le cas dans le Sud de la France avec les « événements cévenols » qui arrivent avec des flux de Sud-Est). Les cyclones sont donc la cause de la majorité des phénomènes d'intenses précipitations dans la région Méditerranéenne (Trigo *et al.*, 2000 ; Lionello *et al.*, 2006).

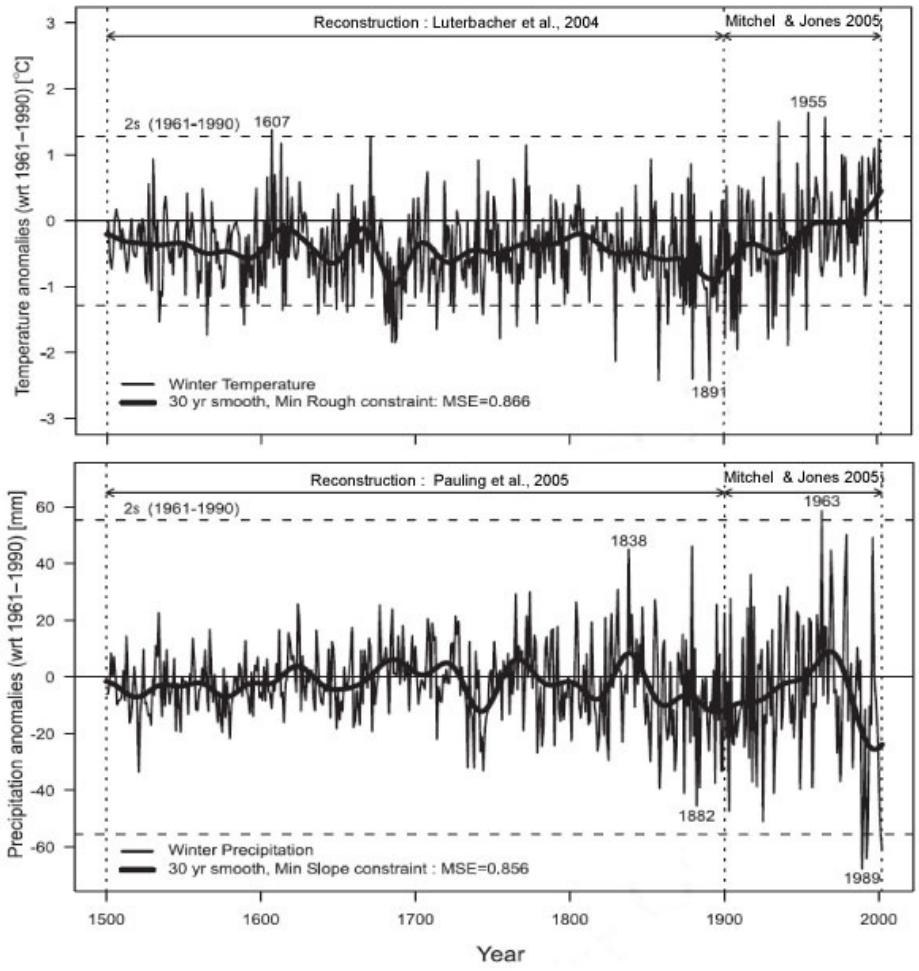

Figure 2.3 : En haut (bas) Anomalies de la moyenne des températures (précipitations) hivernales (DJF) en Méditerranée au cours des 500 dernières années par rapport à celles de 1961-1990. Les valeurs de température sont reconstituées par Luterbacher et al., (2004) et celles de précipitations par Pauling et al., (2005) à partir de l'étude d'archives et de différents proxies, pour la période de 1500-1900. Pour le dernier siècle les données instrumentales ont été publiées par Mitchell et Jones, (2005). Résumé dans Luterbacher et al., (2006).

La tendance générale des cyclones durant l'hiver (DJF, saison des tempêtes) est marquée par une diminution de leur densité dans la partie Ouest de la Méditerranée et une augmentation de leur fréquence dans la partie Est au cours des 120 dernières années (*Figure 2.4,* Maheras *et al.*, 2001 ; Bhend, 2005 ; Lionello *et al.*, 2006). Cette tendance à la diminution des cyclones est confirmée par la diminution de la moyenne de la hauteur des vagues durant l'hiver (Lionello et Sanna, 2005). D'autres études, dans la partie Nord de la Méditerranée suggèrent une distinction entre une tendance à la diminution des cyclones de fortes intensités et une augmentation de ceux de faible intensité en lien avec un déplacement vers le Nord des vents d'Ouest depuis 1979 (Trigo *et al.*, 2000).

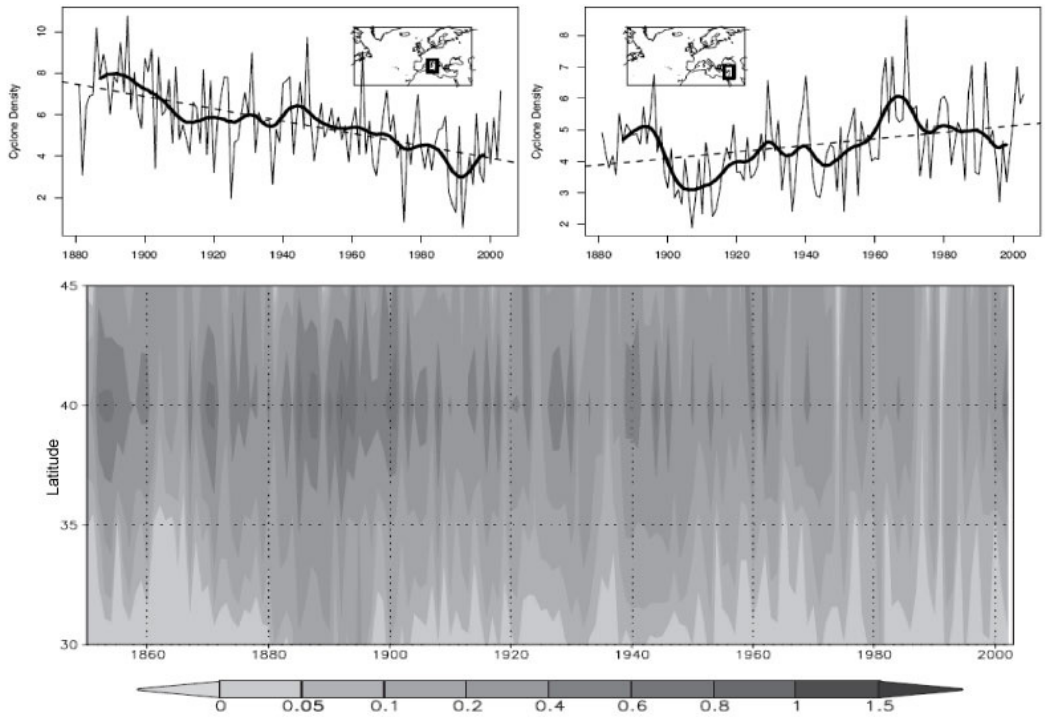

Figure 2.4 : En haut : densité moyenne des cyclones au cours des 120 dernières années pour la Méditerranée de l'Ouest (à gauche) et la Méditerranée de l'Est (à droite), d'après Bhend, (2005). En bas : la variabilité de densité moyenne des cyclones en fonction du temps (1850-2003) et de la latitude à la longitude 10°W (Lionello et al., 2006).

A l'heure actuelle, il n'y a pas encore été démontré que le comportement des événements extrêmes typiques du climat Méditerranéen à une échelle interannuelle ne soit pas lié à des fluctuations climatiques naturelles de basses fréquences depuis le début du siècle. En effet

certains mécanismes climatiques naturels comme la NAO ou l'EAP (Eastern Atlantic Pattern) ont des influences importantes sur les températures et les précipitations selon la fenêtre de temps étudiée (Quadrelli *et al.*, 2001 ; Sánez *et al.*, 2001 ; Krichak et Alpert, 2005 ; Lionello *et al.*, 2006 ; Luterbacher *et al.*, 2006 ; Trigo *et al.*, 2006).

2.1.3 Conclusions

Tous les auteurs s'accordent à dire que la région Méditerranéenne est une des plus sensible au réchauffement actuel tant d'un point de vue climatique (augmentation des températures, diminution des précipitations) que d'un point de vue vulnérabilité socio-économique (ressource en eau, tourisme). Cependant, dans ce contexte, il apparaît important d'obtenir une meilleure lisibilité sur les changements futurs de l'intensité et de la fréquence des événements extrêmes (cyclones, pluies intenses, sécheresses). Pour cela, il est essentiel d'obtenir de longues séries de données, afin de s'affranchir de la variabilité interannuelle à pluri décennale, pouvant être liée aux cycles de certains modes climatiques (NAO, EAP...), afin d'extraire des tendances statistiquement représentatives, dans les différentes régions du bassin Méditerranéen. De plus, comme nous venons de le voir, les cyclones dans cette zone sont à l'origine de la plupart de ces phénomènes extrêmes, tels que les pluies intenses, les vents puissants, les fortes houles et les surcotes importantes. Le littoral est une des rares zones où tous ces aléas peuvent éventuellement agir ensemble et causer le plus de dommages à l'Homme (d'autant plus que le domaine littoral Méditerranéen est une zone de forte concentration en ressources et en population) faisant ainsi des cyclones, et des tempêtes en domaine côtier un des risques majeurs de notre siècle.

2.2 Les tempêtes en domaine littoral

Selon une estimation des Nations Unies, 80 % de la population mondiale vivra en 2010 sur une bande littorale de 100 kilomètres dans laquelle serait rassemblée d'énormes enjeux socio-économiques. Cette évolution pourrait s'avérer dangereuse, comme en témoigne un rapport publié par l'OCDE en 2007, indiquant que le changement climatique et l'urbanisation pourraient entraîner un triplement du nombre de personnes exposées à des inondations côtières dans le monde d'ici 2070. Dans ce contexte, il apparaît donc primordial de

comprendre la dynamique du littoral, zone très mobile et évolutive en liens avec les phénomènes marins comme les tempêtes.

2.2.1 Submersion et érosion du littoral

La submersion marine et l'érosion brutale de la zone côtière par la mer sont des risques en grande majorité associés à l'activité des cyclones et des tempêtes. Une tempête marine correspond à l'évolution d'une perturbation atmosphérique, ou dépression, issue de la confrontation de deux masses d'air aux caractéristiques bien distinctes (température, humidité). Cette confrontation engendre un gradient de pression élevé, à l'origine de vents violents et le plus souvent de précipitations intenses. Lors des tempêtes marines, le niveau moyen de la mer augmente sous l'effet conjoint de la dépression atmosphérique, des vents (qui massent l'eau vers la côte) et du déferlement des vagues. Ces événements sont en principe de courte durée, de quelques heures à quelques jours et se traduisent généralement par (1) l'invasion d'eau salée dans les terres, (2) d'importants transports sédimentaires vers le large, (3) le transfert de matériel sableux dans des zones situées en arrière du cordon dunaire en cas de rupture de celui-ci (sous l'action des vagues). Lorsque l'eau franchit les ouvrages de défense, les projections de sable ou de galets peuvent avoir des effets dommageables sur les fronts de mer urbanisés. De plus, l'influence de l'Homme, en particulier l'urbanisation et les activités économiques dans la zone côtière, a transformé l'érosion côtière, processus initialement naturel, en un problème d'intensité croissante. Les principaux mécanismes induisant ces phénomènes sont :

- L'action des vagues dont la hauteur dépend à la fois de la vitesse du vent et de la houle rémanente (qui est formée par un champ de vent éloigné de la zone d'observation) caractérisée par son absence de relation avec le vent local.
- Les surcôtes qui sont le résultat de faibles pressions atmosphériques combinées à l'action du vent à la surface de l'eau. Ce phénomène peut être amplifié s'il est associé à un fort coefficient de marée.

L'augmentation actuelle du niveau marin 3,1 ± 0,5 mm/an (Nerem *et al.*, 2006) et les prévisions les plus pessimistes pour l'horizon 2100, atteignant des valeurs de 1 ± 0,5 m (Rohling *et al.*, 2008), cette augmentation peut également avoir des effets sur l'érosion du littoral mais à des échelles de temps plus grandes.

Les dépôts sédimentaires les plus typiques lors du passage d'une tempête au dessus d'un littoral sableux sont les cônes de tempêtes. Ils se forment sous l'action des vagues et du vent érodant le cordon sableux et provoquant le transport et le dépôt de matériel sédimentaire dans les zones situées en arrière du lido, généralement des lagunes (*Figure 2.5* ; Leatherman 1979 ; Oxford et Carter, 1982 ; Morton *et al.*, 2000 ; Morton et Sallenger 2002 ; Buynevich *et al.*, 2004; Houser *et al.*, 2008 ; Matias *et al.*, 2008).

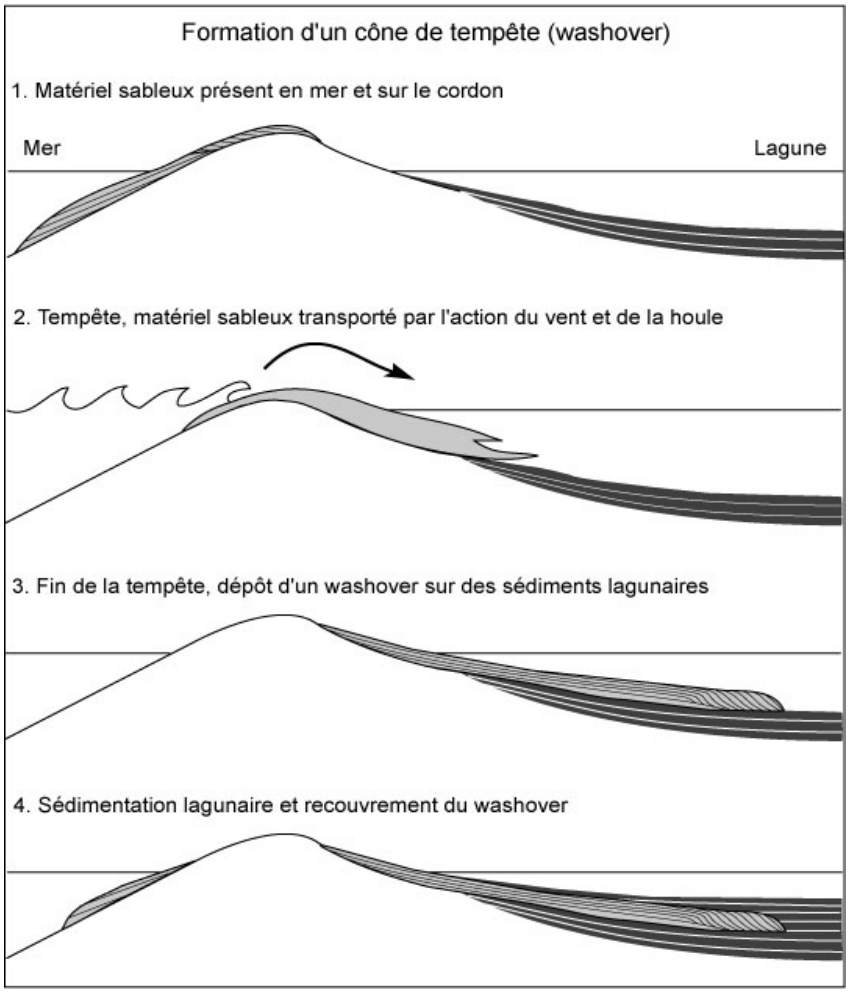

Figure 2.5 : Mécanisme de formation d'un cône de tempête.

Souvent présent sous forme de lobe, l'extension horizontale de ces niveaux sableux sont soumises à différents facteurs comme l'intensité et la durée de la tempête, la hauteur des vagues associées à la surcôte, le coefficient de marée, la direction du vent par rapport au lido, l'épaisseur du lido et la quantité de sable disponible, la configuration de la côte avec la présence ou non de passe, la morphologie de la lagune ainsi que la succession de plusieurs événements extrêmes durant une courte période (Scileppi et Donnelly 2007 ; Matias *et al.*,

2008). Dans la *Figure 2.6* nous constatons l'effet de la tempête de 1982 sur le littoral languedocien. Cette tempête de catégorie 2 sur l'échelle de Saffir-Simpson engendra des vents de plus de 180 km/h levant une houle de près de 10 m (au large) et une surcote atteignant près de 1,5 m NGF (marégraphe de Sète). L'influence de cette tempête sur le littoral se traduit tout d'abord par une submersion du cordon sableux avec la création de passes (grau) lors de l'événement, engendrant une forte érosion du lido et la formation de cône de tempête dans la lagune. De plus, l'effet de cette tempête après sont passage est perceptible à la fois par le recul et par la morphologie du cordon persistant de nombreuses années après l'événement (IMPLIT, 2004).

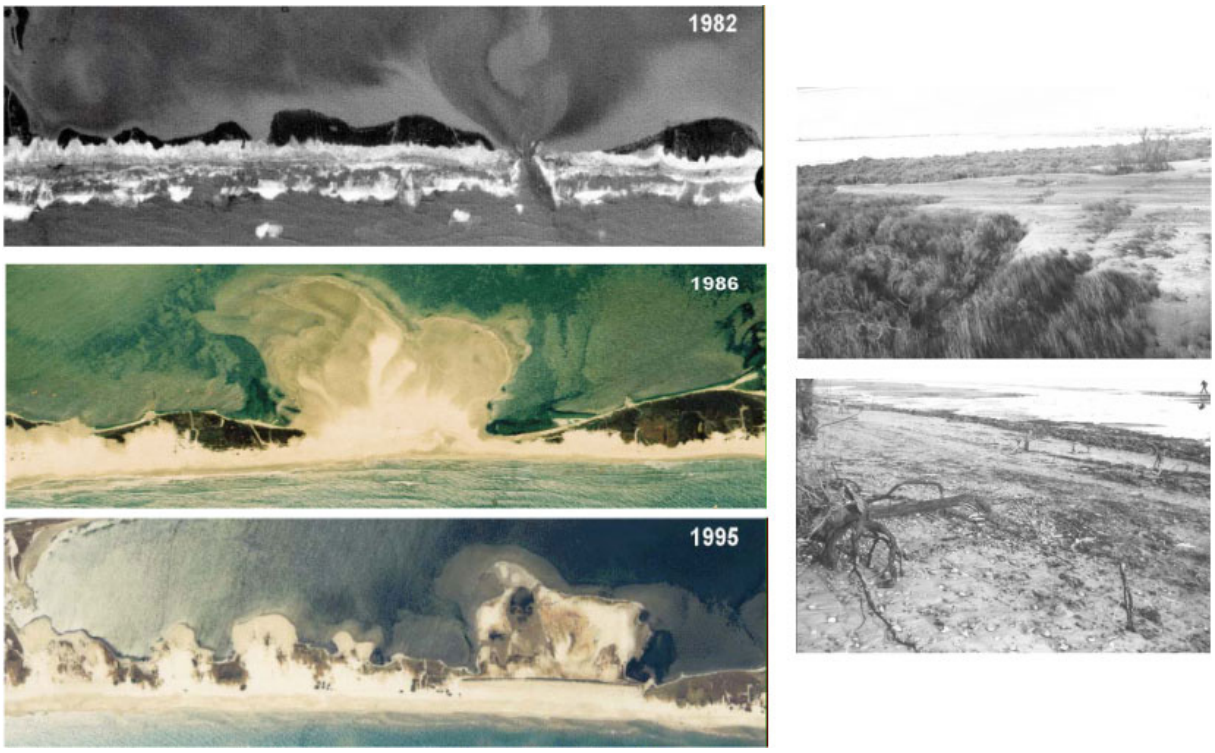

Figure 2.6 : A droite : photos aériennes du cordon sableux de Maguelone durant la tempête de novembre 1982 (haut) puis ce même cordon 4 et 13 ans après, où nous pouvons voir l'influence de cet événement sur la submersion et la morphologie du cordon (IMPLIT, 2004). A gauche : les effets de cette tempête sur le recul du cordon se matérialise par l'érosion au niveau de la plage et le dépôt de sable (washover) dans le domaine lagunaire (Photos : M. Séranne).

2.2.2 La paléotempestologie

La paléotempestologie est une méthode utilisée pour la première fois par Liu et Fearn, (1993) dans une lagune au Nord du Golfe du Mexique (Alabama, USA) puis décrite et synthétisée par Liu et Fearn, (2000). Cette méthode permet de reconstituer les tempêtes et les cyclones du passé à partir d'archives le plus souvent sédimentaires, et elle utilise des traceurs géologiques comme la granulométrie, la géochimie et les bio-indicateurs. Cette méthode est en grande partie basée sur l'étude des cônes de tempête qui se forment à la suite d'un cyclone en arrière d'un cordon littoral sableux (*Figure 2.7*). Ces extensions sableuses dans la lagune ont une épaisseur variable en fonction de critères morphologiques, hydrodynamiques (section 2.2.1.) et varie aussi en fonction de la distance par rapport au cordon, c'est ainsi que la couche de sable est importante sur le bord de la lagune et qu'elle diminue avec l'éloignement.

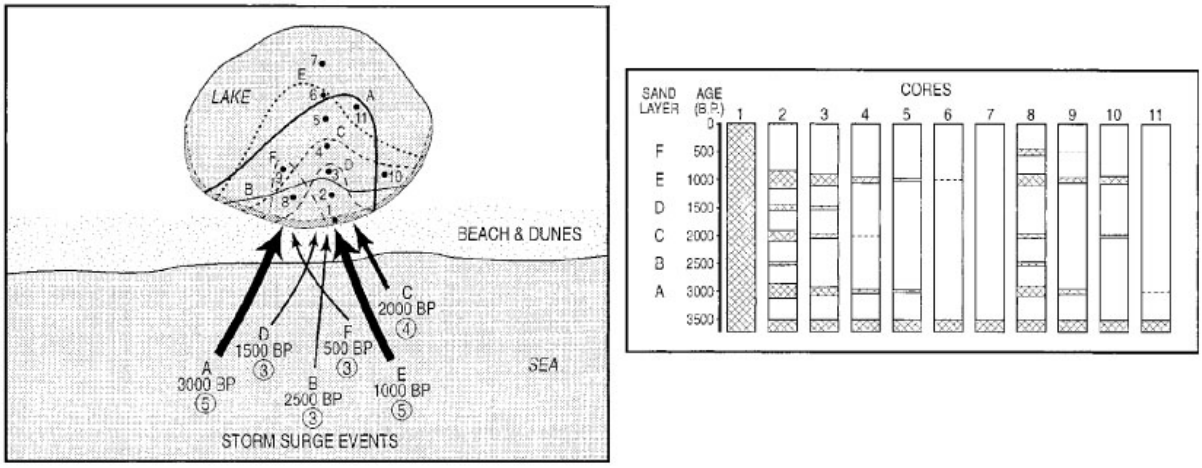

Figure 2.7 : Modèle de dépôt des cônes de tempête dans une lagune située derrière un cordon dunaire sableux (à gauche), l'intensité des tempêtes frappant cette zone est indiquée par la taille des flèches A-F, les numéros entourés indiquent cette intensité sur l'échelle de Saffir-Simpson. L'extension des cônes de tempête dans la lagune est indiquée par les lignes pleines et en pointillés. Les points noirs représentent les différents lieux de carottage (1-11). Ces carottes sont représentées à droite. Le nombre, la taille et l'extension des couches de sable sont fonction de l'intensité de la tempête. Voir le texte pour les explications. D'après Liu et al., (2000).

Liu et Fearn, (2000) montrent donc (1) l'importance de ne pas se situer trop près du cordon si nous voulons enregistrer uniquement les tempêtes les plus extrêmes et (2) l'intérêt de réaliser

des transects reliant plusieurs carottes afin de s'affranchir de l'orientation de l'événement par rapport à la côte. La paléotempestologie permet ainsi de calculer la récurrence des tempêtes les plus extrêmes au cours du temps, souvent exprimée, en pourcentage, ou en probabilité d'avoir un événement par an. Il est également possible de remonter à la fréquence de tels phénomènes en étudiant les successions des dunes et du niveau d'érosion entre ces dunes (Nott et Haynes, 2001 ; Nott, 2004 ; Zazo *et al.*, 2008) ou en analysant les archives historiques (Liu *et al.*, 2001).

Depuis lors, de nombreuses études utilisant cette méthode se sont concentrées sur la compréhension de la récurrence des cyclones en Amérique du nord et dans les Caraïbes (Liu et Fearn, 1993, 2000; Donnelly *et al.*, 2001a, b; Scott *et al.*, 2003; Donnelly *et al.*, 2004; 2005 ; Donnelly et Woodruff, 2007; Scileppi et Donnelly 2007 ; Lambert *et al.*, 2008), ainsi que dans le Pacifique (Goff *et al.*, 2000; Hayne et Chappell 2001; Nott, 2004 ; Woodruff *et al.*, 2009 ; Nott *et al.*, 2009). Peu d'études concernant les côtes Méditerranéennes (Blanc, 1985 ; Bruzzi, 1998 ; Dezileau *et al.*, 2005) existent à ce jour. De plus, l'analyse à haute résolution de nouveaux proxies permet d'étendre l'enregistrement de la fréquence des tempêtes plus loin dans le passée avec des résolutions décennales à saisonnières (Frappier *et al.*, 2007b). Ces proxies basés sur les précipitations exploitent les faibles rapports des valeurs isotopiques de l'oxygène et de l'hydrogène dans les pluies liées aux cyclones tropicaux (Lawrence et Gedzelman, 1996), sont utilisés dans les cernes de croissance des arbres (Miller *et al.*, 2006) et dans les stalagmites (Frappier *et al.*, 2007a ; Nott *et al.*, 2007).

2.3 Le site d'étude

Le littoral du Golfe du Lion est de type microtidal (marée inférieur à 50cm). Il est caractérisé par la présence d'étangs séparés du domaine marin par un cordon littoral sableux étroit (*Figure 2.8*). Le Rhône étant la principale source de sédiment avec près de 94% de la charge solide apporté à la marge (Certain, 2002). Les autres fleuves se situent au centre (Hérault, Orbe, Aude) et à l'Ouest (Têt, Agly). A partir de cette répartition des apports sédimentaires, nous pouvons définir des environnements dominés par la dynamique fluviatile (delta du Rhône) et par la houle comme le système lagunaire palavasien, qui est le site d'étude de cette thèse.

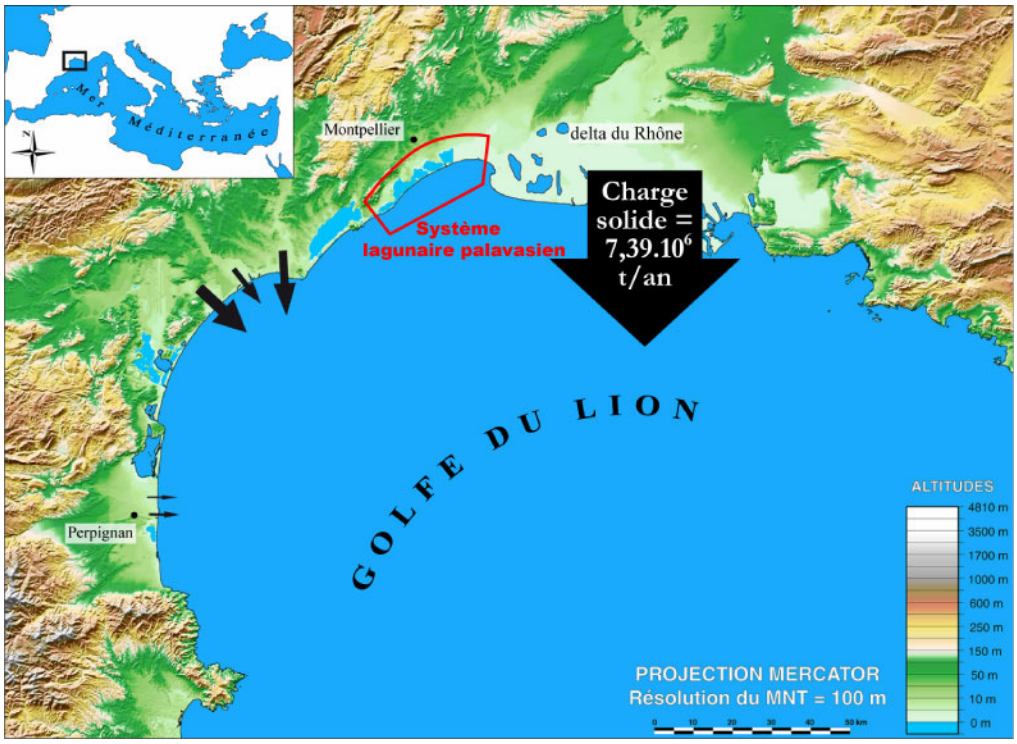

Figure 2.8 : Carte du Golfe du Lion et localisation de l'embouchure des principaux fleuves (la flèche étant proportionnelle à la charge solide annuelle). MNT réalisé par S. Dominguez.

Le système lagunaire palavasien est caractérisé par de faibles apports sédimentaires directs. La seule rivière transportant du matériel sédimentaire au système étudié est la Mosson (*Figure 2.9*). C'est une petite rivière côtière long de 36 km et constitué de deux affluents majeurs (le Coulazou et le Lassédéron) et drainant une superficie de 370 km^2. Son bassin versant est principalement constitué de formations sédimentaires du Secondaire (Calcaire), du Tertiaire (conglomérat, grès, argile) et de dépôts terrigènes du Quaternaire (BRGM, 1967). Le débit de cette rivière est de 1,2m^3/s et peut atteindre des débits nettement plus important lors des périodes de crues, comme le 3 Septembre 2003 avec 258m^3/s (DIREN, 2009). Le Lez, quant à lui n'apporte pas de sédiment dans les lagunes actuelles sauf peut-être en périodes de fortes crues. Mais il contribuait probablement dans le passé à une grande partie de la sédimentation lagunaire. Cependant la géologie du bassin versant du Lez et de celui de la Mosson étant identique nous avons échantillonné uniquement celui de la Mosson ainsi que le cordon littoral (Section 3.3., Article 2).

Les principales caractéristiques climatiques (vents) et hydrodynamiques (houle) du système lagunaire palavasien sont indiquées dans le *Tableau 2-1*.

Vents	Prop. An. (%)	Vitesse Max (m/s)
NW	60	44
NE	20	44
SE-SW	20	46

Fleuves	Débit (m3/s)	Débit crues
Mosson	1.2	258
Lez	2.5	487

	Hs (m)	Tm (s)
Houle annuelle	0.84	4.2

Tableau 2-1 : Principales caractéristiques climatiques et hydrodynamiques du système lagunaire palavasien représentant les proportions annuelles des vents selon leurs secteurs, les données de débits moyens ainsi que ceux en période de crue (3 Septembre 2003) pour la Mosson et le Lez, ainsi que la hauteur et la période de la houle annuelle.

Le système lagunaire palavasien est constitué d'un chapelet de sept lagunes (Méjan, Grec, Arnel, Prévost, Vic, Pierre Blanche, Ingril). Au cours de cette thèse nous nous sommes principalement focalisé sur l'étude de la lagune de Pierre Blanche (*Figure 2.9*). Cette lagune de 267ha est d'une profondeur moyenne de 60 cm. Sa bordure Sud-Est forme le cordon dunaire sur plus de 5 km avec une élévation moyenne de 3 m NGF. Bien que cette lagune ne soit pas directement reliée à la mer, en certain endroit le cordon est large de seulement 60 m ce qui implique lors d'événements de tempêtes une influence marine.

Nous avons réalisé huit carottes courtes (environ 1 m), sept dans la lagune de Pierre Blanche (PRO12, PRO15, PRO14, PRO10, PB08-3, PB08-4 et PB08-5) et une dans celle du Prévost (EG08) selon 3 transects ; un parallèle à la côte (T1) et deux perpendiculaires (T2, T3). Ces carottages ont été réalisés à la main à l'aide de tube en PVC. De plus nous avons réalisé deux carottages longs, un dans Pierre Blanche (PB06) et un dans l'Arnel (AR06). Ces deux carottes ont été prélevées en 2006 à l'aide de la plateforme de carottage UWITEC© (Université de Chambéry, *Figure 2.10*). L'utilisation de ce système permet la récupération de sections de 2m de long et d'un diamètre de 8,5 cm (PVC). Deux séries de 4 carottes ont été prélevées dans Pierre Blanche. Le décalage en profondeur des 2 séries (prélevées à quelques mètres l'une de l'autre) permet d'obtenir une série composite de 7,7 m sur l'ensemble du carottage (*Figure 2.10*). Ce type de carottier fonctionne à l'aide d'un piston hydraulique afin de ne pas perdre de sédiment. Les différentes méthodes d'analyse des carottes sont décrites dans les parties méthodologies de chaque article.

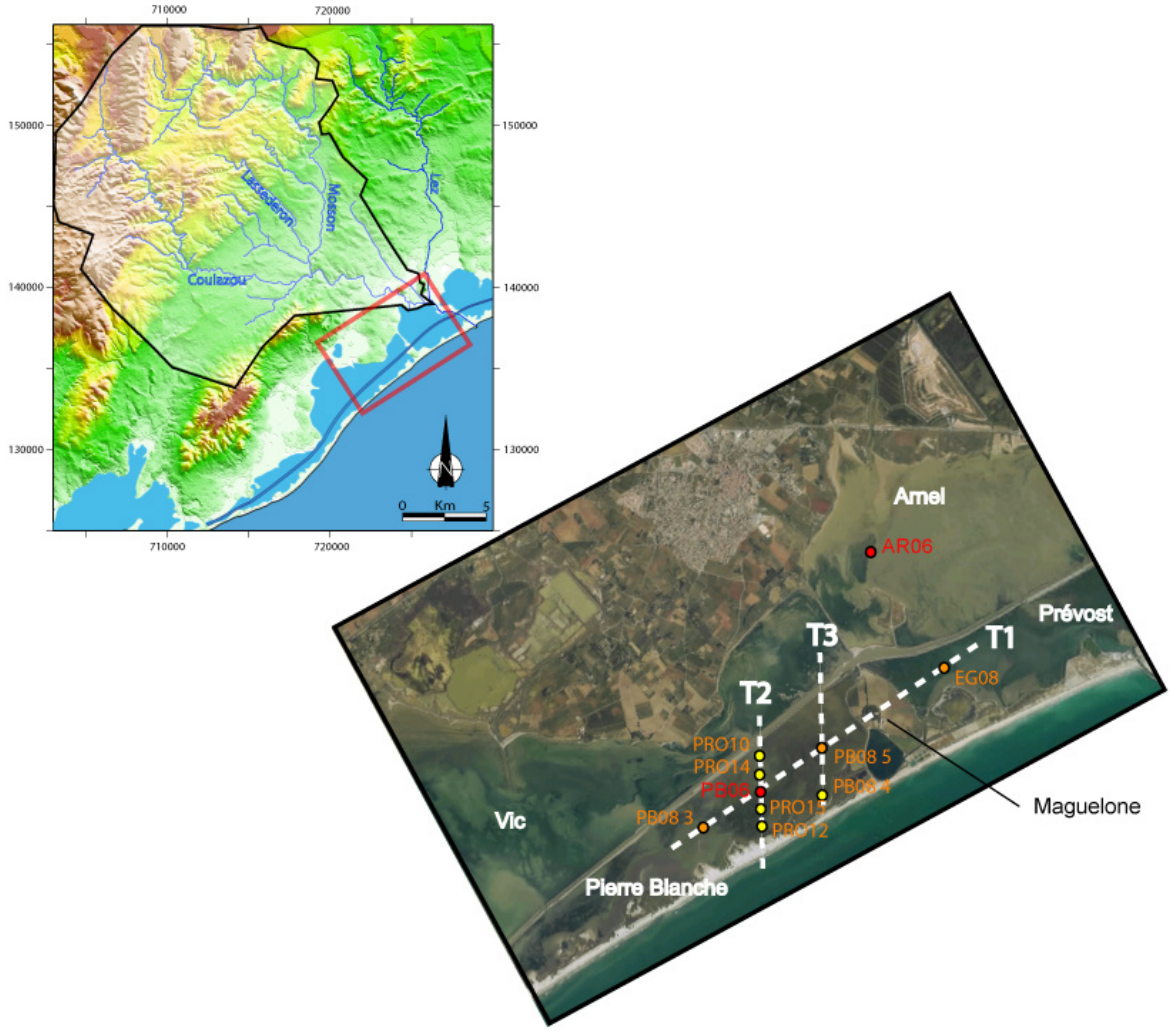

Figure 2.9 : Système lagunaire palavasien où ont été réalisées 10 carottes sédimentaires.

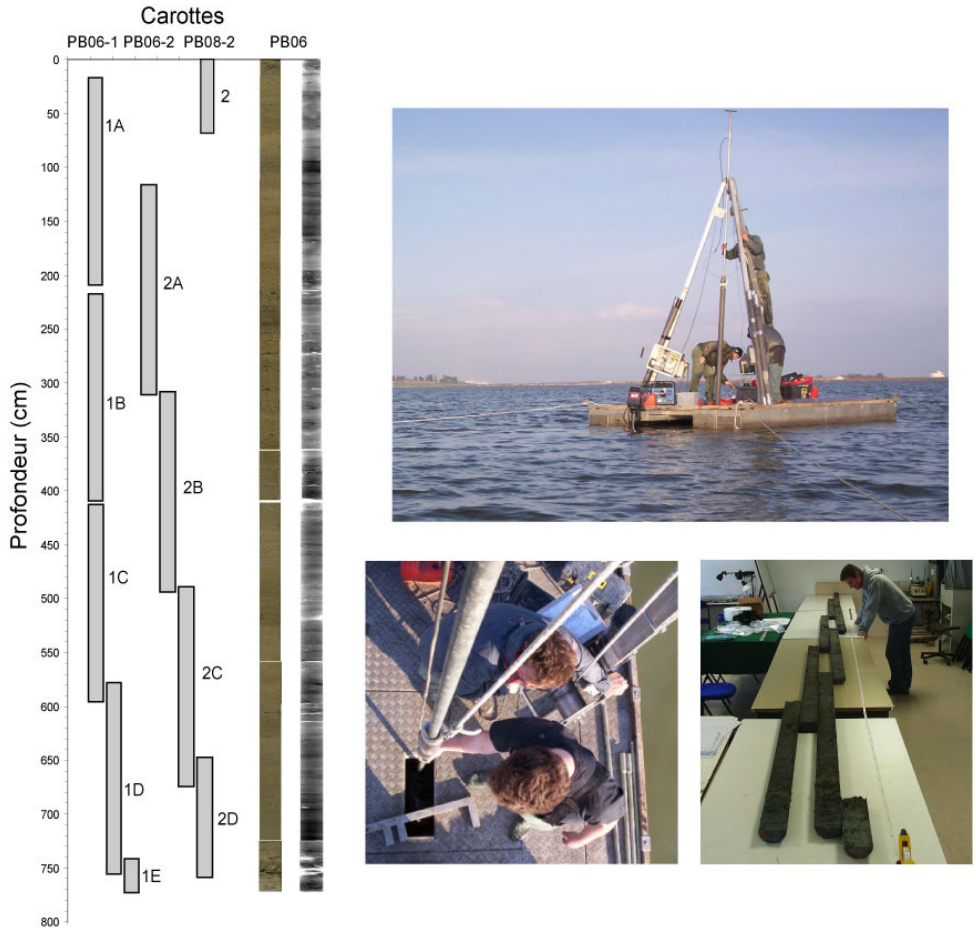

Figure 2.10 : A gauche : Recouvrement et position des carottes utilisées pour obtenir une archive sédimentaire de 7,7 m appelé PB06. A droite : photos de l'échantillonnage.

3. Identification des Paléotempêtes

3.1 Caractérisation d'un cône de tempêtes

Dans le chapitre précédent nous avons vu l'intérêt de caractériser des cônes de tempête pour l'enregistrement des tempêtes du passé. Dans cette partie nous nous intéresserons à l'identification de ces objets par différentes méthodes (sismique, carottage) et à travers divers indicateurs (granulométrie, malacofaune, géochimie, minéraux argileux).

3.1.1 Sismique

Les données de sismique présentées ici ont été acquises au cours d'une campagne de prospection en mai 2009 dans la lagune de Pierre Blanche. L'appareillage utilisé lors de cette campagne est un INNOMAR SES-2000 Standard (plate-forme GLADYS) embarqué sur un zodiac (Université de Perpignan). Cet appareil de prospection sismique acquiert à très haute résolution (5-10 cm de discrimination réelle verticale) et est particulièrement bien adapté aux zones de faible bathymétrie (Raynal, 2008). Durant cette campagne une soixantaine de lignes sismiques a été acquise, avec une forte densité de profils à proximité d'un cône de tempête actif (*Figure 3.1*). La vitesse de 1500 $m.s^{-1}$ a été utilisée pour convertir la vitesse sismique en profondeur. Le but de cette prospection n'est pas de caractériser les différentes unités présentes dans la lagune (thèse Raynal, 2008) mais de mettre en évidence les structures pouvant être associées à l'activité des tempêtes.

Les profils présentés dans la *Figure 3.1* montrent deux faciès sismiques distincts précédemment identifiés dans les remplissages lagunaires (Raynal *et al.*, 2009). Le premier faciès (partie supérieure des profils) est caractérisé par des réflecteurs parallèles sub-horizontaux de grande amplitude, qui correspondent à des dépôts de décantation liés à un environnement de faible énergie (Tessier *et al.*, 2000, Certain *et al.*, 2004, Raynal *et al.*, 2009). Le deuxième faciès (partie inférieure des profils) présente une structure chaotique indiquant la présence de gaz piégés dans le sédiment. Ces gaz sont liés à la dégradation de la matière organique accumulée dans ce type de dépôts lagunaires (Garcia-Gil *et al.*, 2002; Bertin et Chaumillon, 2005). Le gaz perturbe le signal sismique en profondeur et limite ainsi l'interprétation sismique aux premiers 1.5 mètres de sédiment.

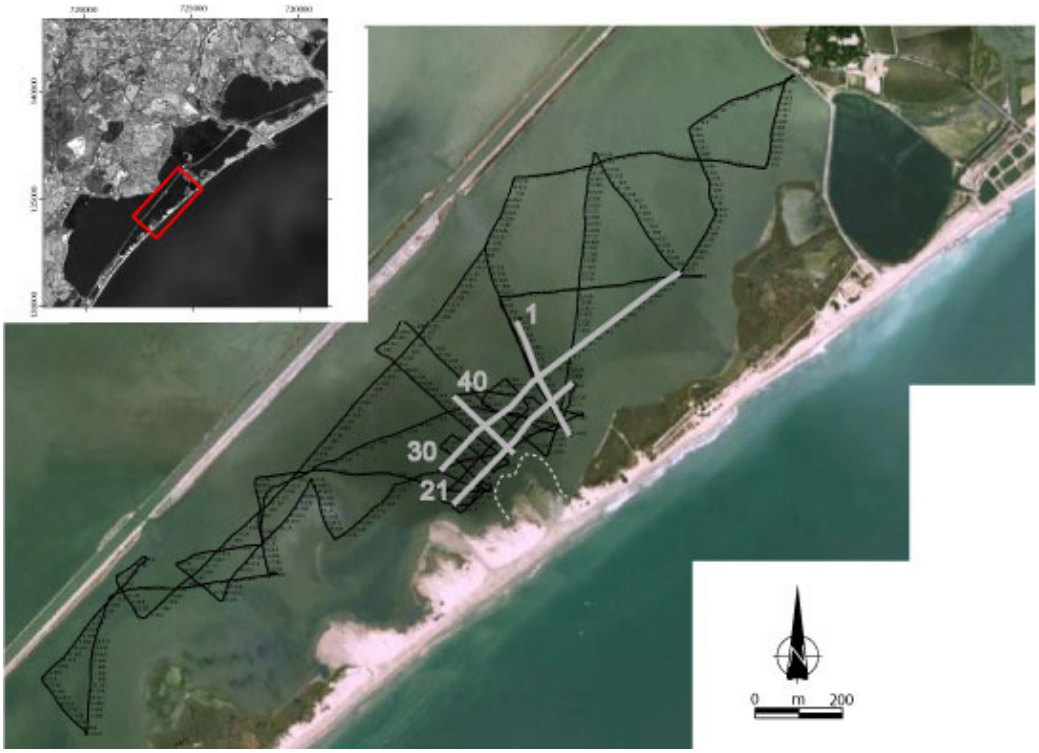

Figure 3.1 : Plan de positionnement avec la localisation des profils sismiques acquis dans la lagune de Pierre Blanche. Les traits gris localisent les profils représentés dans la Figure 3.2, deux le long de la côte (P30 et P21) et deux perpendiculaires à la côte (P1 et P40). Le trait en pointillé représente l'extension actuelle du cône de tempête.

L'analyse détaillée de ces profils permet de mettre en évidence au sein des dépôts lagunaires des réflecteurs plus marqués que d'autres et qui possèdent un léger pendage (*Figure 3.2*). En effet, dans les profils perpendiculaires à la côte, les réflecteurs soulignés en rouge présentent un pendage vers le Nord. Alors que dans les profils longeant la côte, ces mêmes réflecteurs décrivent une forme en dôme possédant une inclinaison à la fois vers le SW et le NE. Cette configuration vue en trois dimensions laisse deviner une forme de lobe (*Figure 3.3*). On note également un raccord tangentiel entre ce réflecteur et celui situé en dessous, tandis que les réflecteurs localisés au dessus décrivent des géométries en onlap (P30, *Figure 3.2*). Une autre observation est la taille de cette structure, bien plus importante dans le profil P21 localisé au plus près de la barrière sableuse que dans le profil P30 situé une centaine de mètre plus loin dans la lagune. De plus, la limite vers le cordon littoral de cet objet (P40, *Figure 3.2*) montre une diminution de la profondeur des réflecteurs suggérant une connexion avec le cordon sableux. Nous pouvons également définir un autre réflecteur plus récent (en jaune), et possédant les mêmes caractéristiques.

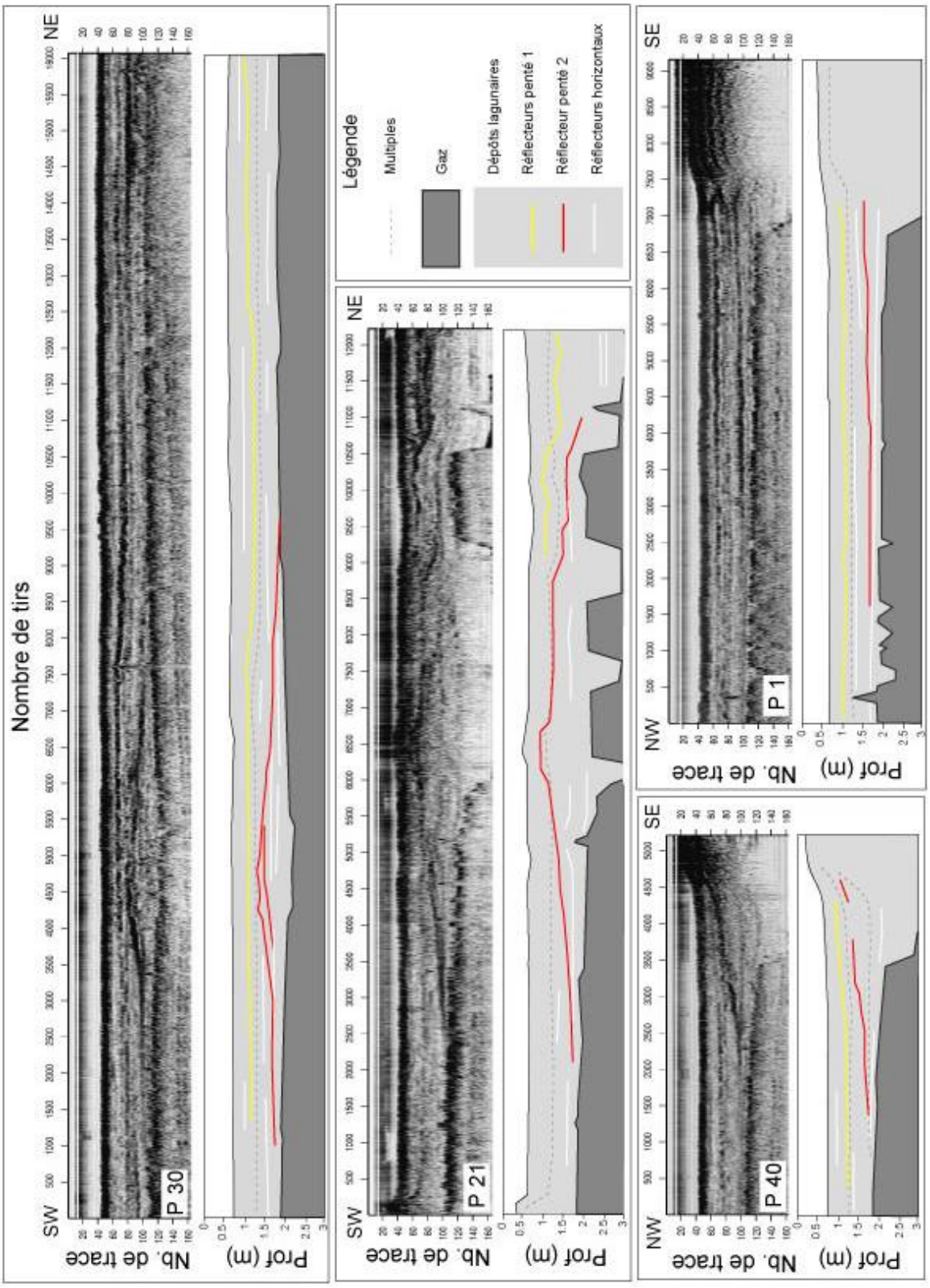

Figure 3.2 : Profils sismiques interprétés acquis dans la lagune de Pierre Blanche. Les profils P30, P21 et P40, P1 sont respectivement parallèles et perpendiculaires à la côte (Figure 3.1).

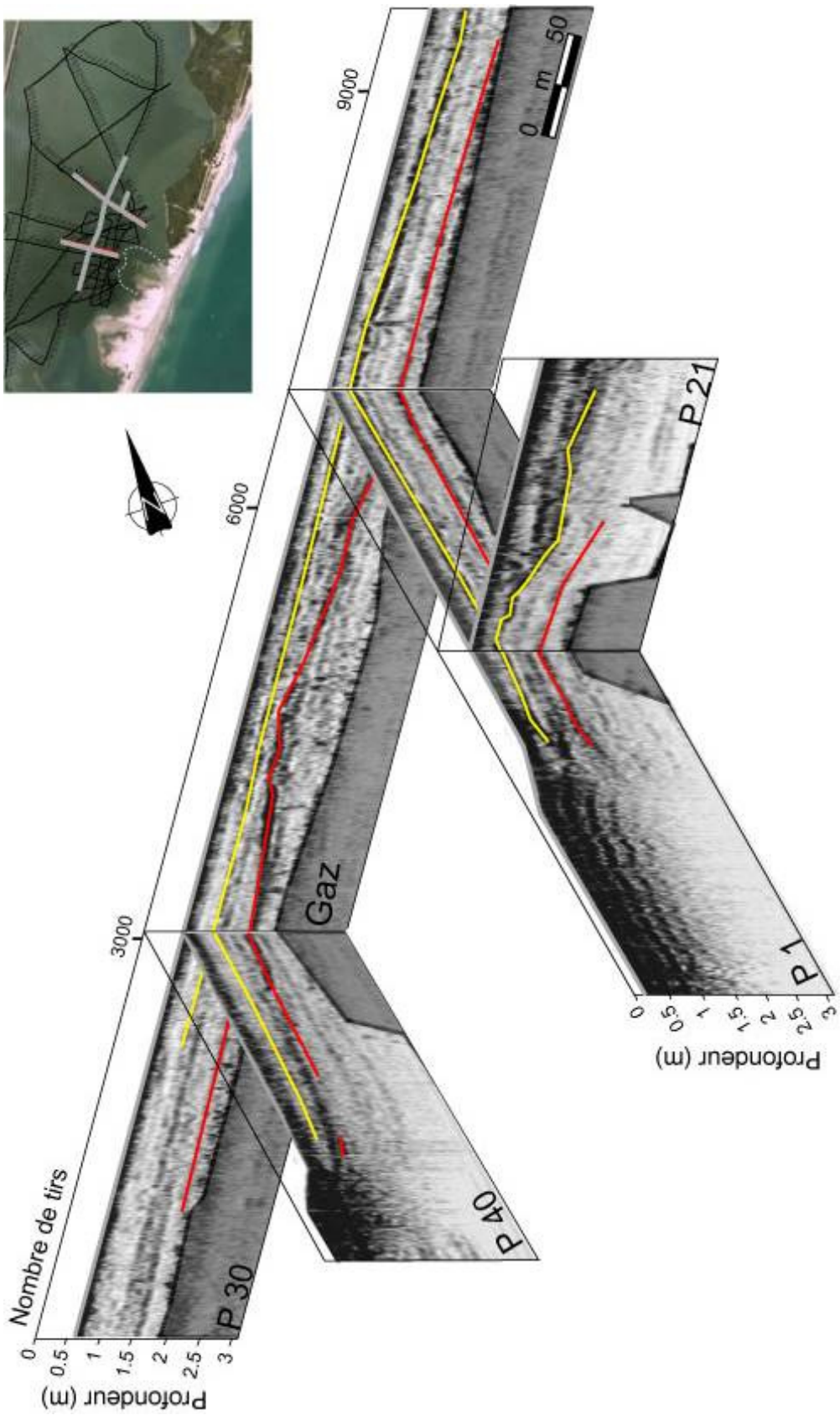

Figure 3.3 : Représentation en 3 dimensions des profils sismiques interprétés (P30, P21, P40 et P1) mettant en évidence des structures de cône de tempêtes au sein des dépôts lagunaires.

Ces observations permettent de mettre en évidence deux structures sédimentaires en forme de lobe s'approfondissant et diminuant de taille lorsque nous nous éloignons du cordon littoral, au dessus de ces structures nous retrouvons des niveaux horizontaux. Nous interprétons donc ces objets comme étant des cônes de tempêtes au sein d'une sédimentation lagunaire, formés à la suite du dépôt de matériel sableux provenant du cordon littoral lors d'un événement de forte houle (Switzer *et al.*, 2006).

D'autre part, les raccords tangentiels à la base de cette structure sont latéralement parallèles aux réflecteurs sous-jacents (*Figure 3.2*), ce qui suggère que ces derniers n'ont pas (ou peu) été remaniés lors du dépôt de lobes de tempêtes. Il en résulte que l'érosion par les cônes de tempête est vraisemblablement minime à l'échelle de la lagune. De plus, l'extension latérale (depuis le cordon littoral) de ces structures étant supérieure à 400 m (*Figure 3.2 et Figure 3.3*), cela nous permet de supposer que ces niveaux sont enregistrés dans une grande partie de la lagune.

3.1.2 Granulométrie

Dans le cadre du Master 1 de Mickael Barbier (2007), une étude granulométrique a été menée sur le cordon littoral et sur un cône de tempête. Un cône de tempête, correspond donc à l'expansion d'un corps sableux en domaine lagunaire. Nous avons prélevé des échantillons de surface selon trois transects de 90 m, dans la lagune (depuis le cône de tempête, CT1, CT2, CT3), et un transect de 30 m côté mer (depuis la plage, M1). Les analyses sont effectuées à l'aide d'un granulomètre Beckman Coulter© (LS 13 320), la méthode est décrite dans l'Article 1 (section 3.2.). Une méthode simple, reposant sur le calcul de l'écart type de chaque fraction granulométrique, permet d'identifier les populations granulométriques présentant les plus importantes variations (Boulay *et al.*, 2003). Cette méthode appliquée à l'ensemble des quatre transects met en évidence trois classes granulométriques possédant un fort écart type (*Figure 3.4*).

La plus fine (5 - 40 µm) correspond à des sédiments argilo-silteux tandis que la population de taille intermédiaire (150 - 400 µm) est définie par des sables moyens à grossiers et enfin la plus grossière (650 – 850 µm) correspond, probablement, à des débris coquillés associés, ou non, à des graviers. Les profils granulométriques, réalisés dans les transects en lagune, reportés dans la *Figure 3.5*, présentent une forte variabilité des deux populations les plus fines. Tandis que le transect en mer présente peu de variabilité et présente uniquement les

fractions les plus grossières. Nous notons également que la population sableuse est bien triée ; nous pouvons ainsi suivre son évolution en lagune, avec sa disparition progressive au détriment de la fraction plus fine correspondant au sédiment lagunaire. Ce sable, ayant la même distribution que ceux définis en Camargue (à la fraction coquillière près), provient donc des apports sédimentaires du Rhône transportés par la dérive la dérive littorale.

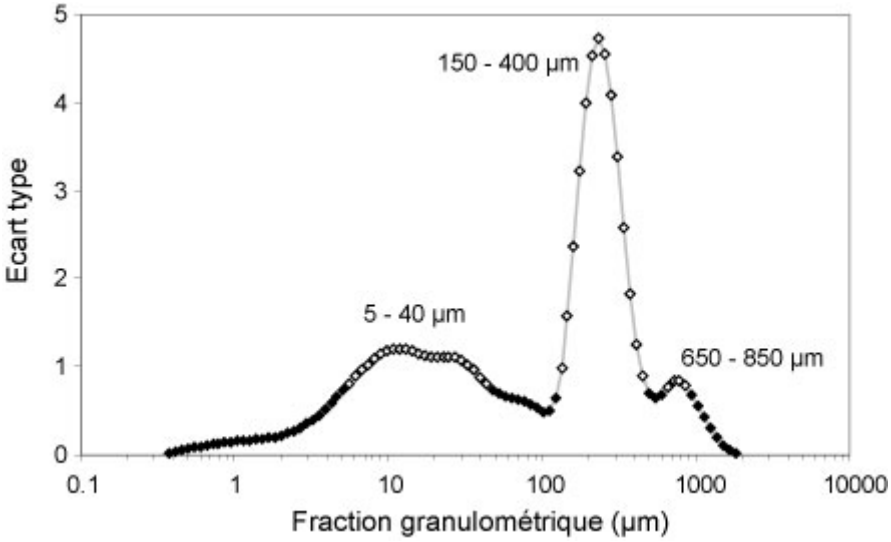

Figure 3.4 : Ecart type en fonction des différentes fractions granulométriques à partir des données des quatre transects. Les losanges blancs représentent les classes granulométriques présentant la plus grande variabilité.

Dans le milieu lagunaire, la diminution de la fraction sableuse traduit la transition entre le cône de tempête et la sédimentation par décantation typique de cet environnement de dépôts. Le profil général reste cependant propre aux trois transects, avec une extension latérale du corps sableux variant selon les différents tracés. Nous pouvons remarquer que cette population granulométrique, apparaît dès 70m le long de CT3 contre 40m et 50m respectivement pour CT1 et CT2 (*Figure 3.5*). Ceci met en évidence une morphologie dissymétrique du cône de tempête.

En résumé, un cône de tempête s'identifie par un passage rapide d'un matériel sableux à une sédimentation lagunaire fine avec cependant une zone de mélange entre ces deux populations jusqu'à disparition de la fraction la plus fine. Une tempête, même de faible intensité, est alors identifiable grâce à la détermination granulométrique du sédiment déposé.

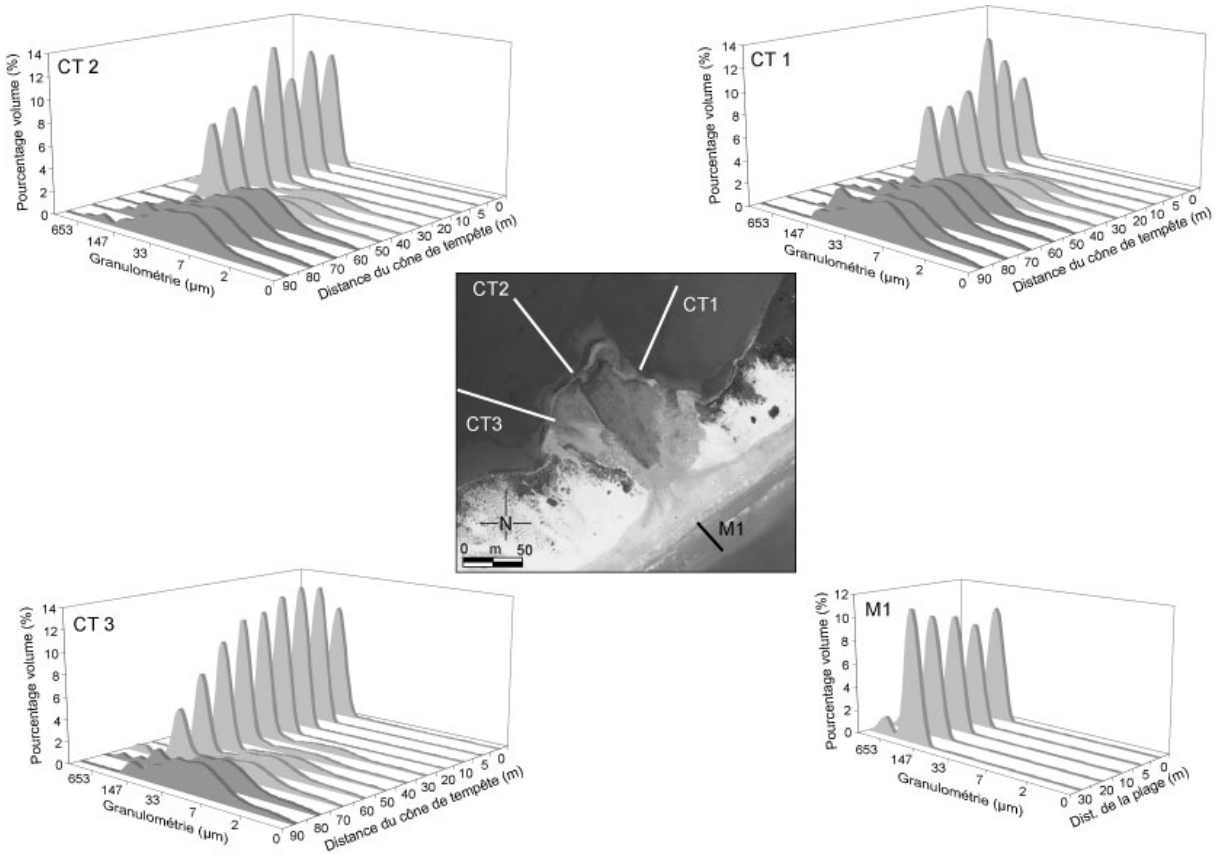

Figure 3.5 : Evolution de la granulométrie d'un cône de tempête selon, 3 transects en lagune de 90 m (CT1, CT2, CT3) et 1 en mer de 30 m (M1). La couleur gris clair définit des profils dominés par les sables alors que ceux dominés par les sédiments plus fins sont en gris foncé (modifié d'après le rapport de M. Barbier, 2007).

3.1.3 Malacofaune

Dans le cadre du Master 2 de Stéphanie Bordelais (2005) et du Master de Mickael Barbier (2007), une étude fine sur la caractérisation faunistique (malacofaune principalement) a été menée sur les lagunes et le cordon littoral. La lagune est le siège d'une intense activité biologique, cent fois plus productive que la mer toute proche. Malgré tout, les lagunes sont beaucoup moins diversifiées en nombre d'espèces que la mer. L'effet de compétition est amoindri, ce qui concourt à la prolifération de certaines de ces espèces. La malacofaune est un très bon indicateur de l'état de confinement des lagunes. En effet, les onzes principales espèces de mollusques que nous avons pu rencontrer dans les lagunes palavasiennes vivent dans des différentes gammes de salinité, de température et d'oxygénation (*Tableau 3-1*).

Photos	Nom de l'espèce	Milieu de vie
	*Hydrobia acuta*	Gastéropode de milieu saumâtre et lagunaire, détritivore, de 2 à 3 mm de long et supportant des conditions anoxiques et de grandes variations de température.
	*Bittium reticulatum* *Cerithium vulgatum*	Gastéropodes marins pouvant atteindre quelques centimètres de long et vivant dans des eaux peu profondes à substrat sableux.
	*Rissoa ventricosa* *Ovatella myosotis*	Gastéropodes marins, de 5mm à 1cm de long vivant dans des substrats sableux et communs dans les herbiers à posidonies.
	*Cerastoderma glaucum*	Bivalve abondant dans milieu lagunaire, fouisseur mesurant jusqu'à 4cm, supportant des variations de salinité et de température mais très sensible à l'anoxie, vit en eau peu profonde sur le sable ou la vase.
	*Abra ovata*	Bivalves lagunaires détritivores, pouvant mesurer jusqu'à 2 cm et vivant enfoui dans la vase jusqu'à 5cm. Ils sont tolérants aux variations de température et de salinité mais sensibles à l'ensevelissement.
	*Loripes lucinalis* *Lucina*	Bivalves vivant dans des milieux sablo-vaseux ou lagunaires à forte influence marine.
	*Venerupis sp.* *Ruditapes sp.*	Bivalves lagunaires, vivant enfouis dans un milieu calme mais avec influence marine, se trouvent généralement près des graus.
	*Gibbula adansoni* *(Gibbule)*	Gastéropode essentiellement marin de taille inférieure à 1,5cm, commun sur les algues fixées au support rocheux et supportant de courtes périodes d'émersion.
	*Cyclope neritea*	Gastéropode lagunaire nécrophage, d'environ 1cm de long, aimant les eaux calmes à faible salinité et les substrats sableux. Souvent trouvé sur les bourrelets coquilliers des berges.
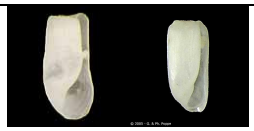	*Retusidae*	Petit gastéropode de quelques mm, surtout présent en milieu lagunaire ouvert.
	*Mytilaster minimus* *(Moule)*	Petit bivalve vivant sur des substrats durs (Rochers) en mer ou dans les lagunes.

Tableau 3-1 : Abaque de reconnaissance des principales espèces présentent dans les lagunes palavasiennes associées à leur milieu de vie, modifié d'après S. Bordelais, (2007).

Les espèces les plus typiques du milieu lagunaire sont *Hydrobia acuta*, *Cerastoderma glaucum* et *Abra ovata*, celles typiques du milieu marin sont *Bittium recticulatum*, *Gibbule adansoni* et *Rissoas ventricosa* tandis que certaines espèces comme *Loripes lucinalis* et *Ruditapes sp.* se rencontrent en lagune sous forte influence marine. Dans les transects en domaines lagunaires (*Figure 3.6*), nous notons la forte anti-corrélation entre les espèces typiques du milieu lagunaire et celles caractérisant les influences marines. Par exemple, nous pouvons compter plus de sept cent individus d'*Hydrobia acuta* en lagune alors qu'à proximité du cône de tempête cette espèce a quasiment disparu au détriment des individus marins comme *Bittium recticulatum*. Plus généralement, la faune lagunaire, en quantité abondante sur un substrat essentiellement argileux, diminue à mesure que la fraction sableuse augmente, sur laquelle se développent les espèces marines.

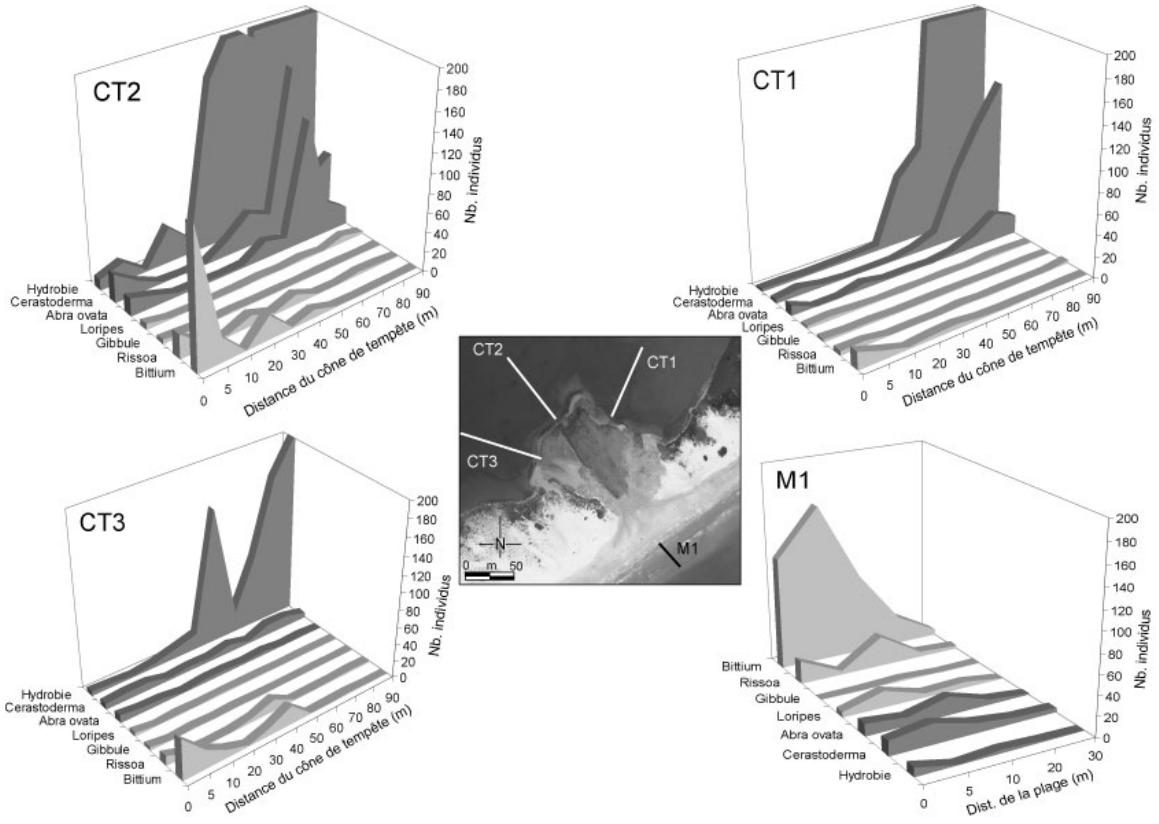

Figure 3.6 : Evolution à proximité d'un cône de tempête des différentes espèces de mollusques selon, 3 transects en lagune de 90 m (CT1, CT2, CT3) et 1 en mer de 30 m (M1). Les espèces sont classées selon leur milieu de vie, environnement lagunaire en gris foncé (Hydrobia acuta, Cerastoderma glaucum, Abra ovata) ; environnement à dominance marine en gris clair (Loripies lucinalis, Gibbule adansoni, Rissoas ventricosa, Bittium recticulatum), modifié d'après M. Barbier, (2007).

Cependant, l'essentiel des coquilles marines rencontrées sur le cône de tempête sont des coquilles mortes et parfois cassées. De plus, la tendance des Bittium recticulatum le long du transect marin, montre qu'il s'agirait, non pas d'un milieu de vie pour cette espèce, mais plutôt d'un milieu de dépôt apporté par les courants et la houle, même si cette espèce se développe en eaux salées.

L'étude faunistique renforce les informations obtenues lors de l'étude granulométrique, traçant donc les périodes d'ouvertures de graus pouvant succéder à une tempête majeure. Cette étude montre également que la malacofaune est un très bon indicateur de l'état de confinement des lagunes.

3.2 Cône de tempêtes, granulométrie et malacofaune : Article 1: Marine Geology

Reconstruction of paleostorm events in a coastal lagoon (Hérault, South of France)

Sabatier Pierre[1], Dezileau Laurent[1], Condomines Michel[1], Briqueu Louis[1], Colin Christophe[2], Bouchette Fredéric[1], Le Duff Michel[3], and Blanchemanche Philippe[4]

[1]Université Montpellier 2, Geosciences Montpellier.
[2]Université Paris-Sud, Laboratoire des Interactions et de la Dynamique des Environnements de Surface, Orsay.
[3]Institut Universitaire Européen de la mer, Laboratoire des Sciences de l'Environnement Marin, Brest.
[4]Université Montpellier 3, Laboratoire d'Archéologie des Sociétés Méditerranéennes, Lattes.

Received 20 March 2007, Received in revised form 30 October 2007, Accepted 2 March 2008
Marine Geology 251 (2008) 224–232

Abstract

Finding records of past catastrophic storm events is essential to evaluate the long term climatic evolution in a given coastal area. This question has been addressed by the study of sediment cores sampled in a small coastal lagoon of the French Mediterranean coast (Pierre Blanche lagoon). Two cores were studied in detail and revealed the presence of three main storm events.

The sedimentation rates calculated using the CFCS ^{210}Pb model, in agreement with ^{137}Cs data, are 3 ± 0.4 and 4.2 ± 0.7 *mm.yr*$^{-1}$ near the border and in the center of the lagoon respectively. This suggests that the 0.6 m deep lagoon could be filled with sediments over the next 150 years. Our study shows that storm events can be characterised in sedimentary sequences identified by facies, grain size and faunal assemblages (lagoonal and marine species). Comparison of ^{210}Pb, ^{14}C chronology and historical accounts suggest that the three identified storm events took place in 1742, 1839 and 1893 A.D. (i.e. about one catastrophic event per century).

Keywords*:* Paleostorms; Lagoon; Mediterranean Sea; Grain size; Accumulation rates; ^{210}Pb

1 Introduction

Storms are one of the most alarming natural hazard due to the recent concentration of resources and population in coastal areas (Pielke et al. 2005; Turner et al., 2006). In view of the last winter storm events having affected the South of France like in 1982 with 46 m/s wind (category 2 in Saffir-Simpson scale), this storm caused the death of 15 people and economic losses estimated at 400 million euros. It is necessary to examine the past decadal- to millennial-scale variability of storm activity in order to determine the frequency of the most extreme events in relation to the climate evolution (Goldenberg et al. 2001; Webster et al, 2005). General circulation models have been used to investigate the variations of the cyclonic activity in the Mediterranean region. Anagnostopoulou et al. (2006) clearly show a decrease of the frequency and an increase of intensity of the severe cyclones for the future (2071-2100). On the opposite, Lionello et al. (2002) do not show a large change in the regime of the cyclone in the same region in relation to the doubling of the CO2 atmospheric content. Both models, based on meteorological data, do not give the same conclusion. This is probably due to a calibration problem because of a lack of instrumental long time series.

In North-Western part of the Mediterranean Sea instrumental records are only available since the last twenty years for surge and waves (wave buoy in Sète) and fifty years for wind speed and direction (meteorological station), we used sediment cores to record the past washover events. Recent studies of some lagoons worldwide have shown that this environment could be a good area to record past climate and environmental changes, like flood and storm events (Liu and Fearn, 1993; Goff et al., 2000; Donnelly et al., 2001; Scott et al., 2003; Andrade et al., 2004; Donnelly, 2005 Donnelly and Woodruff, 2007). But, despite the importance of this subject, this type of study is still scarce.

The Languedoc-Roussillon shoreline is characterized by many coastal wetlands that resulted from the interaction between a process of shore line regularization by migrations of littoral barriers and a slow filling of these areas by the rivers (Certain et al., 2004). Coastal wetlands of North-western of the Mediterranean Sea are mainly characterised by sedimentary system with a fairly high accumulation rate (Monna et al. 1995; Schmidt et al. 2007). This study focused on the wetland complex of the Aigues-Mortes gulf (central part of the Golfe du Lion), more particularly on the Pierre Blanche lagoon (about 10 km South of the city of Montpellier) to identify and characterize the record of environmental changes due to these winter storm (Dezileau et al., 2005). To understand the sediment dynamics, we considered the main sediment sources, i.e. the riverine particulate input, the marine sediment input during storm events, and the organic production resulting from biological activity inside the lagoon. In order to trace the origin of detritic materials, we followed a multi-proxy approach associating sedimentological, granulometric and faunistic data. On the other hand, a chronology needed to be established. Usually, on centennial timescales, the sedimentation rate is calculated through ^{210}Pb radiochronology (Krishnaswami et al., 1971; Noller, 2000). In this study, to date recent paleostorm events, we have compared historical data, from communal archives, and radiochronological data obtained from both ^{210}Pb models (Goldberg, 1963; Krishnaswami et al., 1971; Pennington et al., 1976) and ^{137}Cs activity-depth distrubutions (Robbins and Edgington, 1975).

2 Study area

Pierre Blanche is an elongated lagoon (*Figure 3.7*), 267 ha large and 60 cm water deep. Its northern part is limited by the Rhône-Sète navigation channel (construction started in 1666). The south-east boundary is a 5 km long and ~200 m wide sandy barrier (*Figure 3.8*a.). Even if there is no direct connection with the sea, in some places the barrier is less than 60 m wide

and 3 m high above the mean sea level. This implies a strong marine influence during storm events, as evidenced by the traces of ancient inlets. Languedoc displays a classical microtidal littoral with a maximal tide excursion lower than 50 cm.

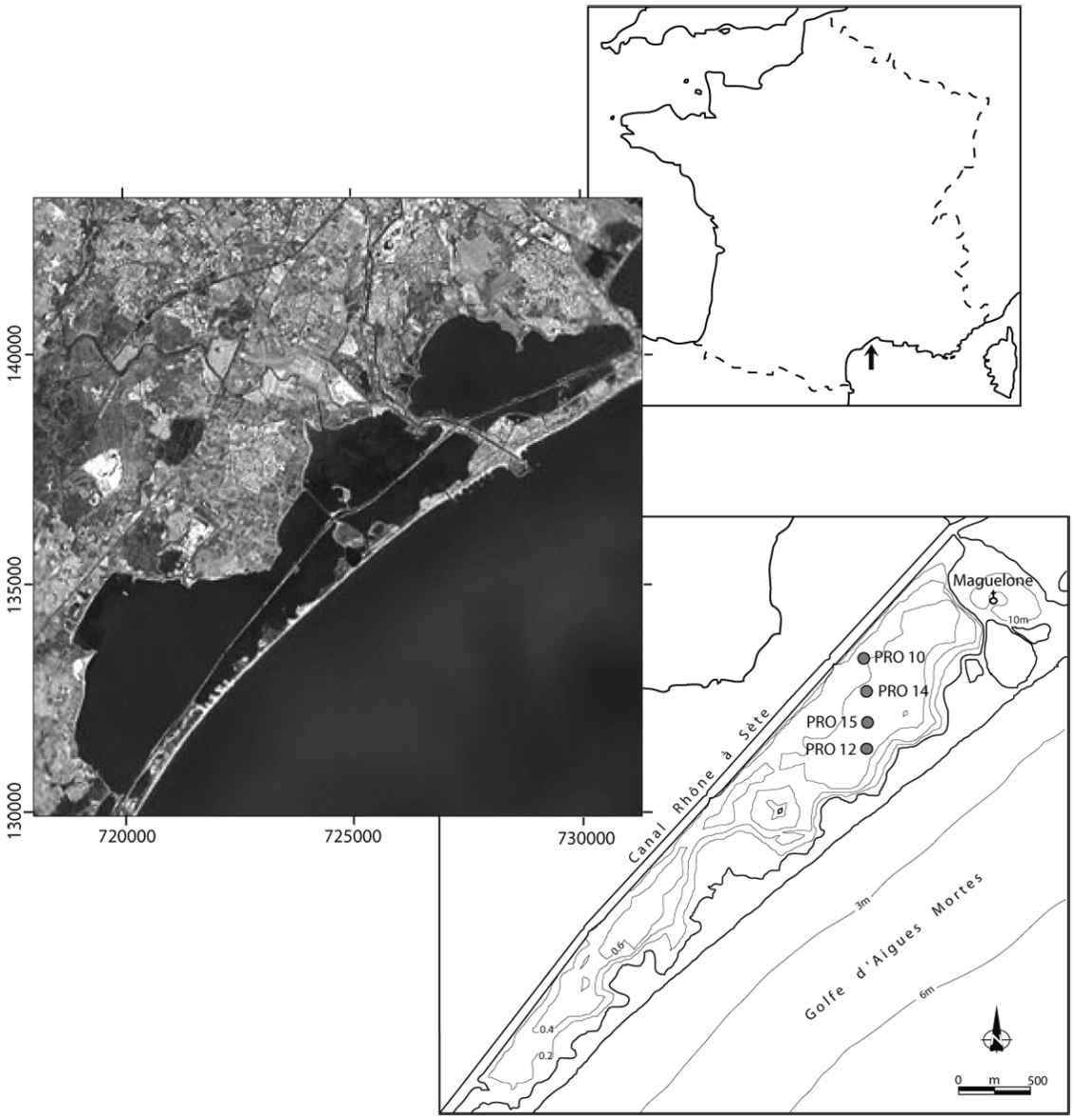

Figure 3.7 : Map of Pierre Blanche lagoon with localisation of the four short cores along a N-S transect (PRO 10, PRO 14, PRO 12 and PRO 15).

In the Western part of Gulf of Aigues-Mortes, North Western wind (Tramontane) blows 60% of the days involved with stronger winds than 5 m/s. Mean velocities recorded since the sixteen are about 10m/s. Maximal velocities exceed 44 m/s. North Eastern wind (Mistral) occurs lesser (20%) and the mean and maximal velocities observed are slightly the same.

South Eastern to South Western winds are not so important (20%) and rarely exceeding 20 m/s. However some rare (1 to 5 events a year) strong winds can exceed this value. The strongest one ever recorded by instrumental stations at Sète was about 46 m/s during the storm of 6-8 November 1982 (category 2 in Saffir-Simpson scale). This value may be compared to that recorded during usual years like 2002 and 2003, when maximal South-Eastern winds recorded were 32 m/s and 25 m/s respectively (Bouchette et al., 2007). These strong winds occurred during winter storms and enhanced along the coastline the effect of the swell generated seaward. In the present day, the coastline is mostly impacted by such a combination of South-Eastern winds and winter swells. The coastal waves are strongly influenced by height period due to east to south-eastern winds. Usual wave period in the Gulf of Aigues-Mortes ranges from 3s and 7s. Wave directions are parted in three main types of climate. South Eastern waves correspond to 69% of the observed waves, Southern waves to 17% and South Western to 14%. The annual significant wave height (Hs) and period (Tm), measured at Sète station under 32 m water depth (10 km far from the studied zone) are fair weather waves during 88% of the year ($Hs = 0.84m$; $Tm = 4.2s$, Guizien K. submitted).

However, this fair weather wave climate is occasionally disturbed by East to South Eastern storms, like that occurred in 1982. The annual proportion of waves higher than 4 m was around 1% and the return period of a 6 m high wave was every 10 years (Guizien K. submitted). However, this wave buoy installed since 1988 does not allow to get back in time far enough to evaluate the decennial to centennial wave climate.

On October 18-19 2006, a storm with 7 m high waves occurred and resulted in the opening of an ephemeral inlet (*Figure 3.8c.),* where an inlet had almost been opened during a previous storm (*Figure 3.8b.*). During this event shoreward flow transported material (sandy sediment and small shells) to the lagoon through the inlet (*Figure 3.8c.*). Two days after, the water flow was reversed and the lagoon was drained, due to the sea set down. Two weeks later, the inlet was closed and the breach was covered up again with sand and pebbles (*Figure 3.8d.*). Aerial photographs analysis demonstrates that influence of this storm on lagoonal sedimentation was almost negligible, except maybe in the direct vicinity of the inlet, where a small washover fan containing some marine shells (small *Bittium reticulatum* and *Rissoa ventricosa* transported by flow) was created. In principle, if cores were collected in more distal area of the lagoon, far enough from this inlet (a few hundred meters), likely contain sedimentological evidence of stronger storms (with low return period), powerful enough to affect the whole lagoonal system.

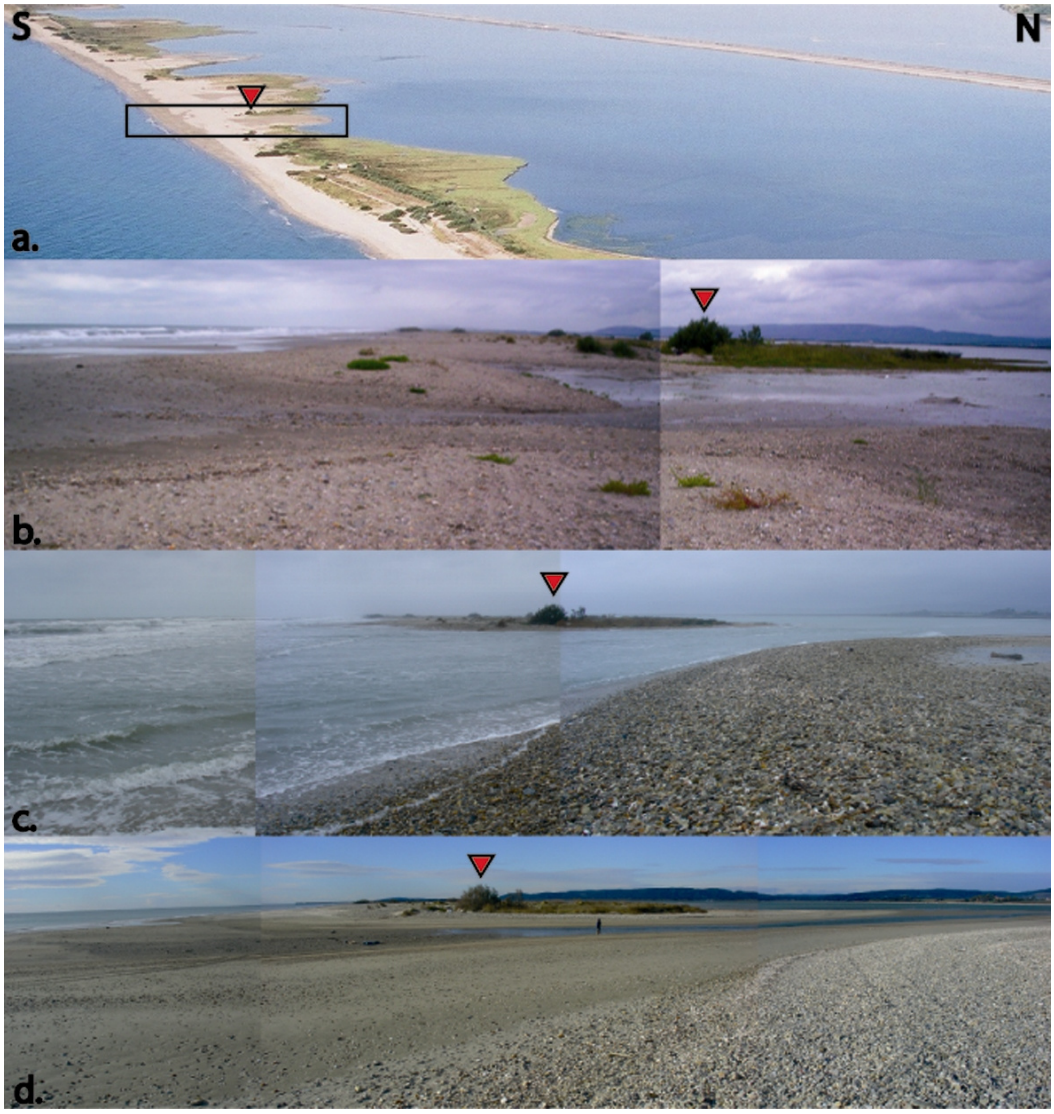

Figure 3.8 : Pictures of a coastal line where an inlet was created, during the 18-19 October 2006 storm. (a) is an air photography taken before the storm where we can see the width of the barrier appears, (b) picture taken in 2005 after a small event which weakened the barrier. (c) shows the inlet created at the same place by the 18-19 October 2006 storm with a strong landward tidal flow. (d) picture taken ten days after this event, where the inlet was covered up again with sand and pebbles. The red triangle shows a landmark present on all photographies.

3 Sampling and analytical methods

Four short cores (< 1*m*) separated by about 200 m (*Figure 3.7*), were collected on a N-S transect in Pierre Blanche lagoon in September 2005 by manually inserting a PVC tube (inner

diameter of 8,5 cm) from a small vessel. Back to the laboratory, cores were X-radiographed (imagery department in ”Clinique du Millénaire”), sliced opened, photographed, logged and divided into 1 cm sections prior to analysis. The two northernmost cores (PRO 10 and PRO 14) were analysed every three centimeters for malacofauna. The two other cores (PRO 12 and PRO 15), closer to the barrier, were analysed in more detail (every centimetres) with the same methods. Their grain size distribution was also determined using a Malvern Mastersizer Hydro 2000G in the laboratory of Interactions and Dynamic of Surface Environment (IDES) at Orsay. In addition, geochemical data were obtained by gamma spectrometry for U, Th series nuclides and ^{137}Cs by Geosciences Montpellier (GM). To study macrofaunal organisms, samples were sieved at 1 mm and the number of individuals of all species were counted. Grain size distribution measurements were made on the less than 1 mm sediment fraction without decarbonatation. Bulk sediments were first suspended in deionized water and gently shaken to achieve desaggregation. After introduction of sediment into the fluid module of the granulometer, ultrasounds were used to avoid particles flocculation. In the laboratory, sediment samples were weighted, washed (three times) with deionised water and dried at 70°C, for four days. Later, samples for gamma spectrometry were crushed and transferred into small polystyrene cylindrical boxes of known volume. Radionuclide activities were calculated by comparison with the known activities of an in-house standard (volcanic rock) filling the same boxes (Condomines et al., 1995). Since ^{137}Cs is absent in the standard, its activity was calculated from the efficiency curve of the BEGe detector (CANBERRA BEGe 3825). As polystyrene boxes are not gas-tight, ^{222}Rn can be lost through the walls and thus ^{226}Ra activities were determined only from the 186 keV peak of ^{226}Ra (after correction of the interfering 185.7 keV peak of ^{235}U) and not from the peaks of the ^{222}Rn daughters (^{214}Pb, ^{214}Bi). In each sample, the ^{210}Pb (unsupported) excess activities were determined by subtracting the ^{226}Ra (supported) activity from the total ^{210}Pb activity. A self-absorption correction based on major element composition and sample density was systematically applied for all photopeaks. For low-energy gamma rays, such as the 46.5 keV of ^{210}Pb, this correction can be relatively large (around 6%).

Four shell samples were selected for ^{14}C age determinations. ^{14}C analyses were conducted at the Laboratoire de Mesure ^{14}C (LMC14) on ARTEMIS in CEA institute at Saclay (Atomic Energy Commission). ^{14}C ages were converted to calendar years using the Calib 5.0.2 calibration program (Hughen et al, 2004) at two standard deviations.

4 Results and interpretations

4.1 Identification of storm deposits

The lagoon is mostly filled by clay and silt with shell fragments alternating with layers of fine sandy material. This succession accounts for different transport and sedimentation processes: one is the transport of small sized particles carried in suspension then decanted; the other one correspond to coarser sand transport, carried either by wind or by water during a high energy event (e.g., a storm event). Cores PRO 12 and PRO 15 show significant grain size variations with some sand layers. These layers are characterized by few shell fragments. The colour of the sediment was rather dark, grading from olive grey to grey and black. Color also gives information on the amount of organic matter in the sediment and on anoxic conditions in the lagoon.

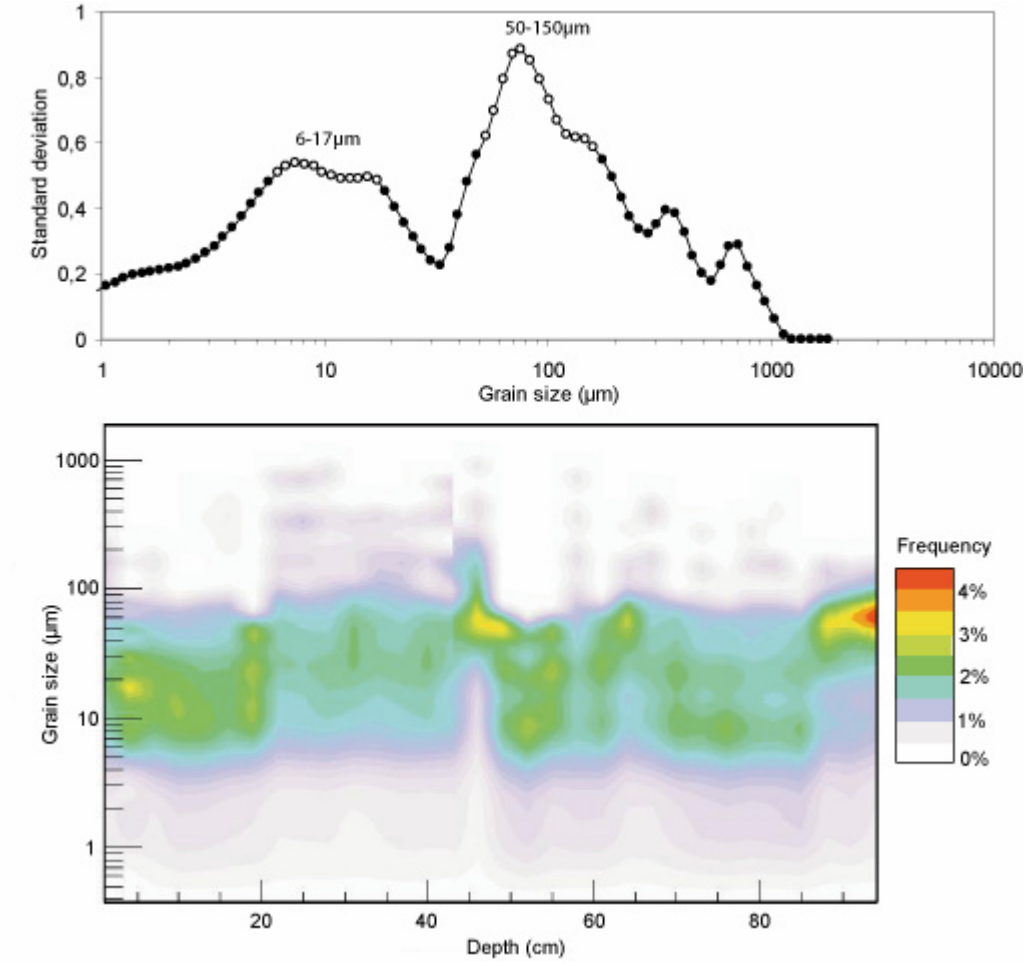

Figure 3.9 : (a) Standard deviation values vs. grain size class diagram of core PRO 15. Open circles are the most important granulometric populations, with one (thin silt) between 6-17 µm, and the other (thin sand) between 50-150 µm. (b) Contour plot of the grain size distribution of the core PRO 15.

Grain size data are generally displayed in a spectrum where the percentages of the populations are plotted *vs.* grain size fraction. They show a combination of different populations of particles. Nevertheless, few methods can discriminate the different populations. Boulay et al. (2003) used a simple method to identify the grain size intervals with the highest variability. Standard deviation quantifies the variability of different measures around the mean values. Using this method, we can determine the grain size classes having the most important variation through time. Standard deviation values *vs.* grain size classes of core PRO 15 are displayed on *Figure 3.9*. Two mean grain populations, presenting the highest variability, can be identified. One between 6-17*μm* (fine silt) and the other coarser, between 50-150 *μm* (fine sand). The evolution with depth of the 50-150 *μm* population in PRO 15 core shows several peaks (*Figure 3.9* and *Figure 3.10*).

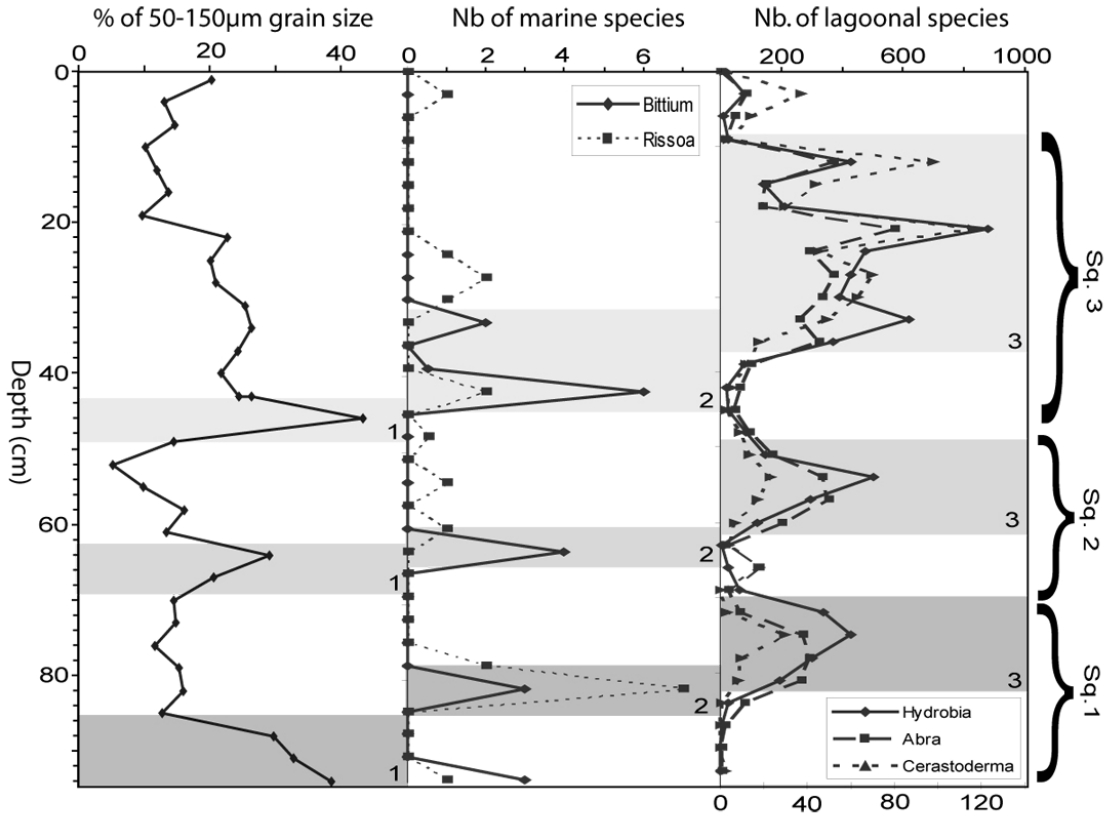

Figure 3.10 : Storm event sequences succession in core PRO 15. From left to right: 50-150 μm grain size population, marine species (Bittium reticulatum and Rissoa ventricosa), lagoonal species (Hydrobia acuta, Cerastoderma glaucum and Abra ovata). Bands shaded in gray were the three main sequences registered in PRO 15 sediment. The different greys correspond to different sequences. The numbers (1, 2 and 3) correspond to facies types described in Figure 3.11.

On the other hand Malacofauna is a good indicator of lagoon isolation state because it develops in different ranges of salinity, temperature and oxygenation. In fact, three species develop typically in a lagoon environment (*Hydrobia acuta, Cerastoderma glaucum* and *Abra ovata*) whereas two other are typical of a marine environment (*Bittium reticulatum* and *Rissoa ventricosa*). The presence of marine species within the lagoon indicates either their transport during a storm event or a change in environmental conditions. *Figure 3.10* shows three peaks of 50-150 *µm* sandy population at 45, 65 and 90 cm, followed, just a few centimeters above, by three peaks of marine species while the lagoonal fauna almost disappears. Data of *Figure 3.10* show a strong anti-correlation between species living in lagoon conditions (*Hydrobia acuta*) and that representative of the marine environment (*Bittium reticulatum*). The close association of sandy layers, marine species and the disappearance of lagoonal fauna suggests that the observed sequences can be interpreted by a succession of marine invasions of the lagoon during storm events, followed by closure of the barrier and return to typical lagoon conditions.

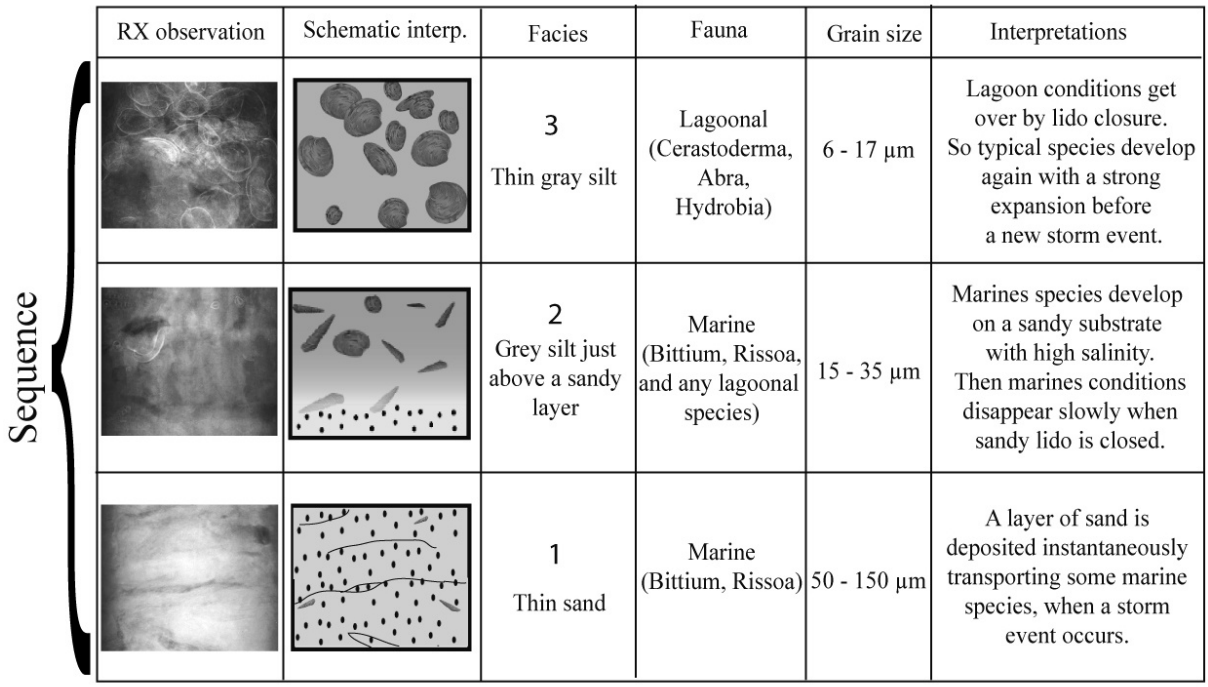

Figure 3.11 : Facies and characteristic sequences for storm layers in the lagoon environment.

Through the multi-proxy analysis of a core, based on grain size and fauna composition, it is possible to recognize typical facies whose succession identifies a storm event (*Figure 3.10* and *Figure 3.11*):

- type 1 facies shows fine sand with some marine species probably carried with this sand.

- type 2 facies, found just above the same fine sand layer. The grey silt contains typical marine fauna (*Bittium reticulatum* and *Rissoa ventricosa*), then grain size becomes finer upwards with the apparition of some lagoonal species.

- type 3 facies is made of fine grey silt with typical lagoonal fauna (*Hydrobia acuta, Cerastoderma glaucum* and *Abra ovata*).

Malacofauna contents were studied in all four cores. Three periods with very low abundances of the lagoonal species (*Hydrobia acuta*) in Pierre Blanche lagoon were observed (*Figure 3.12*). A clear link can be made between all four cores, with the exception of core PRO 10. These lateral correlations, along a 600 m transect, indicate a good preservation of these events in the whole study area and suggest higher accumulation rates in the central part of the lagoon. When a storm occurs, wind and wave energy breaks up the barrier and triggers a landward material transfer, from the barrier to the lagoon. Transported material is mainly sand with some marine fauna and almost instantaneously sinks to the bottom. If the inlet remains open for a sufficiently long time, then the salinity in the lagoon increases and marine species can develop on the sandy substrate to the detriment of lagoonal fauna. When the sandy barrier closes, the lagoon becomes isolated once again, hence environmental conditions change with consequent reappearance of lagoonal species at the expense of marine fauna for which environmental conditions are unfavourable. In all four sediment cores (*Figure 3.12*) we observed three sequences that probably correspond to three main storm events (*Figure 3.10*), with an impact on the whole of the lagoon.

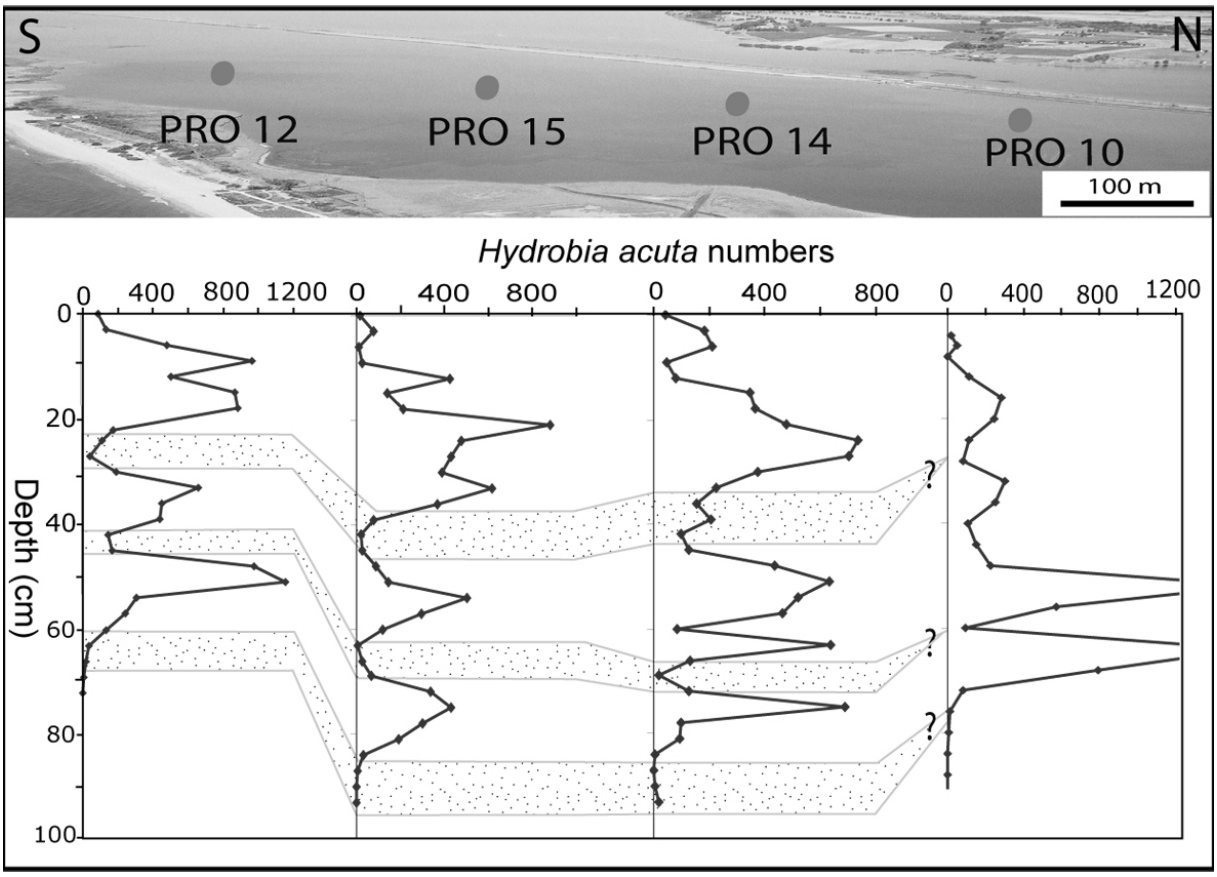

Figure 3.12 : Hydrobia acuta repartition in Pierre Blanche lagoon along an N-S transect. The three Hydrobia acuta minima, corresponding to marine inputs during storm events have been correlated between cores (dotted bands). The same layers are deeper in the center of the lagoon, with a maximum depth between PRO 15 and PRO 14 cores.

4.2 Accumulation rates and Age Model

The basic methodology of ^{210}Pb dating was established in a seminal paper by Goldberg (1963). ^{210}*Pb* precipitates from the atmosphere through ^{222}Rn decay and accumulates in surface soils, glaciers or lakes, lagoons, where successive layers of material are buried by later deposits. Many ^{210}*Pb* models were proposed, allowing to calculate sedimentation rates (Appleby and Oldfield, 1992; Noller, 2000). In the simplest model, the initial (^{210}Pbex), [(^{210}Pb)$_{ex}$ = (^{210}Pb) − (^{226}Ra)] is assumed constant and thus ^{210}*Pbex* at any time is given by the decay law [(^{210}Pb)$_{ex}$ = (^{210}Pb)$_{0,ex}$ exp−λ_{210}.t]. The CFCS model (Goldberg, 1963; Krishnaswami et al., 1971) supposes a constant ^{210}Pb flux and a constant sedimentation rate. Although the sedimentation rate in the lagoon is clearly variable due to the near-instantaneous

sedimentation of sandy storm deposits, the CFCS model can still be applied when typical lagoonal conditions prevail. It is the case of core PRO 12 and PRO 15 above depths of 23 cm and 37 cm respectively. In a logarithmic diagram, ^{210}Pbex should define a straight regression line whose slope allows to calculate an average sedimentation rate (*Figure 3.13*, values in *Tableau 3-2*). Using the average sedimentation rate W (mm.yr^{-1}), the age Tm of the sediment layer can be calculated, for each depth Zm (cm).

$$\ln\left(\left(^{210}Pb_{ex}^{m}\right)\right) = \ln\left(\left(^{210}Pb_{ex}^{0}\right)\right) - \left(\frac{\lambda_{210}}{W}\right) \times Z_m, \quad \text{with:} \quad T_m = \frac{W}{Z_m}$$

This simple model only gives an estimation of the average sedimentation rate and does not take into account possible variations of sediment accumulation rate and/or ^{210}Pb supply. It is thus impossible to precisely date a sedimentologic event. However, any major modification in the sedimentation rate should result in a change of slope in the logarithmic diagram. The post-depositional mixing, by biologic activity (bioturbation) can also affect ^{210}Pb data interpretation. This effect is difficult to estimate because there is no typical mixing surface layer with the same ^{210}*Pb* activity. This potential problem is currently being evaluated, by implantation of luminophores, in order to understand the effect of physical and biological mixing on the ^{210}Pb depth distribution (Gerino et al., 1998; François et al., 2002).

Figure 3.13 shows that the sedimentation rates vary from 3.0 ± 0.4 to 4.2 ± 0.7 *mm.y* $^{-1}$ between the border (PRO 12) and center (PRO 15) of the lagoon. These sedimentation rates are in agreement with those previously obtained for another lagoon (Thau) in the same area by Monna et al. (1995); Schmidt et al. (2007). Both radiochronological dating and faunistic correlation (*Figure 3.12*) indicate that the sedimentation rate is higher in the center of the lagoon. These rates are relatively high in this wetland area where water depth varies between 0.4 and 0.8 m. Extrapolating the present-day sedimentation rate would result in a filling of this lagoon in the next 150 years, without taking account neither the sea level rise nor the littoral antropic impact.

The most usual dating method based on ^{137}Cs data (Robbins and Edgington, 1975) assumes that the depth of the maximum ^{137}Cs activity in the sediment corresponds to the 1963 maximum atmospheric production. A ^{137}Cs peak is well identified in PRO 15 core at 19 cm deep and suggests an average accumulation rate of 4.4 *mm.y* $^{-1}$ similar to the value derived from ^{210}Pbex data. Differently, in core PRO 12 there is no real peak but rather an enlarged

maximum at around 12 cm depths which gives a sedimentation rate of 2.8 *mm.y* $^{-1}$, again in agreement with ^{210}Pbex data.

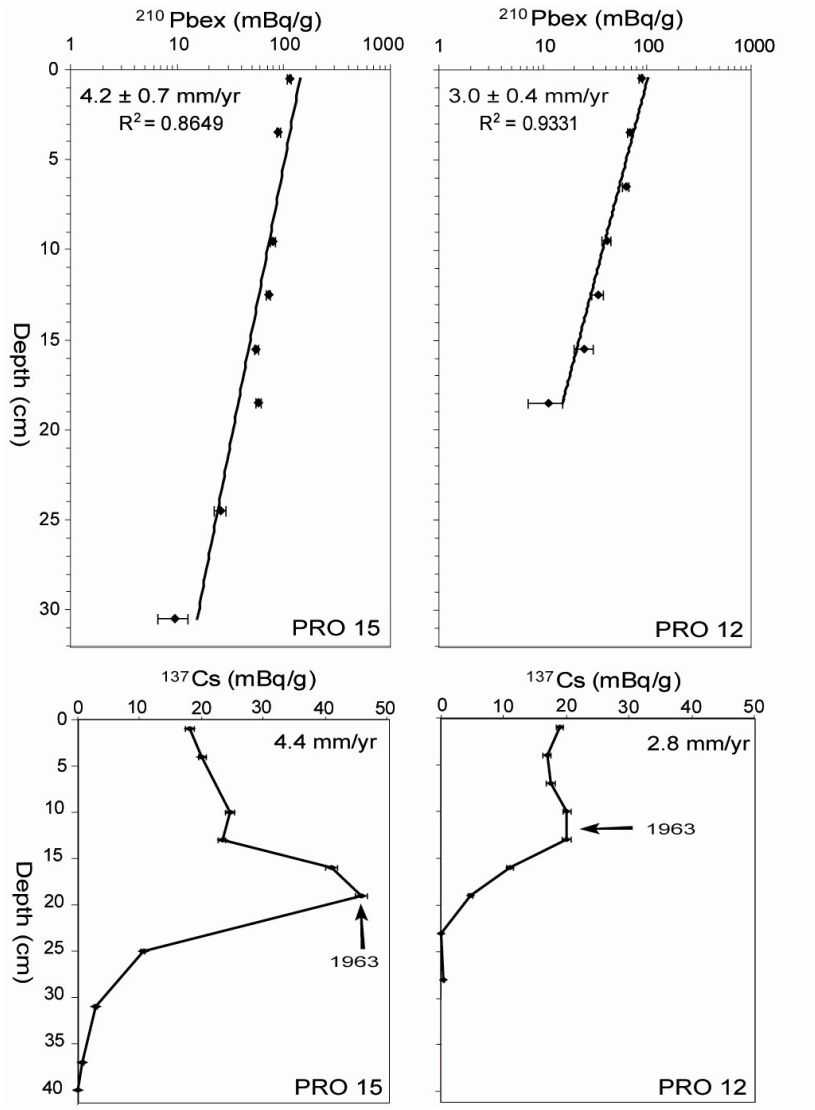

Figure 3.13 : ^{210}Pbex and ^{137}Cs activity-depth profiles in cores PRO 15 (left) and PRO 12 (right) from Pierre Blanche lagoon. ^{210}Pb excess disappears at around 25 cm for PRO 12 and 37 cm for PRO 15. The deepest ^{210}Pbex values were not considered to calculate the sedimentation rate, because of their large associated errors.

However ^{137}Cs is still present at depths of more than 30 cm, whereas this radionuclide has been shown to appear in this area in 1958, a date corresponding to the first high altitude atmospheric tests (Radakovitch et al., 1999). This paradox could be explained by the important mobility of Cs in sea water. Indeed, one of the Cs properties is its high mobility in

marine sediments, with a preferential downward diffusive transport in porewater (Charmasson et al., 1998; Radakovitch et al., 1999). In spite of this mobility, ^{137}Cs can be used to date sediment because the diffusive transport will result in the spreading of the Cs peak and not in its downward move. On both cores the ^{137}Cs activity depth distributions do not show the Chernobyl signal, it is probably due to the low-resolution analysis on these cores (every 3 centimetres) or to its too low concentration in surface soil on the small watershed.

Cores	Depth (cm)	^{210}Pb (mBq/g)	^{226}Ra (mBq/g)	^{210}Pb$_{ex}$ (mBq/g)	^{137}Cs (mBq/g)
PRO 15	0–1	138.6±4.2	25.4±3.9	113.2±5.8	18.1±0.8
	3–4	116.1±2.5	27.3±2.8	88.8±3.7	20.2±0.5
	9–10	100.8±2.8	21.6±3.1	79.3±4.2	24.6±0.8
	12–13	92.2±2.1	20.3±2.3	71.9±3.1	23.4±0.6
	15–16	79.2±1.9	23.7±2.3	55.6±3.0	41.0±0.9
	18–19	78.8±2.0	20.6±2.5	58.2±3.2	45.9±1.0
	24–25	42.7±1.8	17.4±2.8	25.3±3.4	10.5±0.4
	30–31	31.9±1.6	22.3±2.6	9.6±3.0	2.9±0.3
	36–37	25.4±1.7	22.6±3.1	2.8±3.6	0.8±0.2
	39–40	23.8±1.4	27.0±2.8	0	0
PRO 12	0–1	112.8±2.8	25.1±2.9	87.7±4.0	18.9±0.6
	3–4	93.5±2.6	24.2±2.9	69.3±3.9	16.8±0.6
	6–7	84.2±2.8	22.0±3.3	62.2±4.3	17.5±0.7
	9–10	65.5±2.5	24.8±3.1	40.8±4.0	20.1±0.7
	12–13	56.6±2.2	22.8±3.6	33.8±4.2	20.0±0.7
	15–16	48.0±3.0	22.9±4.3	25.1±5.2	11.0±0.6
	18–19	32.6±2.1	21.4±3.5	11.3±4.1	4.6±0.4
	22–23	25.9±1.0	23.9±1.5	1.9±1.8	0
	27–28	22.2±0.9	22.2±1.4	0	0

Tableau 3-2 : Activities of radionuclides in cores PRO 15 and PRO 12.

^{14}C data give a sedimentation rate of 3.15 *mm.y* $^{-1}$, this rate was in good agreement with ^{210}Pb and ^{137}Cs depth distributions. Reservoir age in lagoon environment of Mediterranean region is high, due to a strong continental Carbon contribution (Siani et al. 2000, Zoppi et al. 2001). In this study, we have estimated the reservoir age at around 950 ± 75 yrs (*Tableau 3-3*) by both extrapolating to the surface of sediment and by correlation with ^{210}Pb data (Sabatier et al. Accepted).

The agreement between average sedimentation rates derived from ^{210}Pb, ^{137}Cs and ^{14}C data suggests that the various disturbing processes like bioturbation (Cochran, 1985), grain size effects (Chanton et al., 1983) or instantaneous events (Smith and Walton, 1980; Arnaud et al., 2002) did not play a major role in the studied parts of the cores.

Depth (cm)	^{14}C (yr BP)	^{14}Ccal BP (2σ, Hughen et al. 2004)	^{14}Ccal BP (ΔR = 550 yr)
3–4	Post A.	Post A.	Post A.
20–21	1055±30	610±60	60±60
60–61	1095±30	660±65	110±65
83–84	1285±30	825±80	275±80

Tableau 3-3 : Radiocarbon ages from Pierre Blanche lagoon (core PRO 15).

5 Identification of paleostorms

In the last 400 years, the stronger storm occurred in south of France was in 1666, 1669, 1738, 1742, 1766, 1771, 1790, 1839, 1893, 1956 (historical account) and 1982, 1999 (MétéoFrance data). In communal account, storm events were mentioned because they make damage in the vicinity of the studied city. Sedimentological and paleoecological results described above allow us to identify the most powerful storm events as historical period (i.e. paleostorm) with the presence of sand layer (50-150μm) together with marine species (*Bittium reticulatum*) and the disappearance of lagoonal species (*Figure 3.14*).
Based on our age model the last three catastrophic storm events recorded in this cores-transect occurred in 1742 (with the inlet closing in 1761), 1839, and 1893. These dates were obtained by comparison between ^{210}Pb, ^{14}C data and historical accounts.

- The storm of December 4th, 1742, recorded in many city archives around the Aigues-Mortes gulf, is considered as the most catastrophic event. This storm, probably due to S to SE winds, submerged some local cultivated lands which had been obtained at the expense of old lagoonal parts. This event was not accompanied by coastal river floods. One of the main consequences was the creation of a large inlet, near Maguelone, which remained open until 1761.

- The 1839 tropical storm has for consequence the wreckage of a few ships, like a trading vessel (more than 20 meters long) off the Frontignan village (Serra, 2004). The violence of winds during this storm, associated with the shallow water in this area, explains this shipwreck.

- The most recent event recorded in the PRO 15 core could correspond to the storm of September 21, 1893 which affected the North of France and the Mediterranean region, causing devastations in the Sète area as certified by many engraving illustrations.

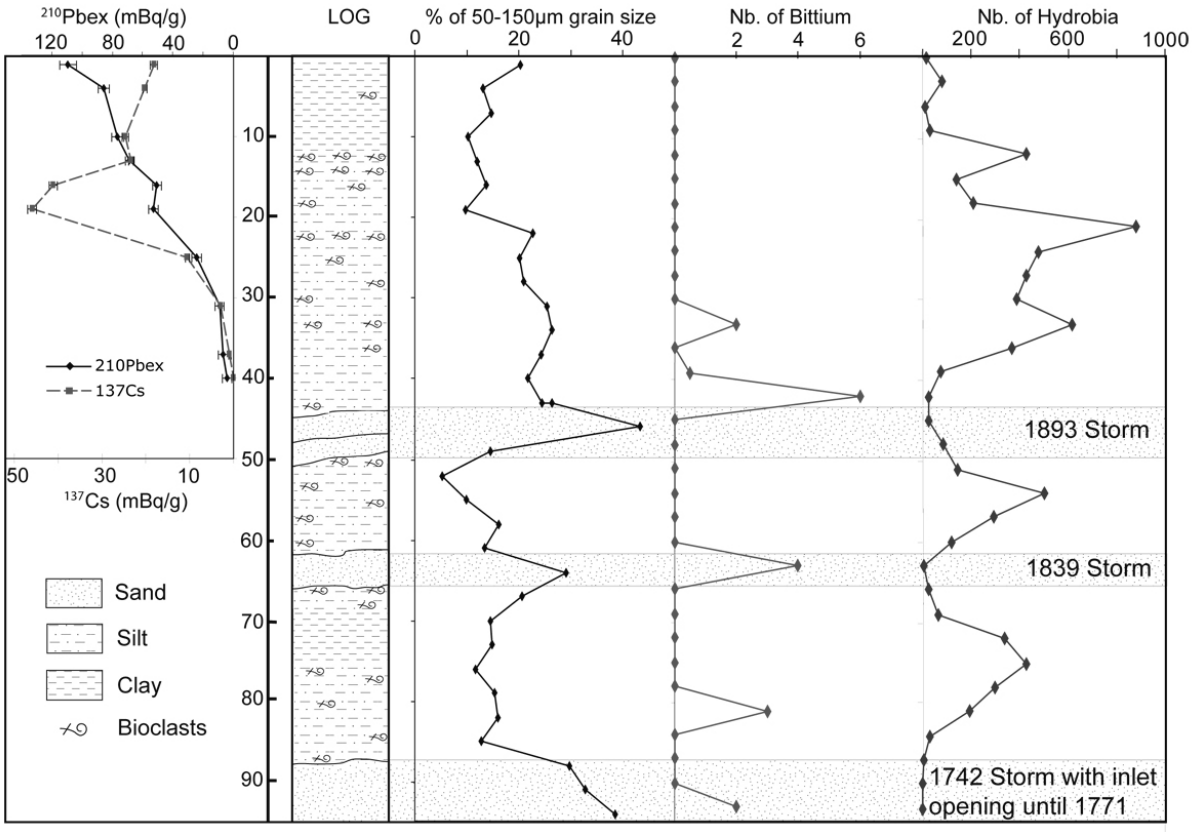

Figure 3.14 : Storm event characterization in core PRO 15. From left to right: 210Pbex and 137Cs activity-depth profiles, 14C date (grey band), sediment description, 50-150 µm grain size population, lagoonal species (Hydrobia acuta). Dotted Bands correspond to the main paleostorms events registered in historical accounts corresponding to different events described in Figure 3.10.

Soft-sediment deformation at the contact between overwash sand and underlying mud in all cores indicates that little sediment may have been removed by the storm deposit inside the lagoon. This was supported by the good agreement between ^{210}Pb extrapolation and ^{14}C data.
It should be noted that the most recent catastrophic event, the 1982 storm, was not registered in the studied sediment cores. One could argue that the storm events described above were of similar intensity as the 1982 event, and that they were recorded in the lagoon sediments because of a thinner barrier in the past centuries. However, examination of old geographical

maps shows that the location and width of the barrier have not changed significantly. It thus appears that the past storm events registered in our cores were stronger than the 1982 event. Although we have not studied a multi-transect cores, the record analysis of washover deposit from a backbarrier marsh provided evidence of three main storms in the past 300 years in Gulf of Aigue-Mortes. If this observation is confirmed, the frequency of such paleostorms, seems to be about one each century.

6 Conclusions

This study of Pierre Blanche lagoon demonstrates that an analysis associating sedimentology, granulometry and faunistic data allows to identify the strongest storms in the Mediterranean area. The record of such events on lagoonal sedimentation is characterized by typical successions (silt with typical lagoonal species, with intercalations of fine sand and marine species). Average sedimentation rates calculated by ^{210}*Pbex* CFCS model are high and vary from 3.0 ± 0.4 $mm.y^{-1}$ near the border to 4.2 ± 0.7 $mm.y^{-1}$ in the center of the lagoon, where water depth is between 0.4 and 0.8 m. We thus expect a complete filling of this lagoon in the next 150 years. Moreover, radiochronological dating (^{210}Pbex and ^{137}Cs) together with historical accounts allows to date the record of past main storms. Three distinct catastrophic events were identified in 1742, 1839 and 1893 over nearly 3 centuries. Therefore, from the presently available and limited data, the recurrence of historic events more powerful than that of 1982, is around one main storm per century. Paleoclimatic recording of Mediterranean storm thus appears clearly possible in lagoonal systems.

The methodology proposed can thereafter be applied over longer time scales, allowing a paleostorm record over the Late Holocene period. To this aim, two long cores have been sampled, in March 2006, in the same lagoon. These cores cross the whole Late Holocene lagoon sediment filling and will allow to identify catastrophic events for at least 6000 years.

Acknowledgements

This research has been undertaken in the framework of the ECLICA Project financed by INSU (ACIFNS ”Aléas et Changement Globaux”, L. Dezileau). The authors wish to thank IFREMER Palavas for allowing storing of the cores in their cold room. Doctor A. Bengana is thanked for making X-ray images with his team of imagery department in ”Clinique du Millénaire”. Thanks to Laboratoire de Mesure ^{14}C (LMC14) on ARTEMIS in CEA institute at

Saclay (Atomic Energy Commission) for the ^{14}C analyses. EID Méditerranée allowed use of their air photographs. S. Bordelais, M. Barbier and all other members of the ECLICA Project team are also thanked for their support and their constructive discussions during the course of this study.

3.3 Minéraux argileux et géochimie : Article 2: Sedimentary Geology

Paleostorm events revealed by clay minerals and geochemistry in a coastal lagoon: a study case of Pierre Blanche (NW Mediterranean Sea)

Sabatier, Pierre[1], Dezileau, Laurent[1], Briqueu, Louis[1], Colin, Christophe[2], Siani, Guiseppe[2]

1 Université Montpellier 2, Geosciences Montpellier, CNRS/INSU, UMR 5243, Montpellier, France.
2 Université Paris-Sud, Laboratoire des Interactions et de la Dynamique des Environnements de Surface, CNRS/INSU UMR 8148 Orsay, France.

Received July 2009
Sedimentary Geology submitted

Abstract

Paleostorm history in lagoon coastal environments (Pierre Blanche lagoon, central part of Gulf of Lions) has been established using a new approach associating clay mineralogy and geochemistry analysis. Clay mineralogy combined with major and trace element concentrations allow us to define four different end members, with Mosson drainage basin, sandy barrier, biogenic and anthropic components. The two main sedimentary sources of the lagoonal system are the Mosson drainage basin with a high concentration of smectite and Al2O3 and the sandy barrier characterized by illite, chlorite, SiO2 and Zr. Smectite/(illite + chlorite), SiO2/Al2O3 and Zr/Al2O3 ratios can be used to reconstruct past storm history of the Pierre Blanche lagoon. Our results indicate that the sensitivity of the smectite/(illite + chlorite) ratio is more important than geochemistry proxies, especially for less intense storms not identified as the most powerful events. This sensitivity could be related 1/ First by the complexity of the mix, two end members for the clay minerals and four end members for the geochemistry; 2/ Second by the storm ability to transport sediment of different sizes.

Keywords : Paleostorm, Mediterranean lagoon, Clay mineralogy, Geochemistry.

1. Introduction

Reconstruction of the recurrence and intensity of past storms in coastal area is an important topic of study due to the recent concentration of resource and population in this area (Pielke and Landsea 1999; Turner et al., 2006; Dezileau et al., submitted). The effects of climate change on extreme events are difficult to assess because of many forms of nonlinearity and long term memory. The lack of instrumental longterm series does not allow us to clearly demonstrate if hurricane activity may increase in relation to anthropogenic climate change (Webster et al., 2005; Emanuel 2006; Landsea et al., 2006). Regional climate simulations have been used to investigate the variations of precipitation and the cyclonic activity in the Mediterranean region. Lionello and Giorgi (2007) show that the reduction of cyclone activity observed in future scenarios could be responsible for the negative change in precipitation on the southern and eastern Mediterranean coast, while positive change occurs in Northern parts in relation to increased strength of mid latitude storm track. It is therefore, important to study

the past storm activity in order to better understand the possible regional and local long term trends of these events, associated to past climate conditions.

Geological data offers opportunities to reconstruct a long term record of intense events and can extend the documented record well beyond the observational record in order to identify how cyclone activity has responded to past shifts in climate (Nott, 2004; Frappier et al., 2007). The Gulf of Lions shore line is characterized by many coastal wetlands that are a result of the interaction between a process of shore line regularization by migrations of sandy barriers due to the sediment transfer through littoral hydrodynamics; and a filling of these areas by the fluvial and marine inputs (Certain et al., 2004; Raynal et al., 2009). This study focused on the Palavasian lagoonal system, characterized by fairly high accumulation rate, more particularly on the Pierre Blanche lagoon, where land-falling storms have previously been identified (Sabatier et al., 2008; Dezileau et al., submitted).

Usually, reconstruction of paleostorm events in coastal environment is made by identifying the recurrence of overwash coarse grained deposits and associated fauna contents (Liu and Fearn 1993, 2000; Collins et al., 1999; Donnelly et al., 2001a, b; Nott 2004; Donnelly, 2005; Dezileau et al., 2005; Donnelly and Woodruff, 2007; Scipelly and Donnelly, 2007; Sabatier et al., 2008). However, recent study in Shelby coastal lake, used different proxy as stable isotopes composition on organic matter ($\delta^{15}N$ and $\delta^{13}C$), where sand laminae/transported shells are indistinguishable or absent, in order to understand hurricane history on Holocene time scale (Lambert et al., 2008). In this study, we test for the first time, the sensitivity of clay minerals and geochemistry to identified paleostorm in a Mediterranean coastal lagoon. This approach was traditionally applied in palaeoclimatology to reconstruct palaeoenvironmental changes linked, for example, to Asian Monsoon intensity (Liu et al., 2004; Boulay et al., 2005; Colin et al., 2006) to El Niño-Southern Oscillation (Lamy et al., 2001) or to cold Atlantic events (Bout-Roumazeilles et al., 2007). In this study we use clay minerals and geochemistry to characterise the main sediment sources, in the aim of defining new proxies, on sediment core, to reconstruct paleostorm land-falling history in this coastal lagoon.

2. Geological setting

The Palavasian lagoonal complex is located to the West of the Rhone delta, in the central part of the Gulf of Lions, South of France (*Figure 3.15*). This area consists of several small lagoons, with low water depth (<1 m), limited to the South by a narrow sandy barrier and to

the North by calcareous Mesozoic hills. This wetland complex is now crossed by the artificial Rhône-Sète navigation channel constructed in the 18th century. In some places, the sandy barrier is less than 60 m wide and 3 m high above the average sea level; this implies an extreme sensitivity to high energy events, enabling temporary but strong marine influence during storm events. This is commonly highlighted by traces of over-wash fans and ancient temporary inlets (Dezileau et al., 2005; Sabatier et al., 2008). This coastal area displays a classical microtidal littoral zone with a maximal tide excursion of less than 50 cm.

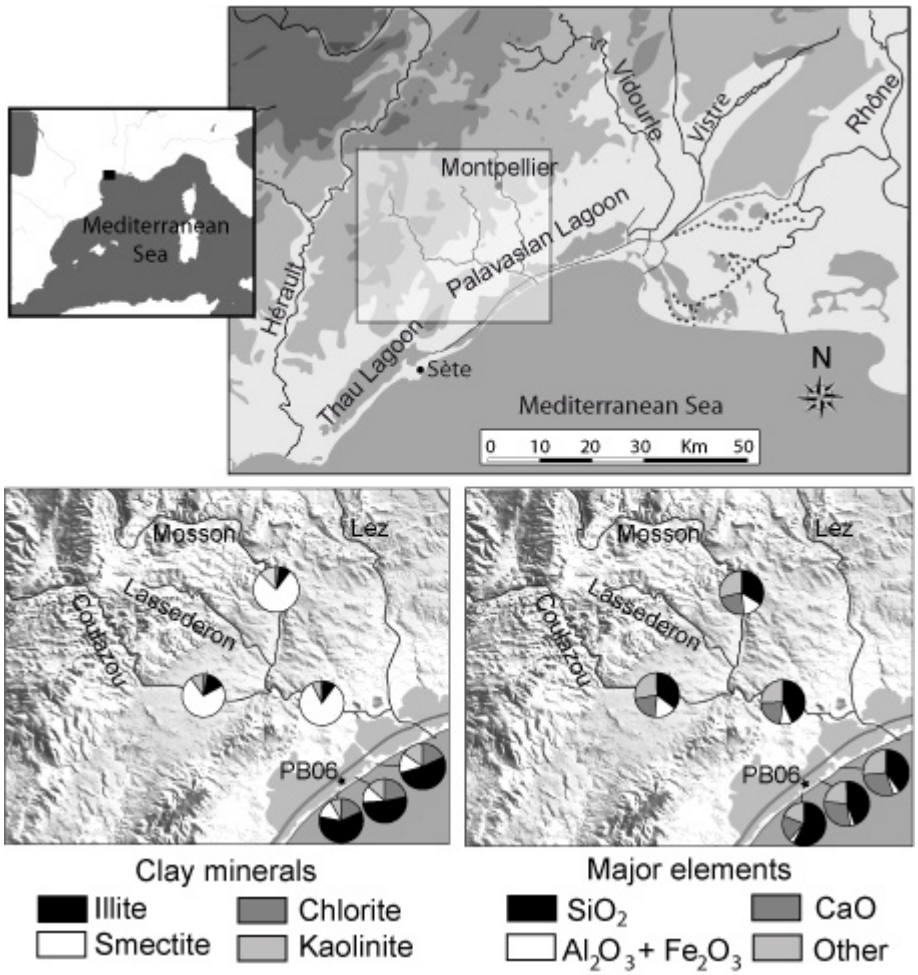

Figure 3.15 : a. Map of the Western Mediterranean Sea and the central part of the Gulf of Lions (South of France) within the light rectangle the Palavasian lagoonal system. b. Sample location and concentration of clay minerals on Mosson drainage basin and sandy barrier. Location of core PB06 sampled in Pierre Blanche Lagoon. c. Concentration of selected major elements.

The Mosson River, drains an area of 370 km^2, is constituted by three main channels: Coulazou, Lassédéron and Mosson, which is 36 km in length (*Figure 3.15*). Most of the sediments transported by rivers and supplied to the studied lagoonal system are carried during flash flood events. The Mosson average flow is 1.2 m^3/s but can reach the values of 258 m^3/s measured during 3 December 2003 flash flood events (DIREN, 2009). The Mosson drainage basin is mainly constituted of Mesozoic (limestone) and Cenozoic (conglomerate, carbonated sandstone and clay) sedimentary rock with Quaternary deposits.

3. Materials and Methods

3.1. Sample location

A piston core of 7.9 m long (PB06) was collected in the Pierre Blanche lagoon in March 2006 (Figure 1) with the UWITEC© gravity coring platform (University of Chambery). In this study, we focus on the first 1.30 m of this core. In addition, 8 samples were collected in the muddy channel deposit from the Mosson drainage basin during the dry season. Suspended sediments were also sampled, with sediment trap during flash flood events (September 2005), at three different locations (4 samples). Moreover, fine sediments were picked up in different geologic sedimentary rocks present on the Mosson drainage basin. Samples were also collected from the sandy barrier in front of the Pierre Blanche lagoon located in the Southern part of the Palavasian system.

3.2. Analytical Methods

Core PB06 was split, photographed, logged in detail (noting all physical and biogenic sedimentary structures and vertical facies successions), and divided into 1 cm long vertical sections prior to analysis. In this study, the upper 1.3 m of sediment of this core was sampled every 2-3 cm in order to analyse clay mineral content as well as major and trace elements.
Clay minerals were identified by X-ray diffraction (XRD) using a PANalytical diffractometer at the Laboratoire IDES (Université de Paris XI) on oriented mounts of non-calcareous clay-sized (<2 μm) particles. The oriented mounts were obtained following the methods described in detail by Colin et al. (1999). Three XRD runs were performed, following air-drying, ethylene-glycol solvation for 24 hours, and heating at 490ºC for two hours. Identification of

clay minerals was made mainly according to the position of the (001) series of basal reflections on the three XRD diagrams. Semi-quantitative estimates of peak areas of the basal reflections for the main clay mineral groups of smectite (including mixed-layers) (15–17 Å), illite (10 Å), and kaolinite/chlorite (7 Å) were carried out on the glycolated curve using the MacDiff software (Petschick, 2000). Relative proportions of kaolinite and chlorite were determined based on the ratio from the 3.57/3.54 Å peak areas.

Major and trace elements analyses were realised by flow injection ICP-MS using a Sciex Perkin Elmer ELAN 5000a at the Service d'Analyse des Roches et des Minéraux (SARM, Nancy, France) using the method described by Carignan et al. (2001). Samples are powdered (300 mg) and fused in Pt crucibles along with 900 mg of ultra-pure LiBO2 at 980 °C in an automatic tunnel oven on a rail over a period of about 60 minutes. After cooling to room temperature, the fusion glass was dissolved in a HNO3 (1 mol l-1)-H2O2 (~ 0.5% v/v)-glycerol (~ 10% v/v) mixture in order to obtain a dilution factor of 333 relative to the amount of samples fused.

4. Sedimentological and chronological framework

Lithological description of PB06 core based on grain size, sedimentary structure and fauna content allow identification of different facies interpreted in terms of lagoon depositional environments (Sabatier et al., 2010). Sabatier et al. (2008) and Dezileau et al. (submitted) recognized, in a core transect including PB06, three main historical storm events. Comparison of ^{210}Pb, ^{137}Cs, ^{14}C chronology and historical accounts suggest that the three identified storm events took place in 1742, 1848 and 1893 A.D. (*Figure 3.16*), these events allow us to specify PB06 chronology. The age of these paleostorm, considered as instantaneous events, are in good agreement with the average sedimentation rate of 2.7 mm/yr defined by Sabatier et al., (2010), for the last 700 yrs. Therefore the 1.3 meter of this core represented the last 480 years.

5. Results

5.1. Mineralogy results

For the Mosson River suspended sediment during a flood event, including the three main channels: Coulazou, Lassédéron and Mosson, smectite (73% - 81%) is the dominant clay mineral with an average of 77%. Illite (8% - 14%) and kaolinite (8%-13%) are less abundant with a similar average content of about 10%. Chlorite is very scarce with an average content of about 3% (*Figure 3.15*).

For the sandy barrier sediment, illite (45% - 59%) is the dominant clay mineral, with an average content of 52%; chlorite (17% - 26%) and smectite (8% -28%) are less abundant with average contents of 20% and 18%, respectively. Kaolinite (6% - 16%) is a minor component averaging at 10% (*Figure 3.15*).

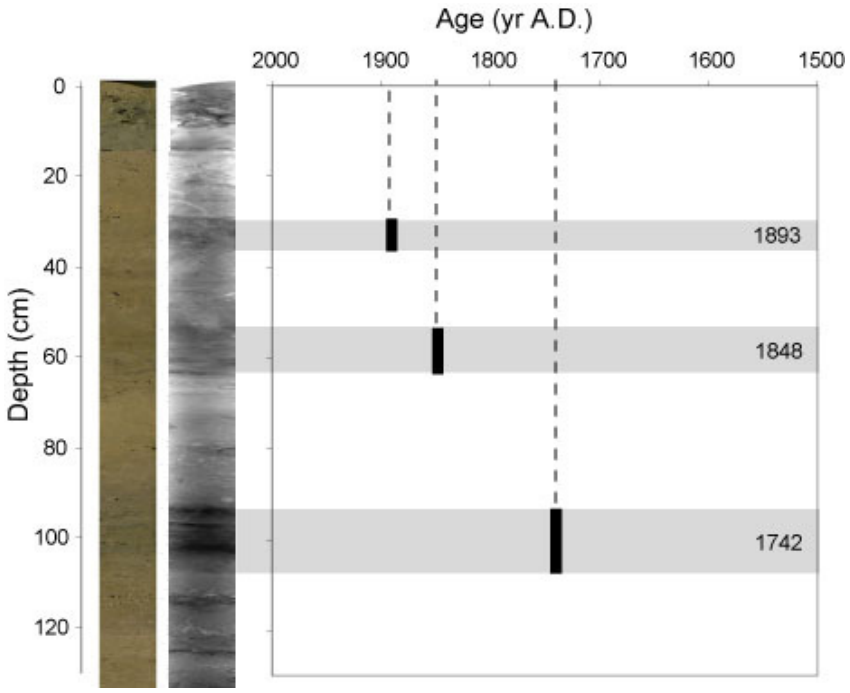

Figure 3.16 : Core PB06 with from left to right: Photography, X-ray and Age Model. Grey band are storm events previously identified and dark rectangle are the age of these events.

The relative abundance of the main clay mineral groups in core PB06 is reported in *Figure 3.17*. In core PB06 values of clay mineral contents are included between the two End Members, the Mosson drainage basin and the sandy barrier. This core is predominantly characterized by high contents of smectite (20% - 64%) and illite (19% - 50%) and low contents of chlorite (5% - 24%) and kaolinite (8% - 17%). Their average percentage is 49% for smectite, 28% for illite, 10% for chlorite and 12% for kaolinite (*Figure 3.17*). Clay minerals can be subdivided into three groups along PB06. Changes of illite and chlorite

display similar variations with two main increases in concentration between 46 and 70 cm and between 92 and 110 cm. A general trend of smectite is inversely correlated to illite and chlorite. Kaolinite contents do not vary significantly with depth.

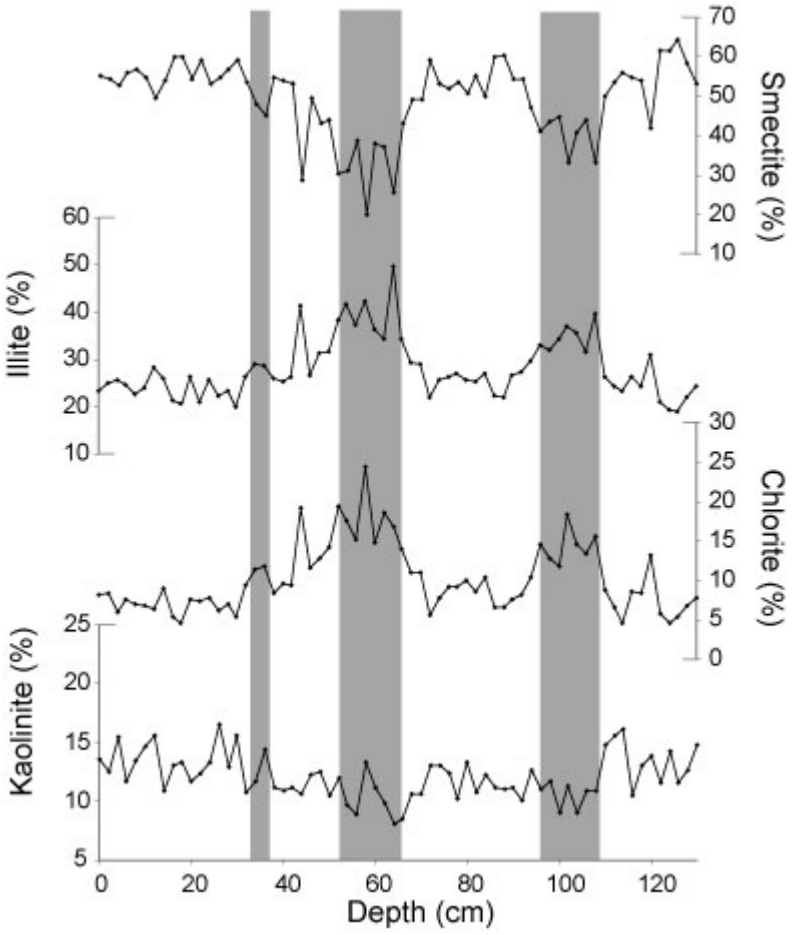

Figure 3.17 : 1.3 m of PB06 clay mineral analyses contents (%) obtained on the carbonated-free <2 µm size fraction. Smectite and illite are dominant (up to 75% of the total clay minerals). Illite and chlorite co-vary opposed to that of smectite. Kaolinite contents do not vary significantly with time. Shaded areas mark the main variations.

5.2. Geochemistry results

Bulk sediment from Mosson drainage basin, sandy barrier and core PB06 consist mainly of high content of SiO_2, CaO, Al_2O_3 and Fe_2O_3 and low concentrations of MgO, K_2O, Na_2O, TiO_2, P_2O_5 and MnO (*Tableau 8-4, annexe 9.5.*). Sediments from the Mosson river basin are characterized by a relatively high concentration of Al_2O_3 and Fe_2O_3 while materials from the sandy barrier consist mainly of SiO_2 and CaO (>70%, *Figure 3.15).*

In *Figure 3.18,* we have reported contents of selected 7 major and trace elements, which present the most important variations through depth. Content variations of these elements can be subdivided into three groups in core PB06. SiO_2, Na_2O and Zr exhibit similar variations with three layers of high concentration. In general, trends in Fe_2O_3 and Al_2O_3 are inversely correlated to those of SiO_2, Na_2O and Zr. In addition, CaO and Cu concentrations display two other trends which are not related to the first two groups.

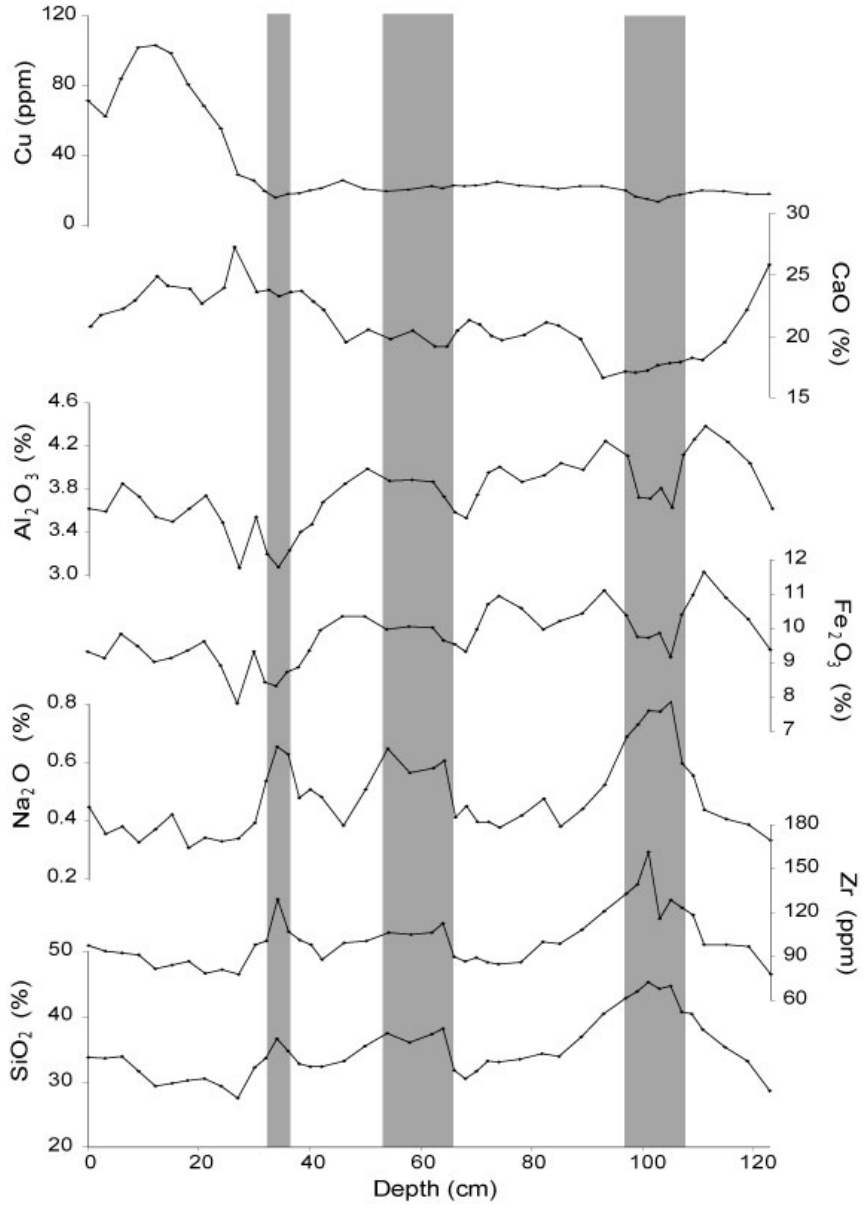

Figure 3.18 : 1.3 m of PB06 selected geochemistry data. SiO_2, Na_2O and Zr co-vary opposed to Fe_2O_3 and Al_2O_3. CaO and Cu contents vary in different phases. Shaded areas mark the main variations.

Different strategies of multivariate data analysis are used to interpret a database from sediment samples. Principal component analysis (PCA) is a technique that transforms a large number of variables (concentration of elements) into a smaller number of independent variables in order to visualize the relation between the first variables and objects of interest (sediment sample). The major elements data and Loss Of Ignition (LOI) from PB06 core were subjected to "centered logratio transformation" (clr-transformation, Aitchinson et al., 2002) and then the PCA calculation was performed, as summarized by Tolosana-Delgado et al. (2005). All statistical calculations were conducted on ''R'' software using the package ''compositions'' (van den Boogaart and Tolosana-Delgado, 2008). The multivariate data analysis applied makes it possible to interpret data in terms of source influence of samples. The first principal component (CP1) explains 63% of the variance and shows high positive loadings for Na_2O, SiO_2, K_2O and MnO and high negative loadings for P_2O_3, CaO, LOI and MgO (*Figure 3.19*a). PC2 explains 17% of the variance and gives high positive loadings for Na_2O, P_2O_3 and CaO and negative loadings for MnO, K_2O, Al_2O_3, Fe_2O_3, TiO_2 and MgO. Samples with high positive PC1 score indicate a strong influence of marine component (sandy barrier) defined above while high negative PC2 score is correlated to the Mosson drainage basin. Moreover, surface sediment samples (<30cm) show high negative PC1 scores that indicate either a strong influence of phosphate or important biogenic component with a lot of shells.

Trace elements were selected in order to trace the origin of sediment, with lithogenic signature (Th, Rb, Ni, Zr, Hf, La, Ta, Nb, Ba), biogenic source (Sr, >1000 ppm into aragonite, <200 ppm into calcite) and related to the pollution (Cd, Cu, Pb). REEs present the same variance. Therefore only two REEs were used (Th, La) not to "swamp" the analysis (Pe-Piper, et al., 2008). PC1 (81% of variance) show high positive loadings for Cu, Pb, Cd and Sr and negative loadings for all the other elements. The PC3 (4% of the variance) was chosen instead of PC2 (12% of the variance) to better discriminate elements with a negative loading on PC1 (*Figure 3.19b*). Thus PC3 displays positive loadings for Zr, Hf and Ba and weaker negative loadings for Ta, Th, La, Ni, Rb and Nb. Samples with high positive PC1 scores indicate a strong influence of pollution-related minor elements (upper <20 cm). Samples with positive PC3 scores are correlated with Zr and Hf, mostly current in heavy minerals (zircon) and are not present in sedimentary formation of the Mosson watershed but are one of the components for the sandy barrier (Dezileau et al., submitted). Samples characterized by high negative scores on PC3 are related to Th and Ni elements, generally associated with clay minerals, mainly transported by the Mosson river.

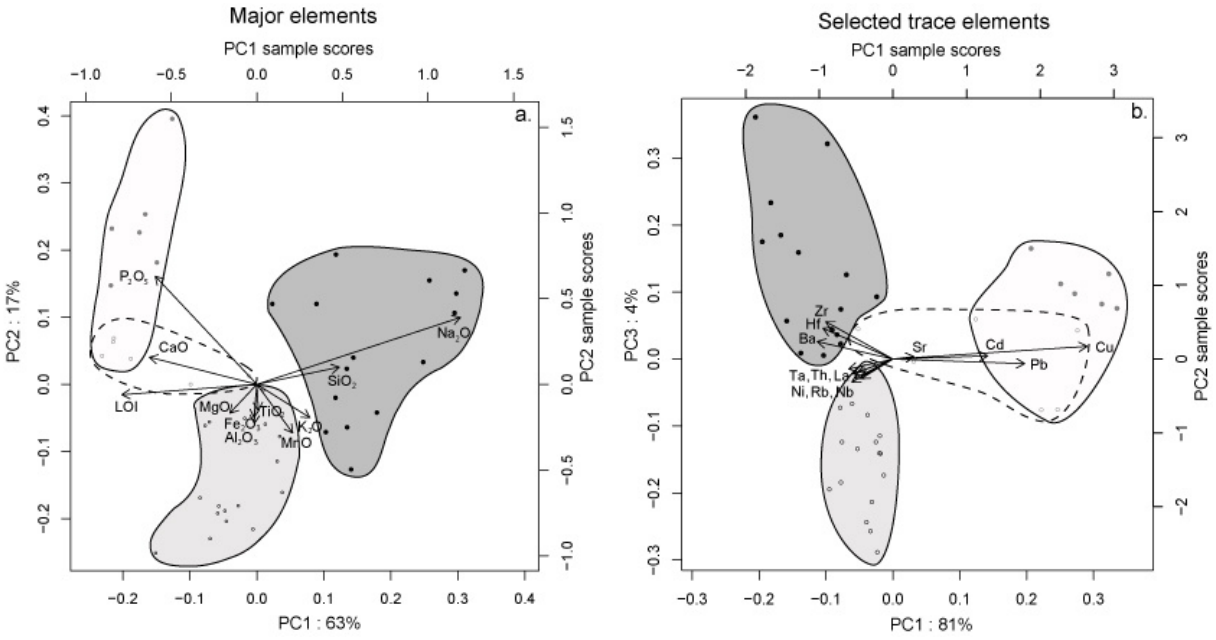

Figure 3.19 : a. Biplots of PC1 and PC2 loadings and sample scores for ten major elements and LOI. PCA was performed on centered logratio transformation of samples. Four different groups of samples were identified in relation to the variable. a. Biplots of PC1 and PC3 loadings and sample scores for thirteen selected trace elements. The same groups of samples were identified.

6. Discussion

The interpretation of clay mineral and detrital geochemical records requires knowledge of the potential source areas, as well as the mode and strength of the transport processes involved (Gingele et al., 2001; Boulay et al., 2003; Liu et al., 2007). An effect of global sea level fluctuations on the sedimentation of the Mediterranean coastal lagoon can not be invoked on the Late Holocene timescale. In addition, the change from chemical to physical erosion on land cannot occur on centennial timescale (Thiry, 2000; Egli et al., 2001). Consequently, for modern sediments of the Pierre Blanche lagoon, mineralogical variations are induced by fluctuations in source sediments.

6.1. Sediment sources

To understand the cause of mineralogical variations in PB06 core, it is necessary to document the origin and source areas of the minerals present in the Pierre Blanche lagoon. Clay mineral composition significantly varies from the Mosson drainage basin, with high concentration of smectite (73% - 81%) to the sandy barrier characterized by high illite (45% - 59%) and chlorite (17% - 26%) contents. Smectite derives mainly from erosion of smectite-rich Cenozoic conglomerates (Vitrollien, 55-70 %) and in its muddy channel deposits outcropping in the upper part of the Mosson drainage basin (BRGM, 1967). In general, illite is related to strong physical erosion and moderate hydrolysis conditions on land (Chamley, 1989). In the Gulf of Lions, the clay mineral distribution has been studied since the 90's (Croup and Monaco, 1990; Giresse et al., 2004; Bout-Roumazeilles et al. 2007). The main marine sediment source in the central part of Gulf of Lions is the Rhône River receiving its detrital materials from the Alps where illite and chlorite are mostly found (>75%).

In the Mediterranean Sea, eolian dust, supplied from North Africa, could account for 20% of the sediment deposition on the Gulf of Lions margin, as previously reported by Zuo et al. (1997) and Guerzoni et al., (1997). African dust can reach the central part of Gulf of Lions by SW-NE transport, mostly during winter when a large atmospheric depression system develops between The Canary Islands and The Iberian Peninsula (Rodriguez et al 2001, Bout-Roumazeilles et al. 2007). The mineralogy of the dust transported from North Africa is mostly characterized by quartz, feldspars associated with kaolinite and illite (Guerzoni et al., 1999). Another clay mineral typical of the arid and semi-arid climate is the palygorskite, commonly used as an indicator of African dust contribution (Coudé-Gaussen et al., 1987; Molinaroli, E. 1996; Caquineau et al. 1998; Bout-Roumazeilles et al. 2007). The occurrence of palygorskite was identified in some Mediterranean areas with, for example an average concentration of 5% in Holocene sediments of the Alboran Sea (Bout-Roumazeilles et al. 2007). In low sedimentation rates areas, such as Corsican lakes, the palygorskite can account for more than 25% of the clay size fraction (Robert et al., 1984). Nevertheless, no evidence of palygorskite was found in core PB06 suggesting a negligible contribution of eolian material in the Pierre Blanche lagoon.

Moreover, applying the eolian flux estimation of 8 $g.m^{-2}.yr^{-1}$ (Guerzoni et al., 1999), and mean terrigenous fluxes of around 600 $g.m^{-2}.yr^{-1}$ calculated for core PB06 (Sabatier et al., 2008), we can estimate eolian flux contributions to the terrigeneous fraction of 1.3 %.

Figure 3.20 displays illite % versus smectite % in Mosson drainage basin (grey), in sandy barrier (dark) and in core PB06 sediments. Samples from core PB06 have been separated into

two groups corresponding to normal sedimentation and to layers influenced by previously identified paleostorm events (*Figure 3.17*). Samples from PB06 are reported on a linear model between these two end members suggesting that no other major sedimentary sources influence the clay size sedimentation of the Pierre Blanche lagoon.

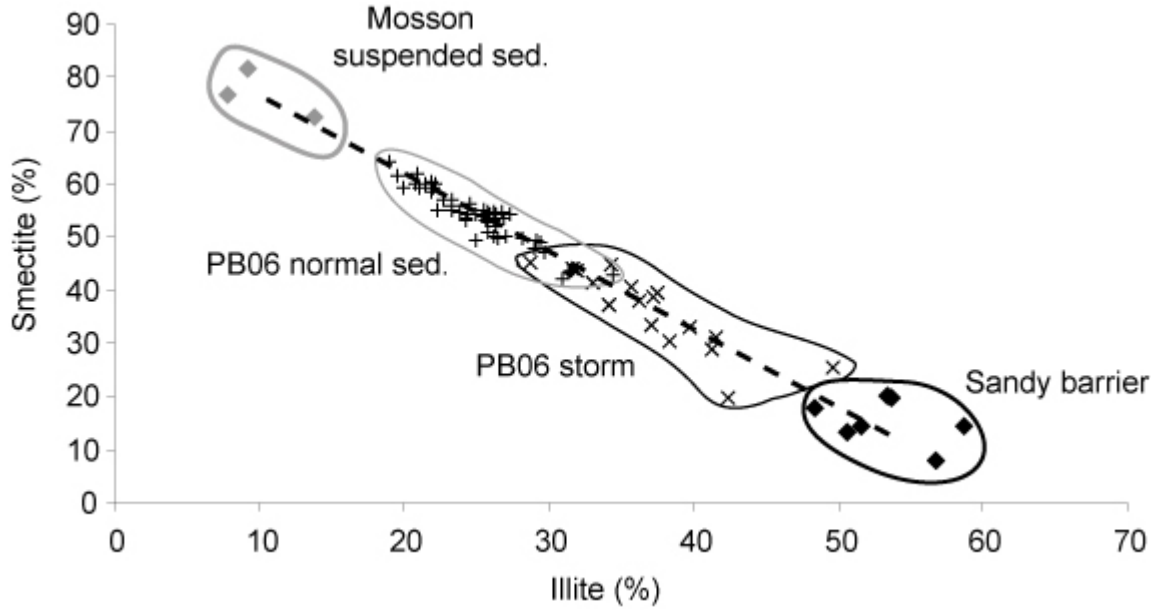

Figure 3.20 : Illite versus smectite with sample from Mosson drainage basin (grey) from sandy barrier (dark) and from PB06 separated into two groups corresponding to normal sedimentation and to layers influenced by previously identified paleostorm events (Figure 3.16).

PCA of major and trace elements on core PB06 shows four groups of samples influenced by different geochemistry end members while clay minerals allow definition of two fine sediment sources (*Figure 3.19*). One of the main sources is characterized by Al_2O_3 and Th. These elements are generally associated with clay minerals, mainly transported by the Mosson drainage basin during flood events. Another source is defined by SiO_2, Na_2O, Zr and Hf, respectively abundant in quartz, salt and heavy minerals present in the sandy barrier. Biogenic contents variations are evident in lagoonal sediment by shell abundance with high concentration in CaO and Sr. Finally, domestic, agricultural and industrial effluents have been released, partly treated, for the last several decades. The high levels of phosphate and metal elements (Cu, Pb, C Cd) in the surface sediment (*Figure 3.18*) are the result of the anthropic component.

In order to characterize different end members, geochemistry analyses were performed on the various components of the system including Mosson drainage basin and barrier samples (Figure 7). Results obtained from core PB06 are also displayed but separated into two groups previously identified by clay minerals as normal lagoonal sedimentation and layers influenced by storm events (Figure 7). Samples from sandy barrier seem to be a ternary mix between quartz (SiO_2), carbonated shell (aragonite with high concentration in CaO and Sr) and aluminosilicate minerals (illite, chlorite and probably mica). Sample from Mosson channel deposit is a mix of aluminosilicate minerals end member (i.e. clay sample from Mosson drainage basin, mainly characterized by smectite) and limestone (calcite, CaO and low Sr in comparison to shell contents). Suspended sediments collected during flood events are intermediate between clay from Mosson drainage basin (smectite) and material from channel deposit (with carbonate component). Core PB06 is mainly characterized by sediments transported by flood events and by carbonated shell with some layer influenced by sandy barrier during storm events (Figure 7d). Therefore, the mineralogical components of this system are quartz, illite chlorite and probably mica for marine end member and derive mainly from the Rhone River, limestone and clay minerals mainly smectite for the Mosson drainage basin, carbonated shell for the biogenic productivity inside the lagoon and an anthropic component with phosphate and some metal elements.

6.2. Identification of storm events with clay mineralogy and geochemistry

Mosson drainage basin and sandy barrier represent the main source of sediment to the Palavasian lagoonal system. They are characterized by different mineralogical and geochemical signatures. Dezileau et al. (2005) and Sabatier et al. (2008) show that strong marine influence in this area occurs during storm events, when wind and wave energies break up the barrier and trigger a landward material transfer, from the barrier to the lagoon. Clay mineralogy and geochemistry display significant variations between these two major sedimentary sources and can therefore, be used to reconstruct the marine influence in the Pierre Blanche lagoon that could be linked to past storm events.

Considering that smectite, illite-chlorite reveal a distinct temporal evolution and that kaolinite abundance does not exhibit significant changes, it is possible to use smectite/(illite+chlorite) ratio to describe the mineralogical variations within the clay size fraction. This mineralogical ratio can be used to reconstruct the history of paleostorm events. In core PB06, the smectite/(illite+chlorite) ratio ranges from 0.4 to 2.4. Variations of this ratio show low values

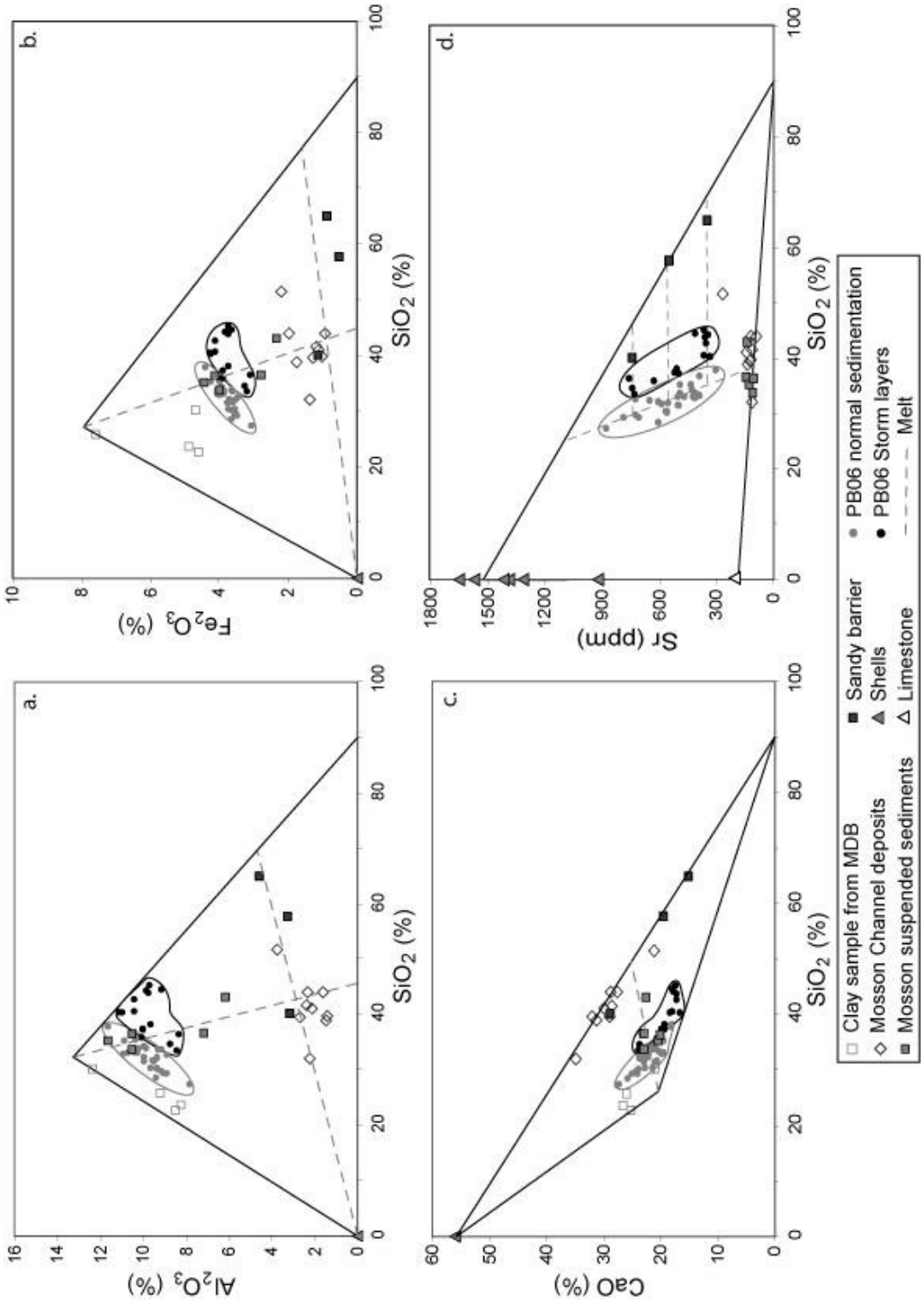

Figure 3.21 : Binary plots of geochemistry data with SiO_2 versus a. Al_2O_3, b. Fe_20_3, c. CaO, d. Sr. These diagrams specify the different end members. Dotted lines represent the main linear melt. All the samples from the studied system are displayed and samples from PB06 are separated into two groups corresponding to normal sedimentation and to layers influenced by previously identified paleostorm events (Figure 3.18).

in correlation to previously identified storm events (*Figure 3.22*). Moreover, two other storm events seem to be identified at 44 and 120 cm (*Figure 3.22*). The relatively higher ratios observed during the rest of time indicate the dominance of Mosson river sediment inputs. We also suggest that minerals with a high concentration in SiO_2 and Zr could correspond mainly to the silt and sand fraction present on the littoral barrier (quartz and heavy minerals as zirconium) while Al_2O_3 is the major component of clay minerals, mostly transported from the watershed. In core PB06, SiO_2/Al_2O_3 and Zr/Al_2O_3 ratios increase in relation to storm events (*Figure 3.22*). Good correlations between smectite/(illite + chlorite), SiO_2/Al_2O_3, Zr/Al_2O_3 ratios and paleostorm events suggest that these proxies determined in different size fractions of the sediment can be used to reconstruct the past storm history.

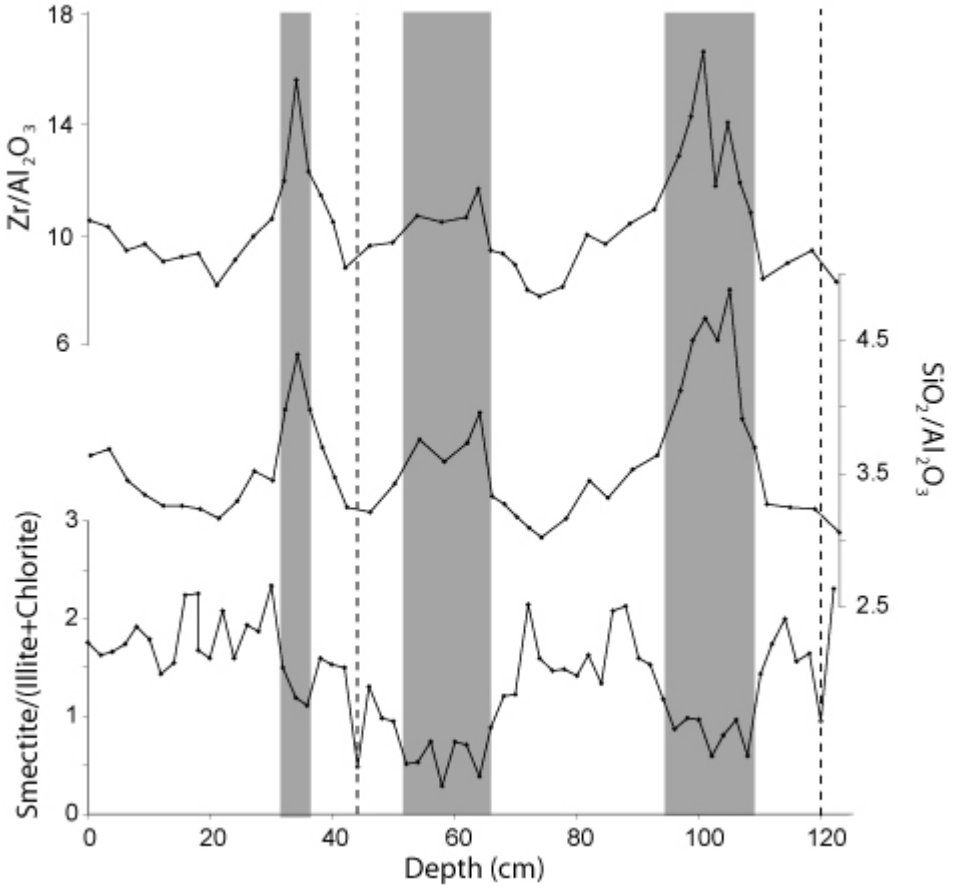

Figure 3.22 : Smectite/(illite + chlorite), SiO2/Al2O3 and Zr/Al2O3 ratios for the PB06 cores. Grey bands are paleostorms events previously identified, dotted lines are new paleostorms identified just with the clay mineral ratio.

However, the sensitivity of smectite/(illite + chlorite) ratio seems to be more important than SiO_2/Al_2O_3 and Zr/Al_2O_3 ratios, especially for storms not identified as a main event. The sensitivity could be related to the complexity of the mix, two ends members for the clay mineral distribution and four ends members for the geochemistry. In addition, there is a possible improved ability of a storm event to transport sediment of different sizes from the barrier to the lagoon. We can assume a constant morphology of the sandy barrier for the last 500 yrs (Dezileau et al., Submitted). During a main storm event, wind and wave energies are strong enough to transport to the central part of the lagoon, coarse sediment as silt and sand with high concentration in quartz and heavy minerals with high ratios of SiO_2/Al_2O_3 and Zr/Al_2O_3. However, the intensity of wind and wave energies is not powerful enough to transport coarse sediment (silt or sand) but can trigger a landward transfer of clay. Moreover, if the breaking up of the sandy barrier occurred far away from the core location, coarse material can not be transported over large distances while clay may record this influence over more distal location. In both cases, the record of this event is just identified by a decrease in smectite/(illite + chlorite) ratio. These analyses allow to specify the layers influenced by marine input in relation to storm events (*Figure 3.20*). These storm layers are in pretty good agreement with a storm previously identify (Sabatier et al., 2008; Dezileau et al., Submitted).

6.3. Clay minerals as indicator of storm intensity?

Clay mineralogy distributions through time clearly show an increase of illite content as a consequence of paleostorm (*Figure 3.20*) in relation to its high concentration in the sandy barrier. In core the relative contribution of illite within layers identified as storm events could be interpreted as an indicator of land-falling intensity. Nevertheless, Woodruff et al., (2008) associate the local flooding intensity to the competence for each overwash event to transport coarse-grained sediment at a fixed distance in the lagoon. Clay minerals are the smallest sediment component and can thus be exported landward across large distances during a storm event while coarser material such as sand and silt need more energy to be transported over the same distance. The storm of September 4th, 1742, recorded in many city archives around the Aigues-Mortes Gulf, is considered the most catastrophic event (around 100 cm depth) but its smectite/(illite + chlorite) ratio suggests that this storm was less intense than in 1848 (64 cm depth). Moreover, two other events seem to be identified at 44 and 120 cm of depth and present values of this same ratio, almost equalling the most powerful hurricane despite the fact that these events seem to be less intense. Therefore, clay minerals can not be used as an

indicator of land-falling intensity but as a very sensitive proxy in order to identify storm events, even if sand layers are indistinguishable or absent.

7. Conclusion

Clay mineralogy and geochemistry analyses of Pierre Blanche lagoonal system had been realized in order to determine sediment sources of this coastal area and to test these proxies to reconstruct paleostorm events, which affected the North western parts of the Mediterranean sea.

The Pierre Blanche lagoonal clay fraction (<2 μm) contains four main clay mineral groups. Smectite and illite accounting for more than 75% of the clay assemblage. Chlorite and kaolinite contents are of secondary importance. Illite and chlorite co-vary (in core PB06) and are mainly present in the sandy barrier and are inversely correlated with smectite abundant on the Mosson drainage basin. Kaolinite contents do not present significant variations.
Major and trace element concentrations allow us to define four main components in the Palavasian lagoonal system. The first source was the sediment from the Mosson drainage basin transported during flood events and is characterized by Al_2O_3, Fe_2O_3, and Th and is mostly constituted of clay (mainly smectite minerals) and limestone. The second end member presents high concentration in SiO2, Zr, Hf and allow to define mineralogical components of this sandy barrier with quartz, illite chlorite, mica and shell, these sediments come from Rhone River by littoral drift. The third component is characterized by CaO and Sr, mainly due to carbonate shell accumulation in relation with biogenic productivity inside the lagoon. The last end member of this system is the anthropic component with phosphate and some metal elements (Cd, Cu, Pb) for the surface sediment (<30 cm).
The main sources to the lagoonal sedimentation are Mosson drainage basin and sandy barrier with landward transport of sand and silt materials during storm events. The important discrepancy of clay minerals and geochemistry between these two end members allow to trace land-falling events. Good correlations between smectite/(illite + chlorite), SiO_2/Al_2O_3, Zr/Al_2O_3 ratios and paleostorm events suggest that these proxies can be used to reconstruct the past storm history. Smectite/(illite + chlorite) ratio are more sensitive than SiO_2/Al_2O_3 and Zr/Al_2O_3 ratios, especially for storms not identified as the main events or triggers of sandy barrier break-ups at a location distal from a core sampled area.

Acknowledgments

This research has been undertaken in the framework of the ECLICA Project financed by INSU (ACIFNS “Aléas et Changement Globaux”, coord.: L. Dezileau) and INTEMPERIES project (“Appel à projets 2008 du Conseil Scientifique de l’Université Montpellier 2, coord.: L. Dezileau). The authors are also grateful to Anis Bel Haj Mohamed and Estelle Ricard from IDES laboratory (CNRS/INSU UMR 8148 - University of Paris XI), who helped us to process clay mineral analyses by DRX. The authors wish also to thank IFREMER Palavas for allowing storage of the cores in their cold room. GLADYS platform (www.gladys-littoral.org) and all other members of the ECLICA Project team are also thanked for their support and their constructive discussions during this study. The authors are grateful to Dr Aurélien Gay and Jessica Cole for English corrections.

3.4 Discussions complémentaires

Le croissement des différents traceurs associés à des données historiques et de radiochronologie nous permet d'identifier trois événements extrêmes de tempête de catégorie 3 sur l'échelle de Saffir-Simpson, au cours du Petit Age Glaciaire. De plus, la corrélation latérale, selon un transect Nord-Sud, des différentes carottes met en évidence l'extension de ses dépôts de tempêtes dans la lagune.

L'analyse des profils sismiques, montrent également une extension latérale importante des réflecteurs interprétés comme étant la continuité, en lagune, des cônes de tempêtes. Ces réflecteurs les plus marqués sont globalement horizontaux sur les profils perpendiculaires à la côte, dès que nous nous éloignions d'une cinquantaine de mètre du cordon (*Figure 3.3*). Bien que les profils sismiques ne recoupent pas exactement les sites de prélèvement des carottes, nous pouvons tenter de lier ces données entre elles. La corrélation, entre les données de sismiques et celles obtenues sur les carottes, met en évidence que les deux réflecteurs majeurs précédemment identifiés (jaune et rouge section 3.1) correspondent à des niveaux de granulométrie relativement grossiers associés aux tempêtes de 1742 et 1893 (*Figure 3.23*).

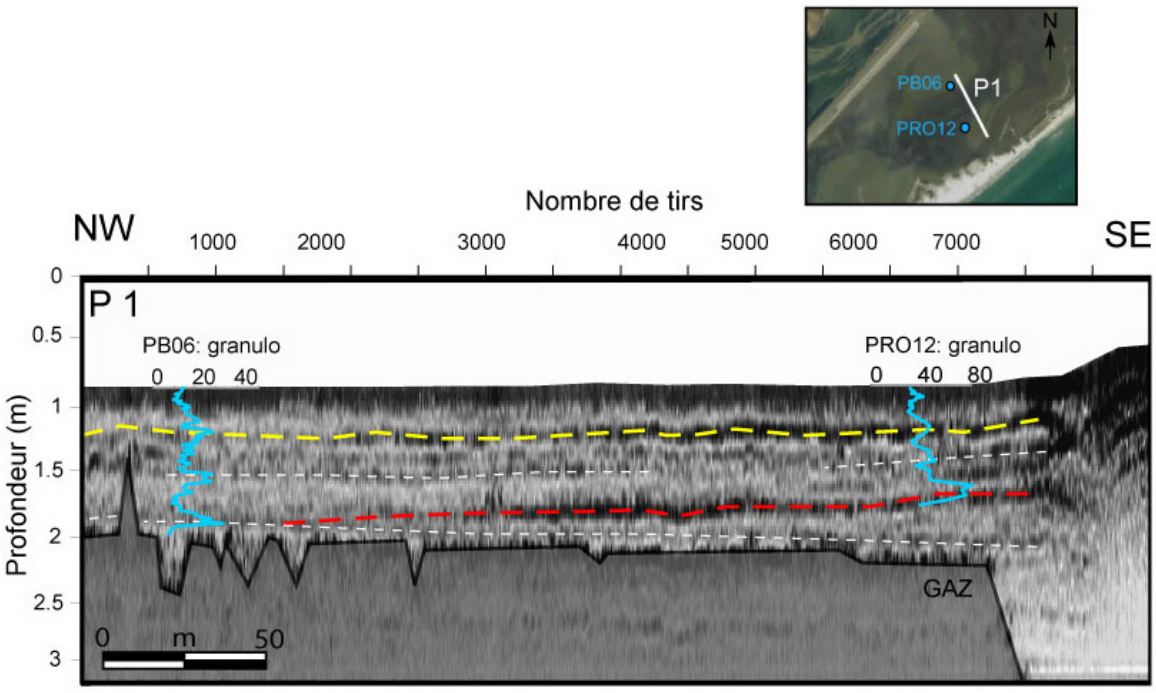

Figure 3.23 : Corrélation entre les réflecteurs sismiques les plus marqués (§3.1.1) et les données granulométriques des carottes PB06 et PRO12.

De plus, un petit réflecteur (pointillé blancs) situé juste au dessous du multiple, semble pouvoir être associé à la tempête de 1848. Cette corrélation n'est pas surprenante car les niveaux de sables et de silts apparaissent comme des réflecteurs idéals au sein d'une sédimentation fine.

4. Cadre chronologique

4.1 Le dernier siècle

4.1.1 Les modèles de ^{210}Pb

En se basant sur des modèles qui prédisent la distribution du ^{210}Pb en profondeur, il est possible de donner un âge aux différents niveaux d'une colonne sédimentaire et donc d'estimer le taux de sédimentation. Les activités de ^{210}Pb sont déterminées à l'aide d'un spectromètre gamma CAMBERRA à détecteur puits (méthode décrite dans l'article 3, section 4.2.). Il existe plusieurs modèles (résumés dans Appleby et Oldfield, 1992) permettant de calculer les vitesses de sédimentation à partir des profils en profondeur de ^{210}Pb. Cependant, sa distribution en profondeur dépend également de l'équilibre entre les transferts atmosphériques et fluviatiles, de la rythmicité de la sédimentation et de la bioturbation. Ces phénomènes de mélange biologique et d'altération des structures sédimentaires entraînent un biais dans la datation si on ne les prend pas en compte.

> Le modèle le plus simple est le CFCS (Constant Flux, Constant Sedimentation Rate) qui suppose constant le flux en ^{210}Pb ainsi que le taux d'accumulation ce qui sous entend que l'activité initiale est constante (Goldberg, 1963 ; Krishnaswami *et al.*, 1971). Le flux *P* et le taux de sédimentation *W* sont exprimés respectivement en mBq.cm^{-2}.an^{-1} et g.cm^{-2}.an^{-1}. L'activité *A* (en mBq.g^{-1}) est donnée par $A=P/W$. L'activité du ^{210}Pb en excès à la profondeur *z* est :

$$(^{210}Pb_{ex}^{z}) = (^{210}Pb_{ex}^{0}) \times e^{-\lambda t} \quad avec \quad (^{210}Pb_{ex}) = (^{210}Pb_{mes}) - (^{226}Ra_{mes}) \qquad (1)$$

Où λ représente la constante de désintégration du (^{210}Pb) (λ=ln(2)/22.3 an^{-1}), (^{210}Pb$^{z}_{ex}$) l'activité en mBq.g^{-1} à la profondeur *z* et (^{210}Pb$^{0}_{ex}$) l'activité en surface, valant *P/W*. Le temps t est égal à la masse de sédiment sec accumulé par cm^2 de surface jusqu'à une profondeur *z*, (M_z) divisée par le taux de sédimentation (*W*). En supposant que le plomb et le radium sont immobiles dans les échantillons, on peut écrire d'après l'équation précédente :

$$\ln(^{210}Pb_{ex}^{z}) = \ln(^{210}Pb_{ex}^{0}) - \left(\frac{\lambda_{210}}{W}\right) \times M_z \quad avec \quad t_z = \frac{M_z}{W} \qquad (2)$$

Lorsque l'on reporte les mesures expérimentales dans un diagramme $ln(^{210}Pb^{z}_{ex}) - M_z$, elles définissent théoriquement une droite dont la pente $-\lambda/W$ permet de calculer le taux de sédimentation. Ce modèle appliqué au profil de $^{210}Pb_{ex}$ de la carotte PB06 nous permet d'obtenir un taux d'accumulation de 0.088 ± 0.005 g.cm^{-2}.an^{-1} soit 2.81 ± 0.15 cm.an^{-1}, en considérant une densité moyenne (DBD) de 0.314 g.cm^{-3} (*Figure 4.1*). On peut alors calculer l'âge de chaque profondeur *z*. Cette méthode très simple à mettre en œuvre, permet de déterminer la vitesse de dépôt moyenne du système sédimentaire, cependant cette approximation dans le modèle d'âge ne rend pas compte des variations de la vitesse d'accumulation pouvant exister à chaque profondeur par rapport à la moyenne, ce qui ne permet pas de dater précisément un événement sédimentologique.

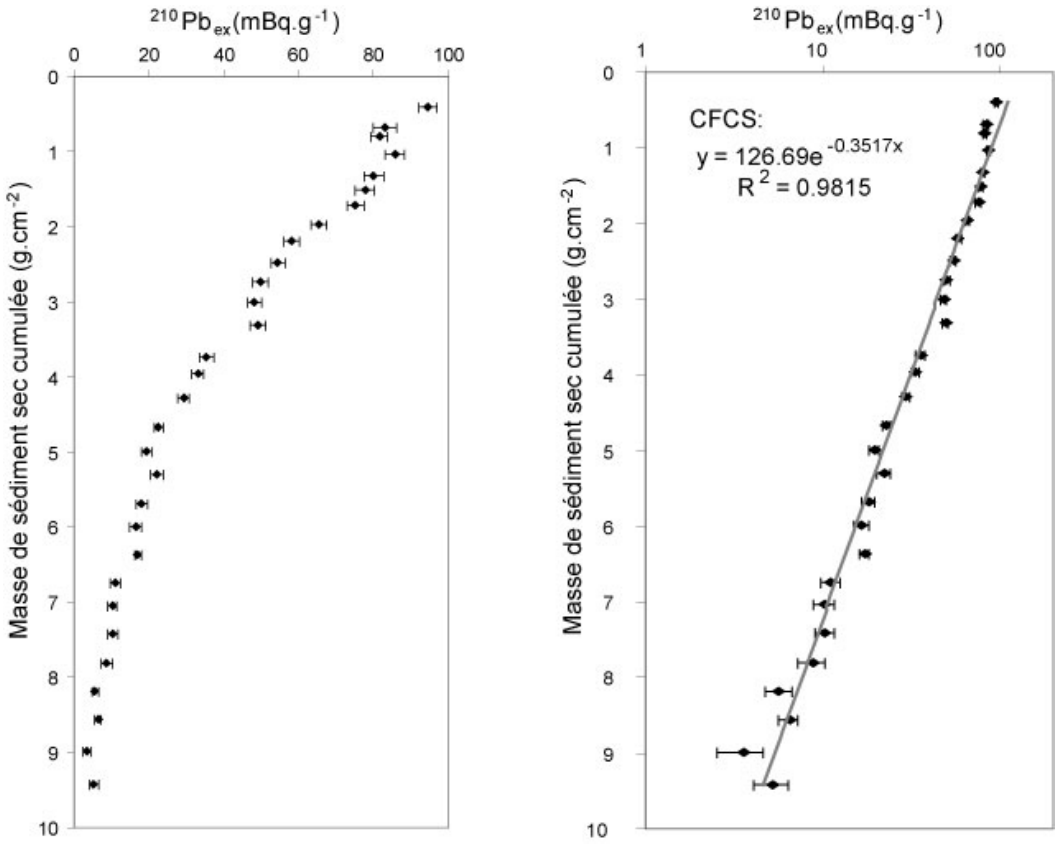

Figure 4.1 : A gauche : profil de $^{210}Pb_{ex}$ exprimé en mBq.g^{-1} en fonction de la masse de sédiment sec cumulée (g.cm^{-2}). A droite Modèle CFCS appliqué à l'ensemble du profil.

> Le second modèle, CIC (Constant Initial Concentration) repose sur l'hypothèse que si le flux en ^{210}Pb ou le taux de sédimentation varient, ces variations sont opposées de telle sorte que l'activité initiale dans le sédiment de surface reste constante (Pennington *et al.*, 1976, Noller, 2000). A partir de l'équation (1) on obtient la relation suivante :

$$t_z = \frac{1}{\lambda} \times \ln\left[\frac{(^{210}Pb^0_{ex})}{(^{210}Pb^z_{ex})}\right] \qquad (3)$$

Bien que l'hypothèse repose sur des conditions de bases qui semblent assez peu probables, on peut calculer un âge pour chaque horizon en utilisant l'équation précédente. Cependant ce modèle repose entièrement sur l'hypothèse que l'activité $(^{210}Pb)^0_{ex}$ mesurée dans la couche de surface est bien représentative de l'activité initiale.

> Le troisième modèle proposé par Appleby et Oldfield 1978, appelé CRS (Constant Rate of Supply) suppose que le flux de ^{210}Pb (*P0*) est constant mais que le taux de sédimentation (*W*) est variable au cours du temps. Ainsi, la concentration de ^{210}Pb diminue lorsque les apports de matière, et le taux de sédimentation, augmentent. Ce modèle définit l'activité accumulée *A(t)* (en mBq.cm^{-2}) durant un certain temps t correspondant à une profondeur z par l'équation suivante

$$A(t) = \int_0^t P(t).\partial t$$

En tenant compte de la décroissance de l'excès de ^{210}Pb au cours du temps, on peut en déduire *I*, "l'inventaire" de $^{210}Pb_{ex}$ sur toute la colonne sédimentaire grâce à la formule suivante

$$I = P_0 \int_0^\infty e^{-\lambda t} \partial t = \frac{P_0}{\lambda} = \sum_{z=0}^{\infty} (^{210}Pb)^z_{ex} m_z \qquad (4)$$

Ou $\sum_{z=0}^{\infty} (^{210}Pb)^z_{ex} m_z$, représente en pratique l'activité du ^{210}Pb en excès intégrée sur l'ensemble de la colonne sédimentaire, m_z étant la masse de sédiment sec dans la couche à la profondeur *z*. On peut également définir l'activité du ^{210}Pb en excès accumulée en dessous de la profondeur *z* par:

$$I_Z = P_0 \int_{t_z}^{\infty} e^{-\lambda t} \partial t = \frac{P_0}{\lambda} e^{-\lambda t} = \sum_{z=Z}^{\infty} (^{210}Pb)_{ex}^{z} M_z \qquad (5)$$

Avec $\sum_{z=Z}^{\infty} (^{210}Pb)_{ex}^{z} m_z$, représentant l'activité du ^{210}Pb en excès intégrée en dessous de la profondeur *Z*. On obtient ainsi, l'âge t_Z du sédiment à la profondeur $Z \leq z$ par la formule suivante :

$$\frac{I}{I_Z} = e^{-\lambda t} \qquad d'où, \quad t_Z = \frac{1}{\lambda} \ln\left(\frac{I_Z}{I}\right) \qquad soit : \qquad t_Z = \frac{1}{\lambda} \times \ln\left[\frac{\sum_{z=0}^{\infty} (^{210}Pb)_{ex}^{z} m_z}{\sum_{z=Z}^{\infty} (^{210}Pb)_{ex}^{z} m_z}\right] \qquad (6)$$

Cette méthode suppose une mesure de l'activité en ^{210}Pb pour toutes les profondeurs, afin de pouvoir calculer les différents termes de l'équation (6). Ce modèle d'âge paraît, dans sa formulation, le mieux adapté au système lagunaire étudié car il ne suppose pas de vitesse de sédimentation constante.

Ces trois modèles de datation sont appliqués au profil de ^{210}Pb de la carotte PB06 (*Figure 4.1*). Les résultats obtenus par ces trois modèles sont présentés dans la *Figure 4.2*. Sur cette figure nous avons également indiqué les datations obtenues par le ^{137}Cs à l'aide des pics de Tchernobyl (1986) et des essais nucléaires (1963) (*Figure 4.2*), méthode décrite dans l'article 3 (section 4.2.), ainsi que la position de la tempête de 1893, le sommet de cette couche étant à 33,5 cm.

Dans la *Figure 4.2* il y a une assez bonne adéquation entre le modèle CFCS considérant un taux d'accumulation constant de 0.088 ± 0.005 g.cm^{-2}.an^{-1} (ou 2.81 ± 0.15 mm.an^{-1}en tenant compte d'une DBD moyenne de 0.314 g.cm^{-2}), et les datations indépendantes (^{137}Cs, tempêtes de 1893) avec cependant un écart significatif pour le pic des essais nucléaires de 1963. Les modèles CIC et CRS s'écartent des autres méthodes de datation avec néanmoins une meilleure adéquation pour le modèle CRS dans la partie supérieure alors que le modèle CIC semble être plus juste pour la partie inférieure. Ces deux modèles supposant rendre compte des variations dans le taux de sédimentation (Boer *et al.*, 2006) suggèrent (1) que les variations du taux d'accumulation sont mineures et (2) qu'un processus perturbe le signal. Le milieu lagunaire étudié étant riche en mollusques et annélides (vers) on peut supposer que l'activité biologique (bioturbation) doit être prise en compte dans cette étude. Pour décrire

mathématiquement le comportement du ^{210}Pb le long d'une colonne sédimentaire soumise à de la bioturbation, nous pouvons utiliser des modèles biodiffusifs.

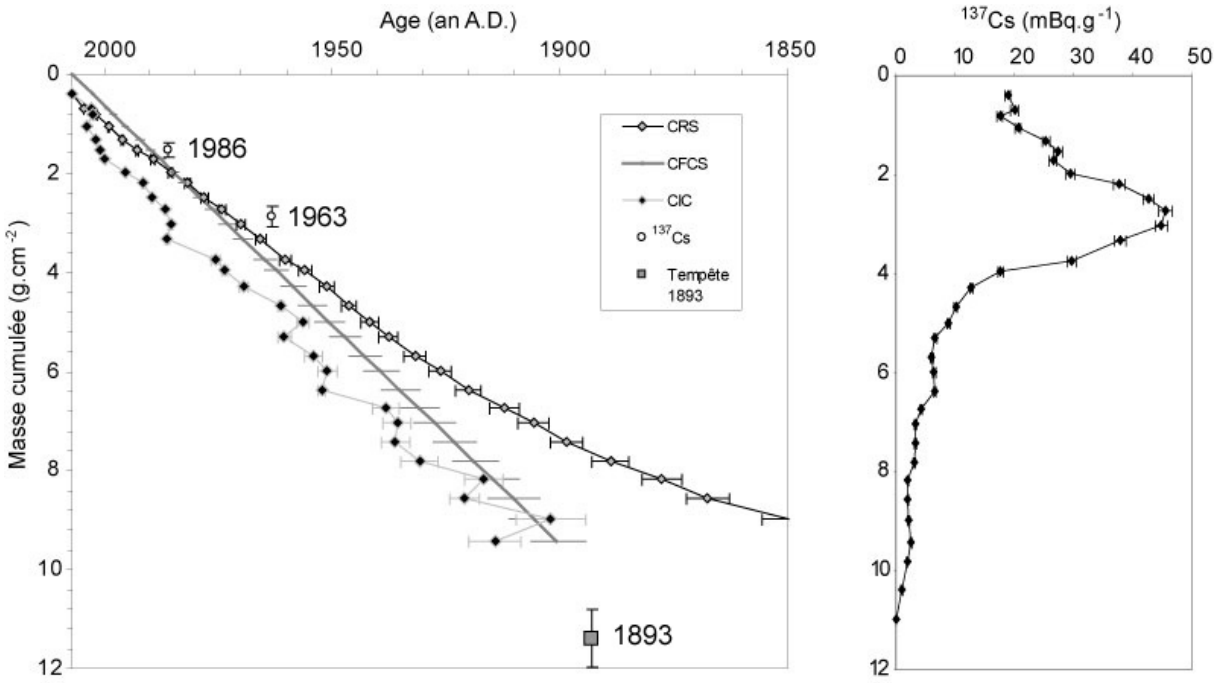

Figure 4.2 : A gauche : Résultats des différents modèles de datation par le ^{210}Pb appliqués à la carotte PB06. Sur cette figure est également représenté l'âge obtenu par la datation des deux pics de 1963 et 1986 de ^{137}Cs (définit par le profil de droite) ainsi que l'âge de la tempête de 1893.

4.1.2 Les modèles de bioturbation

> Dans un modèle simple de bioturbation, on peut considérer que l'activité biologique crée une homogénéisation des activités de ^{210}Pb en excès, notée $\left(\overline{^{210}Pb}\right)_{ex}$, dans les sédiments de surface jusqu'à une profondeur h où une masse M_h de sédiment sera bioturbée, soit :

$$\left(\overline{^{210}Pb}\right)_{ex} = \frac{1}{T}\int_0^T \left(^{210}Pb\right)_{ex}^0 e^{-\lambda t}\partial t = \frac{W}{M_h} \times \frac{\left(^{210}Pb\right)_{ex}^0}{\lambda}\left(1 - e^{-\lambda\frac{M_h}{W}}\right) \quad avec \quad T = \frac{M_z}{W} \qquad (7)$$

Alors qu'en dessous de cette profondeur *h* on peut écrire :

$$\left(^{210}Pb\right)_{ex} = \left(\overline{^{210}Pb}\right)_{ex} e^{-\lambda\frac{(M-M_h)}{W}} \qquad \text{avec} \quad 0 < M_h < M \qquad (8)$$

D'où (7) + (8) $$\left(^{210}Pb\right)_{ex} = \frac{W}{M_h \times \lambda}\left(^{210}Pb\right)^0_{ex} e^{-\lambda\frac{M}{W}}\left[e^{\lambda\frac{M_h}{W}} - 1\right]$$

Soit : $$\ln\left(^{210}Pb\right)_{ex} = -\frac{\lambda}{W}\cdot M + \ln\left[\frac{W}{M_h \times \lambda}\left(e^{\lambda\frac{M_h}{W}} - 1\right)\left(^{210}Pb\right)^0_{ex}\right] \qquad (9)$$

Dans l'équation (9) on remarque que la pente donne toujours la vitesse de sédimentation (*W*) malgré les perturbations liées à la bioturbation, mais que l'ordonnée à l'origine de la droite définie par les mesures au dessus de la profondeur h ne fournit pas directement le ($^{210}Pb^0_{ex}$). Cependant, une fois le taux de sédimentation calculé grâce à la pente de la droite on peut alors calculer, à partir de l'ordonnée à l'origine, le ^{210}Pb en excès initial au moment du dépôt, avant qu'il ne soit affecté par la bioturbation.

> L'application du modèle d'Advection-Diffusion (Bourdeau, 1986 ; Sharma *et al.*, 1987) sur les profils observés, permet de prendre en compte de façon plus complète la bioturbation afin de calculer un taux d'accumulation, mais aussi de déterminer la valeur des coefficients de mélange, c'est-à-dire le degré de perturbation des couches superficielles. Le modèle est décrit par l'équation suivante,

$$\frac{\partial A}{\partial t} = D_b \times \frac{\partial^2 A}{\partial z^2} - V \times \frac{\partial A}{\partial z} - \lambda \times A \qquad (10)$$

Avec D_b : coefficient de biodiffusion ($cm^2.y^{-1}$) et V : vitesses de sédimentation (en $cm.an^{-1}$), la résolution de cette équation (10) donne selon Lecroart *et al.*, (2007) :

$$D_b = \frac{\lambda z^2}{(\ln(A_0 / A_z))^2} - \frac{Vz}{\ln(A_0 / A_z)} \qquad (11)$$

Le profil de $^{210}Pb_{ex}$ de la carotte PB06 (*Figure 4.3*) présente une couche de surface de 3,5 cm (Surface Mixed Layer, S.M.L.) dans laquelle l'activité du $^{210}Pb_{ex}$ est perturbée. Le profil est donc composé d'une couche bioturbée en surface et d'une couche sous-jacente non mélangée. Dans la couche bioturbée, le profil de ^{210}Pb est issu de la combinaison entre le mélange et la sédimentation (V, D_b), alors que dans la couche sous-jacente, seule la sédimentation détermine le profil ($D_b=0$). La solution du modèle consiste à calculer le taux de sédimentation dans la couche non mélangée (profondeur > 3.5 cm) puis d'en déduire grâce à l'équation (11) le coefficient de biodiffusion. On obtient alors un couple (V, D_b) valable dans la couche mélangée de surface.

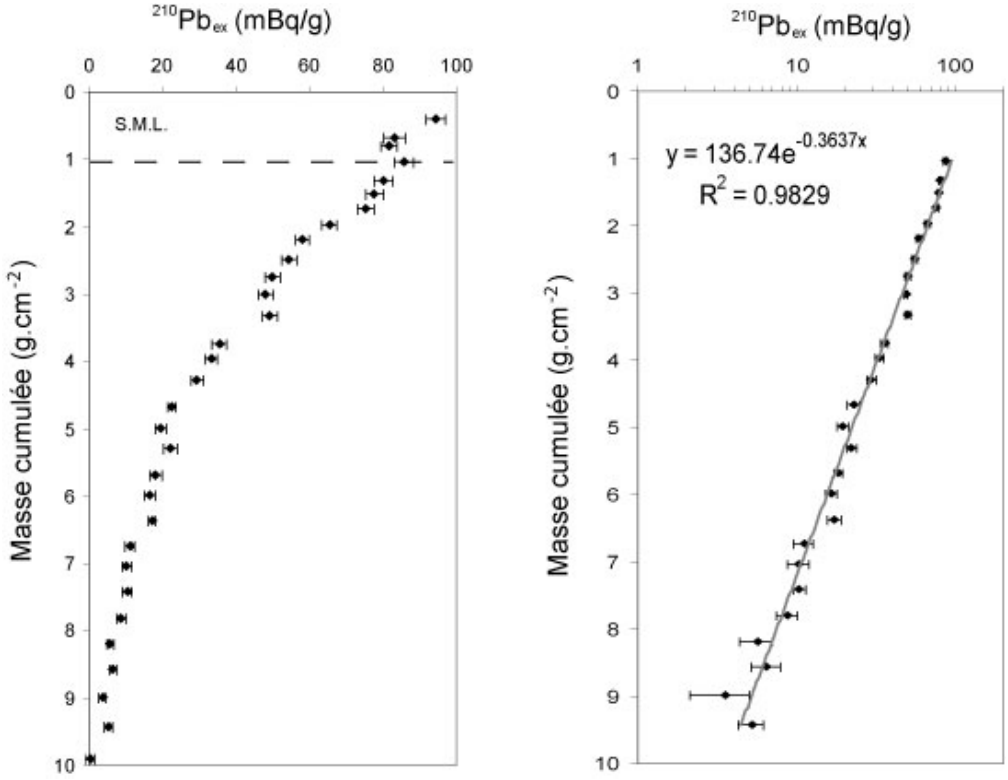

Figure 4.3 : A gauche : profil de $^{210}Pb_{ex}$ de la carotte PB06, mettant en évidence une couche de surface mélangée (S.M.L.). A droite : Application des modèles de bioturbation correspondant au modèle CFCS appliqué en dessous de la S.M.L.

La vitesse de sédimentation, déterminée par les modèles tenant compte de la bioturbation (grâce à l'équation (9) (correspondant au modèle CFCS appliqué aux couches au dessous de 3,5 cm) donne un taux de 0.085 ± 0.005 $g.cm^{-2}.an^{-1}$ avec un ^{210}Pb en excès initial, avant qu'il ne soit affecté par la bioturbation, estimé à 110 $mBq.g^{-1}$ (eq. 9) (*Figure 4.3*). Le modèle

d'advection-diffusion, décrit par l'équation (10) considère lui, une vitesse de sédimentation *V* constante.

Si les données de $(^{210}Pb)_{ex}$ sont reportées en fonction de la profondeur et non de la masse cumulée, on obtient une vitesse *V* de 2.66 ± 0.2 mm.an^{-1} (avec un coefficient de corrélation R^2=0.98). Cette vitesse permet de calculer avec l'équation (11) le coefficient de biodiffusion dans la couche supérieure est égal à 32 cm^2.an^{-1}, valeur en accord avec celles rencontrées dans ce type de milieu (résumé dans Lecroart et al., 2007). Cependant, une des critique que l'on peut apporter à ces modèles est la non prise en compte de la bioturbation liée aux diffuseurs à galerie (Nereis diversicolor). En effet l'activité de ces vers entraîne la chute ou le transport du sédiment de surface jusqu'à des profondeurs pouvant atteidre 20 à 25 cm (François *et al.*, 2002).

4.1.3 Discussions

Nous nous proposons dans cette discussion de comparer les âges obtenus à partir des modèles de ^{210}Pb incluant les effets de bioturbation et la chronologie basée sur le ^{137}Cs et la position de la tempête de 1893.

Le modèle CFCS suppose un flux constant de $^{210}Pb_{ex}$ (*P*, exprimé en mBq.cm^{-2}.an^{-1}) et un taux de sédimentation *W* constant (exprimé g.cm^{-2}.an^{-1}). L'activité *A* (mBq.g^{-1}) du ^{210}Pb en excès déposée dans le sédiment de surface est donc aussi supposée constante, puisque $A=P/W$. L'activité de ^{210}Pb en excès mesurée dans la carotte est alors décrite par l'équation (2). Cela se traduit, dans un diagramme en fonction de la masse de sédiment cumulée M_z à une profondeur *z* par une droite dont la pente est égale à $-\lambda/W$, permettant ainsi de calculer le taux de sédimentation *W*. C'est ce que nous avons fait dans la *Figure 4.3* et *Figure 4.4-1*.
Si la masse volumique apparente ρ (masse de sédiment sec par unité de volume, DBD) reste constante dans la carotte sédimentaire, on peut alors reporter les résultats de $^{210}Pb_{ex}$ en fonction de la profondeur, pour obtenir une vitesse de sédimentation *V* (exprimée par exemple en cm.an^{-1}). En effet $W=V.\rho$ et *V* est aussi constante dans le modèle CFCS où *W* est constant. Par contre, à cause de teneurs en eau (en partie liées à la compaction) et en éléments grossiers > 1 mm (en particulier des coquilles) très variables en fonction de la profondeur, il n'y a pas de proportionnalité directe entre la masse cumulée et la profondeur dans la carotte. Dans un

modèle où l'on considèrerait que *P* et *V* sont constants, mais que ρ varie, alors, puisque $P=A.V.\rho$, c'est le produit $A.\rho$ qui serait constant initialement, et qui varierait avec le temps et la profondeur dans la carotte. Le diagramme à utiliser serait alors $ln\{(^{210}Pb)^{z}_{ex}.\ \rho_z\} - z$. Si les données définissaient un bon alignement, la pente de la droite donnerait $-\lambda/V$ (*Figure 4.4-2*).

Si on reporte *ln(A)* en fonction de *z* dans le cas où ρ varie, pour en déduire une vitesse constante *V*, cela revient à considérer que l'activité initiale A_0 est constante au cours du temps, c'est-à-dire que le rapport P/ρ reste constant. Autrement dit, le flux de radioélément piégé est proportionnel à la masse volumique du sédiment donc, également, au taux d'accumulation en masse *W*, puisque *W* est proportionnel à ρ ($W=V.\rho$). Cette hypothèse est celle qui sous-tend le modèle CIC (Constant Initial Concentration). Les âges des différentes couches peuvent être déterminés en considérant la vitesse d'accumulation *V* déduite de la pente dans le diagramme logarithmique (*Figure 4.4-3*), ou calculés pour chaque profondeur à partir de l'équation (3). Notons que cette dernière technique n'est pas applicable si l'activité en surface a été perturbée et ne représente plus l'activité initiale supposée constante, ce qui se produit fréquemment dans le cas de bioturbation active.

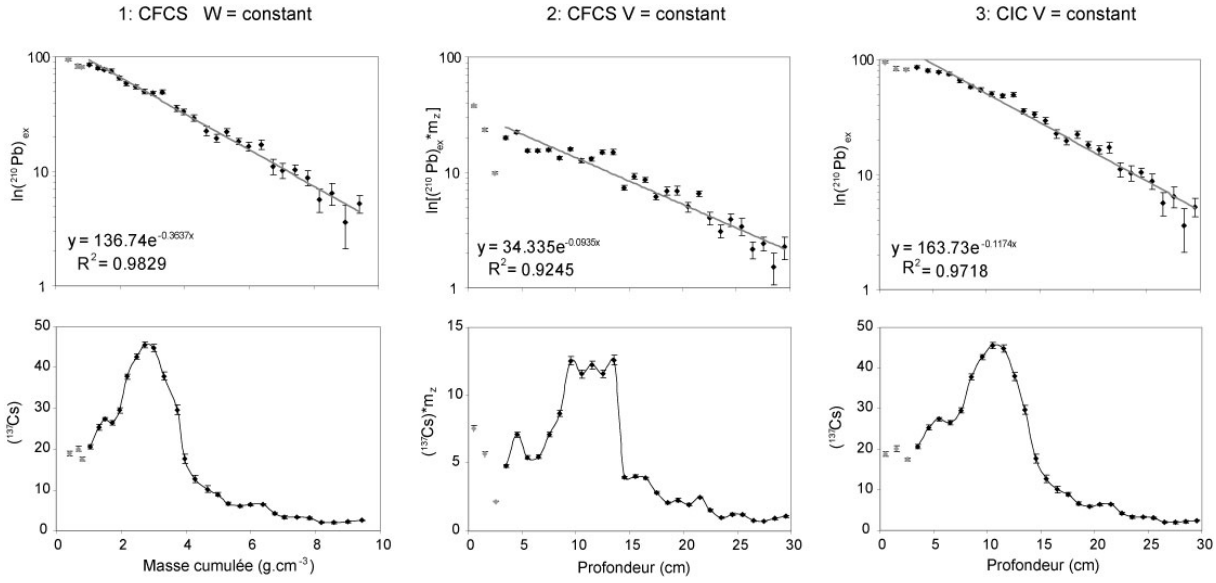

Figure 4.4 : 1 : modèle CFCS avec taux d'accumulation constant ; 2 : modèle CFCS avec vitesse de sédimentation constante ; 3 : modèle CIC avec vitesse de sédimentation constante. Les points gris correspondant à la zone bioturbée ne sont pas pris en compte dans les modèles.

Ces différents modèles dans le cas de la carotte PB06 sont illustrés dans la *Figure 4.4*, où sont reportées les données de $^{210}Pb_{ex}$ et de ^{137}Cs. Il est clair que le meilleur alignement dans le diagramme logarithmique est obtenu pour les modèles CFCS à *W* constant et CIC à *V* constante (*Figure 4.4-1 et -2*).

Si l'on compare les âges obtenus par ces deux modèles avec les âges des pics de ^{137}Cs et de la tempête de 1893, l'accord est meilleur pour le modèle CIC en fonction de la profondeur. L'écart observé entre l'âge calculé, en utilisant la masse cumulée, et le pic du ^{137}Cs censé correspondre à 1963 pose le problème de la validité de la chronologie par le ^{137}Cs. Il est bien connu que le ^{137}Cs peut diffuser dans la colonne sédimentaire après son dépôt, dans les milieux saumâtres ou marins. Ce phénomène peut se manifester par une migration de ^{137}Cs vers le bas de la carotte sédimentaire à des profondeurs correspondant à des âges bien antérieurs à l'apparition du ^{137}Cs atmosphérique (~1954), ce qui est le cas dans la carotte PB06 (Figure E), ou par un étalement du pic de ^{137}Cs vers le haut et le bas (Charmansson *et al.*, 1998 ; Cochran *et al.*, 1998 ; Radakovitch *et al.*, 1999 ; Bellucci *et al.*, 2007). Le coefficient de diffusion est estimé pour ce profil à $1.6*10^{-7}$ $cm^2.s^{-1}$, valeur en accord avec celle connue pour les milieux marins (Radakovitch *et al.*, 1999). Il n'est pas impossible que la migration de fluides interstitiels due à la compaction du sédiment entraîne un déplacement vers le haut du pic de ^{137}Cs, ce qui pourrait expliquer l'écart d'âge observé (*Figure 4.5-1*). Cependant ce processus ne semble pas avoir été clairement mis en évidence jusqu'ici.

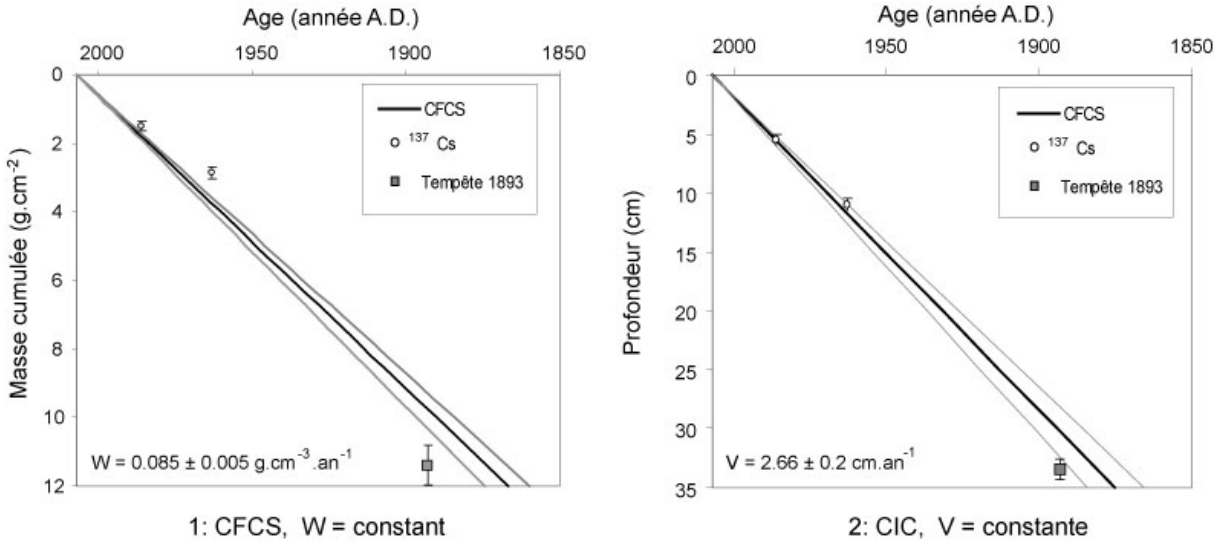

Figure 4.5 : Modèles d'âge de la carotte PB06 défini à l'aide des modèles de bioturbation, obtenu à gauche (1) avec la masse cumulée et à droite (2) avec la profondeur.

Si l'on fait confiance à la chronologie donnée par le ^{137}Cs et la position de la tempête de 1893, alors le modèle d'âge basé sur les profondeurs (*Figure 4.5-2*) est en très bonne adéquation avec cette chronologie. C'est la raison pour laquelle nous avons retenu ce modèle dans l'article qui suit (section 4.2).

4.1.4 Les "inventaires"

A partir de la somme de l'activité totale de $^{210}Pb_{ex}$ et de ^{137}Cs dans la carotte PB06 il est possible de réaliser des inventaires, qui correspondent à l'activité intégrée du ^{210}Pb en excès par unité de surface. Ces inventaires permettront de contraindre les différentes sources des radionucléides. Ils sont réalisés à partir de l'équation (4) généralisée à tous les radionucléides:

$$I = \sum_{z=0}^{\infty} \rho_z A_z \Delta z \qquad (12)$$

Avec pour une couche de sédiments à la profondeur z, ρ_z représentant la DBD (Dry Bulk Density) exprimée en g.cm^{-3}, Δz l'épaisseur de la couche analysée à la profondeur z et A_z l'activité (Bq.g^{-1}) du radionucléide dans la couche d'épaisseur Δz. Le calcul des inventaires respectifs du $^{210}Pb_{ex}$ et de ^{137}Cs donne 3251 ± 158 Bq.m^{-2} et 2084 ± 60 Bq.m^{-2}. On peut alors remonter au flux annuel P_0 du radionucléide étudié exprimé en Bq.m^{-2}.an^{-1}. Il est également possible d'obtenir ce flux à partir de l'activité de surface du sédiment A_0, si celle-ci a été calculée à partir des modèles tenant compte de la bioturbation.

$$I = \frac{P_0}{\lambda} \qquad et \qquad P_0 = A_0 \times W \qquad (13)$$

La valeur du flux atmosphérique de ^{210}Pb, calculée à partir de l'inventaire avec l'équation (13) est de 101 ± 5 Bq.m^{-2}.an^{-1} tandis que celle obtenue à partir du calcul de l'activité de surface (équation (9)) est de 95 ± 5 Bq.m^{-2}.an^{-1}. Ces valeurs sont en très bon accord avec la valeur moyenne estimée à environ 98 ± 10 Bq.m^{-2}.an^{-1} dans le Golfe du Lion (Heyraud et Cherry, 1983 ; Hussain *et al.*, 1990 ; Radakovitch *et al.*, 2003). Cette bonne adéquation, entre le flux atmosphérique de ^{210}Pb estimé dans le Golfe du Lion et celui calculé à partir de nos données,

suppose que tout le $^{210}Pb_{ex}$ présent dans notre zone d'étude provient exclusivement des retombées atmosphériques. Pour le ^{137}Cs, la somme des retombées totales est estimée à nos latitudes (entre 40 et 50° de latitude) par Charmasson *et al.*, (1998) à 2690 $Bq.m^{-2}$ pour la fin de 1990. Soit environ 1860 $Bq.m^{-2}$ après correction de la décroissance par rapport à la date de prélèvement de la carotte (début 2007) grâce à l'équation (1) appliquée au ^{137}Cs. Cependant les effets de l'accident de Tchernobyl ne sont pas homogènes et dépendent fortement des pluies locales au moment de l'accident. Ce qui explique certainement le petit écart entre la valeur calculée sur PB06 et celle estimée par Charmasson *et al.*, (1998). Ces faibles écarts entre les inventaires et les valeurs liés uniquement aux retombées atmosphériques, suggèrent que le ^{210}Pb en excès de la carotte PB06 provient presque exclusivement des apports atmosphériques directs et très peu des apports latéraux, c'est-à-dire du ^{210}Pb en excès fixé sur les particules sédimentaires avant leur dépôt dans la lagune.

4.2 L'Holocène : Article 3 : Radiocarbon

Holocene variation of radiocarbon reservoir ages in a Mediterranean lagonnal system

Sabatier, P.[*, 1], Dezileau, L.[1], Blanchemanche, P.[2], Siani, G.[3], Condomines, M.[1], Bentaleb, I.[4,5], Piquès, G. [2]

1 Université Montpellier 2, Geosciences Montpellier, CNRS/INSU, UMR 5243, Montpellier, France.
2 Université Montpellier 3, Laboratoire d'Archéologie des Sociétés Méditerranéennes, CNRS, UMR 5140, Lattes, France.
3 Université Paris-Sud, Laboratoire des Interactions et de la Dynamique des Environnements de Surface, CNRS/INSU UMR 8148 Orsay, France.
4 Université Montpellier 2, Institut des Sciences de l'Evolution de Montpellier, CNRS, UMR 5554, Montpellier, France.
5 Laboratoire des Sciences du Climat et de l'Environnement LSCE/IPSL UMR CNRS-CEA-UVSQ UMR 1572, Gif sur Yvette, France

Received March 2009, Received in revised from June 2009, Accepted July 2009
Radiocarbon accepted

Abstract

In order to obtain precise radiocarbon Holocene chronology in coastal areas it is necessary to estimate the modern ^{14}C reservoir age R(t) and its possible variations with time in relation to palaeoenvironmental changes. The modern reservoir ^{14}C age was estimated by comparing AMS ^{14}C ages of two recent mollusk shells found in sediment cores sampled in the Palavasian lagoonal system (South of France), with the ages derived from both ^{210}Pb and ^{137}Cs data and historical accounts of identifiable storm events. The calculated modern R(t) value of 943 ± 25 ^{14}C yr is around 600 yr higher than the global mean sea surface reservoir age. This high value, probably due to the relative isolation of the lagoon from marine inputs, is in good agreement with other R(t) estimates in Mediterranean lagoonal systems (Zoppi et al., 2001; Sabatier et al., 2008). ^{14}C ages were also obtained on a series of Holocene mollusk-shells sampled at different depths of the near 8m-long PB06 core. A careful examination of the ^{14}C ages vs depth relationships suggests that R(t) in the past was lower and similar to the value presently measured in the Golfe du Lion (618 ± 30 ^{14}C yr, Siani et al., 2000). The inferred change in R(t) from 618 to 943 yr is interpreted as the result of the final closure of the coastal lagoon by the sandy barrier, due to the along-shore sediment transfer.

Keywords: ^{14}C reservoir age, lagoon, Holocene, coastal area, ^{210}Pb, ^{137}Cs

1 Introduction

On the Holocene timescale, absolute chronology is usually based on Radiocarbon measurements providing a precise dating of carbonaceous samples and allowing accurate palaeoenvironmental and archaeological interpretations. However, when the ^{14}C method is applied to date samples equilibrated in marine or continental water masses, it requires a correction, called the reservoir age correction. While the correction for marine reservoir age is well established, many recent studies focused on climate record in coastal areas, which are strongly influenced by continental river inputs (Spennemann and Head, 1998; Oldfield et al., 2003; Dezileau et al., 2005; Sabatier et al., 2008; Sorrel et al., 2009). Indeed a sample from estuarine or lagoonal systems, could be affected by a reservoir age offset (R) due to a mixture between Marine Reservoir Effect (MRE) and Hard-Water Effect (HWE) (e.g. Little 1993). The reservoir age of the global mixed marine surface layer is a quantitative measure of the

offset between the activities of marine ^{14}C variations in response to atmospheric ^{14}C changes. It is induced by the significant lapse of time required for CO_2 exchange between the atmosphere and the ocean (i.e. to the long residence time of C in the ocean, compared to the ^{14}C half-life) (Stuiver et al., 1986; Stuiver and Braziunas, 1993). The HWE refers also to the dilution of ^{14}C activity in the marine reservoir by the influx of ^{14}C-free inorganic carbon originating from sub-aerial dissolution of old carbonate rocks (Spennemann and Head, 1998).
The pre-industrial global reservoir age is estimated at 405 ± 22 ^{14}C yr and the time dependent correction is available on MARINE04 calibration curve (Hughen et al., 2004). Several studies have suggested the possibility of significant deviations in regional marine reservoir signature from this average value (Ingram and Southon 1997; Goodfriend and Flessa 1997; Siani et al., 2001; Reimer and McCormac 2002; Southon et al. 2002; Fontugne et al., 2004). The reservoir age in coastal areas may also vary with time in relation with environmental changes, which would modify the respective proportion of marine and freshwater inputs. These changes include modification of river discharge rates and variation of marine inputs, due to the build up of a delta or to a change in the sandy barrier morphology. Some examples of lagoonal environment in the Mediterranean area show that R(t) is high and could vary between 600 to 1200 years (Zoppi et al., 2001; Sabatier et al., 2008 ; Court-Picon et al., submitted). These R(t) values can be estimated by comparing dated pre-industrial marine shells of known age or by comparison of the ^{14}C ages of lagoonal mollusks and the ages of the sediment derived from the $^{210}Pb/^{137}Cs$ methods or paleostorm events dated from historical accounts.
The latter method is applied in this study. This work is a part of the ECLICA project (Dezileau et al., 2005), one of the aims of which was to estimate the modern R(t) in a coastal lagoon of the Northwestern part of the Mediterranean basin and to understand the relation between palaeoenvironmental changes and variations in R(t). When appropriate R(t) corrections are applied, a precise and high-resolution chronology of the studied sediment core can be derived. It then provides valuable information on the relations between climate, sediment dynamics and the implications on human society, in an area inhabited since prehistoric times (Sabatier et al., 2010; Dezileau et al. submitted).

2 Location of the sampling site

This study focuses on the Palavasian lagoonal complex located to the West of the Rhône delta, in the central part of the Gulf of Lion, 10 km south of the city of Montpellier (South of France, *Figure 4.6*). These coastal wetlands are the result of the interaction between a process

of shore line regularization by migration of littoral barriers and filling of these areas by the fluvial and marine particulate inputs (Certain et al., 2004). This area consists of several small lagoons, with low water depth (<1m), limited to the South by a narrow sandy barrier and to the North by calcareous Mesozoic hills. Most of the sediments supplied to the area are carried during flash flood events by two short coastal rivers (Mosson and Lez). This wetland complex is now crossed by the artificial navigation channel built in the 18th century. In some places, the sandy barrier is less than 60 m wide and 3 m high above the mean sea level. This implies an extreme sensitivity to high energy events, enabling temporary but strong marine influence during storm events (Dezileau et al., 2005; Sabatier et al., 2008).

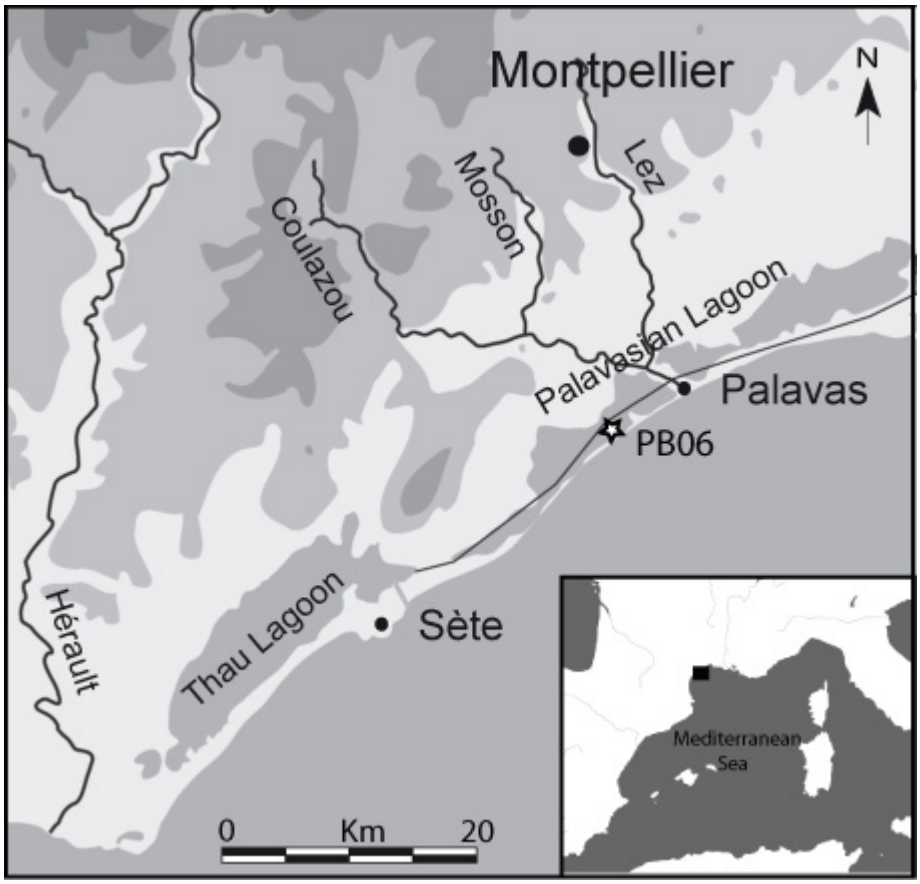

Figure 4.6: Map of the Western Mediterranean Sea and the central part of the Gulf of Lion (South of France) with the location of PB06 core sampled in Pierre Blanche Lagoon (part of the Palavasian Lagoonal Complex).

PB06 core is 7.9 meters long and was collected in Pierre Blanche Lagoon (PBL), in the southern part of the Palavasian lagoonal complex *(Figure 4.6*), in March 2006 with the Uwitec coring platform (University of Chambéry and Laboratoire des Sciences du Climat et

(espace à enlever) de l'Environnement). Twenty-eight lagoonal shells (*Cerastoderma Glaucum*, *Abra Ovata* and *Rissoa sp*.) were selected on PB06 core at different depths for ^{14}C age determinations. In addition, another shell recovered at 62 cm depth from a nearby core (PRO 15, sampled less than 100 m away from the PB06) was also dated.

3 Analytical methods

^{14}C analyses were conducted at the Laboratoire de Mesure ^{14}C (LMC14) on the ARTEMIS Accelerator Mass Spectrometry (Accélérateur pour la Recherche en sciences de la Terre, Environnement, Muséologie Installé à Saclay) in CEA Institute at Saclay (Atomic Energy Commission). These ^{14}C analyses were done with the standard procedure described by Tisnérat-Laborde et al., (2001). ^{14}C ages were converted to calendar years using the Calib 5.0.2 calibration program (Stuiver and Reimer, 1993; Hughen et al., 2004). X Ray Diffraction (XRD) analyses of shells were performed at the University of Montpellier 2 (Laboratoire de Mesures Physique).

On a centennial time-scale, dating of sedimentary layers was carried out with the ^{210}Pb and ^{137}Cs methods. Both nuclides together with U, Th and ^{226}Ra were determined by gamma spectrometry at the Géosciences Montpellier Laboratory (Montpellier, France). The 1 cm-thick sediment layers were washed in de-ionised water and sieved. The fraction smaller than 1 mm was then finely crushed after drying, and transferred into small gas-tight PETP (Polyethylene Terephtalate) tubes (having internal height and diameter of 38 and 14 mm respectively), and stored for more than 3 weeks to ensure equilibrium between ^{226}Ra and ^{222}Rn. The activities of the nuclides of interest were determined using a CANBERRA Ge-well detector, by comparison with the known activities of an in-house standard. Activities of ^{210}Pb were determined by integrating the area of the 46.5 keV photo-peak. ^{226}Ra activities were determined from the average of values derived from the 186.2 keV peak of ^{226}Ra and the peaks of its progeny in secular equilibrium ^{214}Pb (295 keV and 352 keV) and ^{214}Bi (609 keV). In each sample, the (^{210}Pb) (unsupported) excess activities were calculated by subtracting the (^{226}Ra) (supported) activity from the total (^{210}Pb) activity (note that, throughout this paper, parentheses denote activities). A self-absorption correction based on major element composition and sample density was systematically applied for all photo-peaks, using a modified version of the program written by J. Faïn (Pilleyre et al., 2006). The self-absorption corrections were rather small, even for the low energy peaks (less than 4%).

4 Results

Since Goldberg (1963) established for the first time the methodology based on ^{210}Pb chronology, this method has provided a very useful tool for dating recent sediments. Several ^{210}Pb models were later proposed, allowing a precise calculation of sedimentation rates (e.g. Appleby and Oldfield, 1992). In the simplest model, the initial $(^{210}Pb)_{ex}$ is assumed constant and thus $(^{210}Pb)_{ex}$ at any time is given by the radioactive decay law. In the CFCS ("constant flux, constant sedimentation rate") model (Goldberg, 1963; Krishnaswami et al., 1971), ^{210}Pb flux and sedimentation rate are assumed to be constant. The sedimentation rate in the Pierre Blanche lagoon is clearly variable due to the near-instantaneous sedimentation of sandy storm deposits; however the CFCS model can be applied when typical lagoonal conditions prevail (Sabatier et al., 2008). Using the CFCS model, the ^{210}Pb data indicate a sedimentation rate of 2.65 ± 0.2 mm.y^{-1} (Figure 4.7 and Table 4-1).

The most usual dating method based on ^{137}Cs data (Robbins and Edgington, 1975) assumes that the depth of the maximum ^{137}Cs activity in the sediment corresponds to the maximum atmospheric production in 1963. On the other hand the 1986 Chernobyl fallout is used to date most recent part of cores (Appleby et al., 1991). One of the Cs properties is its high mobility in marine sediments, with a preferential downward diffusive transport in pore-water (Radakovitch et al., 1999). Despite the potential Cs mobility by diffusive transport leading to the spreading of the Cs peak, we can see on the *Figure 4.7* that the ^{137}Cs profile shows a clear maximum corresponding to 1963. The ^{137}Cs activity depth profile thus gives an accumulation rate of 2.6 mm.y^{-1} and 3 mm.y^{-1} respectively for 1963 and 1986 depth (*Figure 4.7, Table 4-1*). These rates are in good agreement with ^{210}Pb data.

Conventional ^{14}C measurements performed on shells of the PB06 core result in model ages covering a time interval between 7600 B.P. to 1050 B.P.. The ^{14}C ages are expressed in *Table 4-2* as B.P. according to convention (Stuiver and Polach, 1977). The XRD analysis of the shells shows a >99% aragonite composition excluding any recrystallization process. These conventional ages display two inversions between 139 and 173 cm, and between 567 and 610 cm respectively. Moreover, a large age plateau is observed between 264 and 289 cm. The dated mollusks live within the first 5 cm of sediment. Therefore, bioturbation or mollusk habitat depth can not explain these inversions. This uncalibrated ^{14}C chronology adopted for core PB06 let us suppose important reservoir age fluctuations since the modern period, and/or variations in sedimentation rate.

Depth (cm)	Pb-210 (mBq/g)	Ra-226 (mBq/g)	Pb210ex (mBq/g)	Cs-137 (mBq/g)
0.5	113.49 ± 2.47	19.12 ± 0.32	94.38 ± 2.49	18.89 ± 0.53
1.5	102.50 ± 2.93	19.47 ± 0.43	83.03 ± 2.97	20.09 ± 0.68
2.5	101.23 ± 2.22	19.73 ± 0.20	81.50 ± 2.23	17.54 ± 0.45
3.5	104.61 ± 2.59	18.94 ± 0.26	85.67 ± 2.60	20.60 ± 0.56
4.5	99.11 ± 2.66	19.05 ± 0.23	80.06 ± 2.67	25.36 ± 0.64
5.5	99.47 ± 2.50	21.78 ± 0.25	77.68 ± 2.51	27.40 ± 0.70
6.5	97.17 ± 2.16	21.97 ± 0.23	75.20 ± 2.18	26.55 ± 0.67
7.5	83.06 ± 2.10	17.61 ± 0.23	65.45 ± 2.12	29.53 ± 0.75
8.5	76.28 ± 1.93	18.18 ± 0.22	58.10 ± 1.95	37.78 ± 0.93
9.5	72.25 ± 1.97	17.77 ± 0.22	54.48 ± 1.98	42.73 ± 1.04
10.5	66.90 ± 2.03	17.03 ± 0.22	49.87 ± 2.04	45.63 ± 1.11
11.5	65.30 ± 1.91	17.18 ± 0.21	48.12 ± 1.92	44.91 ± 1.09
12.5	65.68 ± 2.01	16.48 ± 0.22	49.20 ± 2.03	37.94 ± 0.93
13.5	55.60 ± 2.02	20.13 ± 0.42	35.47 ± 2.06	29.69 ± 0.82
14.5	49.23 ± 1.54	16.04 ± 0.19	33.20 ± 1.55	17.67 ± 0.46
15.5	48.99 ± 1.65	19.70 ± 0.22	29.28 ± 1.66	12.71 ± 0.36
16.5	41.71 ± 1.13	19.10 ± 0.21	22.61 ± 1.15	10.13 ± 0.27
17.5	39.20 ± 1.33	19.75 ± 0.28	19.45 ± 1.36	8.89 ± 0.31
18.5	39.27 ± 1.73	17.18 ± 0.24	22.09 ± 1.75	6.58 ± 0.24
19.5	35.32 ± 1.57	17.17 ± 0.33	18.15 ± 1.60	5.98 ± 0.32
20.5	36.13 ± 1.53	19.65 ± 0.32	16.48 ± 1.57	6.39 ± 0.32
21.5	35.16 ± 0.95	18.04 ± 0.18	17.13 ± 0.97	6.45 ± 0.19
22.5	31.08 ± 1.33	20.03 ± 0.30	11.05 ± 1.37	4.16 ± 0.23
23.5	29.00 ± 1.27	18.78 ± 0.28	10.22 ± 1.30	3.29 ± 0.21
24.5	28.83 ± 1.32	18.48 ± 0.32	10.35 ± 1.35	3.26 ± 0.24
25.5	28.18 ± 1.43	19.40 ± 0.33	8.78 ± 1.47	3.06 ± 0.24
26.5	22.58 ± 0.93	16.92 ± 0.20	5.67 ± 0.95	1.98 ± 0.11
27.5	22.22 ± 0.83	15.77 ± 0.20	6.45 ± 0.85	1.96 ± 0.11
28.5	24.57 ± 1.05	20.98 ± 0.23	3.58 ± 1.08	2.14 ± 0.16
29.5	26.08 ± 1.15	20.85 ± 0.23	5.23 ± 1.17	2.48 ± 0.20
30.5	21.84 ± 1.21	21.60 ± 0.30	0.24 ± 1.25	1.83 ± 0.18
34.5	20.88 ± 1.13	21.23 ± 0.28	-0.35 ± 1.16	0.94 ± 0.14

Table 4-1: Activities of radionuclides in PB06 core.

5 Discussion

5.1 Modern Reservoir age estimation

Compared to the average modern ^{14}C marine reservoir age (R(t)) of 405 ± 22 yr, the Mediterranean Sea ^{14}C reservoir age displays higher R(t) values with a deviance from the global mean sea surface reservoir age (ΔR) of 58 ± 85 yr. Its Western part presents a ΔR of 40 ± 15 yr (Siani et al., 2000; Reimer and McCormac 2002). For the central part of the Gulf

of Lion, Siani et al., (2000) found a higher ΔR estimated at 245 ± 30 yr (R(t) = 618 ± 30 ^{14}C yr), which is the average of 3 samples collected at Sète and Banyuls and recalculated by using Hughen's et al., (2004) calibration model. This offset from MARINE04 model has been explained as a result of biological processes or hard-water effects due to the discharge of coastal rivers after dissolution of limestone via several brackish lagoons, before reaching this part of the Mediterranean Sea.

Here we estimate the modern ^{14}C reservoir age in the Pierre Blanche Lagoon by comparing radiocarbon values with both historical events and ^{210}Pb and ^{137}Cs chronologies. Sabatier et al., (2008) and Dezileau et al., (submitted) recognised, in several cores, three main storm events related to events recorded in communal account in 1742, 1848 and 1893 A.D.

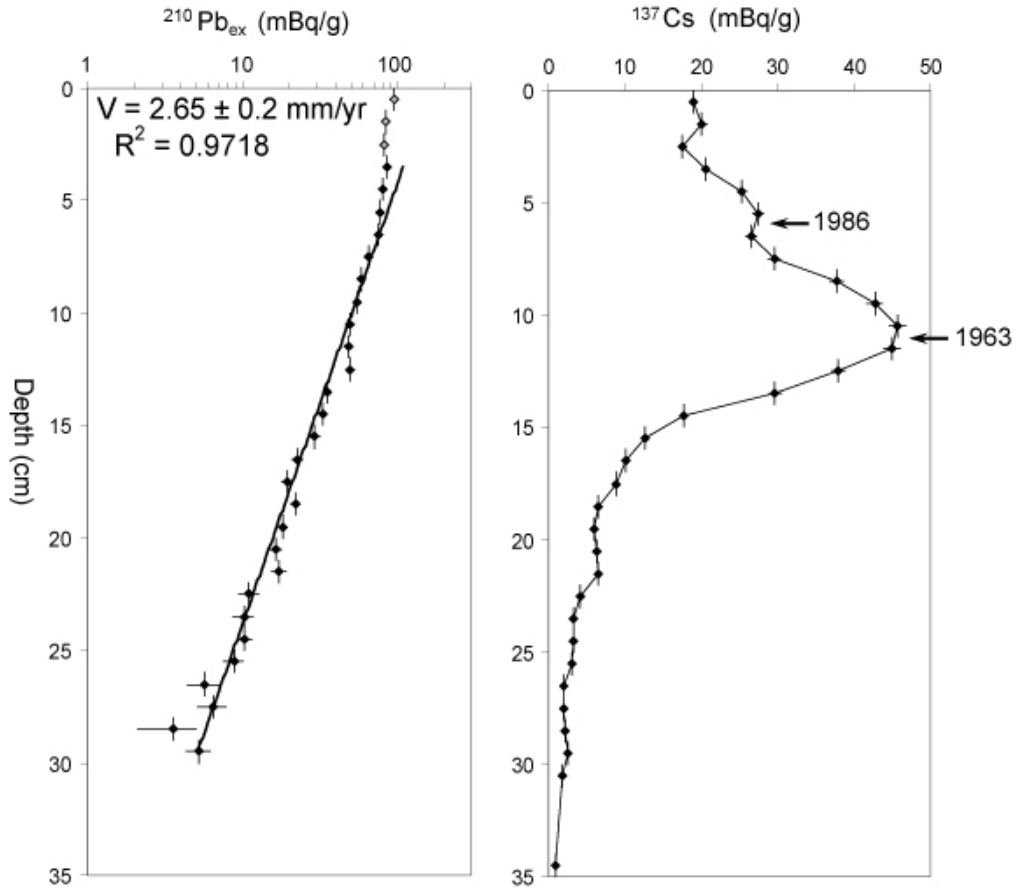

Figure 4.7: $^{210}Pb_{ex}$ and ^{137}Cs activity-depth profiles in cores PB06 from Pierre Blanche lagoon. ^{210}Pb excess disappears at around 30 cm, using the CFCS model the ^{210}Pb data indicates a sedimentation rate of 2.65 ± 0.2 mm.y^{-1}. The ^{137}Cs activity depth profile displays 2 peaks at 6 and 11 cm and gives an accumulation rate of 2.6 mm.y^{-1} and 3 mm.y^{-1} respectively for 1963 and 1986 depth.

Lab codes	Depth (cm)	Species	Conv. age BP	Marine04 (cal BP, 2σ)	Age Model 1 (cal BP, 2σ)	Age Model 2 (cal BP, 2σ)
SacA 6253	20	C. g.	1055 ± 30	551 - 673	0 - 149	0 - 149
SacA 6254	83	C. g.	1285 ± 30	745 - 907	255 - 430	255 - 430
SacA-10833	127	C. g.	1780 ± 30	1264 - 1389	644 - 818	644 - 818
SacA 6160	131	C. g.	1955 ± 30	1404 - 1597	776 - 989	776 - 989
SacA 10720	139	C. g.	2090 ± 30	1562 - 1771	929 - 1143	929 - 1143
SacA 6161	173	C. g.	1645 ± 30	1133 - 1277	531 - 674	842 - 1054
SacA 10834	199	C. g.	1820 ± 30	1283 - 1447	670 - 871	1029 - 1249
SacA 6162	225	C. g.	2100 ± 30	1578 - 1787	940 - 1157	1301 - 1505
SacA 10835	255	C. g.	2615 ± 30	2169 - 2365	1455 - 1696	1881 - 2113
SacA 6163	264	C. g.	3090 ± 35	2757 - 2959	2012 - 2290	2447 - 2726
SacA 10722	267	C. g.	2950 ± 30	2771 - 2794	1858 - 2094	2300 - 2572
SacA 10725	267	A. o.	3045 ± 30	2737 - 2895	1955 - 2243	2385 - 2691
SacA 6164	278	C. g.	3050 ± 30	2741 - 2903	1966 - 2253	2390 - 2695
SacA 10723	278	C. g.	3230 ± 30	2935 - 3165	2163 - 2429	2687 - 2855
SacA 10724	289	C. g.	3065 ± 30	2749 - 2920	1986 - 2268	2417 - 2708
SacA 6255	311	C. g.	3145 ± 30	2831 - 3045	2101 - 2319	2515 - 2760
SacA 6165	354	Ris.	3360 ± 30	3131 - 3331	2340 - 2618	2768 - 3021
SacA 6166	398	C. g.	3805 ± 30	3647 - 3846	2867 - 3150	3347 - 3562
SacA 6256	451	C. g.	4105 ± 30	4053 - 4279	3266 - 3493	3689 - 3949
SacA 6257	498	C. g.	4400 ± 30	4432 - 4678	3616 - 3861	4091 - 4373
SacA 6167	531	C. g.	5050 ± 30	5300 - 5484	4497 - 4786	4944 - 5258
SacA 6168	567	C. g.	4965 ± 35	5236 - 5434	4377 - 4653	4825 - 5123
SacA 6169	610	C. g.	5440 ± 35	5719 - 5901	4976 - 5275	5452 - 5648
SacA 6258	635	A. o.	5645 ± 30	5946 - 6159	5288 - 5509	5658 - 5883
SacA 6170	657	C. g.	5855 ± 35	6189 - 6360	5507 - 5721	5900 - 6148
SacA 6171	684	C. g.	2120 ± 60	1548 - 1852	926 - 1220	1282 - 1567
SacA 6260	710	A. o.	6220 ± 30	6568 - 6754	5906 - 6146	6286 - 6484
SacA 6259	744	A. o.	7175 ± 30	7569 - 7708	6966 - 7209	7354 - 7540
SacA 6261	758	A. o.	7600 ± 30	7976 - 8149	7417 - 7565	7711 - 7923

Table 4-2 : ^{14}C data for mollusk shells of cores POR 15 (one sample) and PB06. The ^{14}C ages are calibrated in the last two columns using the Marine04 calibration curve with different values of the reservoir age ΔR. They correspond to Figure 4.9b and c respectively. Age model 1 uses a constant ΔR of 605 ± 30 yr while age model 2 are calibrated with ΔR of 605 ± 30 yr for the upper 5 samples and with ΔR of 245 ± 30 yr (see text and Figure 4.9). Cerastoderma glaucum (C.g.), Abra ovata (A.o.), Rissoa ventricosa (Ris.)

In another core PRO15, collected less than 100 m away from the PB06 core, one shell (SacA 6270) was recovered at 62 cm depth, just above the 1848 A.D. event. This shell was dated at 1095 ± 30 ^{14}C yr (*Table 4-2*). On the other hand the youngest age on PB06 at 20.5 cm depth is 1055 ± 30 ^{14}C yr. This age corresponds to a date of 1930 ± 5 yrs A.D., derived from the ^{210}Pb

CFCS model ages and ^{137}Cs chronology (with an average sedimentation rate of 2.65 ± 0.2 $mm.y^{-1}$).

The estimation of the sea surface reservoir ^{14}C ages R(t) for the first modern shell SacA 6270, on core PRO15 was made by subtracting the atmospheric ^{14}C value estimated at the historical date 1848 A.D. (113 ± 9 ^{14}C yr by Reimer et al., 2004) from the measured apparent ^{14}C ages of the mollusks (1095 ± 30 ^{14}C yr, *Tableau 4-3, Figure 4.8*). This gives a R(t) value of 982 yrs. The deviance from the global mean reservoir age (ΔR) is then obtained by subtracting the marine model age value estimated at the historical date 1848 A.D. (485 ± 24 ^{14}C yr, Hughen et al., 2004), from the measured apparent ^{14}C age of the shell (1095 ± 30 ^{14}C yr, *Tableau 4-3, Figure 4.8*). ΔR value is thus estimated at 610 ± 40 yrs with the errors added in quadrature (*Figure 4.8*). By adopting a similar approach for shell (SacA 6253) on PB06 dated by ^{210}Pb and ^{137}Cs chronology at 1930 A.D. (*Tableau 4-3*) we obtain a R(t) = 903 ^{14}C yr (ΔR = 600 yr). These two dated shells suggest that, in the Pierre Blanche lagoon, the average reservoir age R(t) is 943 ± 25 ^{14}C yr, (ΔR = 605 ± 30 yr). This high R(t) value compared to the Mediterranean Sea in the studied area (R(t) = 618 ± 30 ^{14}C yr, Siani et al., (2000)) can be explained either by variable discharge of coastal rivers, after draining a watershed mostly composed of limestone, and/or by the non-permanent marine influence in relation to the lagoonal system.

Lab codes	Samples	Age of shells (yr AD)	^{14}C (BP)	Tree-ring ^{14}C (BP). InterCal04	R(t) (yr)	Model age Marine04	ΔR (yr)
SacA 6270	PRO15-60	1848	1095 ± 30	113 ± 9	982	485 ± 24	610
SacA 6253	PB06-20	1930	1055 ± 30	152 ± 7	903	454 ± 23	601

Tableau 4-3: ^{14}C dates of modern pre-bomb shell samples in PBL and their reservoir ages.

5.2 Reservoir age correction during the Holocene

In order to apply an accurate ΔR correction for ^{14}C dating of marine shells, it is necessary to estimate past R(t) fluctuations (Ingram and Southon 1997; Goodfriend and Flessa 1997; Siani et al., 2001; Reimer and McCormac 2002; Southon et al. 2002; Fontugne et al., 2004). The same precaution has to be taken in coastal areas especially when high R(t) variability may occur.

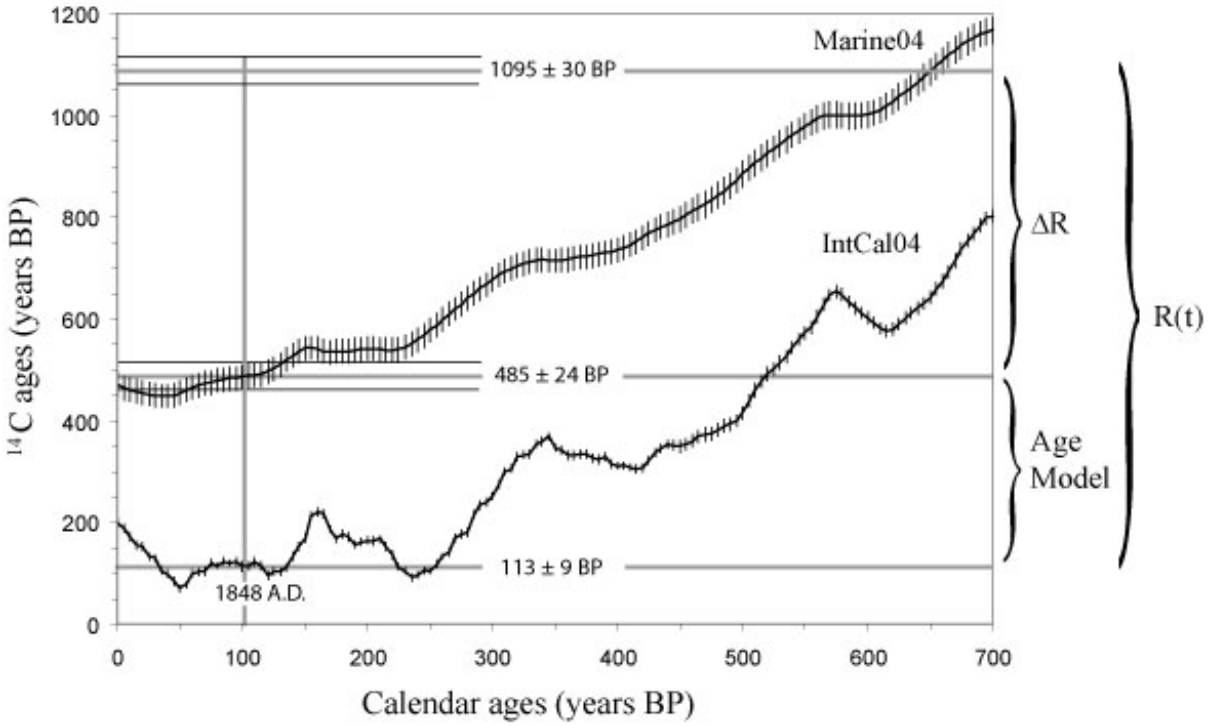

Figure 4.8: Conversion of the ^{14}C conventional ages into calendar ages for sub-aerial samples equilibrated with atmosphere (lower curve) and marine samples (upper curve). The age difference between the two curves for a given calendar date corresponds to the marine reservoir age R(t). The dating of the 1848 A. D. mollusk shell SacA 6270 found in core PRO 15 gives a conventional ^{14}C age of 1095 yr and thus a reservoir age of 1095 – 113 = 982 yr. The deviance from the global mean reservoir age (ΔR) for this same mollusk shell is obtained by subtracting the marine model age value estimated at the historical date, from the measured apparent ^{14}C age and gives 1095 – 485 = 610 yr.

Figure 4.9: Ages Models for PB06 core: Lithologic description, and (a) faunal depth distribution of Bittium recticulatum (marine species) and Hydrobia acuta (lagoonal species); (b) Age model 1 obtained on lagoonal mollusk shells (Table 4-2) with a ΔR of 605 ± 30 yr; (c) Age model 2 calculated with a ΔR of 605 ± 30 yr for the isolated lagoonal environment (since around 950 A. D.) and a ΔR of 245 ± 30 yr for the more open lagoonal environment (before 950 A. D.). PLC palaeoenvironmental evolution before and after the closure of the sandy barrier around 1000 yrs cal B.P.

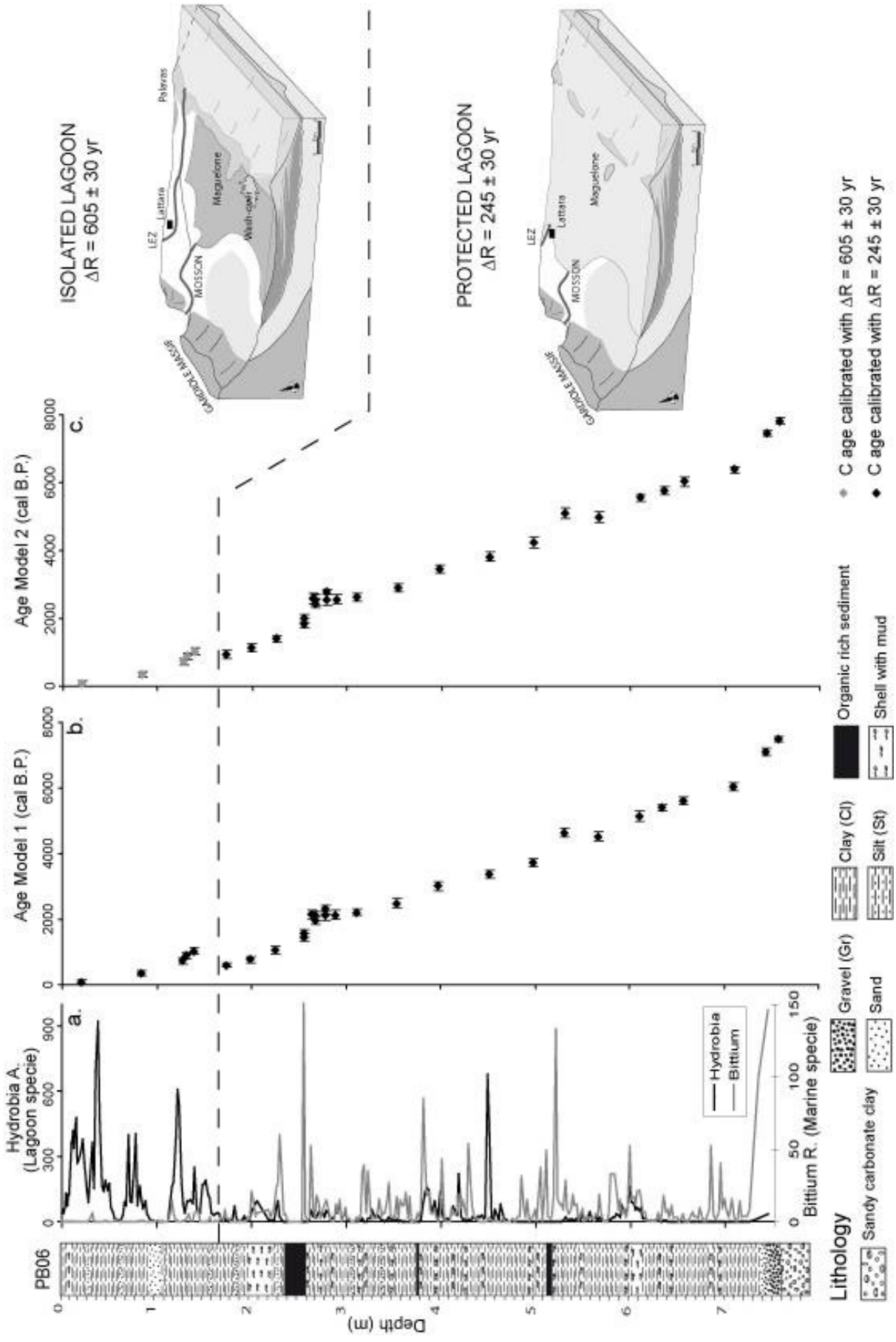
ISOLATED LAGOON
ΔR = 605 ± 30 yr
PROTECTED LAGOON
ΔR = 245 ± 30 yr
LEZ
Lattara
MOSSON
Maguelone
Palavas
CAMBROUE MASSIF
Wash-over
a.
b.
c.
PB06
Hydrobia A. (Lagoon specie)
Bittium R. (Marine specie)
Hydrobia
Bittium
Age Model 1 (cal B.P.)
Age Model 2 (cal B.P.)
Depth (m)
Lithology
Sandy carbonate clay
Gravel (Gr)
Sand
Clay (Cl)
Silt (St)
Organic rich sediment
Shell with mud
C age calibrated with ΔR = 605 ± 30 yr
C age calibrated with ΔR = 245 ± 30 yr

From a sedimentological point of view, the study of core PB06 (*Figure 4.9*) indicates a relative homogenous lagoonal deposit characterised by grey clays and silts with some sand layers (corresponding to paleostorm events). However the high-resolution stratigraphy of fauna indicates a clear shift in mollusk population between 190 and 170 cm (Sabatier et al., 2010) with an increase of lagoonal species (*Hydrobia acut*a), whereas the number of marine species (*Bittium recticulatum*) decreases (*Figure 4.9a*). These data suggest a variation in environmental conditions (salinity, temperature, nutriments, oxygen content). This change is interpreted as the result of the final closure of the coastal lagoon, by a sandy barrier due to the sediment transfer along the littoral. In this area the sandy barriers built up as the result of along-shore progradation of sand spits from inherited topographic highs, by East-West coastal drift carrying sand material from the Rhône river (Raynal et al., submitted). Therefore, the fauna content clearly shows a shift from a protected lagoon (with permanent inlet) to an isolated lagoon environment at around 170 cm core depth.

The correction of the reservoir age, as calculated above ($\Delta R = 605 \pm 30$ yr), was first applied to the whole ^{14}C data set in PB06 (*Table 4-2*) and defined the age model 1 displayed in *Figure 4.9b*. The results indicated the persistence of significant ^{14}C age inversions occurring between 130 cm and 200 cm along the core. By taking into account the mollusk fauna record, we can assume that apparent ^{14}C age inversions could be related to a change in R(t) between the two lagoonal palaeoenvironments (one open to the sea and the other one closed to the sea). Therefore, we suggest to correct ^{14}C ages with (1) $\Delta R = 245 \pm 30$ yr due to the local marine reservoir age, during a protected lagoon environment (similar to the value of 618 yr found for the Golfe du Lion by Siani et al. (2000), and (2) $\Delta R = 605 \pm 30$ yr when isolated lagoonal conditions prevailed. Therefore, the age model 2 presented in *Figure 4.9c* are calculated with a $\Delta R = 245 \pm 30$ yr for 173-758 cm and a $\Delta R = 605 \pm 30$ yr for the depth 0-139 cm. The very slight ^{14}C inversion (*Figure 4.9c*) between 139 cm (i.e., 1036 ± 107 yr cal B.P.) and 173 cm (i.e., 948 ± 106 yr cal B.P.) is within the uncertainties.

The ^{14}C chronology presented in *Figure 4.9c* displays between 250cm and 300cm the same ^{14}C age (between 2500 and 2600 yr cal BP). This apparent strong increase of sedimentation rate around 270cm is more probably the result of a ^{14}C age plateau. Indeed between 2350 and 2700 yr cal BP the calibration curve presents a ^{14}C age plateau, which is caused by a strong increase of ^{14}C production in the atmosphere at 2750 yr cal BP (Reimer et al., 2004), well known as the “Hallstatt disaster”. Another age inversion occurred at around 550 cm, between 4875 and 5275 yr cal BP and is probably also due to the increase of ^{14}C production in the

atmosphere around 5300 yr cal BP, a similar scenario previously observed during the "Hallstatt disaster".

In the Pierre Blanche lagoon, the final age model (age model 2) of PB06 core (*Figure 4.9c*) suggest a low sedimentation rate of 0.18 $mm.yr^{-1}$, at the base of the core. This rate increases from 1 $mm.yr^{-1}$ between 6385 to 948 ^{14}C yr to 2.72 $mm.y^{-1}$ over the last millennium, between 1036 ^{14}C yr to the present time. For the modern part of the core the accumulation rate is the same than that estimated through the ^{210}Pb and ^{137}Cs chronology (2.65 $mm.y^{-1}$).

5.3 R(t) comparison with other Mediterranean lagoons.

In the Northern part of the Venice lagoon, Zoppi et al., (2001) estimated a high R(t) value of about 1200 years by comparing benthic foraminifera and continental leaf at 1900 cal yr B.P. This area seems to be more isolated from the sea than the Pierre Blanche lagoon, with a strong input of freshwater which explains larger R(t) values. On the other hand, in the Thau lagoon (Figure 1) two radiocarbon dates were obtained in an archaeological site on continental seed (2935 ± 35 BP) and on a lagoonal shell (3535 ± 35 BP, *Cerastoderma glaucum*). The estimation of R(t) gives a value of 600 ± 50 ^{14}C yr (Court-Picon et al., submitted). Such an R(t) value is similar to that obtained by Siani et al., (2000) at Sète for the same species but for modern period (1907-1892 A.D. : R(t) = 618 ± 30 ^{14}C yr). This value, smaller than the modern value in the Pierre Blanche lagoon, is probably due to a strong marine water input through the large permanent inlet. These R(t) discrepancies between different Mediterranean lagoonal environments seem to be in good agreement with the system isolation state with an increase of R(t) when the lagoonal environment is less opened to the sea and more influenced by river inputs.

Conclusion

The modern ^{14}C reservoir age in the Pierre Blanche Lagoon was estimated by comparing radiocarbon ages of two mollusk shells, with the ages of the sediment layers derived from historical storm events and from the ^{210}Pb and ^{137}Cs chronologies. The high value found (943 ± 25 ^{14}C yr) compared to the average marine reservoir age results from a Hard-Water Effect explained by the discharge of coastal rivers and/or by the relative isolation of the lagoon from the sea. This interpretation is in good agreement with literature data reporting high R(t) values

for different Mediterranean lagoons, in variable isolation state (Venice, Thau). Our data further suggest that R(t) has probably changed with time, with an increase of more than 350 years, between the mid and late Holocene. This change most likely results from the final closure of the coastal lagoon with the growth of the sandy barrier. The age model of PB06 core indicate, a low sedimentation rate of 0.18 $mm.yr^{-1}$ between 7817 and 6385 ^{14}C yr, corresponding to the last stand of post glacial sea level rise. The sedimentation rate is then relatively constant at 1 $mm.yr^{-1}$ over the period of protected lagoonal environment (from 6385 to 948 ^{14}C yr), and it increases to 2.72 $mm.y^{-1}$ during the isolated lagoonal condition (from 1036 ^{14}C yr to the present time). This latter rate is in good agreement with the rate derived from ^{210}Pb and ^{137}Cs chronologies. This study confirms that a careful estimation of R(t) is necessary, when accurate radiocarbon ages are to be derived in high-resolution studies of coastal areas. This would avoid misinterpretation of archaeological or palaeoenvironmental data.

Acknowledgments

This research has been undertaken in the framework of the ECLICA Project financed by INSU (ACIFNS “Aléas et Changement Globaux”, coord.: L. Dezileau) and ARMILIT project (ANR n° NT_NV_27 / 2005, P. Blanchemanche). The Laboratoire de Mesure ^{14}C (LMC14) on ARTEMIS in CEA institute at Saclay (French Atomic Energy Commission) is thanked for the ^{14}C analyses (ECLICA and INTEMPERIES projects, coord. Dezileau). I. Bentaleb thanks the members of the “Paleocean” team, especially Fabien Dewilde, Elsa Cortijo and Elisabeth Michel for offering her their facilities during the academic sabbatical she spends at the CNRS-LSCE. Michel Fontugne (LSCE), and the members of the GLADYS platform (www.gladys-littoral.org), and of the ECLICA Project are also thanked for their constructive discussions during the course of this study. We are also grateful to J. Faïn (Université Blaise Pascal, Clermont-Ferrand) for allowing us to use his program for self-attenuation corrections in γ-ray spectrometry. This article benefited through constructive reviews by Paula Reimer.

5. Reconstitution Paléoenvironnementale

5.1 Article 4: Bulletin de la Société Géologique Française

Late-Holocene evolution of a coastal lagoon in the Gulf of Lions (South of France)

Sabatier P. [1], Dezileau L.[1], Barbier M.[1], Raynal O.[1], Lofi J.[1], Briqueu L.[1], Condomines M.[1], Bouchette F.[1], Certain R.[2], von Grafenstein U.[3], Jorda C.[4] and Blanchemanche P.[4]

1 Université Montpellier 2, Geosciences Montpellier, CNRS, UMR 5243.
2 Université de Perpignan, Institut de Modélisation et d'Analyse en Géo-Environnement Santé.
3 Laboratoire des Sciences du Climat et de l'Environnement, CNRS/CEA, Saclay.
4 Université Montpellier 3, Laboratoire d'Archéologie des Sociétés Méditerranéennes, CNRS, UMR 5140.

Received October 2008, Received in revised from February 2009, Accepted March 2009
Bulletin de la Société Géologique Française, in press

Abstract

The central part of the Gulf of Lions shoreline is characterized by many coastal wetlands that resulted from the interaction between a process of shoreline regularization by migrations of littoral barriers and a slow filling of the back-barrier areas by the riverine and marine inputs. Analyses of Late-Holocene deposits with a very high-resolution multi-proxy study of two sediment cores, allow us to reconstruct the evolution of this coastal system. Two main Holocene sediment units are identified overlying a Pliocene carbonate continental formation. The lower unit consists of sandy and pebbly marine sediments deposited around 7800 B.P., during the final stand of the last sea level rise. Just above, the upper unit displays lagoonal grey clay silts with shells and some intercalated layers of silty sands related to paleostorm events. The age model was established from radiocarbon dating, for the oldest part of the core. Over the last century, sedimentation rates were calculated using the CFCS ^{210}Pb model, together with ^{137}Cs data. Radiocarbon data show an increase in the accumulation rate from the base to the top of cores. Marine sand units related to the last transgressive deposit allow to refine the curve of Holocene post-glacial sea level rise. Sedimentological and faunal analyses associated with chronological data provide a means for reconstructing the Late-Holocene paleoenvironments along this part of the coast and suggest that the final closure of the coastal lagoon by the sandy barrier occurred at around 730 ± 120 yr cal B.P. The beginning of this closure, together with the progradation of the coastal plain, could be responsible for the decline in economic activity of the Lattara harbour during the Roman period.

Keywords: Coastal lagoon; Mediterranean sea; Sediment filling; ^{210}Pb; ^{14}C; Paleoenvironments; Gulf of Lions.

Abstract

La partie centrale du littoral du Golfe du Lions est caractérisée par de nombreuses lagunes qui résultent de l'interaction entre un processus de régularisation du trait de côte par migration de barrières littorales et d'un lent remplissage des zones situées en arrière de ce cordon par des apports continentaux et marins. Les analyses des dépôts tardi holocène avec une étude multi-traceurs à très hautes résolutions de deux carottes sédimentaires nous permet de reconstruire l'évolution de ce système côtier. Deux unités sédimentaires Holocène sont identifiées recouvrant une formation Pliocène carbonatée. L'unité inférieure est constituée de sables et de

galets d'origine marine déposés vers 7800 B.P., durant les stades ultimes de la dernière remontée marine. Au dessus, l'unité supérieure montre des dépôts d'argile et de silt gris coquillées d'origine lagunaire, intercalées de niveaux de sable silteux révélant la présence d'événements de tempêtes. Le model d'âge est établit à partir de dates radiocarbones pour les parties les plus anciennes des archives sédimentaires, tandis que pour le dernier siècle, les taux de sédimentations sont calculés en utilisant le modèle CFCS pour le ^{210}Pb, associé aux données de ^{137}Cs. Les données ^{14}C montrent une augmentation du taux d'accumulation depuis la base jusqu'en surface des carottes. Les unités de sables marins liées aux dépôts de la dernière transgression marine permettent de préciser la courbe post glaciaire de remontée du niveau marin. Les analyses sédimentologiques et faunistiques associées aux données chronologiques fournissent une méthode permettant de reconstituer les paléoenvironments littoraux tardi-Holocène dans la zone d'étude et suggèrent que la fermeture finale de ces lagunes, par le cordon sableux, survient autour de 730 ± 120 an cal B.P. Le début de cette fermeture associé à la progradation deltaïque pourrait être responsable du déclin des activités économiques du port de Lattara durant la période Romaine.

Mots clés: Lagune ; Mer Méditerranée ; Remplissage sédimentaire ; ^{210}Pb; ^{14}C; Paléoenvironnements ; Golfe du Lions

1. Introduction

High-resolution stratigraphy is an important tool in determining the distribution of Late quaternary sediments. In coastal areas, such a high-resolution approach is uncommon due to the relatively short time scales represented by modern deposits. In the Gulf of Lions (Western Mediterranean), the Holocene evolution of coastal environments has been strongly influenced by the extremely rapid relative sea-level rise before 7000 yr B.P. [10.6 mm/an from Aloisi et al., 1978] and the much slower rise since then [around 1 mm/an from Vella & Provansal, 2000]. The interplay between relative sea-level rise, decrease of erosion and of sediment transport by rivers has led to the development of coastal areas favouring the establishment of lagoon environments where it is possible to accumulate Holocene deposits [Mazzini et al., 1999].

The central part of the Gulf of Lions shoreline is characterized by many coastal wetlands with an actual fairly high accumulation rates [between 2,5 and 4 mm per year, Monna et al., 1995; Dezileau et al., 2005; Sabatier et al., 2008]. Such sedimentation rates allow the preservation

of an almost continuous record of lagoonal sedimentation over the last centuries, mainly characterized by silty clay with some intercalated marine sand layers. These sediments generally have a biogenic component (molluscs and plants), which characterizes the depositional environment. Mollusc fauna is usually abundant in lagoon depositional systems. Occurrence and distribution of this proxy is strongly linked to environmental parameters, such as water depth, salinity and type of substrate, and is very useful for interpreting the complexity of subenvironments that characterise wetland systems [Yum et al., 2003; Amorosi et al., 2005 ; Ricci Lucchi et al., 2006]. The aim of this study is to understand the link between sedimentary dynamics of the Palavasian wetland complex, located on the central part of the Gulf of Lions coastal area, and Holocene paleo-environmental evolution in relation to the sea level rise.

Holocene stratigraphy of these lagoons is based on a high resolution study of two several meter long cores. A set of shell radiocarbon data helped to constrain the evolution of the Holocene sedimentation rates in relation to the stratigraphy. In order to understand the actual filling modalities of these lagoons, ^{210}Pb models and ^{137}Cs depth-distribution profiles were used.

2. Study area

This study focuses on the Palavasian wetland complex located to the West of the Rhône delta, 10 km south of the city of Montpellier (*Figure 5.1*). This area consists of seven small lagoons, with shallow water depth, limited to the South by a narrow sandy barrier, attached from place to place to subdued rocky capes (Aresquier wood or Maguelone Church peninsula), and to the North by calcareous Mesozoic hills (Gardiole Mountain). Most of the sediments supplied to the area are carried during flash flood events by two short coastal rivers (Mosson, Lez). This wetland complex is now crossed by the artificial Rhône-Sète navigation channel constructed in 17th century. This study focuses on two lagoons, the Pierre Blanche and Arnel lagoons, located in the Southern and Northern part of this system (*Figure 5.1*), with water depths of 60 and 40 cm respectively.

This coastal area is characterized by a classical microtidal environment with maximal tide ranges < 50 cm. The annual significant wave height (Hs) and period (Tm), measured at the Sète station (located 10 km offshore, at a water depth of 32 m) are fair weather waves during 88% of the year (Hs=0.84 m; Tm=4.2 s). At the present time, there is only one small artificial connection between the Palavasian lagoons and the sea, in the eastern part (central part of

Prevost lagoon, *Figure 5.1*). However, in some places, the barrier is weak and highly sensitive to high energy events, enabling temporary but strong marine influence when the barrier breaks during storm events. This is commonly evidenced by traces of over-wash fans and ancient temporary inlets.

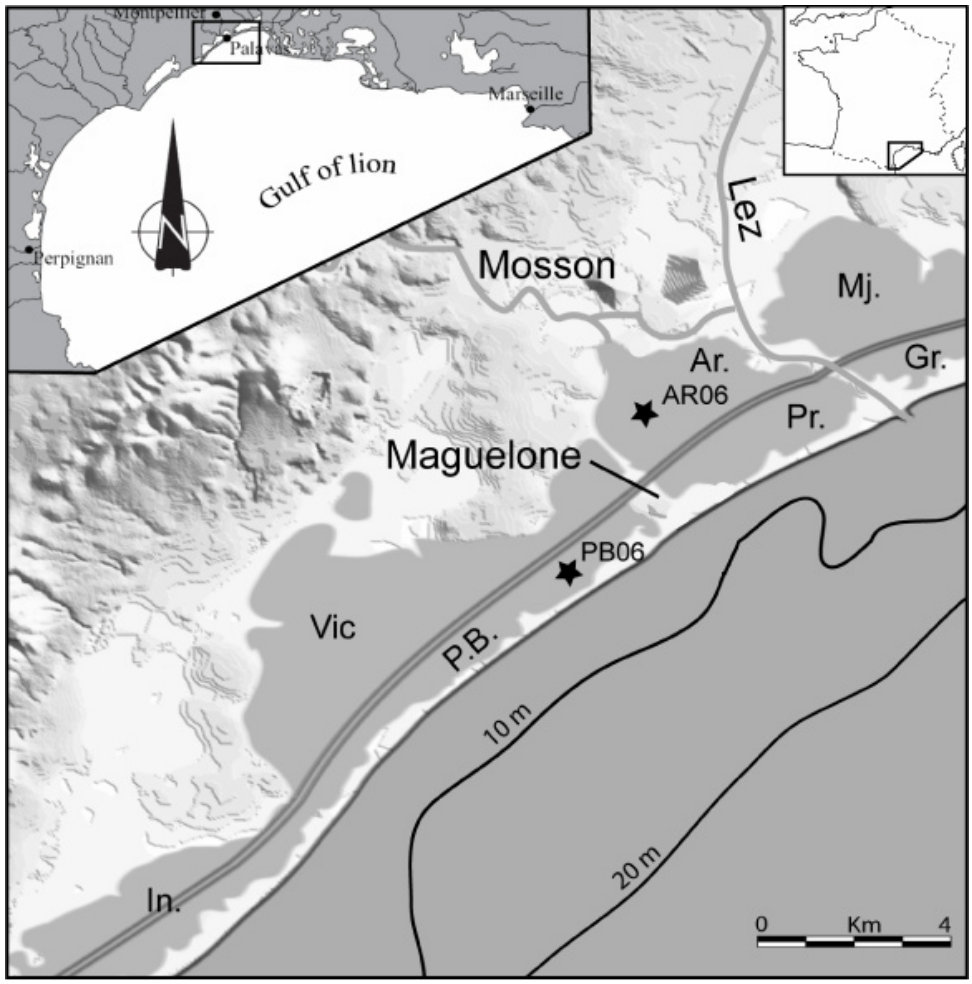

Figure 5.1 : Map of the Palavasian wetland complex, composed by seven lagoons (Mj: Méjan, Gr: Grec, Ar: Arnel, Pr: Prévost, Vic, PB: Pierre Blanche, In: Ingril) with the location of cores PB06 and AR06 (dark stars) used in this study.

Seismic data acquired during the CALAMAR IV cruise in the Vic Lagoon (*Figure 5.1*) illustrate the organisation of the deposits in this area, highlighting the various morphologies and stacking patterns related to the late Quaternary history of the coastal system [Raynal et al., 2009]. In the lower part of the sedimentary column, these authors described two distinct units interpreted as Pliocene in age (Upl). These units are topped by an irregular erosion surface. Above, a more recent unit is characterised by a seismic facies with horizontal parallel

continuous high-amplitude reflections that are typical of a low energy depositional environments and which correspond to quiescent mud accumulation [Tessier et al. 2000, Certain et al. 2004]. This unit is interpreted as the most recent, Holocene in age, depositional unit corresponding to the filling of the lagoonal system by river input [U3, Raynal et al., 2009]. Those Holocene deposits, from which the cores described in this study have been collected, constitute an interesting sedimentary archive allowing the restitution of the Holocene high-stand history of this system.

3. Sampling and analytical methods

Two piston cores (*Figure 5.1*) were collected in March 2006 in the Pierre Blanche (PB06) and Arnel (AR06) lagoons. These cores are 7.9 m and 3.6 m long respectively. They were sampled with the UWITEC© gravity coring platform (University of Chambery). This device consists of a 2 m transparent plastic liner mounted with an "orange-peel" core catcher. No compaction due to the coring system was observed. At the laboratory, cores were split, photographed, logged in detail (noting all physical and biogenic sedimentary structures and vertical facies successions), and divided into 1 cm vertical sections prior to analysis. Grain size and macro-fauna content analyses were performed on 2 cm long sections. To study mollusc shells, samples were sieved at 1mm and the number of individuals of all species was counted (every 2 cm). The most representative molluscs of lagoonal environments are *Hydrobia acuta*, *Abra ovata, Cerastoderma glaucum*. Those typical of marine hard substrate environment are *Bittium recticulatum* and *Rissoa ventricosa* [Dezileau et al., 2005; Sabatier et al. 2008]. Grain size distribution was determined using a Beckman Coulter© LS 13 320. Only the <150µm fraction was analysed due to the high concentration of shells fragments of a size exceeding 200 µm. Bulk sediments were first suspended in deionized water and gently shaken to achieve disaggregation. After introduction of sediment into the fluid module of the granulometer, ultrasounds were used to avoid particles flocculation.

Sediment geochronology for the modern period was determined by gamma spectrometry on a BEGe detector (CANBERRA BEGe 3825) for U and Th series nuclides and ^{137}Cs. We followed the analytical method described in Condomines et al. [1995] and Sabatier et al., [2008] and already tested on two short cores (PRO15 and PRO9) located at less than 100 meters from respectively PB06 and AR06 cores. In each sample, the ^{210}Pb (unsupported) excess activities were determined by subtracting the ^{226}Ra (supported) activity, determined through the ^{214}Pb and ^{214}Bi photopeaks, from the total ^{210}Pb activity. A self-absorption

correction based on major element composition and sample density was systematically applied for all photopeaks.

Shell samples were selected for ^{14}C age determinations. ^{14}C analyses were conducted at the Laboratoire de Mesure ^{14}C (LMC14) on the accelerator mass spectrometer (AMS) ARTEMIS in CEA institute at Saclay (Atomic Energy Commission) in the framework of the ECLICA and INTEMPERIES projects. ^{14}C ages were converted to calendar years using the Calib 5.0.2 calibration program [Hughen et al., 2004] at two standard deviations.

The compaction on 7.6 m of Holocene sediment on PB06 is estimated at 1.9 cm (0.25%) by an accepted decompaction algorithm established on deltaic sediment [Springer, 1993]. Although water content for lagoonal sediment is more important than deltaic sediment, we assumed that compaction is negligible in the sedimentation rate calculation.

4. Cores descriptions

Two cores were collected in the lagoonal system in order to characterize lithologies, determine sedimentary environments from primary structures and mollusc assemblages, and obtain chronostratigraphic constraints through radiocarbon dating. The top of these to cores corresponds to the present day lagoon sea-floor.

4.1. Sedimentary facies

Lithological description of core is based on grain size, sedimentary structure and fauna content. It allows to identify four distinct sedimentary facies interpreted in term of depositional environments (*Figure 5.2*).

- L Facies (LF): grey clays and silts with a grain size median around 10 µm. It contains lagoonal shells (*Hydrobia acuta*, *Abra ovata*, *Cerastoderma glaucum*) and some seeds of *Ruppia maritima* (an aquatic lagoonal plant). This fine sediment is locally laminated (less than 5% of the whole core) and can present continental plant fragments and traces of organic matter. L Facies is typical of a low energy environment and is interpreted as typical lagoonal deposit.
- S Facies (SF) : grey fine sands to silts with a grain size median between 70 to 30 µm with some marine shells (*Bittium recticulatum*, *Rissoa ventricosa*). The thickness of these deposits varies from 1 to 15 cm, the thickest layers showing a basal erosional surface. SF characterizes

relatively high energy deposits and is interpreted as back-barrier wash-over deposits created during storm events.

- M Facies (MF): grey clays and silts with many large molluscs (mostly *Cerastoderma glaucum* of 1-5 cm) recovered in living position. MF could be interpreted as lagoonal deposits with low sedimentation rate or high biogenic productivity.

- T Facies (TF): heterometric conglomerate with centimetric pebbles of quartz and limestone mixed with sands in its upper part. The base of this layer presents a sharp erosive surface. The sand is mostly constituted by shell fragments with some large marine shells (*Pectinidae, Hexaplex trunculus, Bittium recticulatum*). TF is interpreted as transgressive deposits (see part 6.1).

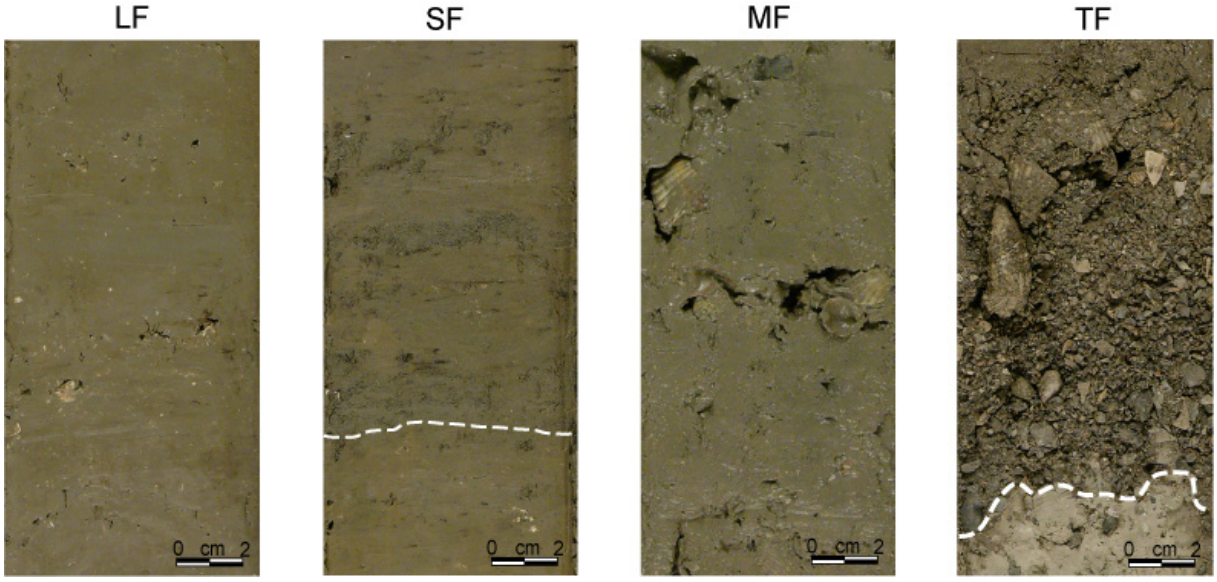

Figure 5.2 : Core photography illustrating the different sedimentary facies identified in the Palavasian wetland complex. (LF): grey clays and silts are typical of a low energy environment; (SF): grey fine sands to silts characterizes relatively high energy deposits; (MF): grey clays and silts with many large molluscs; (TF): heterometric conglomerate mixed in its upper part with sand. Note the sharp erosive surface at the base of TF. This facies is characterized by a very high energy deposits.

4.2. Core PB06

At the base, core PB06 (Fig. 3) displays white clay with chalky limestone nodules interpreted as Pliocene deposits by correlation with the lacustrine Pliocene deposits outcropping onshore

at the Aresquiers (Fig. 1). These deposits are crosscut at the top by an erosional surface. Just above, we observed 20 cm of TF. Then, the core displays a long interval of L-type facies interrupted by several cm-thick levels MF (e.g. at 210 and 610 cm). Some organic-rich levels containing plant fragments with no shells are observed at 515, 377 and from 240 to 260 cm; moreover seeds of a lagoonal plant were found in the upper part of this core at 109 and 134 cm. We observed also the occurrence of cm-thick high energy sedimentation layers of marine origin (SF, e.g. at 30, 100, 185, 340, 520 cm deep). This coarse material represents less than 10% of the total sedimentation along the core.

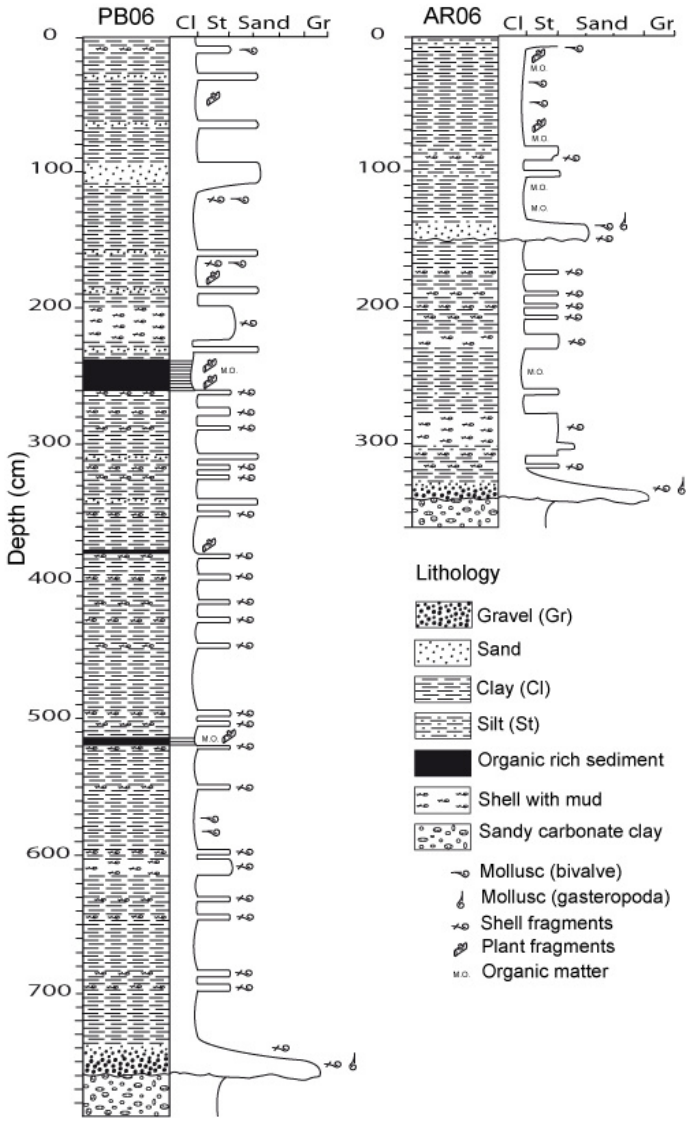

Figure 5.3 : Lithologic descriptions of PB06 and AR06 cores (positions in Figure 5.1).

4.3. Core AR06

Sedimentary succession in core AR06 (*Figure 5.3*) is very similar to the one observed in PB06. The Pliocene substratum is reached at 340 cm, beneath an erosional surface. It is covered by a 15 cm thick layer of TF. From 335 cm to the top, the core consists of grey clays and silts (LF) interrupted by bioclastics (MF, at 90, 230, 290 cm), fine sand layers (SF at 80, 150, 280 cm) and traces of organic matter. An important erosion surface is observed at 150 cm with the presence of marine shells.

5 Chronology

5.1 210Pb and 137Cs dating

Goldberg [1963] established the methodology based on ^{210}Pb chronology. Many ^{210}Pb models have successively been proposed, allowing the calculation of sedimentation rates. In the simplest model, the initial excess of ^{210}Pb activity ($^{210}Pb_{ex}$) is assumed constant and thus ($^{210}Pb_{ex}$) at any time is given by the radioactive decay law [Appleby & Oldfield, 1992; Noller, 2000]. In the CFCS (for Constant Flux, Constant Sedimentation rate) model [Goldberg, 1963; Krishnaswami et al., 1971], ^{210}Pb flux and sedimentation rate are assumed to be constant. In this study, we can apply such a model when typical lagoonal conditions prevail [Sabatier et al., 2008].

Concerning the ^{137}Cs chronology, the most usual dating method based on ^{137}Cs data [Robbins & Edgington, 1975] assumes that the depth of the maximum ^{137}Cs activity in the sediment corresponds to the 1963 maximum atmospheric production. However, one of the Cs properties is its high mobility in marine sediments, with a preferential downward diffusive transport in pore-water [Charmasson et al., 1998; Radakovitch et al., 1999]. In spite of this potential mobility, it was possible to date sediment because when a diffusive transport occurs it only results in the spreading of the Cs peak, while its maximum remains at the same depth.

The ^{210}Pb and ^{137}Cs chronology were determined on two short cores (PRO15 and PRO9) collected in the Pierre Blanche and Arnel lagoons at less than 100 meters from PB06 and AR06 respectively. For core PRO15 (Pierre Blanche lagoon), the ^{210}Pb and ^{137}Cs chronologies are in good agreement and give an accumulation rate of 4.2 ± 0.7 and 4.4 mm.y^{-1} respectively (*Figure 5.4*). On core PRO9 (Arnel lagoon), ^{210}Pb and ^{137}Cs activity depth profiles have the same shape with a typical surface mixing layer (0-4 cm) following by a rapid decrease (4-10 cm) and by an excess of ^{210}Pb until at least 22 cm depth. The discrepancy between the two

cores may be related to the depositional environments. Indeed, the Arnel lagoon, with a water depth < 40 cm is characterised by an important population of molluscs (*Cerastoderma Glaucum*, *Abra Ovata*) and polychaete (*Nereis diversicolor*) while the Pierre Blanche lagoon (core PRO15) , a little deeper, contains fewer molluscs. Thus, we suggest that in the Arnel lagoon, the ^{210}Pb and ^{137}Cs profiles may have been mainly controlled either by bioturbation processes with advection-diffusion in the upper first centimetres and gallery-diffusion in the deepest parts [François et al., 2002], and/or by reworking processes by bottom currents during strong wind periods. Thus, the ^{210}Pb and ^{137}Cs profiles do not permit to estimate a sedimentation rate into the Arnel lagoon for the modern period.

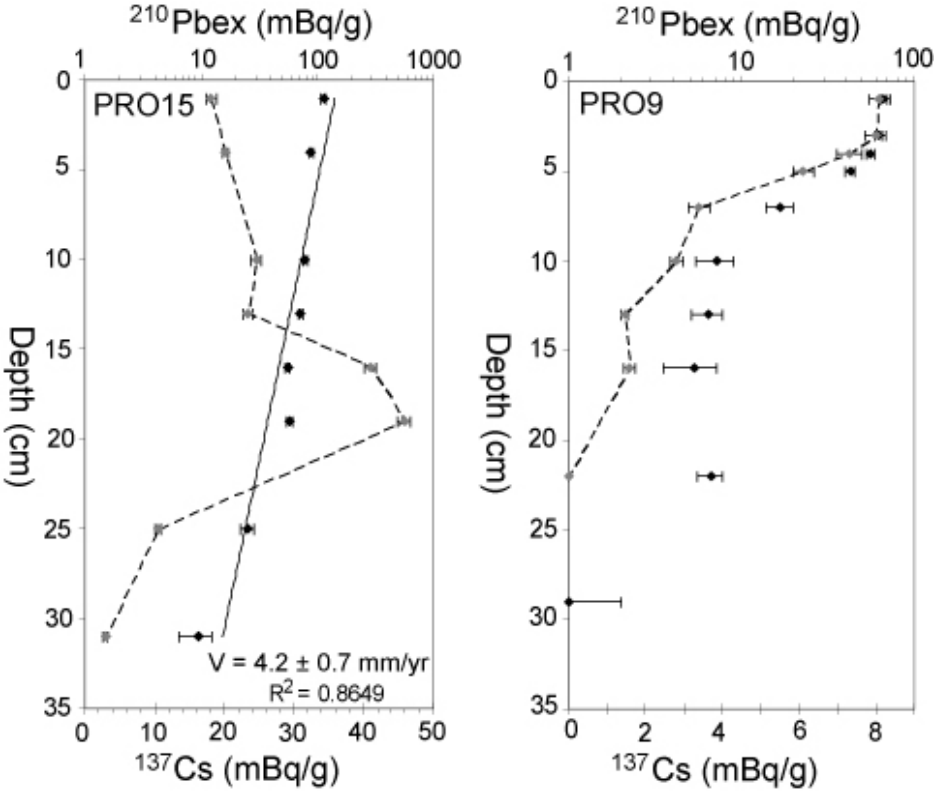

Figure 5.4 : 210Pb excess activity and 137Cs activity versus depth for cores PRO15 (left) and PRO9 (right), located in Pierre Blanche and Arnel Lagoon respectively.

5.2 Radiocarbon chronology

In this study 18 lagoonal molluscs (Bivalves *Cerastoderma Glaucum* and *Abra Ovata*) were collected from PB06 (11 samples) and from AR06 (7 samples). Results are reported in *Tableau 5-1* and *Figure 5.5*. The ^{14}C ages, reservoir ages (R(t)) and deviations from modelled

marine reservoir ages in response to local oceanic conditions (ΔR) are expressed in yr cal. B.P.

Cores	Depth (cm)	Species	^{14}C Age BP	Age cal BP R(t)=600±50	Age cal BP R(t)=1000±50
PB06	20	Cerastoderma sp.	1055 ± 30	450 ± 115	115 ± 115
	83	Cerastoderma sp.	1285 ± 30	640 ± 105	350 ± 125
	173	Cerastoderma sp.	1645 ± 30	1015 ± 135	610 ± 95
	225	Cerastoderma sp.	2100 ± 30	1445 ± 135	1055 ± 135
	311	Cerastoderma sp.	3145 ± 30	2695 ± 160	2200 ± 140
	398	Cerastoderma sp.	3805 ± 30	3505 ± 145	3020 ± 175
	498	Cerastoderma sp.	4400 ± 30	4270 ± 170	3740 ± 160
	610	Cerastoderma sp.	5440 ± 35	5595 ± 130	5125 ± 170
	710	Abra sp.	6220 ± 30	6440 ± 145	6035 ± 140
	744	Abra sp.	7175 ± 30	7475 ± 100	7090 ± 100
	758	Abra sp.	7600 ± 30	7850 ± 125	/
AR06	68	Cerastoderma sp	2185 ± 30	1540 ± 150	1135 ± 130
	136	Cerastoderma sp	1950 ± 30	1185 ± 120	885 ± 140
	159	Cerastoderma sp	3185 ± 30	2785 ± 135	2260 ± 155
	230	Cerastoderma sp	3425 ± 30	3040 ± 175	2550 ± 165
	283	Cerastoderma sp	3735 ± 30	3435 ± 145	2925 ± 160
	332	Cerastoderma sp	4995 ± 30	5075 ± 185	4570 ± 165
	335	Cerastoderma sp	5675 ± 30	5845 ± 140	/

Tableau 5-1 : Radiocarbon ages for PB06 and AR06 cores. Marine calibration with reservoir age R(t)=600±50 yr (Siani et al., 2000) has been performed with Calib 5.0.2 program at 2σ (Hughens et al., 2004) and marine calibration with R(t)=1000±50 yr (Sabatier et al., 2008).

To date the shells with accuracy, we need to have an estimation of reservoir age R(t). In the Mediterranean Sea, the average reservoir age for the modern period R(t0), over the considered time interval (1830–1950 AD), is calculated by Siani et al, [2000] at 420±110 yr. However, these authors find a higher reservoir age at around R(t)=600 ± 50 yr (ΔR=200 yr) for the Gulf of Lions area. This discrepancy can be explained as a result of biological processes or hardwater effects due to the discharge of coastal rivers after draining through limestones via several brackish lagoons, before reaching the Mediterranean Sea [Siani et al., 2000; Zoppi et al., 2001].

Based on a comparison between a radiocarbon age of 1055 ^{14}C yr BP at 20 cm depth, and the age derived from ^{210}Pb and ^{137}Cs profiles converted to ^{14}C atmospheric age, Sabatier et al. [2008] estimated at 1000 yrs the ^{14}C reservoir age (ΔR=600 yr) in the studied lagoonal system. This estimation was made just for the upper part of the PB06 core and may be different for the rest of the Holocene, since the lagoon was not totally isolated from the sea

during sediment deposition. Nevertheless, we assume that, whatever the deviation from the modelled marine reservoir ages is, it does not play a major role in the calculation of the Holocene average sedimentation rate. Two dates were calibrated with the ΔR=200 yr because those dating have been performed on shells that were samples in marine sand, at the bottom of the two cores.

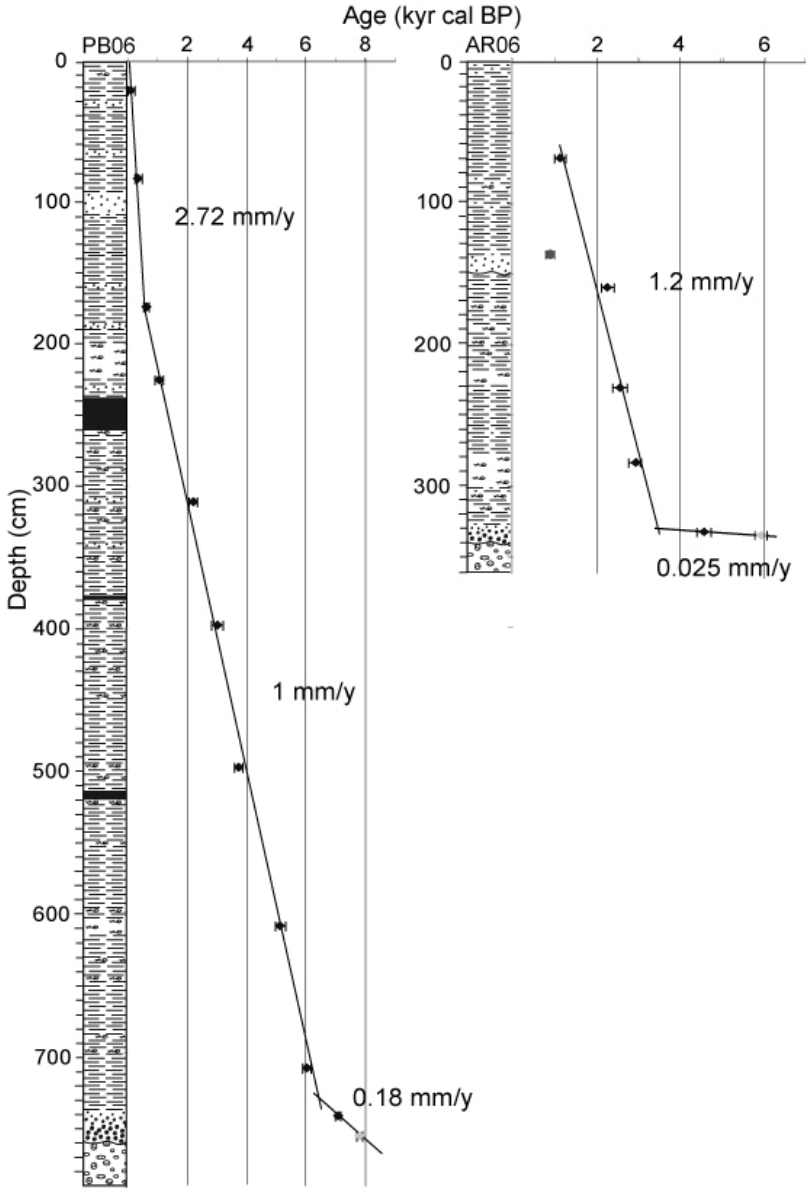

Figure 5.5 : Simplified lithologic description of PB06 and AR06 with 14C age vs. depth. Average accumulation rates are calculated through linear regression. The light grey points were calibrated with a marine reservoir age (R(t) = 600 ± 50 yr). Uncertainty is included within the symbols. The date AR06-138 is excluded from the sedimentation rate calculation.

Considering the age profile along the cores, based on the radiocarbon data, an inversion appears in core AR06 around 136 cm, corresponding to a dating performed on a bivalve shell of marine origin (see AR06-136 in *Tableau 5-1* and *Figure 5.5*). At this depth, we observed a 15 cm-thick marine sand layer. A possible explanation might thus be related to the diminution of the R(t) of this shell, probably link to marine conditions when those sands deposited.
In order to estimate the Holocene average sedimentation rate from ^{14}C data, it was chosen to interpolate linearly between all the accepted ages, centred on the 2σ age range. The accumulation rates on the figure 5 represent the age/depth relationship defined for each one of the best-fit lines, its illustrates some major changes in sedimentation rate. In the Pierre Blanche lagoon, core PB06 shows, at the base, a low sedimentation rate of 0.18 $mm.y^{-1}$. Then this rate increases from 1 $mm.y^{-1}$ between 700 and 170 cm to 2.72 $mm.y^{-1}$ over the last millennium, between 170 and 20 cm. In the Arnel lagoon, AR06 core shows, in the deepest part, a negligible accumulation rate. Then when lagoonal sedimentation prevails this rate increases to 1.2 $mm.y^{-1}$. We have not enough age control in the uppermost part of this core to discuss accumulation rate evolution over the last millennium.

6. Holocene paleoenvironmental evolution of the lagoonal system

Detailed facies characterization, based on lithostratigraphy and macropaleontology, together with the radiocarbon and ^{210}Pb, ^{137}Cs chronology, allow us to reconstruct the depositional history of the Palavasian lagoonal system since 8000 yr cal BP.

6.1 Early Holocene and sea level tracks

The complex basal polygenic surface (consisting of the ravinement surface and above conglomerate (*Figure 5.2* and *Figure 5.3*) probably originated from subaerial erosion during times of relative sea-level low-stand and subsequent reworking during the ensuing transgression [Cattaneo & Steel, 2003]. The coarse marine sands above are interpreted as transgressive shoreface deposits [eg. Cattaneo & Steel, 2003] laterally associated with an erosional surface. This lateral difference is likely due to various sedimentary regimes linked to the pre-existing topography. These sands with young marine shells are dated in their upper part at 7850 ± 125 cal B.P. at 8.2 ± 0.2 NGF in core PB06 and 5845 ± 140 cal B.P. at 3.8 ± 0.2 m NGF in core AR06 (*Tableau 5-1*). These shells show good preservation state and thus have not been reworked over large distances. However, they may not be in growth position

and may have been slightly reworked either seaward or landward by wave action. Thus the ages determined for the shells may refer to a sea-level located either slightly above or, more probably, because of the transgressive context, slightly below the relative sea-level position at shell growth time [Lambeck & Bard 2000]. Despite these uncertainties, these ages and depths are in good agreement with relative sea level curves (*Figure 5.6*) in NW Mediterranean Sea over the last 8000 yrs [Aloisi et al., 1978, Dubar & Anthony, 1995, Vella & Provansal, 2000, Berné et al., 2007], with the Tahiti sea level curve [Bard et al., 1996] and with the glacio-hydro-isostatic model of Lambeck & Bard [2000].

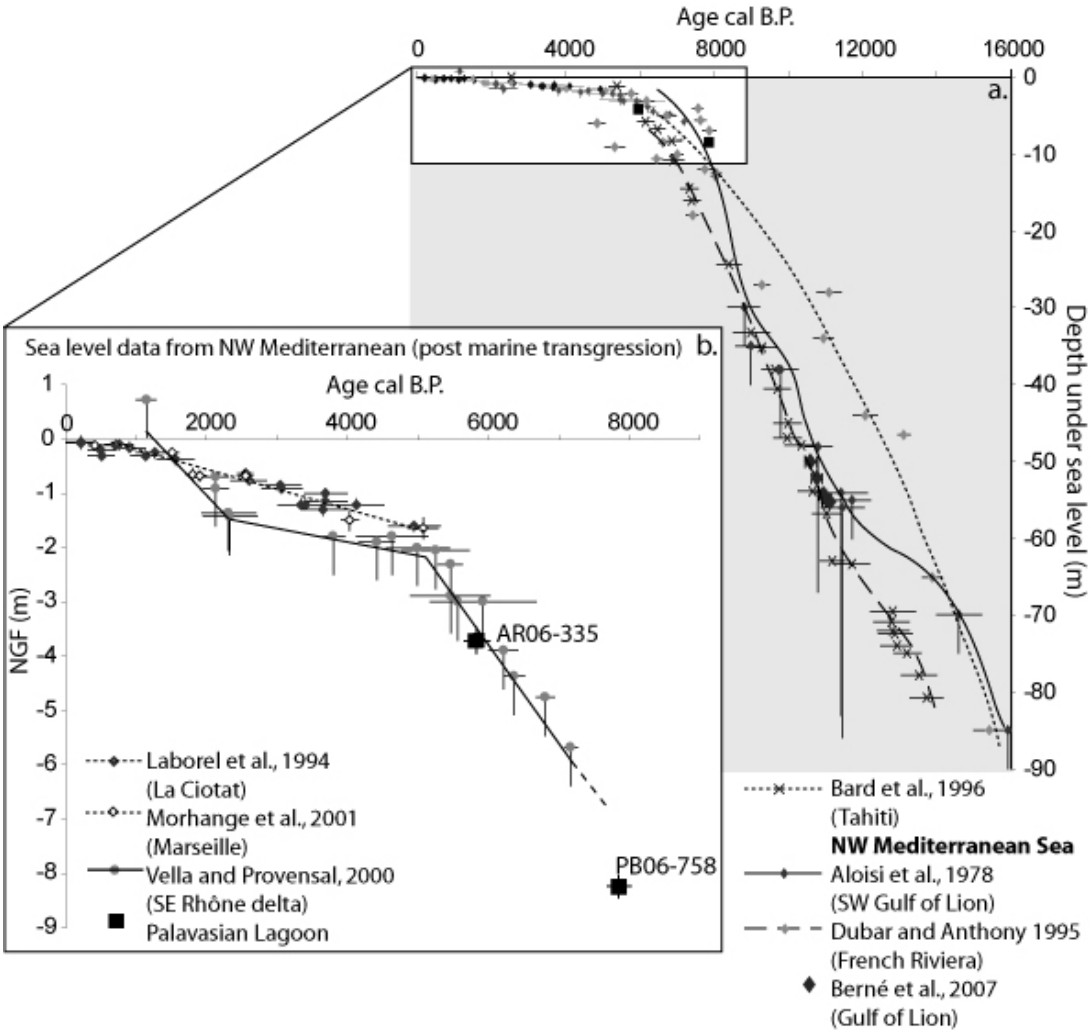

Figure 5.6 : Relative sea level curve in the NW Mediterranean Sea (a) for the last 16000 yr cal B.P., and (b) for the last 9000 yr cal B.P. The two black dots represent the relative elevation of the dated sand layer due to the last transgressive high-stand deposit in PB06 and AR06 cores.

6.2 Lagoonal paleoenvironments

These coastal wetlands result from the interaction between a process of shoreline regularization by migration of littoral barriers and a filling of these subsequently isolated areas by fluvial and marine inputs [Certain et al., 2004]. These barriers result from alongshore progradation of sand spits from inherited topographic highs by East-West coastal drift carrying sand material from the Rhône river [Raynal et al., 2009]. According to this author the closure of these lagoons began around 7100 yr cal B.P., the age of the first lagoonal deposit, during the last stages of eustatic rise stabilization.

Using lithostratigraphy and macropaleontology analyses it is possible to interpret the complexity of subenvironments that characterise wetland systems [Mazzini et al., 1999; Amorosi et al., 2005; Ricci Lucchi et al., 2006]. Thus we can separate the lagoonal Holocene history into two paleoenvironmental intervals which record the evolution of the area in relation to the closure of the system by sandy barriers due to the interaction between the rising relative sea level and the progradational activity of coastal rivers. From a purely sedimentological point of view, study on core PB06 (*Figure 5.3*) suggests a relative homogenous lagoonal depositional environement from 744 cm (i.e., 7090 ± 100 yr cal B.P.) to the present day, characterised by grey clays and silts with locally intercalated sand layers (less than 10% of the total sediment) interpreted as paleostorm events. The high-resolution stratigraphy performed on fauna however indicates a tendency towards the closure of the lagoon that started at around 220 cm (i.e. about 1050 yr cal B.P.) This tendency is marked by a clear shift in mollusc population at around 190-170 cm (i.e. about 730 ± 120 yr cal B.P.) characterised by an increase of the most typical lagoonal specie *Hydrobia acuta* whereas the number of marine specie *Bittium recticulatum* decreases (*Figure 5.7*). This suggests a change in environmental conditions (salinity, temperature, nutriments, and oxygenation) from a lagoonal depositional environment, with marine influence to a more isolated lagoonal environment. Such a change could result from local paleo-morphological modifications such as a closure of the communications between the lagoon and the sea. We thus suggest that the change in mollusc population may reflect the creation of physical barriers such as the final closure of a continuous sandy barrier with probably no permanent inlet or channel which controlled inflow of marine water into the Palavasian lagoon system. A main change in environmental conditions corresponding to the progressive closure of the lagoon occurs at a depth of about 220 cm (i.e. about 1050 yr cal B.P.), with a moderate increase of lagoonal species. The final closure of this system occurred between 190 and 170 cm depth, with a

strong decrease of marines species. Therefore fauna contents clearly show a shift from a protected lagoon to an isolated lagoon environment around 730 ± 120 yr cal B.P. (*Figure 5.7*). Nevertheless this environmental change could also imply a change in the ^{14}C reservoir age R(t), which is difficult to estimate from the presently available and limited data.

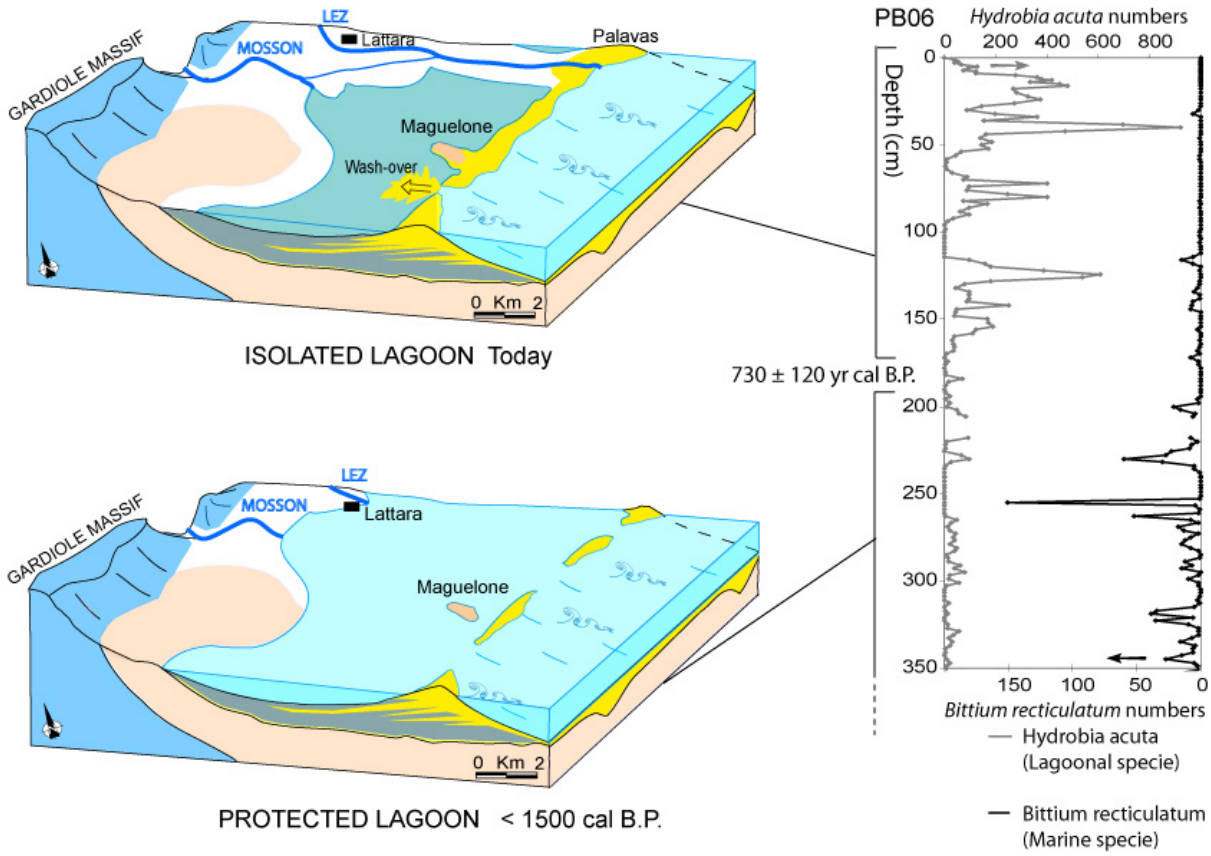

Figure 5.7 : Paleoenvironmental evolution of the Palavasian coastal lagoon before and after the final closure of the sandy barrier at around 190-170 cm depth (i.e., 730 ± 120 yr cal B.P.).

6.3 Holocene filling in relation to relative sea level rise

Following the deposition of the transgressive sands above the ravinement surface (*Figure 5.6*), we propose that the relative constancy of marine sea level rise, around 1 mm.y^{-1} [*Figure 5.6*, Vella & Provensal, 2000] allowed the establishment of a proto-sandy barrier which protected the lagoonal system against waves (*Figure 5.7*) before 7100 yr cal BP, age of the fist lagoonal deposit. This interpretation is testified by the low energy depositional environments dominated by clays that are observed in the cores. However, as attested by the

fauna in core PB06 this protected system was still influenced by marine conditions. During this period the sedimentation rate was almost equal to the average sea level rise of about 1 $mm.y^{-1}$, other authors documents that the sea-level rise rate decreased to 0.3 $mm.y^{-1}$ since 5000 yr cal B.P. [Laborel et al., 1994; Morhange et al., 2001]. Since 190 to 170 cm (i.e., 730 ± 120 yr cal B.P.), we observed an increase of lagoonal species possibly related to the closure of the sandy barrier giving rise to a permanent isolation of the lagoon (*Figure 5.7*). This observation suggests that, in the context of a progradation of the coastal plain, we may have an increase in the accumulation rate in the lagoon since that time, because the riverine inputs can no longer be exported directly seaward, through the inlets. Such an increase in sedimentation rate is observed, with a mean 2.72 mm/yr over the last 750 yrs (*Figure 5.5*). In the centre of Pierre Blanche Lagoon, where water depth is around 0.6 m, even higher sedimentation rates (4.2 mm y^{-1}) have been calculated from ^{210}Pb and ^{137}Cs chronology (for the last century). Extrapolating these constant rates toward the future, we could expect a complete filling of this lagoon in the next 150 yr. However, the actual increase of sea level rise, estimated to 3.1 ± 0.4 $mm.y^{-1}$ [Nerem et al., 2006] due to the global warming, will partially compensate for the filling tendency, by creating accommodation space in the lagoon. In such a case, we could expect a delayed complete filling of this system. On the other hand, the present-day sea level rise associated to wave action during storm may result in the progressive retrogradation of the barrier/lagoon system, thus reducing the lagoonal surface and increasing also the accumulation rate. The anthropogenic component from erosion in the watershed and increased sedimentation in the deltaic and lagoonal system is also difficult to estimate, especially with demographic rises, deforestation and changes in land use (e.g., agriculture, buildings). Therefore, at the present time, it is difficult to predict the final filling of this lagoonal system.

7. Implication for human activity during the Roman period

Since the Iron Age (2700-2100 B.P.), the lagoonal environment was a habitat favourable for human activity. During the VIth century B.C., the development of Greco-Etruscan trade favours, in the western Mediterranean Sea, the development of a littoral harbour like at Agde, le Cailar and Lattara [Blanchemanche et al., 2003]. The Lattara harbour was populated by almost 4000 persons in the IVth century B.C. and was located on a small peninsula at the Lez mouth, on the northern border of the Palavasian lagoonal system [Chabal et al., 2008], thus facilitating economic shipping through permanent inlet (*Figure 5.7*). At the end of the IInd

century A.D. (1800 yr BP), during the Roman period (2100-1500 B.P.), the activity and the population of this ancient harbour shown a strong decrease. Raynal et al. [submitted] have estimated the beginning of construction of the actual barrier at 1800 ± 150 yr cal BP thanks to a ^{14}C age at the base of the present day sandy barrier. This date is in good agreement with the decrease of Lattara harbour activity. We propose that the morphological changes related to the growth of the sandy barrier since 1800 yr cal PB may have perturbed the marine shipping in the lagoon Therefore, we propose here that one possible explanation for the decline of the harbour is the decrease of maritime transport due to a change in environmental conditions in relation to the sedimentary evolution of the lagoonal system with: (1) the build up of the Lez and Mosson delta plain; (2) the filling of the lagoon with a decrease of bathymetry to around 2 m (taking into account the prevailing sea level) and (3) the creation of physical barriers such as sandy barrier.

8. Conclusion

High-resolution stratigraphy correlated with detailed chronology of the deposits is used to reconstruct Holocene filling of a lagoonal system along the Languedoc Mediterranean coast. Above an erosional surface interpreted as a ravinement surface, some marine sands are interpreted as Holocene transgressive deposits allowing identification of the onset of stable sea level rise around 8000 and 6000 yr cal BP. Sedimentological and faunal analyses of the lagoonal deposits accumulated above this transgressive level give information about the paleoenvironmental changes since 7000 yr BP., from a protected lagoon with marine influence to an isolated lagoon. The beginning of this evolution can be dated at around 1050 yr cal B.P., with a slow increase of lagoonal species, and the final closure of the lagoonal system occurred at around 730 ± 120 yr cal B.P., with a strong decrease of marines species. The combination between the closure of the lagoonal system by the sandy barrier (probably as a result of coastal hydrodynamics and alongshore sediment transfer) and the progradation of the coastal plain, may explain the increased sedimentation rates over the last 750 yrs, resulting in the progressive filling of the lagoon. We suggest that such a filling may be responsible for the decline in economic activity of Lattara harbour during the Roman period. During the latest part of the Holocene sea-level rise and subsequent high-stand, sandy barrier evolution may thus play a key role in the formation of the lagoonal system and associated sedimentary deposits.

Acknowledgements

This research has been undertaken in the framework of the ECLICA Project financed by INSU/CNRS (ACIFNS “Aléas et Changement Globaux”, coord.: L. Dezileau) and ARMILIT project (ANR n° NT_NV_27 / 2005, P. Blanchemanche). The authors wish to thank IFREMER Palavas for allowing storing of the cores in their cold room. Thanks to Laboratoire de Mesure ^{14}C (LMC14) on ARTEMIS in CEA institute at Saclay (French Atomic Energy Commission) for the ^{14}C analyses (ECLICA and INTEMPERIES projects, coord. Dezileau). Bernadette Tessier (Université de Caen) and the members of the GLADYS platform (www.gladys-littoral.org) and all other members of the ECLICA Project team are also thanked for their support and their constructive discussions during the course of this study.

5.2 Synthèse formation des lagunes palavasiennes

La partie centrale du littoral du Golfe du Lion est caractérisée par des systèmes lagunaires résultant de l'interaction entre un processus de régularisation du trait de côte par migration de barrière littorale, et par un lent remplissage des zones situées en arrière de ce cordon par les apports continentaux et marins (Certain *et al.*, 2004). L'étude multi-traceurs à très hautes résolutions des dépôts tardi holocène (§5, Article 4), associée à de la prospection sismique (Raynal *et al.*, 2009 ; Raynal *et al.*, Soumis) nous permet de reconstruire l'évolution du système lagunaire palavasien.

Durant le dernier maximum glaciaire (20 000 ans B.P.), le niveau de la mer étant près de 120 m plus bas (Lambeck et Bard, 2000), le segment de Maguelone est complètement émergé. Cette zone est donc sujette à l'érosion, comme attestée par les vallées incisées de la Mosson et du Lez (Raynal *et al.*, Soumis), induisant ainsi une topographie très irrégulière (plateau des Aresquiers et de Maguelone). Au cours de la transgression marine post-glaciaire (début de l'Holocène) le niveau de la mer remonte pour atteindre entre -8 et -10 m NGF vers 8000 ans B.P. (*Figure 5.8A*). L'eau envahit donc toute la zone, déposant des niveaux transgressifs de sables bioclastiques (Cattaneo et Steel, 2003). Cette interprétation est validée par la bonne corrélation entre l'âge de ces niveaux sableux et la courbe locale du niveau marin (section 5.1, Article 4).

L'unité située au dessus montre des dépôts d'argile et de silt gris coquillés d'origine lagunaire, intercalés de niveaux de sable silteux révélant la présence d'événements de tempête. L'enregistrement continu de ces dépôts fins est lié à une faible hydrodynamique. Ces premiers niveaux lagunaires sont datés à 7665 ± 110 ans Cal B.P. à -20 m NGF, dans la vallée incisée du Lez, située juste au dessus d'un niveau marin transgressif (Raynal *et al.*, Soumis ; section 5.1., Article 4). Cela implique la mise en place très rapide de l'environnement lagunaire au cours des derniers stades de la transgression marine, associée à la formation d'un cordon littoral. L'analyse des géométries en mer, montre que la fermeture de l'environnement lagunaire est due à la progradation de flèches sableuses, vers le Sud-est, parallèlement à la côte. La formation de ces corps sableux est liée au transport des sédiments rhodaniens par l'intermédiaire de la dérive littorale (Raynal *et al.*, 2009). Ces flèches s'accrochent sur les

plateaux rocheux, comme celui des Aresquiers et de Maguelone, situés à près de 2 km au large (*Figure 5.8B*).

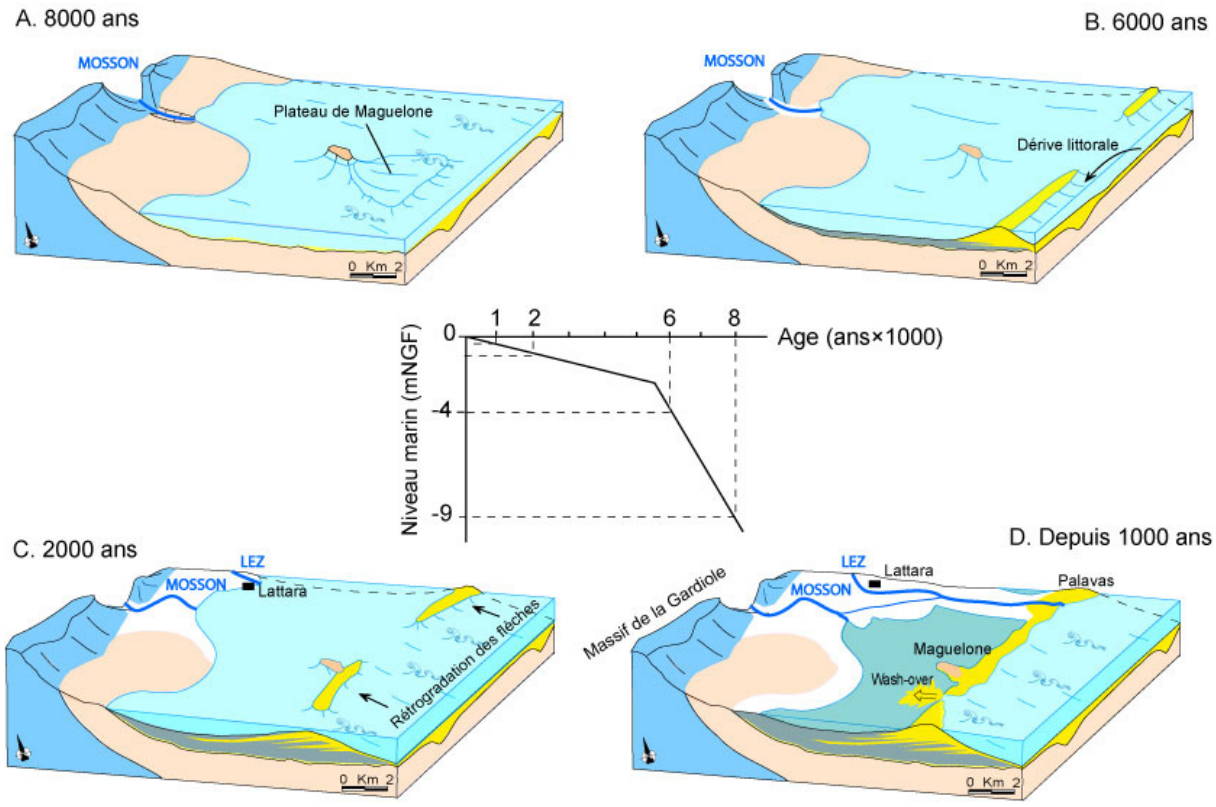

Figure 5.8 : Modèle en trois dimensions de l'évolution du système lagunaire palavasien depuis 8000 ans B.P., en fonction de l'évolution du niveau marin (Raynal et al., 2009 ; Sabatier et al., 2010).

La diminution du taux d'élévation du niveau marin vers 5500 ans B.P. et sa stabilisation autour de -2,5 m NGF, provoquent le début de rétrogradation de la barrière littoral sur les dépôts lagunaires. A l'aide d'une datation à la base du cordon sableux actuel (1745 ± 120 ans Cal B.P., échantillon M377, carotte MAG-1) on estime que la barrière littorale a quasiment atteint sa position actuelle vers 1800 ans B.P.. La barrière est bloquée dans son retrait par des points topographiquement hauts, affleurant, comme la presque île de Maguelone (*Figure 5.8C*). La lagune enregistre une sédimentation fine, durant la période comprise entre 5500 et 1800 ans B.P.. Cependant ces dépôts sont associés à des indicateurs biologiques (faune marine) traduisant un environnement fortement ouvert sur la mer avec probablement un système de type lagune protégé (section 5.1, Article 4).

Depuis 1800 ans B.P., le niveau de la mer ayant peu monté (maximum 1 m), la dérive littorale induit une fermeture progressive de la barrière ancrée sur des points hauts (*Figure 5.8D*). Dans la lagune on observe un changement majeur dans l'activité biologique. Des nouvelles espèces de mollusques dominent ce milieu, plus adaptées aux grandes gammes de variations des paramètres physico-chimiques de l'eau (température, salinité, oxygénation). Les espèces ayant des affinités pour les milieux ouverts disparaissent progressivement. Ce remplacement graduel se termine autour de 1050 ans B.P. (Section 4.2 et 5.1 ; Article 3 et 4) date à partir de laquelle la présence d'espèces marines dans la lagune est uniquement liée à l'activité des tempêtes (Section 3.2, Article 1). Ce changement s'interprète comme étant dû à la fermeture définitive du cordon sableux par l'hydrodynamique côtière, rendant les échanges mer/lagune quasi inexistant, on parle alors de système lagunaire isolé. De plus, cette fermeture induit une augmentation du taux de sédimentation passant de 1 $mm.an^{-1}$ à 2,7 $mm.an^{-1}$ durant cette période (Section 4.2, Article 3). En effet, les sédiments apportés par la Mosson ne peuvent plus être exportés en mer et se retrouvent piégés en lagune, participant ainsi à son comblement (Section 5.1, Article 4).

Les stades ultimes de l'évolution de ce système lagunaire restent très incertains. D'un côté l'érosion du cordon sableux (en partie liée aux activités humaines) associée à la progradation du delta de la Mosson, a tendance à diminuer l'espace lagunaire. Tandis que l'augmentation actuelle du niveau marin, estimée à 3.1 ± 0.4 $mm.an^{-1}$ (Nerem *et al.*, 2006), crée de l'accommodation qui contrebalance le taux de sédimentation et retarde ainsi le comblement final de ce milieu.

6. Reconstitution des Paléotempêtes et implications climatiques

6.1 Les deux derniers millénaires : Article 5 : Palaeogeography, Palaeoclimatology, Palaeoecology

Increase of intense storm activity during the Little Ice Age on the French Mediterranean Coast

Dezileau L [1], Sabatier P.[1], Blanchemanche P.[2], Joly B.[3], Swingedouw D.[4], Cassou C.[4], Castaings J.[1], Martinez P [5].and von Grafenstein U.[6]

1 Université Montpellier 2, Geosciences Montpellier, CNRS, UMR 5243.
2 Université Montpellier 3, Laboratoire d'Archéologie des Sociétés Méditerranéennes, CNRS, UMR 5140.
3 RECYF, Centre National de Recherche en Météorologie, Toulouse
4 Centre Européen de Recherche et de Formation Avancée en Calcul Scientifique, Toulouse
5 Université Bordeaux 1, EPOC, CNRS, UMR 5805
6 Laboratoire des Sciences du Climat et de l'Environnement, CNRS/CEA, Saclay.

Received June 2009
Palaeogeography, Palaeoclimatology, Palaeoecology, Submitted

Abstract

Understanding long-term variability in the frequency of intense storm activity is important for assessing whether changes are controlled by climate evolution. Understanding this variability is also important for predicting present and future community vulnerability and economic loss. Our ability to make these assessments has been limited by the short (less than 50 years) instrument record of storm activity. Storm-induced deposits preserved in the sediments of coastal lagoons offer the opportunity to study the links between climatic conditions and storm activity on longer timescales. Here we present a record of these extreme climatic events in the French Mediterrannean coast over the past 1,500 years based on sediment cores from Gulf of Aigues-Mortes lagoons that contain a specific sedimentary and geochemical signature associated with intense storms.

Overwash deposits correlate with the most intense documented floods in the area. There is no evidence of intense storm landfalls in the region for several hundred years prior to the late 17th century A.D. The apparent increase in intense storms around 250 years ago occurs during the latter half of the Little Ice Age, a time of lower continental surface temperatures. Comparison of the sediment record with palaeoclimate records indicates that this variability was probably modulated by atmospheric dynamics. We found that the Eastern Atlantic Pattern could be responsible for much of these extreme wind events in the North Western Mediterranean region. A complete understanding of the relationship between climate fluctuations, storm activity, and the coastal response will be crucial to predicting the impacts of future climate change.

Keywords: lagoon, storm, flood, Little Ice Age, North Atlantic Oscillation, East Atlantic Pattern, Mediterranean Sea, risk assessments.

I. Introduction

It has been clearly established that our planet has been warming since pre-industrial times (Solomon et al., 2007). The effects of climate change on extreme events are difficult to assess because of many forms of nonlinearity and long term memory. If several storms and floods have hit France and Europe in the recent years, the link between these events and climate change is not yet proven. The effect of man on his environment, the development of our societies and our greater wealth are at increasing risk and are more likely to be destroyed

because of the destructive impact of climate intense episodes. However, the issue of extreme events remains: are they linked to global warming or are they part of natural climate variability? To answer this question, it is essential to place such events in a broader context of time, and trace the history of climate changes over several centuries or several millennia, because these extreme events are inherently rare and therefore difficult to observe in the period of a human life.

In this study, we focus mainly on the Languedoc-Roussillon (*Figure 6.1*), a region of the French Mediterranean coast. This area is particularly sensitive in terms of societal issues for the risks of floods (the Mediterranean Heavy Precipitating Events) and the risk of coastal erosion/submersion during storm events. The Languedoc-Roussillon, which stretches from the Cevennes Mountains to those of the Pyrenees was hit several times by climatic events of great intensity. In September 2002, large floods hit the Gard. There were 23 victims and damage estimated at over one billion Euros. The 50 mm isohyet spanned more than 26 000 km2. The volume of water rushed over the area is estimated at 3.6 billion m3, almost three times the capacity of the Serre Ponçon dam on the Durance, the biggest reservoir in Europe. For the most recent period (1958-1994), Meteo-France has recorded 110 episodes of rain exceeding 190 mm in 24 hours, with sometimes extremes above 350 mm. The intensity of rain and the configuration of the drainage basin cause the emergence of flash floods. These floods are real breaking waves: "At the bridge of Herault, upstream of Ganges, water was moving in the form of a wall of trees and debris that an invisible hand seemed to push all of a piece" (ancient text of 1900, cf. Antoine et al., 2001). Linked or not to these rainy episodes, the region is also prone to frequent storms. These events can have dramatic actions when the waves are associated with high sea levels (heavy sea, offshore winds) attacking coastal sand dunes, sometimes breaking the sandy barrier (Pierre Blanche lagoon in 1999), and weakening certain human infrastructure (ports, defense barriers, housing). For the last few decades, the most important storms are those of 1982, 1997 and 1999. From the fifteenth-century to present-day, historical documents reveal many periods of hydrological irregularities particularly during the Little Ice Age (Blanchemanche et al., 2003; Berger et al., accepted). Over longer periods of time, we have no information on the existence of extreme climatic events. The frequency of these events is difficult to estimate from the instrumental and documentary records due to the relative rarity of these events and the short historical period of instrumental observation. Therefore, geological data offer the only hope of reconstructing a long historic record of intense events and deciphering any long-term changes in storm or flood activities.

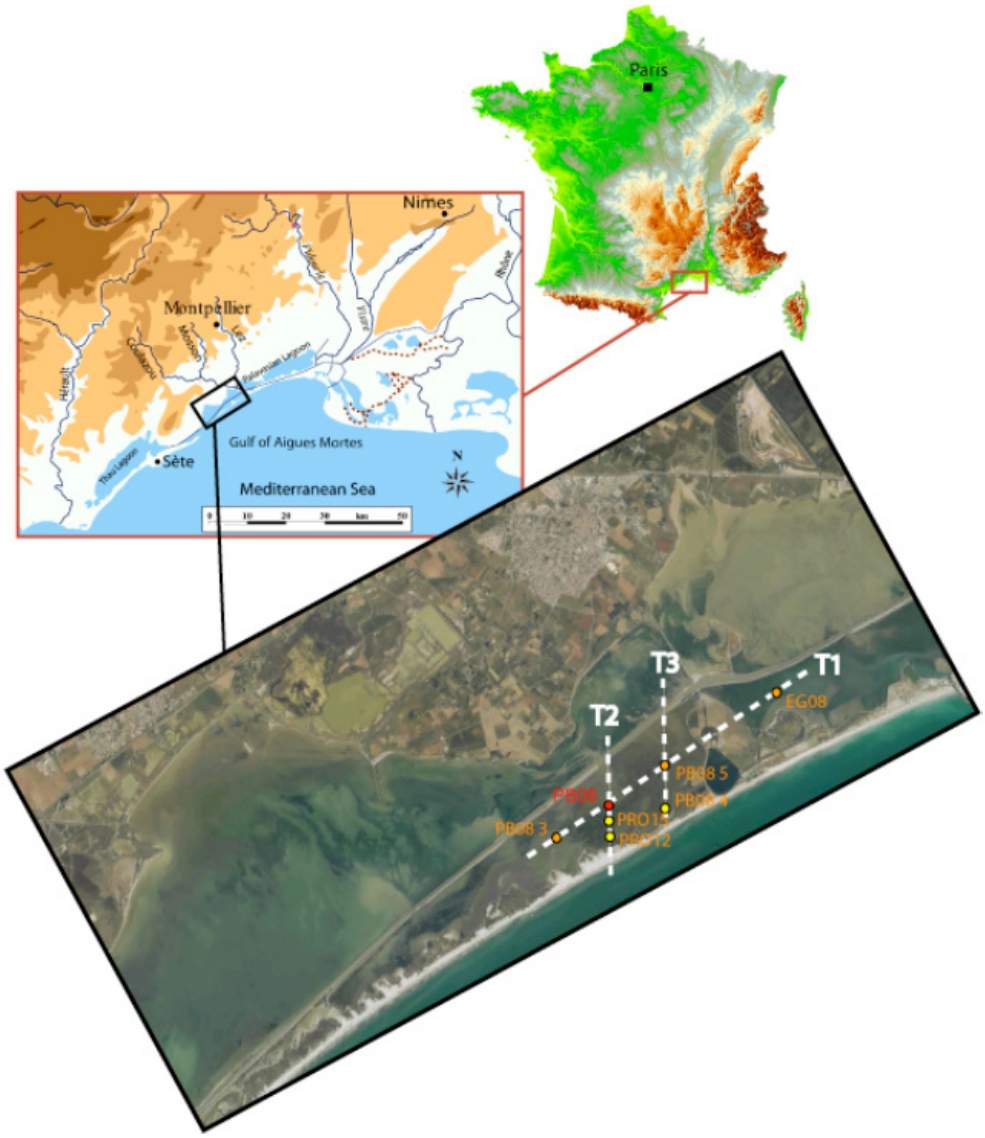

Figure 6.1 : Study area and cores location in Pierre Blanche and Prevost lagoons. Seven short cores and one long core were extracted from the two lagoons along three transects (One longitudinal transect T1 and two transverse transects T2 and T3).

In this study, we propose to use bio- and geo- indicators (proxies) from sedimentary archives to reconstruct past storm activities in the Languedoc-Roussillon region. Pioneer studies from this area demonstrated that overwash sand layers preserved in the sediments of coastal lagoons can provide a record of catastrophic storms during the last 250 years (Dezileau et al., 2005; Sabatier et al., 2008). Here a multi transect approach is used to assess the frequency and intensity of these events during the last 1,500 years and to study the possible links between past climatic conditions and storm activities. To date, the study of historic and prehistoric

storms, named Paleotempestology by Liu and Fearn, (2000) has been confined to the study of tropical cyclones in tropical Australia (Chappell et al., 1983; Chivas et al., 1986; Hayne and Chappell, 2001; Nott, 2004) and southern and eastern United States (Liu and Fearn, 1993, 2000; Collins et al., 1999; Donnelly et al., 2001a, b; Donelly et al., 2004, 2007 ; Scilleppi and Donnelly, 2007). Up to now, this relatively new branch of science was not applied to mid- and high-latitude events (Nott, 2004). The identification of storm events in the Mediterranean region is a new area of study. This study has been undertaken in the framework of ECLICA project (INSU, ACI-FNS « Aléas et changements gobaux » in 2004, coordinator L. Dezileau) which aims to identify and assess the recurrence of extreme climatic events (floods and storms) from the study of documentary records and geological data in lagoons and river deltas that have affected the western Mediterranean basin during the Holocene.

2. Large Scale Environments for Heavy Precipitating Events in the Mediterranean

Today, the Mediterranean Heavy Precipitating Events (HPEs) often occur within very similar synoptic (large scale) contexts. When a dynamical clustering is performed to a set of 1200 days which samples the major part the rainfall variability over the region including events of high intensity we obtain two classes of configuration that gather more than 70% of the HPEs (*Figure 6.2*). The left panel displays the Cyclonic SoutherWesterly (CSW) pattern which depicts a very typical situation. A strong trough is moving forward over Western Europe and is associated with a strong mid-level SW flow over the French Mediterranean coast. In this configuration, interactions between upper level tropopause anomalies and baroclinicity in lower levels may lead to cyclone development over western Mediterranean. High low level moisture flux anomalies (c.f. shading areas) are advected from the Gilbraltar strait by a rapid SW low level jet with high wind speed values (up to 15 m/s in average). The Cyclonic Southerly pattern (CS, on right panel) shows a weaker trough, then a less forcing environment. However, the system being isolated from the main stream to the north reinforces thermal contrasts due to the upper level cold air in the trough. Furthermore, the magnitude of the ridge over central Europe is more significant in this cluster and may steer the low level jet more to the SE with still high wind speeds (13 m/s), but also it may help enhancing upper level divergence over the area of interest.

At a regional scale, it is noteworthy to observe that HPEs only occur under two orientations of the strong low level jet, the southwesterly in the CSW and the southeasterly in the CS. These two branches of the low level jet, associated with surface cyclones or not, may be connected

with potential coastal impact on a region extended from the Rhone delta to the east in the CSW configuration, and to the Languedoc-Roussillon seafront for CS cases.

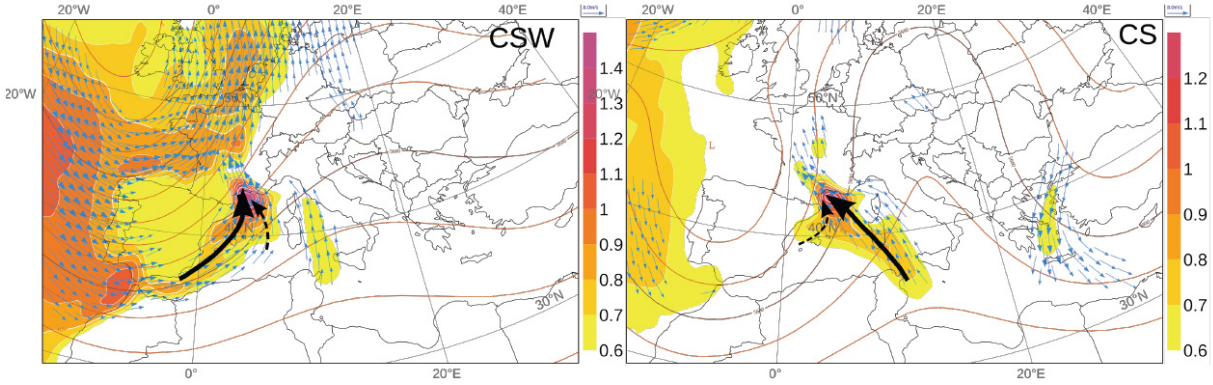

Figure 6.2 : The two classes that gather more than 70% of the Mediterranean Heavy Precipitating Events (HPEs). The left panel displays the Cyclonic SoutherWesterly (CSW) pattern and the right panel shows the Cyclonic Southerly pattern (CS). HPEs only occur under two orientations of the strong low level jet, the southwesterly in the CSW and the southeasterly in the CS.

3. Study site

Pierre Blanche and Prevost lagoons are located in the northwestern part of the occidental Mediterranean Sea (*Figure 6.1*). These hypersaline backbarrier lagoons are separated from the Mediterranean Sea by a wave-produced, sandy barrier 150 m wide and 2–3 m above the mean sea level. These lagoons have a flat bottom with a maximum water depth of approximately 1 m. Modern sediments accumulating at the bottom of this lagoon is clay/silt and no sand. Tidal variability is modest (mean range 0.30 m), which minimizes the influence of dynamic tidal currents. The study site is located along the southeastern-facing shoreline, and is extremely vulnerable to intense storms coming from south and southeast.

4. Materials and methods

4.1 Core material

Six short cores and one long core were extracted from the two lagoons (Pierre Blanche, and Prevost) along three transects (transverse and longitudinal transects, *Figure 6.1*). The long core was extracted using the Uwitec platform. All cores were collected at water depths between 0.5 and 1.5 m. The locations for all coring sites were determined using a handheld GPS unit which provided a horizontal accuracy of 3 to 6 m.

4.2 Physical measures

Back at the laboratory, cores were X-radiographed (imagery department in "Clinique du Millénaire" and University of Bordeaux), sliced open, photographed and logged. Cores were refrigerated at 5°C to prevent dessication. Core PB06 was run through a non-destructive Itrax core scanner to obtain subcentimeter-resolution X-ray fluorescence measurements of the sediment's elemental composition. Grain-size analysis was conducted on contiguous 2-cm samples using a Beckman-Coulter LS13320 laser diffraction particle-size analyser. Grain size distribution measurements were made on the less than 0.3 mm sediment fraction without decarbonatation.

5. Results

5.1 Cores descriptions

Cores collected from the two lagoons contain organic-rich clay and silt interbedded with coarse grained layers comprised of a mixture of siliciclastic sand and shell fragments. X-ray images, X-ray fluorescence and high-resolution grain-size analysis for PB06, PB08-3, PB08-4, PB08-5, PRO 12, PRO 15 and EG08 indicates several thin, coarse-grained layers preserved within mud sediments which were not detected by visual inspection. The more prominent sand layers are typically composed of sand and have often sharp contacts with the organic-rich clay and silt sediments below (*Figure 6.3*). These sand layers preserved in the cores seems to be overwash layers, i.e., coming from marine incursions during intense storm events. However, these coarse grained event layers can have another source such as rivers for example. Consequently, we investigated the origin of the detrital material.

5.2 Detrital input and transport mechanisms

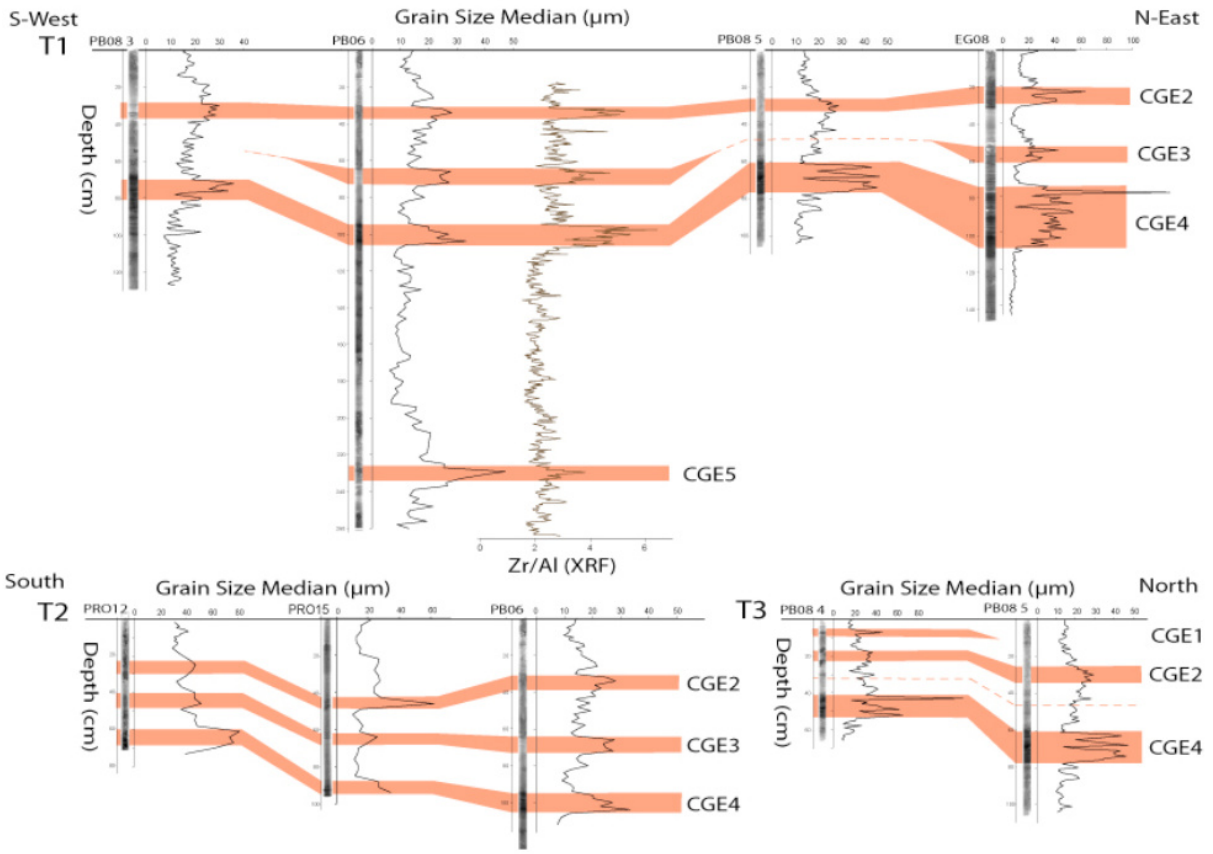

Figure 6.3 : Grain size distribution of the seven short cores (PB08-3, PB08-4, PB08-751 5, PRO 12, PRO 15 and EG08) and one long core (PB06) following three transects (one longitutinal T1 and two transverses T2 and T3). The Zr/Al ratios of core PB06 are well above 3 indicating a higher contribution of terrigenous particle from the sandy barrier. Five different coarse grained event layers have been identified in the different cores (CGE 1 to 5).

In the two lagoons, terrigenous particles may originate from any of the surrounding land masses, i.e., old Mesozoïc/Cenozoïc calcareous watershed sediment and/or that of the sandy barrier. These potential source areas are characterized by different major and trace-element compositions. Thus, by connecting the major and trace-element compositions of source areas to the terrigenous particles in the sediment, the origin of the particles can be identified. In order to characterize temporal changes in detrital fluxes during the last 1,500 years, we chose to focus on core PB06 extracted in the centre of the Pierre Blanche lagoon.

In order to obtain the best resolution in this identification, we chose to use the ratio Zr/Al, which discriminates between the two potential source areas. The high Zr/Al ratio value is explained by a high concentration of heavy minerals (like zircon) from Camargue sand. The Zr/Al ratios of coarse grained event layers are well above 3 (*Figure 6.3*), indicating a higher

relative contribution of terrigenous particle from the sandy barrier. These sand layers preserved in the cores are interpreted as overwash layers given their geochemical and sedimentary characteristics, i.e. all these coarse layers are the result of marine flooding events overtopping or breaching the barrier and transporting these barrier and nearshore sediments into the lagoon. The marine origin of these sand layers were also ascertained through identification of molluscs (*Bittium recticulatum* and *Rissoa ventricosa*), unique to the marine environment (Dezileau et al., 2005; Sabatier et al., 2008).

In conclusion, storm surge associated with an intense storm strike, is the only mechanism that can generate these high-energy events with seawater influx. There is no evidence of earthquakes or tsunamis affecting the Languedoc coast in the historical record. The data cannot be explained by any other fluvial or lacustrine processes.

5.3 Stratigraphic framework and age model

To allow for a more detailed discussion of the markers and their comparison with other records, a chronostratigraphic scale was constructed. Time scales for cores PB06, PRO 12 and PRO 15 are based on ^{137}Cs, ^{210}Pb and AMS ^{14}C dates (Sabatier et al., 2008). Samples shells were radiocarbon-dated at the Laboratoire de Mesure ^{14}C on ARTEMIS in CEA institute at Saclay (ECLICA, INTEMPERIES, PALEOSTORMS projects, coordinator L. Dezileau 2004; 2006; 2008). These measurements were obtained from monospecific samples *Cerastoderma Glaucum* at each level. ^{14}C ages were corrected for reservoir age (see Sabatier et al., 2008 for method) and converted to calendar years using the Calib 5.0.2 calibration program (Hughen et al., 2004) at two standard deviations. For the four cores, PB08-3, PB08-4, PB08-5 and EG08, we have no absolute age constraints. The proposed age scale for these cores was developed by graphic correlation to core PB 06.

5.4 Overwash deposits chronology

In communal archives, intense storm events were mentioned because they caused damage in the vicinity of the studied city (Sabatier et al., 2008). For the last 400 years, eighteen intense storms occurred in the Languedoc. Among all of these, some seem to be more intense. The storm of December 4th, 1742, recorded in many city archives around the Aigues-Mortes gulf, is considered as the most catastrophic event in the study area. This storm, probably due to S to SE winds, submerged some local cultivated lands which had been gained at the expense of the

older parts of the lagoon. The lagoon was covered with a sand layer on “300 toises”, i.e. 500 m. One of the main consequences was the creation of a large inlet, near Maguelone, which remained open until 1761. The storm of November 23, 1848 associated with strong SSE winds induced the wreckage of a few ships in the Sète Harbour, the biggest port in the region. The sea has completely submerged defense barriers in the harbour. This storm caused the death of numerous people. Certified by many engraved illustrations, the storm of September 21, 1893 also resulted in the devastation of the Sète harbour and the wreckage of a few ships. The winter storm of 1982, with 46 m/s wind (category 2 in Saffir-Simpson scale) caused the death of 15 people and economic losses estimated at 400 million Euros. This storm caused a partial devastation of the new Palavas and Carnon harbours.

To determine which historical events left coarse grained layers, we used our detailed age model previously defined. Five different coarse grained event layers (CGE) have been identified in the different cores. The coarse-grained event deposits (CGE-2 and 4) are consistent among all cores (*Figure 6.3*). Historic overwash (CGE-1 and 3) layers are not consistent across the two lagoons, suggesting that these storms may have been nearly absent or less-intense storms that overtopped the barrier in localized areas, producing overwash lobes as opposed to sheet overwash. Nothing may be deduced from the CGE-5, the deeper coarse-grained event in the long core PB 06. CGE-1 is observed only in the core PB 04 which was retrieved near the lagoon shore suggesting the existence of a less intense storm. This layer is consistent with the storm of 1982 (category 2). The three subjacent layers CGE-2, CGE-3 and CGE-4 are consistent with the storm events which occurred in 1893, 1848 and 1742, respectively. These dates were obtained by comparison between ^{210}Pb, ^{14}C data and historical archives (Sabatier et al., 2008). The storm of 1848 was chosen instead of the less intense storm of 1839 (Sabatier et al., 2008). For the last layer CGE-5, dated at 455+/-145 cal AD, we have no communal archives.

On the basis of our age model a quiescent interval is evident between 455 and 1742. After this time, there is a period of intense storms between 1742 and 1900. The interval from 1900 to today was relatively quiet.

6. Discussion

6. 1 Site sensitivity through time

Barrier coasts are dynamic systems and differences in backbarrier sensitivities can result from several factors including sea level change, sediment supply, inlet, and barrier-elevation

changes (Scileppi and Donnelly, 2007; Donnelly and Webb, 2004; Rampino and Sanders, 1981; Hennessy and Zarillo, 1987).

6.1.1 Sea level changes

Sea level rise can increase the sensitivity of backbarrier study sites by moving the shoreline farther inland and narrowing the barrier beach through time. In this context, an increase or decrease in sand layers through time can solely be caused by a sea-level change. Major discrepancies exist about the chronology and shape of postglacial sea-level curves reconstructed for the Mediterranean Sea (Pirazzoli, 1991; Lanbeck and Bard, 2000). However, for the last 1,500 years, no significant sea-level fluctuation (<1 m) has been documented for the Mediterranean Sea (Pirazzoli, 1991; Vella and Provansal, 2000; Morhange et al., 2001). The abrupt increase in sand layer frequency after ca. 1740 A.D cannot be explained by differences in sea levels. The sediment-stratigraphic change also post dates any minor sea-level fall that may have been attributable to the Little Ice Age (Tanner, 1992; van de Plassche et al., 1998). Moreover, as suggested by ancient maps (Service maritime maps of 1819, 1938 and the Cassini map, 1774, *Figure 6.4*) the position of the sandy barrier, has not shifted significantly during the last 300 years (between 30 and 80 metres landward approximately). Therefore, while it is likely that there were minor sea-level fluctuations and shoreline changes during the last 1,500 years these changes were probably inadequate to alter drastically the depositional environment of the lagoon and hence the sensitivity of the site in recording paleostorms.

6.1.2 Sediment supply changes

A change in sand layers through time can be caused by the availability of sand oceanside. The seismic campaign CALAMAR IV (Raynal et al., 2009) demonstrated the various morphologies and the pattern of sediment layers related to the Quaternary history of this coastal system. Different seismic profiles, across the shore shows different seismic units. These units present a seismic facies typical of a high energy environment which corresponds to large sand deposits (Certain et al., 2004). The present huge sand deposits observed with the seismic campaign cannot explain the decrease of sand layers between 1740 and today. It is difficult to estimate sand availability through longer timescale, however the large sand deposits present problems in explaining the changes at the site over last 1,500 years.

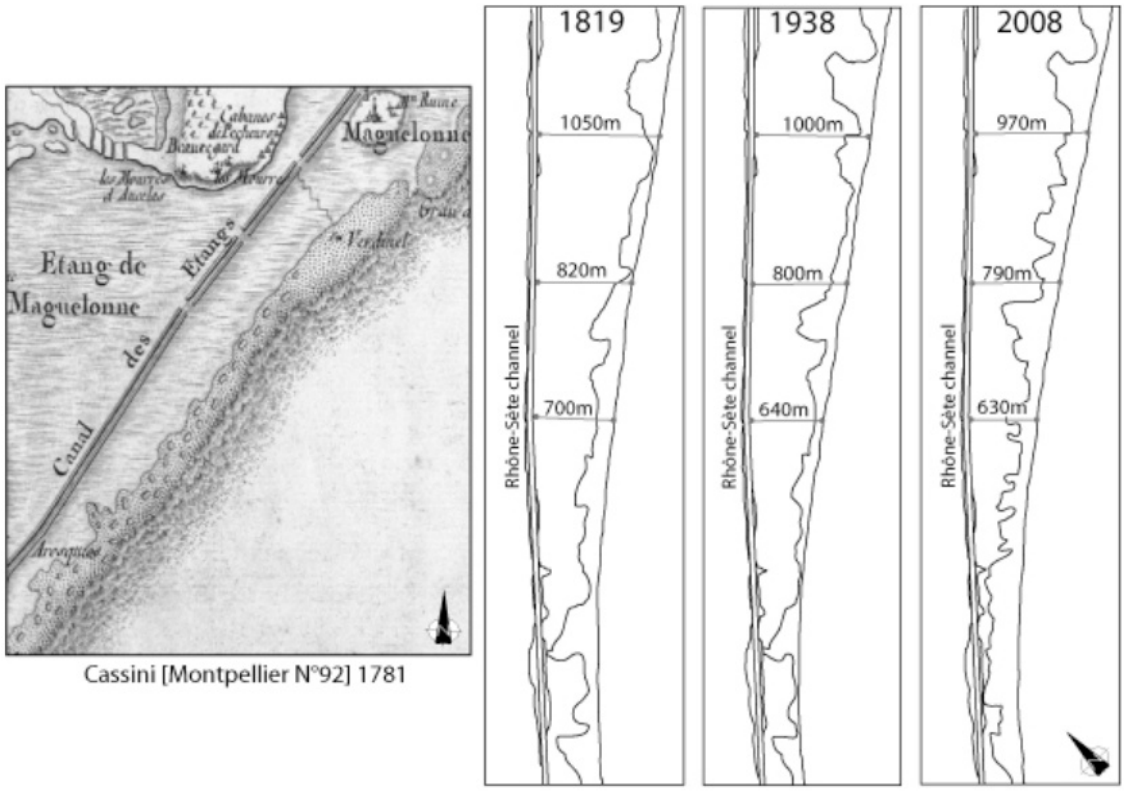

Figure 6.4 : Service martime maps of 1819, 1938 and the Cassini map, 1774. The position of the sandy barrier, has not shifted significantly during the last 300 years (between 30 and 80 metres landward approximately).

6.1.3 Inlet changes

The presence of a nearby inlet may increase the sensitivity of a particular area to storm-induced deposition. It allows for storm energy to more easily penetrate into the backbarrier area, letting a lesser storm with lower wave surge transport coarse sediment into the backbarrier. Texts and maps from the 18th and 19th centuries clearly show that ephemeral small inlets have been created by storm activity along the Pierre Blanche Lagoon and often have not induced longlasting coastal features. If a large inlet had existed over a long period and had provided a ready conduit for sand from the Gulf of Aigues-Mortes to the Pierre Blanche lagoon, this would have been reflected in the cores. However, no evidence of such active tidal connection during a long time is found in sedimentological and geochemical data for the past 1,500 years. Our cores contain overwash sand layers embedded by organic lagoon mud with sharp stratigraphic contacts, again indicating that no active Gulf inlet existed during

the past 1,500 years. The small inlets along the Pierre Blanche lagoon during the 18 and 19th centuries have been the result of increased storm activity.

6.1.4 Barrier-elevation changes

A change in barrier height may change the sensitivity of a particular area to storm-induced deposition. Coastal sand dunes frequently erode when they are overtopped by surges and waves (Nott, 2004). The diminution in height of a dune barrier, will allow subsequent smaller surges and waves generated by lower intensity storms to penetrate inland and deposit sandy sediments into back barrier environments. This situation may remain the case for many centuries and possibly longer. Eventually, the dunes will rebuild to their former height, and over time will show no evidence of once being eroded.

At present, our sandy barrier functions as a barrier with a current height of 2-3 m. Historical topographic information on the evolution of the height of this sandy barrier is limited. The barrier heights appear to have been constant for at least the past 50 years. For a longer period, we cannot assume that the barrier has remained the same height. It is very likely that the increase of intense storms between 1742 and 1900 time interval caused the diminution in height of a dune barrier increasing the sensitivity of this area for the 20th century. Nevertheless, it is clear from sediment cores that this time interval (1900 to 2008) was relatively quiet. The present morphology of the coastal barrier with a succession of overwash sand fans well vegetated is probably the result of the increase of intense storms during the 18 and 19th centuries.

To conclude, the record of paleostorm occurrences can be complicated by different factors (coastal dynamics, sea level changes, sediment supply, inlet, and barrier-elevation changes) however, the organic-rich clay/silt sediment types appearing throughout the record show that these areas were experiencing quiescent sedimentation during at least the past 1,500 years, indicating that the study sites were likely protected behind the barrier system over that time. Finally, the close agreement between documented intense storms and the recent sedimentary record in our study area indicate these backbarrier lagoons have been sensitive to overwash deposition associated with the strongest storms impacting on the area. However, in order to control localized sensitivity changes, it will be necessary in the future to employ a vast multiple site approach, as extreme storms in all the northwestern Mediterranean area would

likely result in storm surges and waves of sufficient height to overtop the barrier across wide stretches of coast and not only at localized areas.

6.2 Intensity of storms through time

The relationship between storm intensity and the size of the overwash sand body deposited in a coastal back-barrier lagoon is complex. We have acknowledged some of these confounding factors, including the abundance of sand supply, emphasizing that our working hypothesis is subject to the assumption that the geomorphic setting remains roughly the same for Pierre Blanche and Prévost lagoons during the last 1,500 years and that storm conditions (e.g., timing, duration, angle of approach) occur randomly over time (Liu and Fearn, 2000; see also Liu and Fearn, 1993). However, recognizing these complexities does not prevent us from generalizing that a positive relationship exists among hurricane and storm intensity, storm-surge height, and the size of the overwash sand body. Donnelly et al. (2001a, 2001b) demonstrates that recent and historic major hurricanes on the Atlantic coast caused significantly higher storm surges than minor hurricanes and winter storms, and that over the past several centuries only the major hurricanes left a stratigraphically distinct and regionally consistent record of overwash sand layers in the sediments of the coastal marshes.

During the past 50 years no catastrophic intense storm has directly struck Pierre Blanche, and Prevost lagoons, except maybe the 1982 storm of category 2 intensity that was not strong enough to directly deposit sand into the centre of the two lagoons, the coarse grained event layers (CGE-1/1982 event) have been identified only in one core PB04, near the lagoon shore. The four thin sand/silt layers in core PB06 have interpolated ages of approximately, 1742, 1848 and 1893 A.D.. If the two lagoons's geomorphic setting has not changed drastically during the last 1,500 years and if a positive relationship exists among storm intensity, storm-surge height, and the size of the overwash sand body, these four thin sand/silt layers recorded in the lagoon at more than 500 m from the sandy barrier, were probably formed by a catastrophic storm of category 3 intensity or more. Taking into account text description of the 1742 storm and the large overwash sand body deposited in the core PB06, the distinct 1742 sand layers were probably formed by overwash processes that occurred during a catastrophic storm of category more than 4 in intensity. This storm is probably the most intense event ever recorded during the last 1,500 years in that region. To conclude, these 4 storms of very high intensity can be called superstorms.

6.3 Comparison between flash floods and intense storms events through the last 400 years

The municipal council archives contain descriptions of meteorological or hydrological aspects concerning a flood event or damage occuring directly. These documentary series were investigated to reconstruct past floods events. Six coastal rivers located in the Mediterranean Languedoc were choosen for collecting data series, i.e. Vidourle, Vistre, Lez and Mosson, Herault and Orb rivers. The hydrosystems are generally short with steep slope longitudinal profile and present a fast response to extrem hydoclimatic events. Communal archives of fifteen villages were analysed, located along these rivers at up- and downstream levels, or in the deltaic plain for five of them. So we could i) cross-validate information using several testimonies for one event and ii) ensure that no flood are missing in the recording series. For the pre-instrumental period, a scale of event magnitude can be established using the descriptions of flood effects on the river bed and surrounding areas (Barriendos et al. 1998, Coeur and Lang, 2002). Three classes of flood magnitude have been adopted : i) ordinary small flood, with some damages to hydraulic installations and local dikes failure (class 1), ii) extraordinary flood overflow the minor bed with a large flood perimeter. River banks and dikes are destroyed on several hundred meters, crops are lost and roads damaged, (class 2) iii) the exceptional or catastrophic flood is very abrupt (flashflood) and cause severe damage to houses, bridges, other infrastructures but also human losses (class 3). These two classes are generally associated to morphogenic changes of the river bed (avulsions, meanders capture) and to regional events. The flood series obtained run since the middle of the thirteenth century, but before 1550 it is probably non exhaustive. So we present here only the results for the period 1550-1950 (*Figure 6.5*).

The historical archives show that the hydrological regime shifted from one characterized by infrequent and moderate floods before 1700 to one characterized by frequent, severe floods between 1700 and 1900 (*Figure 6.5*). The hydrological regime seems to return to moderate conditions after. In the same way, geological data (*Figure 6.3*) do not show any evidence of superstorms in the region for several hundred years prior to the late 17^{th} century A.D. The apparent increase in intense storms around 250 years ago occurs only between 1700 and 1900. This intense meteorological activity seems to return to a quiescent interval after. To conclude, overwash deposits correlate with the most intense documented floods in the area between 1700 and 1900, i.e. during the latter half of the Little Ice Age.

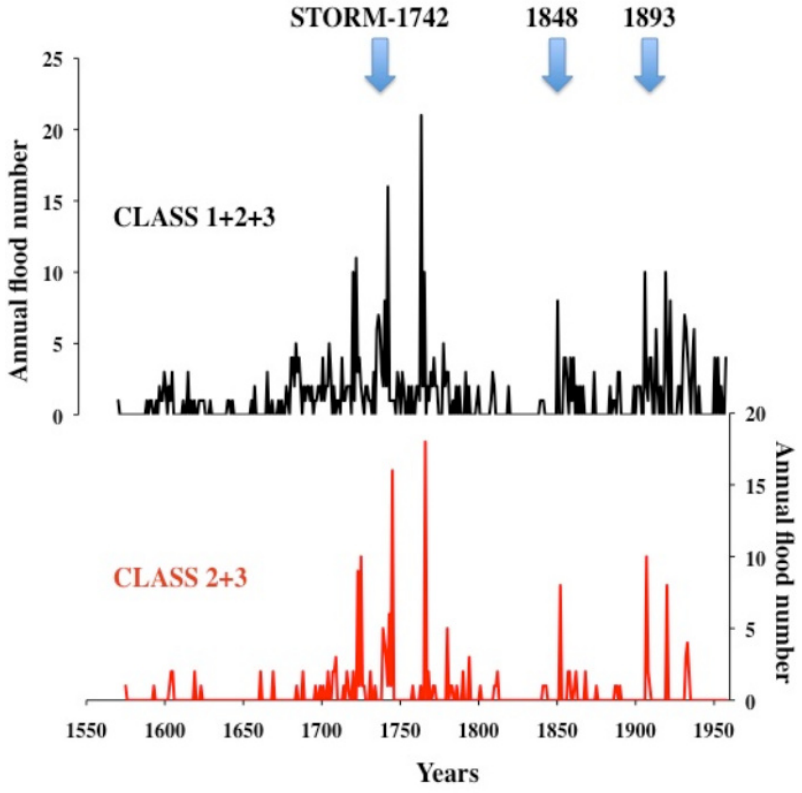

Figure 6.5 : 1565-1955: Annual flood number of Herault, Orb, Mosson, Lez, Vidourle and Vistre rivers from communal archives of fifteen villages.

6.4 Paleoclimatological interpretations

The longest record from Pierre Blanche lagoon reveals intervals of more frequent overwash deposition punctuating intervals of quiescent backbarrier sedimentation. Alternating periods of quiescent conditions and frequent intense storms are recorded in the sedimentary record and historical data and likely indicate that climate conditions may have modulated storm activity on centennial timescales. Although additional long records are necessary to test this hypothesis, one of the most likely explanation of this remarkable increase in storm frequency and intensity affecting the Languedoc region during the latter half of the Little Ice Age is a result of modifications in atmospheric circulation and variability.

6.4.1 Is the North Atlantic Oscillation the main control mechanism?

The North Atlantic Oscillation (NAO) is responsible for much of the climate variability observed in the Mediterranean region (Hurrell, 1995) at present day and possibly during the

last 500 years (Luterbacher et al., 2002). During positive phase of the NAO, the high-pressure gradient between the strong Azores anticyclone and the Iceland depression results in a northward shift and an increase strength of the westerlies (Hurrell, 1995). The “storm track” crosses the northern part of Europe. When the NAO is high, dry conditions develop over southern Europe and North Africa (Pittalwala and Hameed, 1991). Conversely, when the NAO is negative, the pressure gradient between the Azores high and the Iceland low decreases (Hurrell, 1995). The westerlies are shifted to the South providing precipitations over the Mediterranean and the North African continent. In this configuration, the “storm track” crosses the southern Europe. Our historical archives and geological datas show an increase of storm and flood activities in the Languedoc region during the latter half of the Little Ice Age, when tree-ring based reconstructions (Luterbacher et al., 2002; Guiot et al., 2005) indicate a negative (cooler) phase of the NAO. We could thus hypothesized that the active storm period in the Languedoc are the result of shifting storm tracks to the south related to a negative phase of the NAO. However, in our region this assumption is not completly satisfactory for several reasons: First, if the active and inactive intense storm periods are the result of shifting storm tracks between northeastern and southwestern locations, thus we should observe a spatial see-saw pattern of storm activity between the northern part of Europe and the Mediterranean area. However, Jegersma et al., (1995); Aagaard et al., (2007) and Sorrel et al., (2009) clearly show an increase of storm frequency during the little Ice Age in the northern part of Europe. This active period in the northern locations fall within the period of high storm frequency in the southern part of Europe. This synchroneity provides evidence that a millennial-scale spatial see-saw pattern of atmospherically-driven storm tracks may not be a major climate mechanism forcing changes in the superstorm frequency in our region. Secondly, the intense storm events reconstructed from sedimentary archives do not show a correlation with the reconstructed NAO index on the last 500 years (Luterbacher et al., 2002).

6.4.2 What are the other climate mechanisms that may control the frequency of superstorm events?

The physical explanation for the increased occurrence of extreme wind events over the region of Languedoc during the Little Ice Age is therefore not straightforward. Based on an ensemble of six simulations of the Maunder Minimum (MM, going from 1640 to 1715 with time varying forcing) using an Ocean-Atmosphere General Circulation Model (OAGCM), Raible et al. (2006) consistently find an increase in cyclone occurrence in the Mediterranean

during the MM compared to present-day. They attribute this signal to a larger cooling in the high latitudes than in the low latitudes (due to polar amplification effect, Masson-Delmotte et al. 2006), leading to enhanced lower tropospheric baroclinicity over a large Central Atlantic-European domain. This result suggests that the cooling observed during the MM over Europe (Guiot et al. 2005) may be associated with upstream changes in the large scale dynamics of the atmosphere over the Mediterranean and North Atlantic sectors. It is hypothesized here that such a large-scale flow alteration may have modified the occurrence of extreme wind events along the French Mediterranean coast, thus explaining the local signal found here over the region of Languedoc. To demonstrate this hypothesis, it is necessary to adopt a downscaling approach in order to relate the small scale extreme events over the region of Languedoc to the large scale dynamics of the atmosphere.

What is the relationship between southwestern Europe climate variability and strong storms for modern climate conditions ? Using present-day large scale circulation data for the period 1960-2001 (NCEP-NCAR reanalysis, Kalnay et al. 1996), we compute the three leading Functions (EOFs for Empirical Orthogonal Functions) of the 500mb geopotential height for the months September-October-November-December (SOND, the period when events of high intensity occur in the analysed region) on a daily basis. We find three characteristic patterns associated to the NAO, the BL (Blocking, Pavan et al., 2000) and the EAP (East Atlantic Pattern, Barston and Livezey 1987). Then we classify the 204 events of high intensity (c.f. section 2) occurring over the same period within the different EOFs (when statistically significant), it has to be kept in mind, however, that these events are of lower intensity than during the LIA. The results of this classification appear in the *Tableau 6-1*. This table suggests that strong wind events over the region of Languedoc are mostly (26% of the total events) associated with EAP positive phase, while, on the opposite, the negative phase prevents the occurrence of these events (2%). The positive phase is characterized by a low pressure monopole located off Western Europe leading to large-scale southerlies over the western Mediterranean basin (*Figure 6.6*). This general dynamics is favorable to local wind amplification due to both coastal configuration, and to formation of explosive synoptic scale systems leading to strong events.

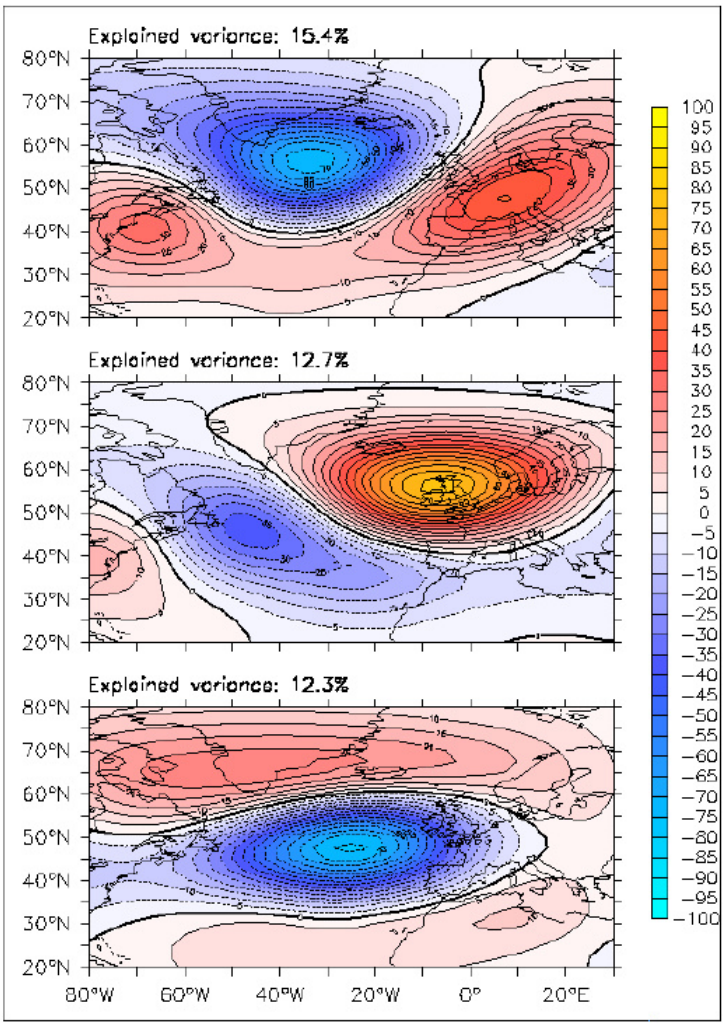

Figure 6.6 : Three leading Empirical Orthogonal Functions (EOFs) of the 500mb geopotential height (in m) computed on a daily basis for the months September-October-November-December (SOND) using the 1960-2001 NCEP reanalysis (Kalnay et al.1996). Are represented the positive phase of each EOF. The first EOF is identified as being the NAO (North Atlantic Oscillation, Hurrel 1995), the second as the BL (Blocking, Pavan et al., 2000), and the third as the EAP (East Atlantic Pattern, Barston and Livezey 1987). The patterns are not canonical, since the analysis is performed over SOND, which are the months when the extreme events occur around the Languedoc region, in place of the classical winter months.

Our results do not suggest a significant link between strong wind events over the region of Languedoc with the NAO. This study clearly demonstrates that on different timescales the NAO is not the main control mechanism. We could suggest that during the Little Ice Age the positive phase of the EAP mode is favored. This assumption has to be verified. This is

planned to be done in a companion study, by using last millennium simulations from the Météo-France CNRM-CM3 (Salas y Mélia et al., 2005) OAGCM.

	Positive phase	Negative phase
EOF1 (NAO)	15 (7%)	28 (14%)
EOF2 (BL)	32 (16%)	21 (10%)
EOF3 (EAP)	53 (26%)	5 (2%)

Tableau 6-1 : Number of extreme events in the Languedoc region for the period going from 1960 to 2001 classified on each EOF (for Empirical Orthogonal Functions) as obtained in Figure 6.6. In parenthesis are the percentages of the events in the EOF with respect to the total number of extreme events (204).

6. 5 Storm risk estimation for the last 1,500 years in the Northwestern Mediterranean area.

This study has implications for risk assessments. During the past 100 years no catastrophic intense storm has directly struck the Languedoc region, the sediment stratigtaphic data suggest an increase of catastrophic storms of category 3 intensity or more during the latter half of the Little Ice Age. The area on average has a 0.2% probability of being struck by a catastrophic storm by years on the last 2000 years. This estimate is higher, 2% during the latter half of the Little Ice Age, the risk is increased by a factor of 10. In the same way, we have shown an increase of flash flood events during this period with sometimes more than 7 intense events (class 3) per year. Communal archives clearly show the terrible impact of these intense events on the society during this period (Blanchemanche, accepted). Today, the lack of familiarity with such extreme events has led to the assumption that they are unlikely to ever occur within the lifetime of many individuals. This has led to the development of inadequate policies governing the location of buildings well within the zone of possible storm tide inundation. In the Gulf of Aigues-Mortes, the development of seaside tourism during the 20th century was marked by the construction of numerous seaside resorts (Carnon, La Grande-Motte, Port Camargue) or extension of small fishing villages (Palavas-les-Flots; Le Grau-du-Roi). These stations were built on the sandy barrier in the 1970s. The town of Carnon is established on a wide washover fan that was probably set up during the "Little Ice Age". The resident population on the coast has increased by a factor of 15 since 1750 with a dramatic

increase since the 1970s. Today, 150 000 people live all the year on the sandy barrier and more than the double in summer (*Figure 6.7*).

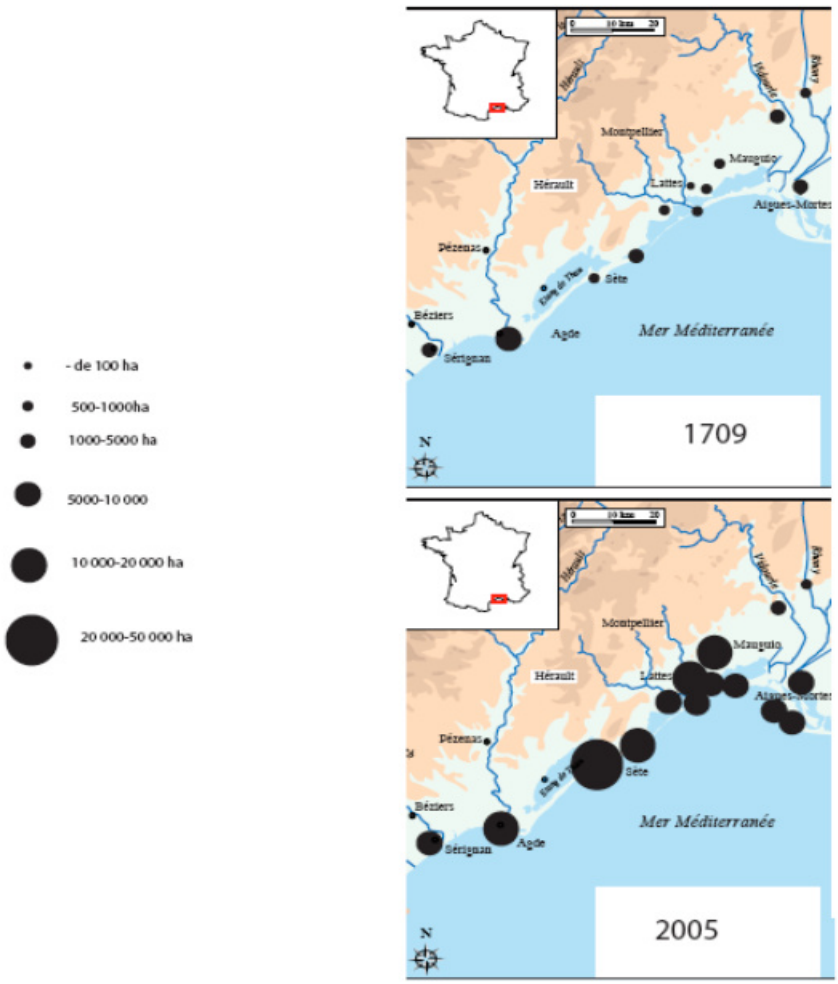

Figure 6.7 : The resident population on the coast has increased by a factor of 15 since 1709 with a dramatic increase since the 1970s. Today, 150 000 people live all the year on the sandy barrier.

The last few centuries have seen a regime shift in the occurrence storms crossing the coast in the Northwestern Mediterranean area. If the regime of the latter half of the Little Ice Age came back today, the implications will be dramatic. The percentage number of housing, accommodation or business buildings and different infrastructures (dams, recent harbours) inundated will increase considerably. To conclude, it is really important to better understand mechanisms causing regime shifts in the Northwestern Mediterranean area for making more accurate predictions of the levels of risk and exposure as human populations, urbanization and tourism grow rapidly along this Mediterranean coast.

7. Conclusion

This study shows that reconstructing the overwash history of two backbarrier lagoons can provide a sedimentary record of intense storms. Four distinct, overwash deposits are identified in these lagoons at more than 500 m from the sandy barrier, which is much more important than the deposit of sand storm of 1982 (category 2 intensity). Since we have demonstrated that the two lagoons's geomorphic setting has not changed drastically during the last 1,500 years we suggest that these four overwash deposits were probably formed by catastrophic storms of category 3 intensity or more.

Overwash deposits correlate with the most intense documented floods between 1700 and 1900, i.e. during the latter half of the Little Ice Age. Comparison of the sediment record with palaeoclimate records indicates that this variability was probably modulated by atmospheric dynamics. We suggest that extreme wind events are associated with a large cooling of Europe and probably link to variations in the Eastern Atlantic Pattern. This study has also implications for risk assessments of intense storms. During the latter half of the Little Ice Age, this risk is increased by a factor of 10. If this regime came back today, the implications will be dramatic.

Acknowledgments

We are grateful with Michel Serrane, Michel Condomines, Patricia Stanley-Russell, Stéphanie Bordelais and Mickaël Barbier for useful comments and discussions. This study was part of the ECLICA program supported financially by the ACI-FNS/ INSU program "Aléas et changements globaux". C. Cassou and D. Swingedouw received support from Ecarsel project (ANR program).

6.2 Echelle Holocène : Article 6: Quaternary Sciences Reviews

Increase of storm events during the Holocene cold events in NW Mediterranean Sea

Sabatier, Pierre[1], Dezileau, Laurent[1], Colin, Christophe[2], Briqueu, Louis[1], Martinez, Philippe[3], Bouchette, Frédérique[1], Raynal, Olivier[1]

1 Université Montpellier 2, Geosciences Montpellier, CNRS/INSU, UMR 5243, Montpellier, France.
2 Université Paris-Sud, Laboratoire des Interactions et de la Dynamique des Environnements de Surface, CNRS/INSU UMR 8148 Orsay, France.
3 Université Bordeaux 1, EPOC, CNRS, UMR 5805, France.

Quaternary Sciences Reviews in prep

Abstract

The effects of climate change on extreme events are difficult to assess because extremes present large variability and consequently, it is difficult to identify significant trends in relation to the lack of instrumental long time series. Here we present a record of these extreme storm events in the French Mediterrannean coast over the past 7000 years based on a long sediment core from lagoonal environment in Gulf of Lions. Using a high resolution multi-proxies approach on core associating grain size, faunal to reconstruct Mid to Late Holocene history of backbarrier deposits in relation to landfalling activity.

Even if change in lagoon geomorphological setting over the Holocene does not allow to compare storm events in terms of intensity trough time, we have recorded six periods of increase in storm activity at 6200, 5500, 4400, 3200, 1500 yr cal B.P. and over the LIA (450 and 100 yr cal B.P.). These evidences of changes in coastal hydrodynamic, inversely correlated to periods of aridification in Western Mediterranean region, are in phase with those observed over the North Atlantic and correspond to Holocene cooling events. This increase in storm activity during Holocene cold events over Mediterranean region was probably due to thermal gradient increase leading to enhanced lower tropospheric baroclinicity over a large Central Atlantic-European domain. This study demonstrates that temperatures in North Atlantic region influence the severe storm activity and therefore the Mediterranean climate at Holocene timescale.

1. Introduction

Across the 20th century, the average global surface temperature has increased by about 0.75°C and predicts a significant warming for the 21st century, mainly due to the increased in greenhouse gases (IPCC, 2007). The Mediterranean region is one of the world's areas most vulnerable to the climate change (Giorgi, 2006). Regional climate simulations have been used to investigate the variations of precipitation and the cyclonic activity in the Mediterranean region. Gibelin and Déqué (2003) predict, using ARPEGE model, an overall warming and drying in all seasons except in winter over North-Western Mediterranean area with an increase in precipitation. Moreover, Lionello and Giorgi (2007) show that the reduction of cyclone activity observed in future scenarios would be responsible for the negative change in precipitation on the southern and eastern Mediterranean coast, while positive change occurs in

Northern parts in relation to increased strength of mid latitude storm track. In addition, Gaertner et al., (2007) detect for the first time a risk of tropical cyclone development over the Mediterranean Sea under future climate change conditions. However, the effects of climate change on extreme events are difficult to assess because extremes present larger variability than average values and consequently, it is more difficult to identify significant trends in relation to the lack of instrumental long time series (Webster et al., 2005; Emanuel 2006a; Landsea et al., 2006). It is therefore, important to study the past storm activity in order to better understand the possible regional and local long term trends of these events, associated to past climate conditions.

In this study, we focus mainly on the Gulf of Lions (*Figure 6.8*), a region of the French Mediterranean coast. This area is particularly sensitive in terms of societal issues for the risks of flooding (the Mediterranean Heavy Precipitating Events) and the risk of coastal erosion/submersion during storm events. In September 2002, large floods hit this region; there were 23 victims and damage was estimated at over one billion Euros. Linked or not to these rainy episodes, the region is also prone to frequent storms. These events can have dramatic actions when the winds and waves are associated with high sea surges (Ullmann et al., 2008) attacking coastal sand dunes, sometimes breaking the sandy barrier. For the last few decades, the most important storm is that of 1982 with 46m/s of wind (category 2 in Saffir–Simpson scale), this storm caused the deaths of 15 people and economic losses were estimated at 400 million euros. Wet season (October to March) rainfall over the Northern Mediterranean which corresponds to the so-called storm season has decreased over the last four decades, mostly forced by the decline in the intensity of cyclogenesis event (Trigo et al., 2000). Cyclones are the cause of most of the heavy precipitations in the whole Mediterranean region (Trigo et al., 2000; Jansá et al., 2001). Lionello et al., (2006) find a significant decrease in winter cyclone density over most of the Western Mediterranean during the last 150 years, this tendency is also confirmed by a work on sedimentary archives (Sabatier et al., accepted a). However, there is no evidence that the behaviour of Mediterranean climate extremes on this timescale is inconsistent with natural climate fluctuation as NAO (North Atlantic Oscillation) or EAP (Eastern Atlantic Pattern) during earlier centuries (Quadrelli et al., 2001 ; Sánez et al., 2001 ; Krichak et Alpert, 2005 ; Lionello et al., 2006 ; Luterbacher et al., 2006 ; Trigo et al., 2006; Dezileau et al., submitted).

Reconstruction of the recurrence and intensity of paleostorms in coastal area is an important topic of study due to the recent concentration of resource and population in this zone (Pielke and Landsea 1999; Turner et al., 2006; Lionello et al., 2006; Dezileau et al., submitted).

Therefore, geological data offers opportunities to reconstruct a long term record of intense events and can extend the documented record well beyond the observational record in order to identify how storm activity has responded to past shifts in climate. This study was a part of the ECLICA project, one of the aims of which was to identify regional storm patterns using systematic, historical and paleostorm data (Dezileau et al., 2003). Usually, reconstruction of paleostorm events in coastal environments has been made by identifying the recurrence of overwash coarse grained and associated deposits (Liu and Fearn 1993, 2000; Collins et al., 1999; Donnelly et al., 2001a, 2001b; Nott, 2004; Donnelly, 2005; Dezileau et al., 2005; Donnelly and Woodruff, 2007; Scipelly and Donnelly, 2007; Frappier et al., 2007; Woodruff et al., 2009).

The Gulf of Lions shore line is characterized by many coastal wetlands that are the result of the interaction between a process of shore line regularization by migrations of sandy barriers due to the sediment transfer through littoral hydrodynamics; and a filling of these areas by the fluvial and marine inputs (Certain et al., 2004; Raynal et al., 2009). In this study we present a high-resolution multi-proxy approach on a long core from the Pierre Blanche lagoon. Part of this record was the subject of a previous work that discussed in detail the link between the sedimentary record of extreme storm events and climate changes of the last 1000 years and the Little Ice Age (Dezileau et al., submitted). Here we extend the record back to the last 7000 years. We then try to assess the most probable mechanisms behind the observed variability of extreme storm events in the area at the millennial scale.

2. Study area

This study focuses on the Palavasian wetland complex located to the West of the Rhône delta, 10 km south of the city of Montpellier (*Figure 6.8*). This area consists of seven small lagoons, with shallow water depth, limited to the South by a narrow sandy barrier, attached from place to place to subdued rocky capes (Aresquier wood or Maguelone Church peninsula, Raynal et al., 2009), and to the North by calcareous Mesozoic hills (Gardiole Mountain). In some places, the barrier is weak and highly sensitive to high energy events, enabling temporary but strong marine influence when the barrier breaks during storm events. This is commonly seen by traces of over-wash fans and ancient temporary inlets (Dezileau et al., 2005). Most of the sediments supplied to the area are carried by the Mosson coastal river. The Mosson drainage basin is mainly constituted by Mesozoic (limestone) and Cenozoic (conglomerate, carbonated

sandstone and clay) sedimentary rock with Quaternary deposits. This wetland complex is now crossed by the artificial Rhône-Sète navigation channel constructed in the 17th century. This study focuses on the Pierre Blanche located in the Southern part of this system (*Figure 6.8*), with water depths of 60 cm.

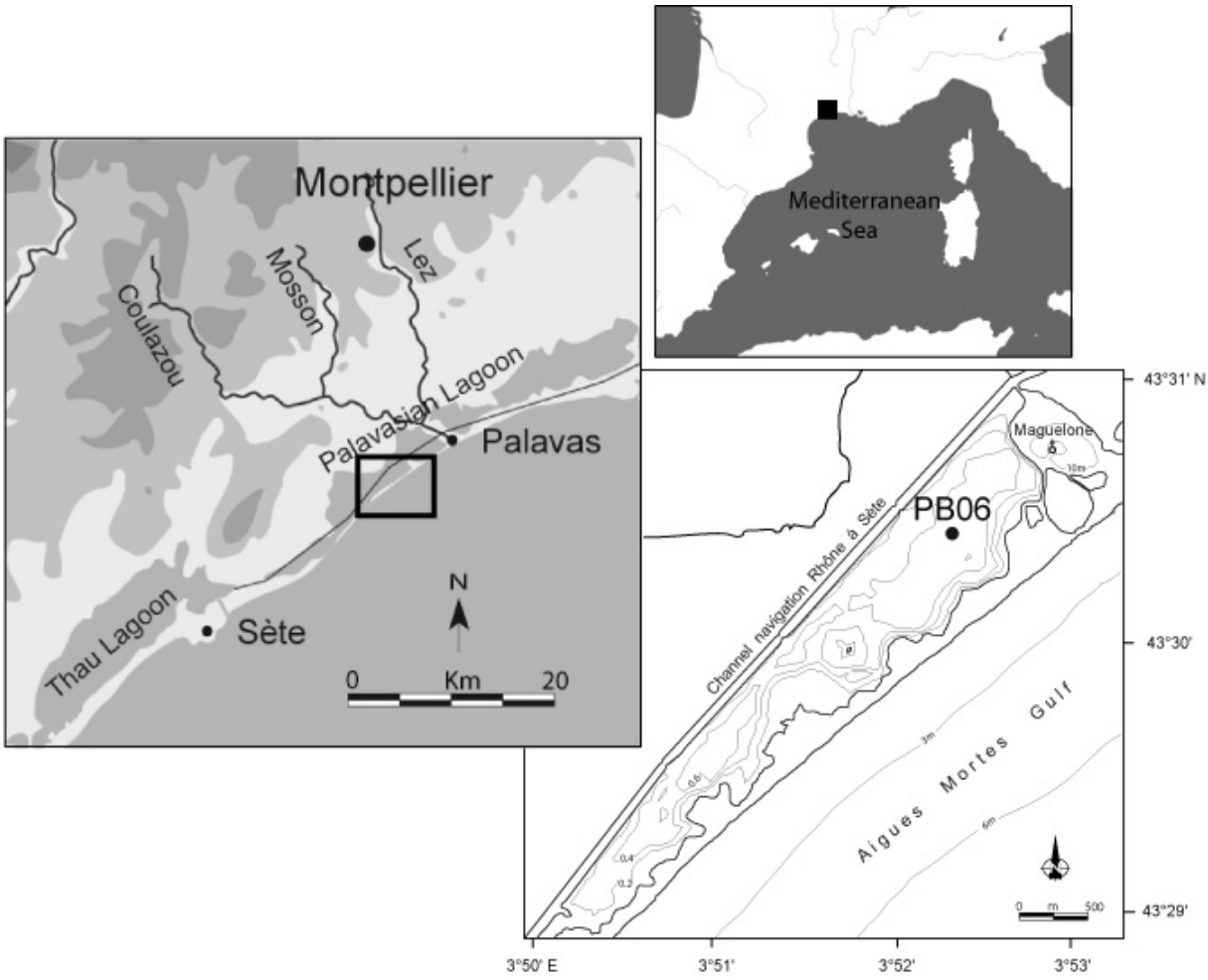

Figure 6.8 : Map of Pierre Blanche lagoon with localisation of the core PB06.

This coastal area is characterized by a classical microtidal environment with maximal tide ranges < 50 cm. The annual significant wave height (Hs) and period (Tm), measured at the Sète station (located 10 km offshore, at a water depth of 32 m) are fair weather waves during 88% of the year (Hs=0.84 m; Tm=4.2 s). However, this fair weather wave climate is occasionally disturbed by east to south-eastern storms, like that of 1982. The annual proportion of waves higher than 4 m was around 1% and the return period of a 6m high wave was every 10 yr (Guizien K. personal communication).

3. Material and methods

A piston core of 7.9 meters long (PB06) was collected in the Pierre Blanche lagoon in March 2006 in the ECLICA project (*Figure 6.8*) with the UWITEC© gravity coring platform (University of Chambery). This device consists of a 2 m transparent plastic liner mounted with an "orange-peel" core catcher. No compaction due to the coring system was observed. At the laboratory, cores were split, photographed, radiographed using the Scopix X-ray scanning (EPOC, University of Bordeaux), logged in detail (noting all physical and biogenic sedimentary structures and vertical facies successions), and divided into 1 cm vertical sections prior to analysis.

Grain size and macro-fauna content analyses were performed on 2 cm long sections. To study mollusc shells, samples were sieved at 1mm and the number of individuals of all species was counted (every 2 cm). The most representative molluscs of lagoonal environments are *Hydrobia acuta, Abra ovata, Cerastoderma glaucum* and those of typical marine hard substrate environment are *Bittium recticulatum* and *Rissoa ventricosa* (Dezileau et al., 2005). Grain size distribution was determined using a Beckman Coulter© LS 13 320. Only the <150µm fraction was analysed due to the high concentration of shell fragments of a size exceeding 200 µm. Bulk sediments were first suspended in deionized water and gently shaken to achieve desegregation. After introduction of sediment into the fluid module of the granulometer, ultrasounds were used to avoid particle flocculation.

Clay minerals were identified by X-ray diffraction (XRD), every 2 cm, using a PANalytical diffractometer at the Laboratoire IDES (Université de Paris XI) on oriented mounts of non-calcareous clay-sized (<2 µm) particles. The oriented mounts were obtained following the methods described in detail by Colin et al. (1999). Three XRD runs were performed, following air-drying, ethylene-glycol solvation for 24 hours, and heating at 490ºC for two hours. Identification of clay minerals was made mainly according to the position of the (001) series of basal reflections on the three XRD diagrams. Semi-quantitative estimates of peak areas of the basal reflections for the main clay mineral groups of smectite (including mixed-layers) (15–17 Å), illite (10 Å), and kaolinite/chlorite (7 Å) were carried out on the glycolated curve using the MacDiff software (Petschick, 2000). Relative proportions of kaolinite and chlorite were determined based on the ratio from the 3.57/3.54 Å peak areas.

Avaatech scanners performed continuous semi-quantitative downcore X-ray fluorescence (XRF) analysis on the surface of split sediment cores. The split core surface has to be covered

with a 4 mm thin Ultralene to avoid contamination of the XRF measurement unit and desiccation of the sediment. Core PB06 was run through a non-destructive ITRAX core scanner at the Laboratory EPOC (Université de Bordeaux 1) to obtain subcentimeter-resolution of the sediment's elemental composition, reported as counts per second. In the present study, the selected step size was 0.5 mm with a XRF count time at each step of 30 s. Geochemical data was obtained at different tube voltage, 10 KeV for Al, Si, S, Cl, K, Ca, Ti, Mn, Fe and 30 KeV for Zn, Br, Sr, Rb, Zr (Richter et al., 2006).

Monospecific shell samples (*Cerastoderma glaucum*) were selected for ^{14}C age determinations. ^{14}C analyses were conducted at the Laboratoire de Mesure ^{14}C (LMC14) on the Accelerator Mass Spectrometer (AMS) ARTEMIS in CEA institute at Saclay (Atomic Energy Commission). ^{14}C ages were converted to calendar years using the Calib 5.0.2 calibration program (Hughen et al., 2004) at two standard deviations.

4. Chronology framework

The chronology of core PB06 has been established using ^{210}Pb and ^{137}Cs chronology associated with Accelerator Mass Spectrometry (AMS) ^{14}C dates on monospecific shell sample (Sabatier et al., Accepted). These authors make an estimation of radiocarbon reservoir age which varies in relation to palaeoenvironmental change (see section 5.2) between 618 ± 30 ^{14}C yr (local marine reservoir age, Siani et al., (2000)) for the deepest part of the core to 943 ± 25 ^{14}C yr (estimated by correlation with ^{210}Pb and ^{137}Cs chronology and historical events) for the last 1.7 m. In the Pierre Blanche lagoon, the final model ages of PB06 core (*Figure 6.9*) suggest a low sedimentation rate of 0.18 $mm.yr^{-1}$, at the base of the core. This rate increases from 1 $mm.yr^{-1}$ between 6385 to 948 ^{14}C yr to 2.72 $mm.yr^{-1}$ over the last millennium. For the modern part of the core, the accumulation rate is the same as that estimated through the ^{210}Pb and ^{137}Cs chronology (2.65 $mm.yr^{-1}$).

5. Results

The lagoon is mostly filled by grey clay and silt with shell fragments alternating with layers of fine sandy material. Lithological description of PB06 core based on grain size, sedimentary structure and fauna content allows us to identify different facies interpreted in terms of lagoon

depositional environments (Sabatier et al., 2010). PB06 is constituted by two main sedimentary units above Pliocene deposits. The first one is a complex basal polygenic surface consisting of the ravinement surface and above conglomerate originating from subaerial erosion during times of relative sea-level low-stand and subsequent reworking during the ensuing transgression. The second one is constituted by clay and silt with shell fragments interpreted as lagoonal depositional environment consequent to the Holocene filling of this coastal area. In this study we focus, in the upper unit, on the variations of sediment properties in order to identify paleostorm events.

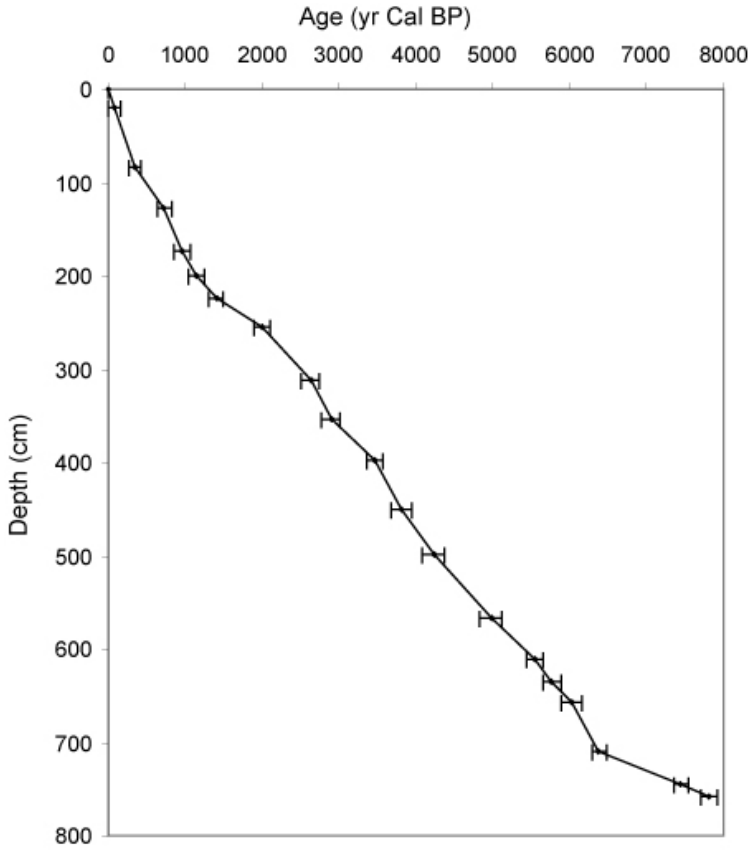

Figure 6.9 : Age versus depth plot of chronological data for core PB06. Solid horizontal lines denote 2 standard deviations for radiocarbon ages.

5.1. Grain size

Grain size data is generally displayed in a spectrum where the percentages of the populations are plotted vs. grain size fraction. They show a combination of different populations of particles, which vary in time describing different deposit mechanisms. Boulay et al. (2003)

used the standard deviation of each grain size interval as a simple method to identify the grain size population with the highest variability. Using this method, we can determine the grain size classes having the most important variation through time. Standard deviation values vs. grain size classes of core PB06 are displayed on *Figure 6.10.* Two main grain populations, presenting the highest variability, can be identified. One between 2 and 10 µm (clay to fine silt) and another coarser, between 30 and 100 µm (fine sand). The evolution with depth of these two populations displays eight main changes in PB06 core with a strong anti correlation between fine and coarse sediment revealed by the grey bands on *Figure 6.11.*

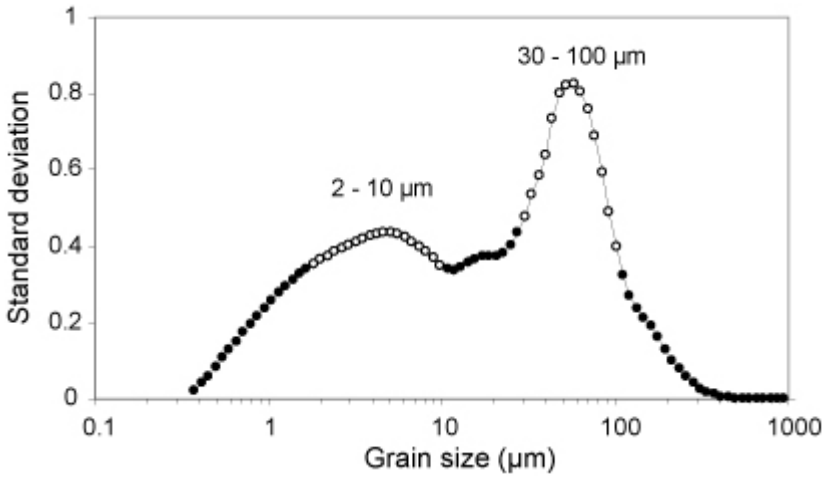

Figure 6.10 : Standard deviation values vs. grain size class diagram of core PB06. Open circles are the most important granulometric populations, with one (clay to thin silt) between 2 and 10 µm, and the other (thin sand) between 30 and 100 µm.

5.2. Fauna contents

Macropaleontology analyses are a good indicator of a lagoon paleo-isolation state because it develops in different ranges of salinity, temperature and oxygenation. In fact, one specie develops typically in a lagoon environment (*Hydrobia acuta*) whereas another is typical of a marine environment (*Bittium reticulatum*) (*Tableau 8-2*). The presence of marine species within the lagoon indicates either their transport during a storm event or a change in environmental conditions. Data of *Figure 6.11* shows a good anti-correlation between species living in lagoon conditions and that representative of the marine environment. Dezileau et al (2005) and Sabatier et al., (2008) suggests that the close association of sandy layers, marine species and the disappearance of lagoonal fauna propose that the observed sequences can be

interpreted by a succession of marine invasions of the lagoon during storm events, followed by closure of the barrier and return to typical lagoon conditions. Nevertheless, this assumption is valid when lagoonal species are dominant in an isolated lagoonal environment.

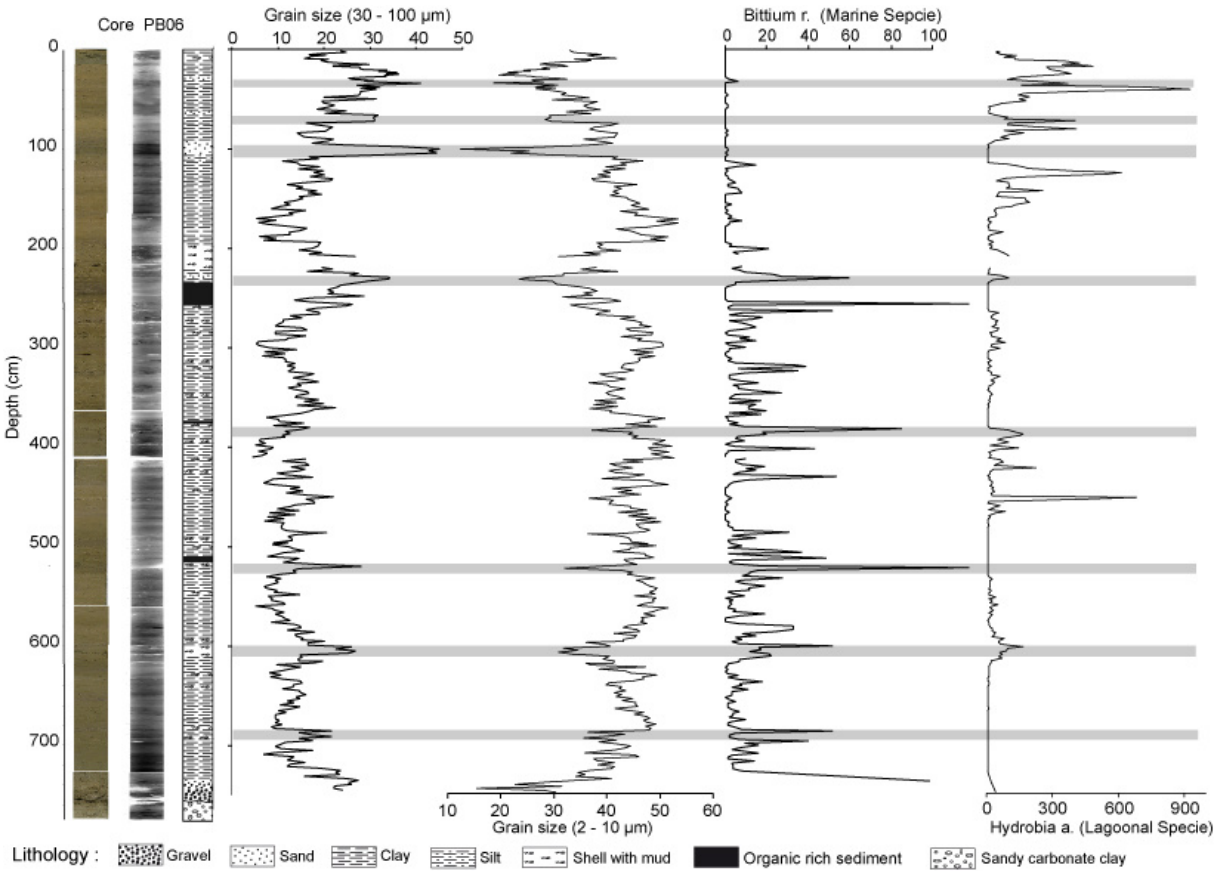

Figure 6.11 : Core PB06 with from left to right: Photography, X-ray, Grain size population of thin sand (30 – 100 µm) and clay to thin silt (2 – 10 µm), Number of Bittium recticulatum (marine specie) and Number of Hydrobia acuta (lagoonal specie). Shaded areas mark the main variations.

Sabatier et al., (2010) show a main change in mollusc population at around 190-170 cm characterized by an increase of the most typical lagoonal specie *Hydrobia acuta*, whereas the number of marine specie *Bittium recticulatum* decreases. These authors suggest a change in environmental conditions (salinity, temperature, nutriments, and oxygenation) from a lagoonal depositional environment, with marine influence to a more isolated lagoonal environment. Such a change could result from local paleo-morphological modifications such as a closure of the communications between the lagoon and the sea. That implies a shift from a protected lagoon to an isolated lagoon environment in relation to the final closure of the

sandy barrier by coastal hydrodynamics. Therefore, numbers of lagoonal and marine specie in the two first meters of PB06 can not be compared to the rest of the core in term storm events.

5.3. Clay minerals

Sabatier et al., (submitted) show that clay minerals display significant differences between the Mosson drainage basin, with high concentration of smectite (73% - 81%) reflecting erosion with reworked processes of ancient formation as Cenozoic conglomerates and the sandy barrier, mostly characterized by high contents of illite (45% - 59%) and chlorite (17% - 26%) related to sediment from the Rhône River. Sediments from PB06 core present mean values for clay minerals included between the Mosson drainage basin and sandy barrier contents. This core consists predominantly of smectite (15% - 70%) and illite (16% - 55%) with less content of chlorite (3% - 25%) and kaolinite (6% - 17%) (*Tableau 8-3*). Theirs average percentages are 44% for smectite, 33% for illite, 12% for chlorite and 11% for kaolinite (*Figure 6.12*). In *Figure 6.12* clay minerals can be subdivided into three groups along PB06. Changes of illite and chlorite display similar variations. Smectite general trend is inversely correlated to illite and chlorite, shaded bands. Kaolinite contents seem to vary in time with the same trend as smectite. Therefore, we adopt the ratios of smectite/(illite + chlorite) as mineralogical indicators to reconstruct the history of paleostorm events in the suited system.

5.4. Geochemistry

X-ray fluorescence core scanning provides high-resolution palaeoenvironmental information in a variety of sedimentary settings. These results are inherently semi-quantitative due to the nature of the surface of split-sediment cores due to the effects of sample inhomogeneity and surface roughness. These characteristics are particularly pronounced for sediments containing abundant medium–coarse sand-sized particles such as shell fragments in coastal environments (Richter et al., 2006). Therefore, we have to represent geochemical data, obtained by XRF measurement, in relation to other elements. In this study, we choose to normalize the different elements by the Aluminium, representative to detritic component from the watershed.

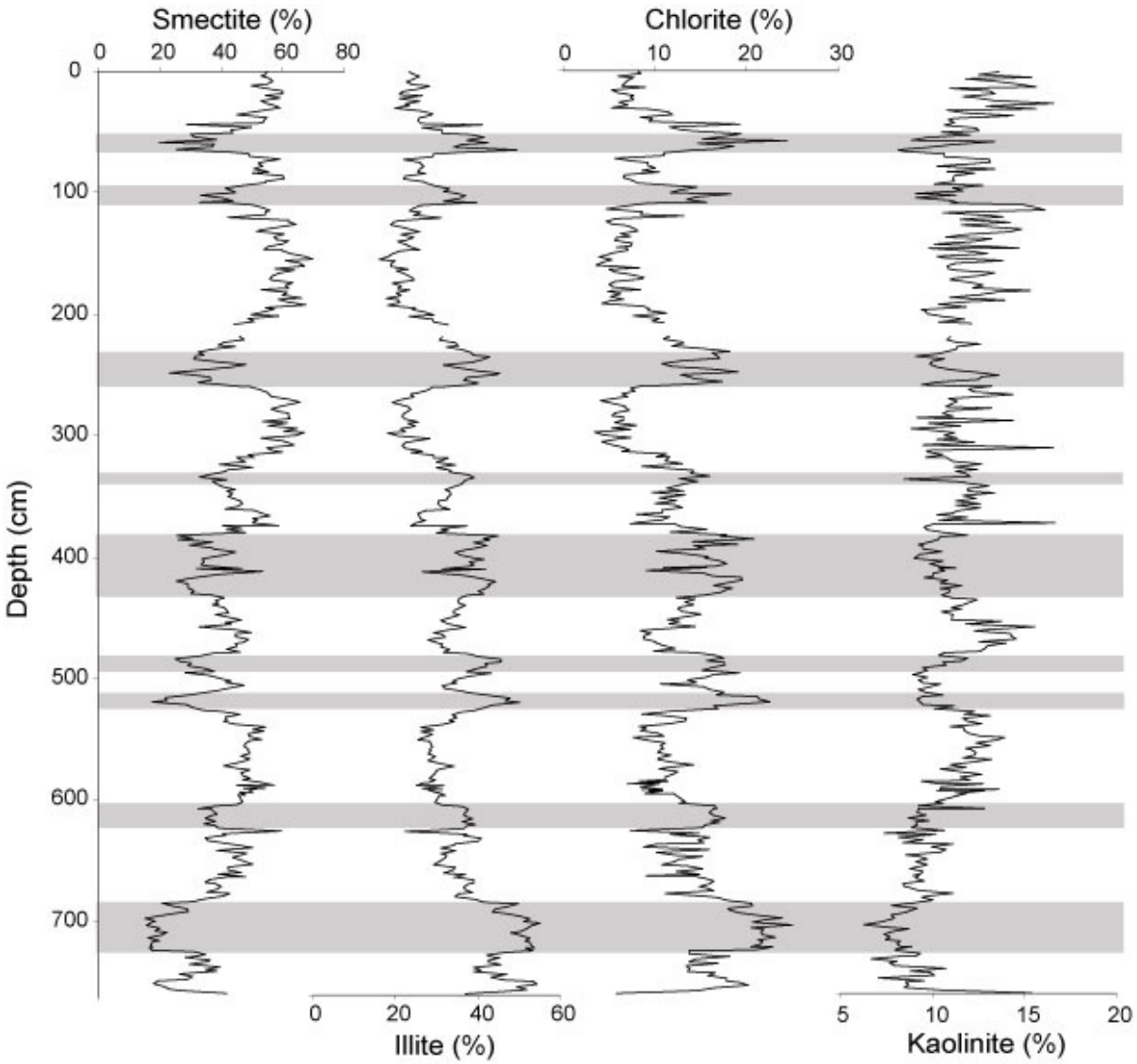

Figure 6.12 : PB06 clay minerals analyses contents (%) obtained on the carbonated-free <2 µm size fraction. Smectite and illite are dominant (up to 75% of the total clay minerals). Illite and chlorite co-vary opposed to that of smectite. Kaolinite contents do not vary significantly with time. Shaded areas mark the main variations.

The Mosson drainage basin is characterized by Al_2O_3, Fe_2O_3 and Th (Sabatier et al., submitted). Another source is defined by SiO_2 and Zr respectively abundant in quartz, and heavy minerals present in the sandy barrier. The authigenic productivity is traced in lagoonal sediment by shell abundance with high concentration in CaO and Sr. In *Figure 6.13*, we represent on one hand Si/Al and Zr/Al ratios in order to reconstruct the influence of marine component during paleostorm events (high values) and on the other hand Ca/Al and Sr/Al ratios to trace periods of large concentration in mollusk population. Si/Al and Zr/Al ratios

display a good correlation, especially for the first five meters of the core (shaded bands). Ca/Al and Sr/Al ratios show also a pretty good correlation, increase of these values could be due either to a strong biogenic productivity or to the reworking and the transport of shells from the sandy barrier during high energy events. These hypotheses explain how increase of Ca/Al and Sr/Al ratios are not systematically associated with Si/Al and Zr/Al ratios related to paleostorm events (*Figure 6.13*).

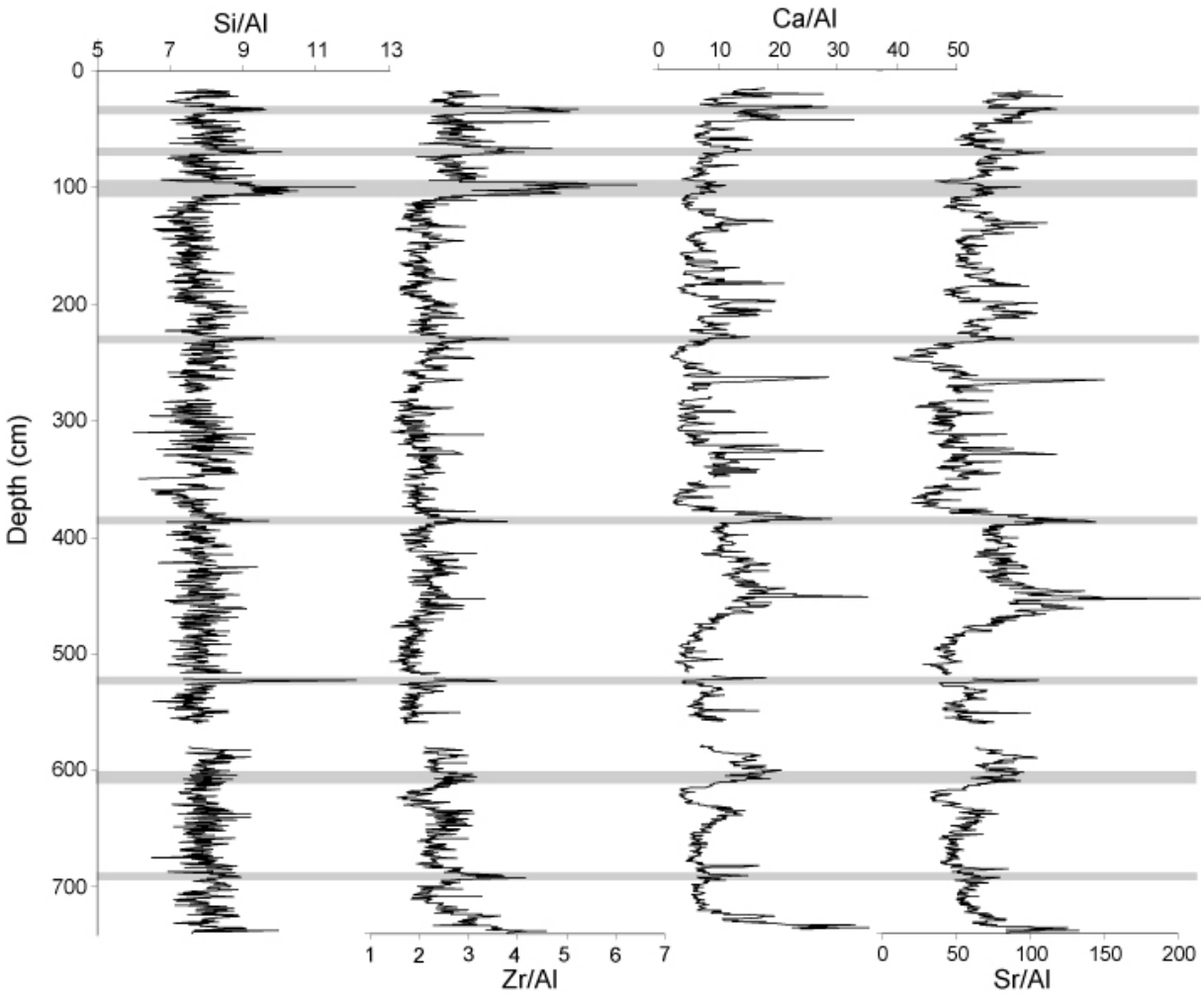

Figure 6.13 : XRF records from core PB06, with down core variations of ratio Si/Al, Zr/Al, Ca/Al and Sr/Al. Shaded areas mark the main variations of Si/Al and Zr/Al ratio.

6. Discussion

6.1. Paleostorms deposits

The multiple deposits identified in PB06 by correlation between grain size, fauna contents, clay minerals and XRF geochemistry suggest that the barrier has been breached numerous times over the last 6500 yrs (*Figure 6.14*). The three last events were previously identified in the whole lagoonal system by lateral correspondences on multiple cores transects. These events were dated using ^{210}Pb and ^{137}Cs chronology associated with ^{14}C dates and historical accounts at 1742, 1848 and 1893 A.D (Sabatier et al., 2008; Dezileau et al., submitted). Several peaks (grey band on *Figure 6.14*) in grain size, Zr/Al and the number of marine specie related to a decrease in Smectite/(Illte + Chlorite) ratio which may suggest the occurrence of eight high energy events likely reflecting recurrent perturbation of coastal hydrodynamics in relation to paleostorm events. Except for the last three deposits, it is difficult to associate these layers to a specific event or to a short period of increase in landfalling activity. Based on our ^{14}C age model, the strongest evidence for this change in storm activity occurred around 6200, 5500, 4400, 3200, 1500 and between 450 and 100 cal B.P. (*Figure 6.14*).

The horizontal extent of the overwash deposit is affected by many complicating factors in relation to storm characteristics such as hurricane intensity and storm surge height, tidal height at time of landfall, angle of storm events and wind direction, and timing and duration of landfall (Liu and Fearn, 2000). In this microtidal study area, we may infer that stronger storms tend to result in a higher storm surges and thus producing a thicker and more widespread overwash layer. However, storm landfall conditions as well as timing, duration and angle of approach occur to randomly over time. Liu and Fearn, (2000) present a model, where a coastal lake was subjected to overwash events caused by landfalling hurricanes of various intensities and direction. This study concludes that a suite of cores taken from different sites is vital for producing a complete record of past hurricane landfalls. In this system three multi-cores transects show a clear link between recent overwashes (last 1000 years), due to a catastrophic storm of category 3 intensity or more, and was described and discussed in Dezileau et al., (submitted). Just one long core was sampled, thus the oldest paleostorm layers were not correlated with other deposits, but we may suppose that the most powerful events are recorded in the whole lagoonal area as suggested by correlation over the upper 1.2 m of sedimentary archives.

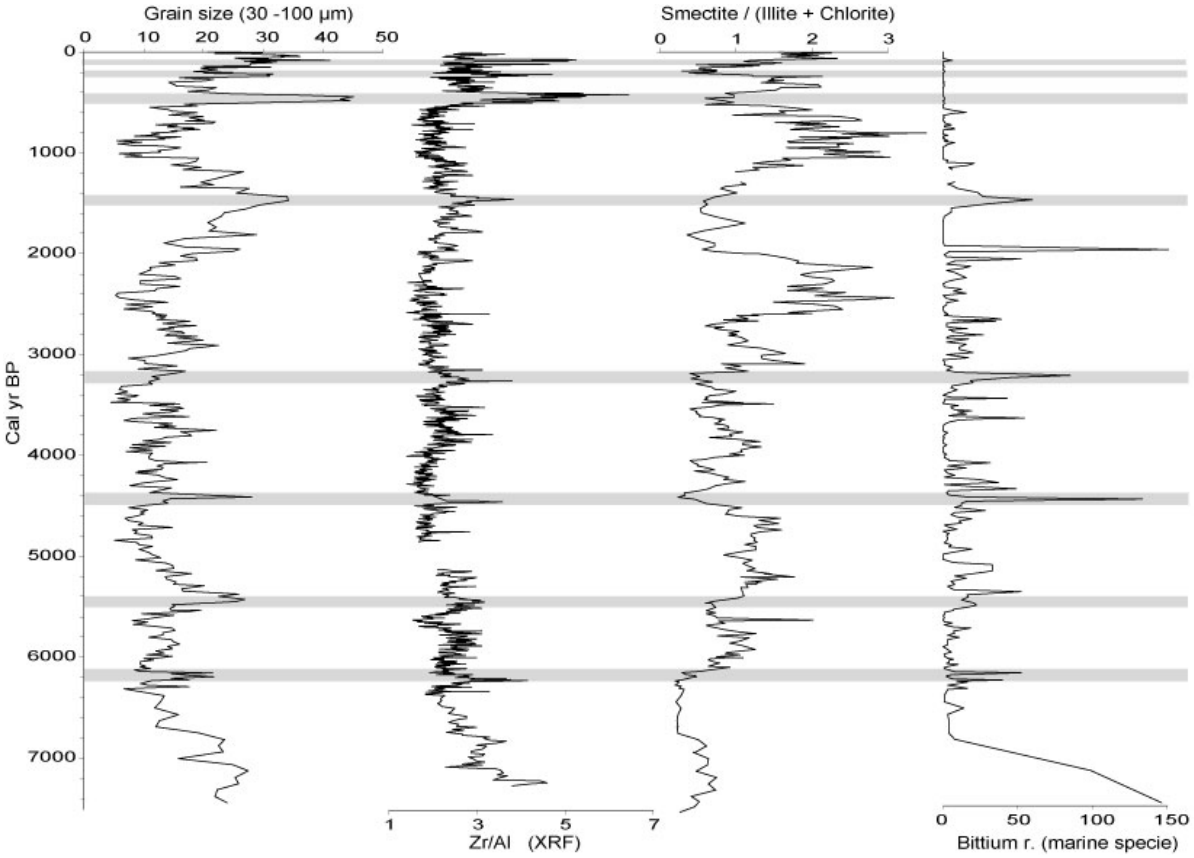

Figure 6.14 : Core PB06 with from left to right: Grain size of 30 to 100 µm population, Zr/Al XRF ratio, Smectite/(illite + chlorite) and Number of Bittium recticulatum (marine specie). Grey bands are the main paleostorms events.

6.2. Site sensitivity through time

Sea level rise can increase the sensibility of backbarrier study site by moving the shoreline farther inland and narrowing the sandy barrier through time. The Languedoc coast has been free of significant vertical tectonic movements (< 0.02 mm/yr) in Late-Quaternary time (Lambeck and Bard; 2000). The relative sea level curve in the NW Mediterranean Sea, for the last 7000 yr cal B.P. (*Figure 6.15*) presents some discrepancies (from observations: Laborel et al., 1994; Vella and Provensal, 2000; Morhange et al., 2001; from glacio-hydro-isostatic model: Lambeck and Bard; 2000). If the relative sea level has remained almost constant for the last 5000 yrs (< 2m), significant changes occurred during the first stand of lagoonal deposit between 6500 (date of the first lagoonal deposit in PB06) and 5000 yrs (1-3 m). The establishment of the sandy barrier has been estimated by Raynal et al., (2009) at around 7500 yrs at 1 km seaward from the present position. Moreover, these authors have dated the actual

barrier at 1800 ± 150 yr cal B.P. thanks to a ^{14}C age at the base of the present day sandy barrier. These dates imply a landward movement of the sandy barrier with an average rate of 0.2 m/yr in relation to the decrease of sea level rising rate (Raynal et al., submitted). While it is likely that there have been minor sea level fluctuations and shoreline landward movements for the last 1800 yrs (Dezileau et al., submitted), changes were most important before this period. The variation of the sea level before the last 1800 years have probably affected the sensitivity of the site in recording paleostorms and the intensity of the different sedimentary records can not be directly compared.

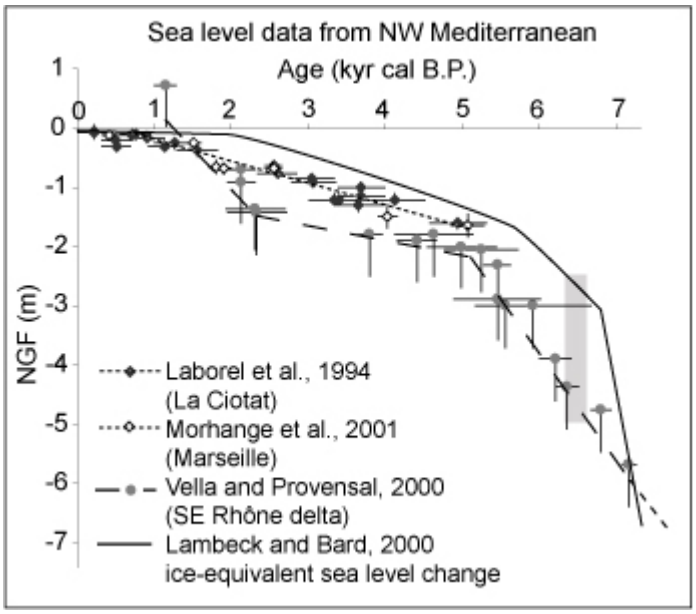

Figure 6.15 : Relative sea level curve in the NW Mediterranean Sea for the last 7000 yr cal B.P. from observations in the Rhône delta (Vella and Provensal 2000), La Ciotat (Laborel et al., 1994) Marseille (Morhange et al., 2001) and from glacio-hydro-isostatic model (Lambeck and Bard; 2000). Shaded area represents the sea level during the first lagoonal deposit.

Fauna content reveals a main palaeoenvironmental change around 1000 yr cal B.P. (Sabatier et al., 2010), after this date the sandy barrier was continuous but with temporal inlet formation in relation to storm events (Dezlieau et al., submitted). Before this date, the lagoonal system was less isolated from the sea and presents probably a weaker barrier with large permanent channel, which controlled inflow of marine water into the system, typical from a protected lagoon environment. However, the fine organic-rich sediment types appearing throughout the record show that this back barrier area was experiencing quiescent sedimentation during at

least the past 6500 yrs, indicating that the study site was probably protected behind the barrier system over that time. This Spatial and temporal variability in barrier beach morphology complicate the sedimentary record of storms, varying the sensitivity of backbarrier locations (Donnelly and Webb, 2004). This morphology can explain why sand material was not clearly found in the deeper identified storm layer deposit (*Figure 6.13*).

Sedimentary records of overwash deposit through time could be influenced by sediment supply, especially during periods when accumulation rates are low. Woodruff et al., (2008), using a model developed by Emanuel et al., (2006b), show that a decreased of sedimentation rate involving a low resolution interval could induce an apparent drop in landfalling activity during this same period (35% of the apparent decrease). In this study, we do not identify periods with an increase in the number of storms but rather a single event or a succession of events involving punctual records of past landfalling deposit, except for the top of the core. The three last prehistoric overwashs (1742, 1848 and 1893) occur during an interval of relatively high sedimentation rate (highest of the core: 2.6 mm/yr). Whereas, during the other periods of increase in storm activity the accumulation rate was lower (1 mm/yr). Therefore, we can suppose that if the accumulation rate was the same all along the core (equal to 2.6 mm/yr) we would have recorded more storm events during these periods of increase in storm activity. In general, if two back barrier storm deposits are not separated by enough time in relation to the sedimentation rate, these two overwash layers can appear as a single unit (Scileppi and Donnelly, 2007).

In the Pierre Blanche lagoon, many mechanisms can perturb the records of overwash deposits such as level variations, barrier morphodynamics, sediment supply to the system and to the complexity of storm conditions. For the last 1000 years, from a multi cores transects approach Dezileau et al., (submitted) show that the study site appears to be sensitive to only the most severe storm events. However, on Mid to Late Holocene the sensitivity of this environment changes in relation to these mechanisms, therefore we can not compare different paleostorm deposits records in core PB06 in terms of intensity.

6.3. Storm activity: region-wide comparison and Holocene climate changes.

The Late Holocene sedimentary archive of Palavasian lagoonal system report from the presently available and limited data the occurrence of six periods of storm activity increase at

6200, 5500, 4400, 3200, 1500 and between 450 and 100 yr cal B.P., based on our ^{14}C age model (*Figure 6.14* and *Figure 6.16b*). Although few studies record Mid to Late Holocene storm activity in Mediterranean Sea, these evidences of perturbation in coastal hydrodynamics could be correlated to other events on a regional scale.

In the Southern Tyrrhenian Sea (Western Mediterranean Sea) to the East of the studied area, in the shallow marine wedge, Budillon et al. (2005) recognized four event beds related to major storms that occurred in the last 1000 years. These landfalling events associated to historical sources display an important storm activity between the 16th and 19th centuries. Dezileau et al., (submitted), show an increase of storm events during the Little Ice Age (LIA) associated to an increase of severe flood events between the 17th and the end of the 19th centuries, recorded in municipal archives of township along six coastal rivers located in the Mediterranean Languedoc (Blanchemanche, Accepted). This high hydrological activity is regionally well correlated to the increase of the Vidourle river detritic component (Berger et al., Accepted), to a higher frequency of flood in the Durance and lower Rhône valley (Miramont et al., 1998; Pichar 1995; Bruneton et al., 2001) and to high Jurassian lake level (Magny et al., 2002). In this Mediterranean area Dezileau et al., (submitted), demonstrated that severe flooding and intense storm are due to the same mechanism, during the last centuries, with a strong mid-level SW flow over the French Mediterranean coast. Moreover, most of the heavy precipitations in the whole Mediterranean region over the last century have had a cyclone in its vicinity (Trigo et al., 2000; Jansá et al., 2001).

To the West of the studied area, in the Alboran Sea, beach ridge systems show evidence of intense erosion produced by storm waves generated by winds from the SW, particularly after 3–2.7 cal kyr BP. In general, cold episodes and cool events reported in the North Atlantic region (Bond et al., 2001), and marine Sea Surface Temperatures (SST) in the South of Iberia (Cacho et al., 2001) are recorded in coastal regions as arid episodes, marked by reduced rainfall and/or increased wind velocity and intensity (Goy et al., 2003; Zazo et al., 2008). Moreover, six major Holocene changes in vegetation have been identified by Jalut et al., (2000) in a transect covering southeast France and south-west Spain. They correspond to aridification phases that took place between 10.9–9.7 cal kyr BP, 8.4–7.6 cal kyr BP, 5.3–4.2 cal kyr BP, 4.3–3.4 cal kyr BP, and 2.8–1.7 cal kyr BP (*Figure 6.16d*). In spite of the uncertainty of the chronology, these phases are inversely correlated to the increase in storm

activity observed in our study. This result seems to confirm the hypothesis of Dezileau et al., (submitted) but on longer timescale.

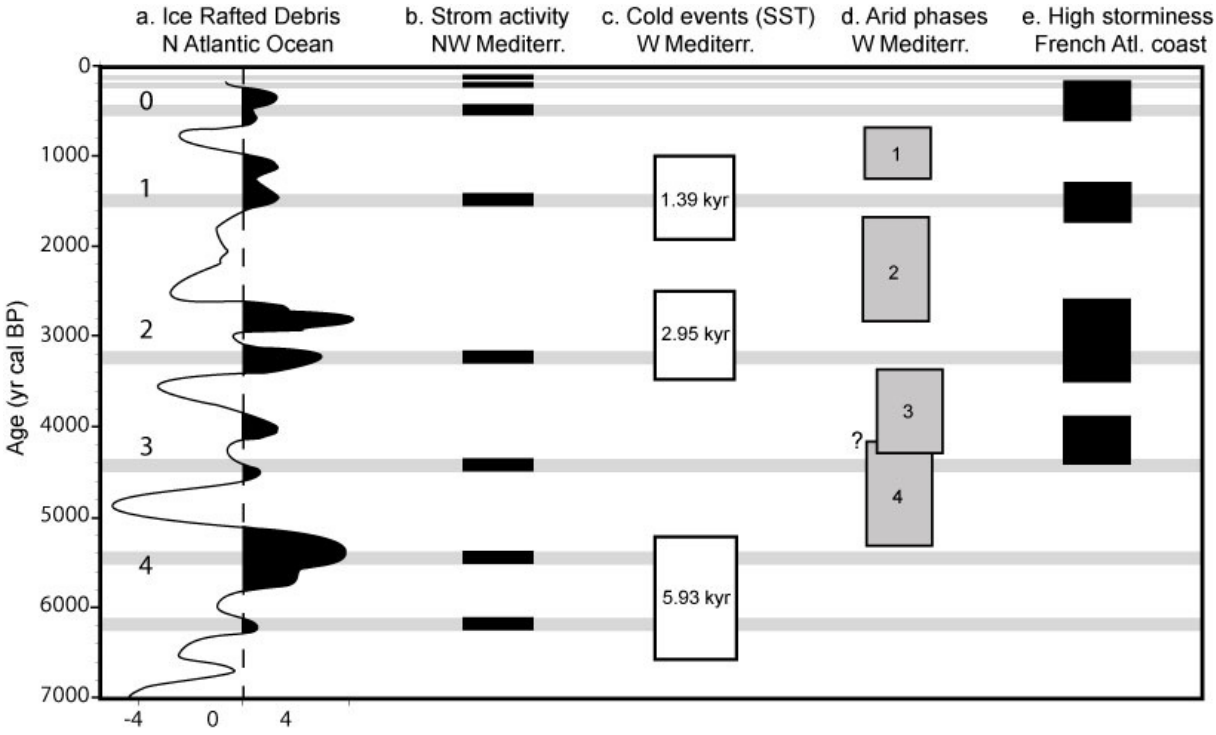

Figure 6.16 : Comparison between (a) Ice Rafted Debris cycles (IRD) in the North Atlantic (Bond et al., 1997; 2001); (b) our record of increase in storm activity in North Western Mediterranean Sea (Palavasian lagoon) based on the multi-proxy correlations defined in Figure 6.14; (c) Sea Surface Temperature (SST) cold events deduced from the core BS79-38 in Tyrrhenian Sea (Western Mediterranean Sea) by Cacho et al., (2001); (d) the aridification phases identified by Jalut et al., (2000) in the North Western Mediterranean region; (e) record of intensified storminess in Seine estuary (French Atlantic coast) by Sorrel et al., (2009). The grey shading bands outline the correlation in increase of storm activity in North Western Mediterranean Sea with other records, see text for discussion.

In the Southern Tyrrhenian Sea, Cacho et al. (2001) show a sequence of short SST cooling events (1.5-3° C) observed in cores studied at high resolution is consistent with a climatic periodicity of ~730 ± 40 years. These coolings took place at 5.93, 2.95, 1.39 Kyr cal B.P. in the Tyrrhenian Sea and are in good agreement with the increase in storm activity (*Figure 6.16c*). Such events, correlated with the cold Bond events were transmitted to the Mediterranean Sea by the Atlantic inflowing water and may have been amplified by strong

winter winds in this Mediterranean region. Therefore, periods of increase in storm activity recorded in this study are well correlated with Holocene cooling events (5.9, 4.3, 2.8, 1.4 and 0.5-0.1 Kyr, *Figure 6.16a*) associated with ice rafted in the North Atlantic (Bond et al., 1997; 2001).

6.4. Climate implication on Mid to Late Holocene storm activity

In a previous work focusing on LIA, Dezileau et al, (submitted) highlight the synchronicity between increases in storm activity, over Western Europe (resume in Clarke and Rendell, 2009) and North Western Mediterranean Sea. During this low solar activity period, the sea ice was extended southward particularly in winter over the North Atlantic basin (Lamb, 1995). Dezileau et al., (submitted) hypothesize that this extend implies a thermal gradient increase, leading to enhanced lower tropospheric baroclinicity over a large Central Atlantic-European domain. This mechanism associated to southward displacement of storm track implies an increase of storm activity in North Western Mediterranean Sea, in agreement with simulation on Maunder Minimum (Raible et al., 2007).

On Holocene timescale some periods of increase in storm activity were described, for example the 8.2 kyr cold event which represents a significant period of abrupt cooling within the early Holocene is associated with coastal sand accretion in Western Europe (resume in Clarke and Rendell, 2009). Moreover, a recent study on the French Atlantic coast, in the Seine estuary, shows strong evidence of changes in coastal hydrodynamics at ca. 4200, 2700, 1250 yr cal. B.P. and during LIA in relation to intensification of storm activity (Sorrel et al., 2009, *Figure 6.16e*). This present study demonstrates that periods of increase in storm activity in North Atlantic and in North Western Mediterranean Sea seem to be well correlated with Holocene cold period (Bond et al., 1997; 2001; Figure 9). Moreover, even if the origin of cold events in Holocene are not straightforward (Mayewski et al., 2004; Wanner et al., 2008), we hypothesized here that the mechanism invoked by Dezileau et al., (submitted) resulting from a decrease of European temperature, implies an increase of storm activity in NW Mediterranean region during these periods, thus explaining our 7000 years sedimentary records. The results of this study suggest that important changes in the Mediterranean "climate" over Holocene timescale have directly influenced the lower frequency of severe local storms.

7. Conclusion

This study provides a 7000 years high resolution record of past storm events using multi-proxy analysis of sedimentary deposits from lagoonal environment in Gulf of Lions in North Western Mediterranean Sea. Lagoon geomorphical setting has clearly changed over the Holocene, we suggest that these modifications altered the sensitivity of the site in recording paleostorms therefore, we can not compare storm events in terms of intensity through time. Nevertheless, from the presently available and limited data, we identify six periods of storm activity increase at 6200, 5500, 4400, 3200, 1500 yr cal B.P. and over the LIA (450 and 100 yr cal B.P.) based on our ^{14}C age model. These periods of high storm activities are inversely correlated to aridification phases over the Western Mediterranean Sea (Jalut et al., 2000). These data confirms, over the Mid to Late Holocene, that the reduction of overall winter precipitation in Northern Mediterranean Basin is related to a significant decrease in intense storm, as observed on shorter timescale by Trigo et al., (2000) and Dezileau et al., (submitted).

These evidences of changes in coastal hydrodynamic are in phase with those observed over the North Atlantic and correspond to Holocene cooling firstly evidenced in the North Atlantic (Bond et al., 1997; 2001). We hypothesize here that this increase in storm activity during Holocene cold events over the North Atlantic and Mediterranean region was probably due to thermal gradient increase leading to enhanced lower tropospheric baroclinicity over a large Central Atlantic-European domain as previously suggested over the LIA (Raible et al., 2007; Dezileau et al., submitted). These results demonstrate that North Atlantic region influence the Mediterranean climate at Holocene timescale, in relation to severe storm activity. In order to confirm these results, it is necessary to realize other studies over the Mediterranean region with the same multi-proxy approach.

Acknowledgments

This research has been undertaken in the framework of the ECLICA Project financed by INSU (ACIFNS “Aléas et Changement Globaux”, coord.: L. Dezileau) and INTEMPERIES project (“Appel à projets 2008 du Conseil Scientifique de l’Université Montpellier 2, coord.: L. Dezileau). The authors also wish to thank IFREMER Palavas for allowing storage of the cores in their cold room. To GLADYS platform (www.gladys-littoral.org) and all other members of the ECLICA Project team are also thanked for their support and their constructive

discussions during the course of this study. The authors are grateful to Jessica Cole for English corrections.

7. Synthèse et conclusions générales

7.1 Rappel des objectifs de l'étude

Ce travail, concernant la reconstruction des événements extrêmes de tempêtes au cours de l'Holocène dans le Golfe d'Aigues-Mortes, s'appuie principalement sur des données sédimentologiques acquises dans le complexe lagunaire palavasien entre 2004 et 2009.

Les principaux objectifs de ce travail étaient (i) de caractériser des sources par une approche sédimentologique (granulométrie, minéraux argileux), géochimique (éléments majeurs et traces) et faunistique afin d'identifier les phénomènes brefs de fortes amplitudes, (ii) d'établir un cadre chronologique (^{210}Pb, ^{137}Cs, ^{14}C et chroniques historiques), (iii) de comprendre l'évolution paléoenvironnementale du système lagunaire étudié, et (iv) de reconstituer les événements extrêmes au cours de l'Holocène afin de comprendre leurs liens avec les variations climatiques passées.

7.2 Principaux résultats

La caractérisation d'un cône de tempête actuel et l'identification des paléotempêtes dans le système lagunaire palavasien ont pu être réalisées avec une approche muli-traceur, principalement à partir de l'étude d'archives sédimentaires prélevées le long de plusieurs transects. L'étude de la géochimie (éléments majeurs et traces) et des minéraux argileux nous permet de définir quatre sources différentes susceptibles de contribuer au remplissage sédimentaire de la lagune: le bassin versant de la Mosson, la barrière sableuse, les rejets anthropiques et l'activité biologique de la lagune (section 3.3.). Les deux pôles principaux sont d'une part le bassin versant de la Mosson caractérisé par des concentrations élevées en Al_2O_3 et Fe_2O_3 et de fortes teneures en Smectite. Et d'autre part, le cordon littoral principalement composé de SiO_2, CaO, et pour les argiles d'Illite et de Chlorite contenant également des minéraux lourds avec d'importante teneur en Zr (apport provenant du Rhône). Cette étude permet de définir les rapports SiO_2/Al_2O_3, $Zr/A_{l2}O_3$ et Smectite/(Illite + Chlorite) traçant les apports sédimentaires provenant du cordon littoral, durant les périodes de tempêtes (section 3.3.). De plus, l'analyse de la taille des grains présents dans les carottes, permet de définir principalement deux populations granulométriques avec une fraction fine (argile - silt)

caractéristique de la sédimentation lagunaire, et une plus grossière (silt - sable) liée au fonctionnement d'un cône de tempête. Les données faunistiques obtenues sur les différentes populations de mollusques permettent d'identifier des espèces spécifiques de l'environnement lagunaire telle que Hydrobia acuta alors que d'autres, comme Bittium recticulatum, se rencontrent dans ce milieu quand il est dominé par une forte influence marine, liée à l'action d'une tempête. Cela nous a amené à définir une séquence de sédimentation caractérisant la présence d'un cône de tempête au sein d'une sédimentation lagunaire (section 3.2.). L'analyse de ces différents traceurs selon plusieurs transects de carottages, trace l'influence de ces dépôts de tempêtes à des distances supérieures à 600 depuis le cordon jusque dans la lagune. De plus, l'analyse des profils sismiques, corrélée aux données obtenues sur les carottes, permet d'associer deux réflecteurs majeurs à des événements de tempêtes affectant l'ensemble de la lagune. Ce milieu apparaît donc comme un environnement idéal pour reconstituer l'histoire des tempêtes du passé.

L'établissement d'un cadre chronologique aux archives sédimentaires étudiées, a été réalisé à deux échelles temporelles distinctes. Sur des courtes périodes de temps, de l'ordre du dernier siècle, nous avons utilisé les données ^{210}Pb et ^{137}Cs, obtenues par spectrométrie gamma, afin de déterminer la vitesse actuelle de comblement. Les taux de sédimentations présentent des variations entre 4.2 et 2.65 mm.an^{-1}, selon les différentes carottes (section 3.2. et 4.2.). Seule la carotte PB06 a été analysée à haute résolution avec un échantillon tous les centimètres. Les vitesses d'accumulations obtenues sur PB06 à l'aide des pics du ^{137}Cs (essais nucléaires, Tchernobyl) et d'un modèle simple de bioturbation pour le ^{210}Pb sont en bonne adéquation et donnent un taux moyen de 2.65 ± 0.2 mm.an^{-1} (section 4.1.). Connaissant la profondeur actuelle de cette lagune (environ 65 cm) nous pouvons nous attendre à un comblement de ce système dans 200 à 250 ans, sans tenir compte de l'élévation actuelle du niveau marin et de la diminution de l'espace lagunaire (progradation du delta et recul du cordon).

Afin d'obtenir une chronologie à l'échelle de l'Holocène, des datations par ^{14}C sur des mollusques ont été réalisées. Cependant, le milieu lagunaire fortement influencé par les apports continentaux présente un âge réservoir important qui varie au cours du temps en fonction du bilan eau douce/eau marine et donc de l'évolution du milieu lagunaire. L'âge réservoir de la lagune actuelle (fortement isolée), est estimé à 943 ± 25 ^{14}C an, par corrélation avec les données de ^{210}Pb, ^{137}Cs et l'utilisation d'archives textuelles (section 4.2.). Cependant, l'étude de la malacofaune présente dans ce milieu, montre un changement important de cet environnement avec, pour les périodes plus anciennes, une forte influence marine typique

d'une lagune protégée (section 5.1.). L'âge réservoir durant cette période est donc plus faible et égal à 618 ± 30 ^{14}C an, valeur marine estimée pour le Golfe du Lion. La chronologie ^{14}C est donc calibrée en corrigeant de la déviance de ces âges réservoirs par rapport à l'âge réservoir marin global (ΔR), selon les différents environnements de dépôts. Nous pouvons ainsi calculer le taux de sédimentation qui varie de 1 mm.an^{-1} (entre 6500 et 1000 ans cal B.P.) à 2.7 mm.an^{-1} (pour le dernier millénaire) (section 4.2.). On remarque que la vitesse de sédimentation obtenue pour les derniers 1000 ans est identique à celle acquise par la chronologie ^{210}Pb et ^{137}Cs pour le XX^{ème} siècle.

Le croissement des différents traceurs associé à des données radiochronologiques, nous permet d'identifier trois événements extrêmes de tempêtes au cours du Petit Age Glaciaire (PAG). Ces trois événements ont une intensité supérieure à celle de 1982, soit au moins de catégorie 3 sur l'échelle de Saffir-Simpson (section 3.2. et 6.1.). Les données historiques présentes dans les délibérations communales, relatent les tempêtes ayant affecté la région, permettant ainsi, par corrélation avec les archives sédimentaires, de donner un âge précis à ces trois niveaux de sables, datés en 1742, 1848 et 1893. Le lien clairement établi entre ces trois événements majeurs nous autorise à conclure que depuis les 500 dernières années les tempêtes enregistrées dans nos archives ont affecté l'ensemble du système lagunaire. Ces événements extrêmes ont probablement ébranlé toute la région en comparaison avec les effets de la dernière grosse tempête datant de 1982, d'intensité trop faible pour être présente dans nos enregistrements (section 6.1.).

La morphologie du cordon littoral ayant varié depuis 7000 ans (section 5.1.), nous ne pouvons pas comparer les événements entre eux, en terme d'intensité (section 6.2.). Notre enregistrement permet de reconstituer la variabilité de ces événements extrêmes au cours de l'Holocène mettant en évidence six périodes d'augmentation de l'activité des tempêtes datées à 6200, 5500, 4400, 3200, 1500 an cal B.P. et durant le PAG (section 6.2.). Le PAG est également une période où l'activité hydrologique des fleuves de la région se trouve perturbée avec une recrudescence des phénomènes de crues (section 6.1.). Les autres périodes de forte activité des tempêtes durant l'Holocène sont en anti-phases avec les phases d'aridification affectant la partie Nord Ouest de la Méditerranée. Cela nous permet de supposer que les phénomènes de fortes précipitations et de tempêtes sont étroitement liés à l'échelle de l'Holocène, comme suggérées par les données instrumentales pour la période actuelle.

L'augmentation de l'activité des tempêtes est corrélée aux périodes froides, décrites dans l'Atlantique Nord au cours de l'Holocène, et associée à une diminution des températures aux

pôles (section 6.1. et 6.2.). De plus ces périodes de forte activité sont en phase avec celles enregistrées à l'échelle du bassin Ouest Méditerranéen et dans l'Europe du Nord, laissant suggérer un mécanisme affectant toute cette zone durant les périodes froides.

L'un des mécanismes climatiques modérant l'activité des tempêtes à l'échelle de cette région est l'Oscillation Nord Atlantique (NAO) (section 6.1.). Cependant ce phénomène oscillatoire affecte l'Europe du Nord lors de sa phase positive et la Méditerranée en phase négative. Il est donc difficile d'associer ce mécanisme à l'augmentation des tempêtes dans ces deux zones. Les reconstitutions de l'indice NAO au cours des 500 dernières années ne montrent pas non plus de corrélation claire avec notre enregistrement lors du PAG. De plus une approche statistique menée en collaboration avec des modélisateurs du climat (section 6.1.), sur la période 1960-2001, montre que les 204 événements de tempêtes, dans la zone d'étude durant cette période, sont principalement associés (26%) à la phase positive du mode de circulation atmosphérique EAP (Eastern Atlantic Pattern). Alors que la phase négative du NAO (North Atlantic Oscillation) ne représente que 14% du signal. Ainsi il semble délicat d'associer les tempêtes au phénomène NAO à cause de l'échelle temporelle, en effet il y a des difficultés inhérentes pour lier des phénomènes d'une durée de 2 à 3 jours avec des moyennes mensuelles de l'index NAO.

Un autre mécanisme peut être invoqué pour expliquer l'augmentation des tempêtes durant les périodes froides. Il est lié à l'amplification du gradient thermique en lien avec la diminution des températures aux hautes latitudes (section 6.1.). Ce gradient thermique à l'origine des courant-jets troposphériques (circulant d'Ouest en Est à nos latitudes) est un milieu favorable, par interaction barocline (isobares recoupant les isothermes), aux cycles d'évolution des dépressions et des tempêtes. Cette altération atmosphérique à grande échelle peut être responsable de l'augmentation des vents violents et des fortes précipitations dans les régions de l'Europe du Nord et de la Méditerranée de l'Ouest, durant le PAG. Bien que les processus induisant les périodes froides au cours de l'Holocène sont encore sujets à discussions, nous supposons que le mécanisme invoqué ci-dessus pour le PAG peut être à l'origine de l'augmentation de l'activité des tempêtes durant ces périodes froides au cours de l'Holocène expliquant ainsi notre enregistrement (section 6.2.).

La reconstitution de la fréquence et de l'intensité des paléotempêtes dans le domaine côtier languedocien est indispensable en regard de l'augmentation de la population vivant sur le littoral actuel (section 6.1.). En effet, le nombre d'habitants a été multiplié par un facteur 15 depuis le milieu du 18ème siècle, avec un fort accroissement surtout au cours des 40 dernières années, avec le développement du tourisme, augmentant d'autant l'impact destructeur des

événements climatiques extrêmes. Les archives sédimentaires étudiées durant ce travail montrent qu'aucun événement catastrophique de tempête n'a directement affecté cette région durant le XX^{ème} siècle. Cependant si le régime de tempêtes enregistré durant le PAG revenait à l'heure actuelle, les implications seraient dramatiques. Enfin, pour conclure il apparaît primordial de mieux comprendre les mécanismes à l'origine de cette augmentation, afin de réaliser des prévisions les plus précises possibles quant à l'exposition des populations et des activités humaines dans cette région au risque de tempête.

7.3 Perspectives

Ce travail ouvre de nombreuses perspectives au regard des implications paléoclimatiques des résultats présentés.

Un des points essentiels qui devra être abordé pour confirmer les résultats de cette étude est l'élargissement du chantier de travail à d'autres lagunes du Golfe du Lion (de la petite Camargue jusqu'au Roussillon, projet INTEMPERIES, coord. L. Dezileau) afin de confirmer la tendance observée au cours de l'Holocène. Puis, d'appliquer cette même approche à d'autres sites d'étude en Méditerranée de l'Ouest (exemple projet Franco-Marocain-Espagnol Paleostorm, coord. L.Dezileau). En effet, la principale question qui reste en suspens est de savoir si cet enregistrement est lié à des phénomènes locaux, ou si toute cette région est sujette aux mêmes implications climatiques.

Il serait également intéressant de confronter les résultats de cette étude aux simulations numériques, en collaboration avec des modélisateurs du climat, pour faire le lien entre les modèles (à grande échelle) simulés et les observations à une échelle régionale. Cette étude qui a débuté sur l'échelle du dernier millénaire dans le cadre du projet INTEMPERIES (coord. L. Dezileau) doit être étendue à tous l'Holocène. Une telle étude permettrait d'une part de mettre en lumière les relations entre les variations séculaires du climat et les événements extrêmes régionaux, afin de confirmer ou non le mécanisme climatique invoqué durant le PAG à l'échelle de l'Holocène. Et d'autre part, si la réponse est concluante, il sera possible de se servir des simulations de scénarios futurs pour déterminer les probabilités de tempêtes et de crues extrêmes dans le futur, afin de déterminer l'aléa lié à ces phénomènes dans cette région.

Certains aspects tel que les effets de la bioturbation sur les modèles de ^{210}Pb ainsi que la mobilité du ^{137}Cs sont des mécanismes à mieux appréhender dans ce type de milieu, afin d'affiner notre compréhension des données chronologiques. De plus la mise en évidence d'importantes variations de l'âge réservoir perturbant les données de ^{14}C dans les environnements côtiers, implique une prise en compte systématique de ces phénomènes dans le but d'obtenir une chronologie la plus précise possible.

Enfin, certains points soulevés dans cette étude mériteront d'être approfondis dans le futur afin de mieux comprendre la dynamique lagunaire soumise à une forte composante anthropique (surtout depuis le siècle), dans le but de protéger ces zones humides dont l'intérêt en terme de biodiversité n'est plus à démontrer. En effet le comblement de ce milieu par les apports sédimentaires (section 3.2.) et les rejets de polluants liés aux activités humaines (section 3.3.) apparaissent comme des enjeux fondamentaux pour une gestion durable de ces zones par les acteurs régionaux.

Bibliographie

Aagaard, T., Orford, J. and Murray, A.S. (2007). Environmental controls on coastal dune formations; Skallingen Spit, Denmark, *Geomorphology*, 83, 29-47.

Aitchison, J., Barceló-Vidal, C., Egozcue, J.J. and Pawlowsky-Glahn, V. (2002). A concise guide for the algebraic–geometric structure of the simplex, the sample space for compositional data analysis. *In*: Bayer, U., Burger, H., Skala, W. (Eds.), Proceedings of IAMG'02-The Eighth Annual Conference of the International Association for Mathematical Geology, Berlin, Germany, 387–392, ISSN 0946- 8978.

Aloisi, J.C., Monaco, A., Thommeret, J. and Thommeret, Y. (1978). Holocene transgression in the Golfe of Lion (southern France): paleogeographic and palaeobotanic evolution. *Geography Physique du Quaternaire*, 32, 145– 162.

Alpert, P., Ben-Gai, T., Baharad, A., Benjamini, Y., Yekutieli, D., Colacino, M., Diodato L., Ramis, C., Homar, V., Romero, R., Michaelides, S. and Manes, (2002). The paradoxical increase of Mediterranean extreme daily rainfall in spite of decrease in total values. *Geophysical Research Lett*ers, 29, 11, 31-1 - 31-4.

Amorosi, A., Centineo, M-C., Colalongo, M-L. and Fiorini, F. (2005). Millennial-scale depositional cycles from the Holocene of the Po Plain, Italy. *Marine Geology*, 222-223, 7-18.

Anagnostopoulou, C., Tolika, K., Flocas, H., and Maheras, P. (2006). Cyclones in the Mediterranean region: present and future climate scenarios derived from a general circulation model (HadAM3P). *Advances in Geosciences*, 7, 9-14.

Andrade, C., Freitas, M., Moreno, J., and Craveiro, S. (2004). Stratigraphical evidence of Late Holocene barrier breaching and extreme storms in lagoonal sediments of Ria Formosa, Algarve, Portugal. *Marine Geology*, 210, 339–362.

Antoine, J.-M., Desailly, B. and Gazelle, F. (2001). Les crues meurtrières, du Roussillon aux Cévennes, *Annales de Géographie*, 622, 597-623.

Appleby, P.G., (1991). ^{241}Am dating of lake sediments. *Hydrobiologia*, 214, 35-42.

Appleby, P. and Oldfield, F. (1978) - The calculation of ^{210}Pb dates assuming a constant rate of supply of unsupported ^{210}Pb to the sediment. *Catena*, 5, 1-8.

Appleby, P. and Oldfield, F. (1992). *Uranium Series Disequilibrium, Application to Earth, Marine and Environmental Sciences.*, chapter Application of lead-210 to sedimentation studies, pages 731–778. Clarendon Press, Oxford.

Arnaud, F., Lignier, V., Revel, M., Desmet, M., Beck, C., Pourchet, M., Charlet, F., Trentesaux, A., and Tribovillard, N. (2002). Flood and earthquake disturbance of 210Pb geochronology (Lake Anterne, NW Alps). *Terra Nova*, 14, 225–232.

Barbier, M. (2007). Comblement sédimentaire et événements climatiques catastrophiques dans les lagunes du haut Languedoc au cours de l'Holocène. *Rapport de stage de Master 1 Reservoir*, Université Montpellier 2.

Bard, E., Hamelin, B., Arnold, M., Montaggioni, L. Cabioch, G., Faure, G. and Rougerie, F. (1996). Deglacial sea level record from Tahiti corals and the timing of global meltwater discharge. *Natur*e, 382, 241-244.

Barriendos, M., Coeur, D., Lang, M., Llasat, M.C., Naulet, R., Lemaitre, F. and Barrera, A. (2003). Stationarity analysis of historical flood series in France and Spain (14th–20th centuries). *Natural Hazards and Earth System Sciences*, 3, 583-592.

Barston, A.G. and Livezey, R.E. (1987). Classification, seasonality and persistence of low frequency atmospheric circulation patterns. *Monthly Weather Reviews*, 115, 1083-1126.

Bellucci, G., Frignani, M., Cochran, J.K., Albertazzi, S., Zaggia, L., Cecconi, G. and Hopkins, H. (2007). ^{210}Pb and ^{137}Cs as chronometers for salt marsh accretion in the Venice Lagoon : links to flooding frequency and climate change. *Journal of environmental radioactivity*, 97, 85-102.

Berger, J.F., Blanchemanche, P., Reynes, C. and Sabatier P. Dynamiques fluviales et lagunaires en basse vallée du Vidourle au cours des 6 derniers siècles : confrontation des données pédosédimentaires à haute résolution temporelle à l'analyse fréquentielle des crues historiques, *In :* Littoraux, lagunes et basses plaines alluviales à l'Holocène, *Quaternaire*, 20, (3), 2009, accepté.

Berné, S., Jouet, G., Bassetti, M-A., Dennielou, B. and Taviani, M. (2007). Late Glacial to Preboreal sea-level rise recorded by the Rhône deltaic system (NW Mediterranean). *Marine Geology*, 245, 65–88

Bertin, X. and Chaumillon, E. (2005). New insights in shallow gas generation from very high resolution seismic and bathymetric surveys in the Marennes-Oleron Bay, France. *Marine Geophysical Research*, 26, 225–233.

Bhend, J. (2005). North Atlantic and European Cyclones: their variability and change from 1881 to 2003. *Masters Thesis*, University of Bern available at http://www.giub.unibe.ch/klimet/publications.html .

Blanc, J.J. (1985). Ruptures d'équilibre au littoral de Provence occidentale : l'action des tempêtes, relations avec les aménagements, *Tethys*, 11, 3-4, 350-359.

Blanchemanche, P., Berger, J-F., Chabal, L., Jorda, C., Jung, C. and Raynaud, C. (2003). Le littoral languedocien durant l'Holocène: milieu et peuplement entre Lez et Vidourle (Hérault, Gard). *In*: Muxart, T., Vivien, F-D., Villalba, B., and Burnouf, J., Eds., Des milieux et des hommes : fragments d'histoires croisées, Bilan du Programme PEVS/SEDD, Elsevier, Coll. Environnement, 79-92.

Blanchemanche, P. Crues historiques et vendanges en Languedoc méditerranéen oriental : la source, le signal et l'interprétation. *In* : Changement global, effets locaux :Le Petit Age

Glaciaire dans le Sud de la France : Impacts morphogéniques et sociétaux », *Archéologie du Midi Médiéval, accepté.*

Boer, W., van den Bergh, G.D., de Haas, H., de Stigter, H.C., Giles, R. and van Weering, Tj.C.E. (2006). Validation of accumulation rates in Teluk Banten (Indonesia) from commonly applied 210Pb models, using the 1883 Krakatau tephra as time marker. *Marine Geology*, 227, 263-277.

Bond, G., Showers, W., Cheseby, M., Lotti, R., Almasi, P., deMenocal, P., Priore, P., Cullen, H., Hajdas, I. and Bonani, G. (1997). A pervasive millennial scale cycle in North Atlantic Holocene and glacial climates. *Science,* 278, 1257–1266.

Bond, G., Kromer, B., Beer, J., Muscheler, R., Evans, M.N., Showers, W., Hoffmann, S., Lotti-Bond, R., Hajdas, I. and Bonani, G. (2001). Persistent solar influence on North Atlantic climate during the Holocene. *Science,* 294, 2130–2136.

Bordelais, S. (2005). Evolution des lagunes du Golfe d'Aigues-Mortes à partir de l'étude de carottes sédimentaires courtes. *Rapport de stage de Master 2 Recherche*, Université Montpellier 2.

Bouchette, F., Denamiel, C., and NAUSICAA team (2007). NAUSSICAA Phase A advancement report. *BEACHMED-E report*, 174pp.

Boulay, S., Colin, C., Trentesaux, A., Pluquet, F., Bertaux, J., Blamart, D., Buehring, C., and Wang, P. (2003). Mineralogy and sedimentology of Pleistocene sediment in the South China Sea (ODP Site 1144). *Proceedings of the Ocean Drilling Program, Scientific Results*, 184, 1–21.

Boulay, S., Colin, C., Trentesaux, A., Frank, N. and Liu, Z. (2005). Sediment sources and East Asian monsoon intensity over the last 450 kyr: Mineralogical and geochemical investigations on South China Sea sediment, *Palaeogeography, Palaeoclimatology, Palaeoecology,* 228, 250–277.

Bourdeau, R. (1986). Mathematics of tracer mixing in sediments: I. Spatially-dependent, diffusing mixing. *Amercican Journal of Science*, 286, 161-198.

Bout-Roumazeilles, V., Combourieu Nebout, N., Peyron, O., Cortijo, E., Landais, A., and Masson-Delmotte, V. (2007). Connection between South Mediterranean climate and North African atmospheric circulation during the last 50,000 ys BP North Atlantic cold events. *Quaternary Sciences Reviews,* 26, 3197-3215.

BRGM, Carte géologique de Montpellier à 1:80 000. , BRGM Éditions (1967).

Bruneton, H., Arnaud-Fassetta G., Provansal, M. and Sistach, D. (2001). Geomorphological Evidence for Fluvial Change during the Roman Period in the Lower Rhône Valley (Southern France). *Catena*, 45, 287–312.

Bruzzi, C., (1998). Les tempêtes et l'évolution morphosédimentaire des plages orientales du delta du Rhône, *Thèse de doctorat de Géograpgie physique, Université d'Aix-Marseille 1*, 403 pp.

Budillon, F., Esposito, E., Iorio, M., Pelosi, N., Porfido, S. and Violante, C. (2005). The geological record of storm events over the last 1000 years in the Salerno Bay (Southern Tyrrhenian Sea): new proxy evidences. *Advances in Geosciences*, 2, 123–130.

Buynevich, I.V., Nichol, S.L. and Asp, N.E. (2004). Sedimentary records of intense storms in Holocene barrier sequences, Maine, USA. *Marine Geology*, 210, 135-148.

Cacho, I., Grimalt, J.O., Canals, M., Shackleton, N., Schönfeld, J. and Zahn, R. (2001). Variability of the Western Mediterranean Sea surface temperature during the last 25,000 years and its connection with the Northern Hemisphere climatic changes. *Paleoceanography*, 16, 40–52.

Caquineau, S., Gaudichet, A., Gomes, L., Magonthier, M-C. and Chatenet, B. (1998). Saharan dust: clay ratio as a relevant tracer to assess the origin of soil-derived aerosols. *Geophysical Research Letters*, 25**,** 983–986.

Carignan, J., Hild, P., Mevelle, G., Morel, J. and Yeghicheyan, D. (2001). Routine Analyses of Trace Elements in Geological Samples using Flow Injection and Low Pressure On-Line Liquid Chromatography Coupled to ICP-MS: A Study of Geochemical Reference Materials BR, DR-N, UB-N, AN-G and GH. *Geostandards Newsletter: The Journal of Geostandards and Geoanalysis*, 25, 187-198.

Cattaneo, A. and Steel, R.J. (2003). Transgressive deposits: a review of their variability. *Earth Science Re*views, 62, 187–228.

Certain, R. (2002). Morphodynamique d'une côte sableuse microtidale à barres : le Golfe du Lion (Languedoc-Roussillon). *Thèse de Doctorat, Université de Perpignan, pages 209*.

Certain, R., Tessier, B., Courp, T., Barusseau, J., and Pauc, H. (2004). Reconnaissance par sismique très haute résolution du remplissage sédimentaire de la lagune de Leucate (Aude et Pyrénées-Orientales - SE France). *Bulletin de la Société géologique de France*, 175, 35–48.

Chabal, L., Jorda, C. and Blanchemanche, P. (2008). Lattara entre terres et eaux: paléogéographie et paléo-boisements autour du port protohistorique de Lattes (Hérault). *Gallia*, 65, 1-12.

Chamley, H. (1989). Clay Sedimentology, 623 pp., Springer, New York.

Chanton, J., Martens, C., and Kipphut, G. (1983). Lead-210 sediment geochronology in a changing coastal environment. *Geochimica et Cosmochimica Acta*, 47, 1791–1804.

Chappell, J., Chivas, A., Rhodes, E. and Wallensky, E. (1983). Holocene palaeo-environmental changes, central to north Great Barrier Reef inner zone. *BMR Journal of Australian Geology Geophysics*, 8, 223-235.

Chivas, A., Chappell, J. and Wallensky, E. (1986). Radiocarbon evidence for the timing and rate of island development, beach rock formation and phosphatization at Lady Elliot Island Queensland, Australia. *Marine Geology*, 69, 273-287.

Charmasson, S., Radakovitch, O., Arnaud, M., Bouisset, P., and Pruchon, A. (1998). Long-cores profiles of ^{137}Cs, ^{134}Cs, ^{60}Co and ^{210}Pb in sediment near the Rhône river (Northwestern Mediterranean sea). *Estuaries*, 21-3, 367–378.

Clarke, M.L. and Rendell, H.M. (2009). The impact of North Atlantic storminess on western European coasts: A review. *Quaternary International*, 195, 31–41.

Cochran, J. (1985). Particle mixing rates in sediments of the eastern equatorial Pacific: Evidence from ^{210}Pb, $^{239,\ 240}$Pu and ^{137}Cs distributions at MANOP sites. *Geochimica et Cosmochimica Acta*, 49, 1195–1210.

Cochran, J.K., Hirschberg, D.J., Wang, J. and Dere, C. (1998). Atmospheric deposition of metals to coastal waters (Long Island Sound, New York U.S.A.): evidence from saltmarsh deposits. *Estuarine Coastal Shelf Sciences*, 46, 503-522.

Cœur, D. and Lang, M. (2002). L'enquête en archives et la connaissance des inondations, in Avalanches et risques. Regards croisés d'ingénieurs et d'historiens, Actes du séminaire du programme Histoval (Grenoble, 16 sept. 1999), Cemagref-université Pierre Mendès France (CRHUPA/HESOP), Grenoble, MSH-Alpes, 133-144

Coudé-Gaussen, G., Rognon, P., Bergametti, G., Gomes, L., Strauss, B. and Le Coustumer, M.N. (1987). Saharan dust on Fuerteventura island (Canaries): chemical and mineralogical characteristics, air mass trajectories, and probable sources. *Journal of Geophysical Research*, 92, 9753–9771.

Colin, C., Bertaux, J., Desprairies, A., Turpin, L. and Kissel, C. (1999). Erosional history of the Himalayan and Burman ranges during the last two glacial-interglacial cycles. *Earth Planetary Science Lett*ers, 171, 647–660.

Colin, C., Turpin, L., Blamart, D., Frank, N., Kissel, C. and Duchamp, S. (2006). Evolution of weathering patterns in the Indo-Burman Ranges over the last 280 kyr: Effects of sediment provenance on 87Sr/86Sr ratios tracer, *Geochemistry Geophysics and Geosystems*, 7, Q03007, doi:10.1029/2005GC000962.

Collins, E.S., Scott, D.B. and Gayes, P.T. (1999). Hurricane records on the South Carolina Coast: can they be detected in the sediment record ? *Quaternary International*, 56, 15-26.

Condomines, M., Tanguy, J., and Michaud, V. (1995). Magma dynamics at Mt Etna: Constraints from *U-Th-Ra-Pb* radioactive disequilibria and Sr isotopes in historical lavas. *Earth and Planetary Science Letters*, 132, 25–41.

Courp, T. and Monaco, A. (1990). Sediment dispersal and accumulation on the continental margin of the Gulf of Lions: sedimentary budget. *Continental Shelf Research*, 10, 1063-1087.

Court-Picon, M., Vella, C., Chabal, L. and Bruneton, H. Coastal palaeoenvironments during the last 8000 years on the Lion Gulf western side: the sand bar of the Thau lagoon coastal lagoon (SETIF coring, Sète, Hérault). Submitted to *Quaternaire*.

Dezileau, L., Bordelais, S., Condomines, M., Bouchette, F., and Briqueu, L. (2005). Evolution des lagunes du Golfe d'Aigues-Mortes à partir de l'étude de carottes sédimentaires courtes (étude géochronologique, sédimentologique et géochimique des sédiments récents). In *Publications ASF, Paris, 51, p. 91*.

DIREN Languedoc-Roussillon, Braudeau, B. (2009). La Mosson à Saint-Jean-de-Vedas., HYDRO-MEDD/DE.

Donnelly, J. P., Roll, S., Wengren, M., Butler, J., Lederer, R., and Webb T. III (2001a). Sedimentary evidence of intense hurricane strikes from New Jersey. *Geology*, 29, 615-618.

Donnelly, J. P., Smith Bryant, S., Butler, J., Dowling, J., Fan, L., Hausmann, N., Newby, P., Shuman, B., Stern, J., Westover, K., and Webb, T. III (2001b). 700 yr sedimentary record of intense hurricane landfalls in southern New England. *Geological Society of America Bulletin*, 113, 714–727.

Donnelly, J.P., and Webb, T., III, (2004). Backbarrier sedimentary records of intense hurricane landfalls in the northeastern United States. *In* : Hurricanes and Typhoons: Past, Present, and Potential, edited by Murnane, R., and Liu, K., *Columbia Univ. Press*, New York.

Donnelly, J. P., (2005). Evidence of Past Intense Tropical Cyclones from Backbarrier Salt Pond Sediments: A Case Study from Isla de Culebrita, Puerto Rico, USA. *Journal of Coastal Research*, SI42, 201-210.

Donnelly, J. P., and Woodruff, J.D. (2007). Intense hurricane activity over the past 5,000 years controlled by El Nino and the West African monsoon. *Nature*, 447, 465-468.

Dubar, M. and Anthony E. (1995). Holocene environmental change and river-mouth sedimentation in the Baie de Anges, French Riviera. *Quaternary Research*, 43, 329-343.

Egli, M., Mirabella, A. and Fitze, P. (2001). Clay mineral formation in soils of two different chronosequences in the Swiss Alps. *Geoderma,* 104, 145–175.

Emanuel, K. (2006a). Hurricanes: Tempests in a greenhouse. *Physics Today,* 59, 74–78.

Emanuel, K., Ravela, S., Vivant, E. and Risi, C. (2006b). A statistical deterministic approach to hurricane risk assessment. *Bulletin of American Meteorological Society*, 87(3), 299–314, doi:10.1175/BAMS-87-3-299.

François, F., Gerino, M., Stora, G., Durbec, J., and Poggiale, J. (2002). Functional approach to sediment reworking by gallery-forming macrobenthic organisms: modeling and application with the polychaete Nereis diversicolor. *Marine Ecology Progress Series*, 229, 127–136.

Frappier, A. B., Sahagian, D., Carpeter, S. J., Gonzalez, L. A. and Frappier, B. (2007a). A stalagmite record of recent tropical cyclones. *Geology*, 7, 111–114; doi: 10.1130/G23145A.

Frappier, A. B., Knutson, T., Liu, K.-B. and Emanuel, K. (2007b). Coordinating paleoclimate research on hurricanes with hurricane-climate theory and modelling. *Tellus*, 59A, 529–537.

Gaertner, M.A., Jacob, D., Gil, V., Domínguez, M., Padorno, E., Sánchez, E. and Castro, M. (2007). Tropical cyclones over the Mediterranean Sea in climate change simulations. *Geophysical Research Letters*, 34, doi:10.1029/2007GL029977.

Garcia-Gil, S., Vilas, F. and Garcia-Garcia, A., (2002). Shallow gas features in incised-valley fills (Rìa de Vigo, NW Spain): a case study. *Continental Shelf Res*earch, 22(16), 2303–2315.

Gerino, M., Aller, R. C., Lee, C., Cochran, J. K., Aller, J. Y., Green, M. A., and Hirschberg, D. (1998). Comparison of different tracers and methods used to quantify bioturbation during a spring bloom: 234-Thorium, Luminophores and Chlorophyll a. *Estuarine, Coastal and Shelf Science*, 46, 531–547.

Gibelin A.-L. and Déqué, M. (2003). Anthropic climate change over the Mediterranean region simulated by a global variable resolution model. *Climate Dynamics*, 20, 327-339.

Gingele, F.X., De Deckker, P. and Hillenbrand, C.D. (2001). Clay mineral distribution in surface sediments between Indonesia and NW Australia - source and transport by ocean currents. *Marine Geology*, 179, 135–146.

Giorgi, F. (2006). Climate change hot-spots. *Geophysical Research Letters*, 33, L08707, doi:10.1029/2006GL025734.

Giorgi, F. and Lionello, P. (2008). Climate change projections for the Mediterranean region. *Global and Planetary Change*, 63, 90–104.

Giresse, P., Wiewióra, A. and Grabska, D. (2004). Glauconitization processes in the northwestern Mediterranean (Gulf of Lions). *Clay Minerals*, 39, 57–73.

Goff, J., Rouse, H., Jones, S., Hayward, B., Cochran, U., a. M. W., Dickinson, W., and Morley, M. (2000). Evidence for an earthquake and tsunami about 3100-3400 yr ago, and other catastrophic saltwater inundations recorded in a coastal lagoon, New Zealand. *Marine Geology*, 170, 231–249.

Goldberg, E. (1963). *Geochronology with lead-210*, chapter radioactive dating, pages 121–131. International Atomic Energy Agency.

Goldenberg, S. B., Landsea, C. W., Mestas-Nuñez, A.M., and Gray, W.M., (2001). The recent increase in Atlantic hurricane activity : Causes and implications. *Science*, 293, 474-479.

Goodfriend, GA., and Flessa, KW. (1997). Radiocarbon reservoir ages in the Gulf of California: roles of upwelling and flow from the Colorado River. *Radiocarbon*, 39(2), 139–48.

Goubanova, K. and Li, L. (2007). Extremes in temperature and precipitation around the Mediterranean basin in an ensemble of future climate scenario simulations. *Global and Planetary Change*, 57, 27-42.

Goy, J.L., Zazo, C. and Dabrio, C.J. (2003). A beach-ridge progradation complex reflecting periodical sea-level and climate variability during the Holocene (Gulf of Almería, Western Mediterranean). *Geomorphology*, 50, 251–268.

Guerzoni, S., Molinaroli, E. and Chester, R., (1997). Saharan dust inputs to the western Mediterranean sea: depositional patterns, geochemistry and sedimentological implications. *Deep-Sea Research II*, 44 (3–4), 631–654.

Guerzoni, S., Chester, R., Dulac, F., Herut, B., Loye-Pilot, M.-D., Measures, C., Migon, C., Molinaroli, E., Moulin, C., Rossini, P., Saydam, C., Soudine, A. and Ziveri, P., (1999). The role of atmospheric deposition in the biogeochemistry of the Mediterranean Sea. *Progress in Oceanography*, 44 (1–3), 147–190.

Guiot, J., Nicault, A., Rathgeber, C., Edouard, J.L., Guibal, F., Pichard, G. and Till, C. (2005). Last millennium summer-temperature variations in Western Europe based on proxy data. *The Holocene*, 15, 489-500.

Hayne, M. and Chappell, J. (2001). Cyclone frequency during the last 5000 yrs from Curacoa Island Queensland. *Palaeogeography, Palaeoclimatology, Palaeoecology*, 168, 201-219.

Hennessy, J.T. and Zarillo, G.A. (1987). The interrelation and distinction between flood-tidal delta and washover deposits in a transgressive barrier island. *Marine Geology*, 78, 35-56.

Heyraud, M. and Cherry, R.D. (1983). Correlation of ^{210}Po and ^{210}Pb enrichments at the sea-surface microlayer with neuston biomass. *Continental Shelf Research*, 1(3), 283–293.

Houser, C., Hapke, C. and Hamilton, S. (2008). Controls on coastal dune morphology, shoreline erosion and barrier island response to extreme storms. *Geomorphology*, 100 (3-4), 223-240.

Hughen, K., Baillie, M., Bard, E., Beck, J., Bertrand, C., Blackwell, P., Buck, C., Burr, G., Cutler, K., Damon, P., Edwards, R., Fairbanks, R., Friedrich, M., Guilderson, T., Kromer, B., McCormac, G., Manning, S., Bronk Ramsey, C., Reimer, P., Reimer, R., Remmele, S., Southon, J., Stuvier, M., Talamo, S., Taylor, F., Van der Plicht, J. and Weyhenmeyer, C. (2004). Marine04: Marine radiocarbon age calibration, 0-26 cal kyr BP. *Radiocarbon*, 46, 1059-1086.

Hurrell, J.W., Kushnir, Y., Visbeck, M. and Ottersen, G. (2003). Atlantic Oscillation. The North Atlantic Oscillation: Climate Significance and Environmental Impact. *In*: J.W. Hurrell, Y. Kushnir, G. Ottersen, and M. Visbeck, Eds. *Geophysical Monograph Series*, 134, 1-35.

Hussain, N., Church, T., Heyraud, M., Fowler, S., Heussner, S., Monaco, A., Biscaye, P.E. and Anderson, R.F. (1990). Systematics of radon daughters (^{210}Pb-^{210}Po). Atmospheric fallout to coastal regions. *EOS Transactions*, 73(2), 72.

Ingram, BL., and Southon, JR. (1997). Reservoir ages in eastern pacific coastal and estuarine waters. *Radiocarbon*, 38(3), 573–82.

IPCC (2000). Emissions scenarios. Special Report of the IPCC (Ed. by Nakicenovic, N., Swart, R.). Cambridge University Press, UK, 570 p.

IPCC, (2007). Climate Change 2007. The physical science basis: contribution of Working Group I to the Fourth Assessment Report of the Intergovernmental Panel on Climate Change, viii. Cambridge University Press, Cambridge, New York, 996p.

IMPLIT, (2004). Impact des évènements extrêmes (tempêtes et surcotes) sur les hydrosystèmes du littoral méditerranéen dans le cadre du changement climatique. *Rapport final*, 90pp.

Jalut, G., Esteban Amat, A., Bonnet, L., Gauquelin, T. and Fontugne, M. (2000). Holocene climatic changes in the Western Mediterranean, from south-east France to south-east Spain. *Palaeogeography, Palaeoclimatology, Palaeoecology*, 160, 255–290.

Jansá, A., Genovés, A., Picornell, M. A., Campins, J., Riosalido, R. and Carretero, O. (2001). Western mediterranean cyclones and heavy rain. Part 2: statistical approach. *Applied Meteorology*, 8, 43–56.

Jelgersma, S., Stive, M.J.F. and van der Valk, L. (1995). Holocene storm surge signatures in the coastal dunes of the western Netherlands. *Marine Geology*, 125, 95-110.

Kalnay, E., Kanamitsu, M., Kistler, R., Collins, W., Deaven, D., Gandin, L., Iredell, M., Saha, S., White, G., Woollen, J., Zhu, Y., Chelliah, M., Ebisuzaki, W., Higgins, W., Janowiak, J., Mo, K.C., Ropelewski, C., Wang, J., Leetmaa, A., Reynolds, R., Roy, J. and Dennis J. (1996). The NCEP/NCAR 40-Year Reanalysis Project. *Bulletin of the American Meteorological Society*, 77 (3), 437-471.

Krichak, S. O., and Alpert, P. (2005). Decadal trends in the East Atlantic/West Russia pattern and the Mediterranean precipitation. *International Journal of Climatology*, 25, 183–192.

Krishnaswami, S., Lal, D., Martin, J.M., and Meybeck M. (1971). Geochronology of lake sediments. *Earth and Planetary Science Letters*, 11, 407–414.

Laborel, J., Morhange, C., Lafont, R., Le Campion, J., Laborel-Deguen, F. and Sartoretto, S. (1994). Biological evidence of sea level rise during the last 4500 years on the rocky coast of continental southwestern France Corsica. *Marine Geol*ogy, 120, 203–223.

Lamb, H.H. (1995). Climate, History and the Modern World, second ed. Routledge, London, 433pp.

Lambeck, K. and Bard, E. (2000). Sea-level change along the French Mediterranean coast for the past 30000 years. *Earth and Planetary Sciences Letters*, 175, 203-222.

Lambert, W.J., Aharon, P. and Rodriguez, A.B. (2008). Catastrophic hurricane history revealed by organic geochemical proxies in coastal lake sediments: a case study of Lake Shelby, Alabama (USA). *Journal of Paleolimnology*, 39, 117–131.

Lamy, F., Hebbeln, D., Röhl, U. and Wefer, G. (2001). Holocene rainfall variability in southern Chile: a marine record of latitudinal shifts of the Southern Westerlies. *Earth Planetary Science Lett*ers, 185, 369-382.

Landsea, C.W., Harper, B.A., Hoarau, K. and Knaff, J.A. (2006). Can we detect trends in extreme tropical cyclones? *Science,* 313, 452–454.

Lawrence, J. R. and Gedzelman, S. D. (1996). Low stable isotope ratios of tropical cyclone rains. *Geophysical Research Letters*, 23, 527–530, doi:10.1029/96GL00425.

Leatherman, S.P. (1979). Migration of Assateague Island, Maryland, by inlet and overwash processes. *Geology,* 7, 104-107.

Lecroart, P., Schmidt, S., Anschutz, P. and Jouanneau, J.M. (2007). Modeling sensitivity of biodiffusion coefficient to seasonal bioturbation. *Journal of Marine Research,* 65, 417–440.

Lionello, P., Dalan, F., and Elvini, E. (2002). Cyclones in the Mediterranean region: the present and the doubled CO2 climate scenarios. *Climate research,* 22, 147-159.

Lionello, P. and Sanna, A. (2005). Mediterranean wave climate variability and its links with NAO and Indian Monsoon. *Climate Dynamics*, 25, 611-623.

Lionello, P. and Giorgi, F. (2007). Winter precipitation and cyclones in Mediterranean region: future climate scenarios in a regional simulation. *Advances in Geosciences*, 12, 153-158.

Lionello, P., Bhend, J., Buzzi, A., Della-Marta, P. M., Krichak, S., Jansá, A., Maheras, P., Sanna, A., Trigo, I. F., and Trigo, R. (2006). Cyclones in the Mediterranean region: climatology and effects on the environment, in Mediterranean Climate Variability. In: Lionello, P., Malanotte-Rizzoli, P., Boscolo, R. (Eds.), Mediterranean Climate Variability, *Developments in Earth & Environmental Sciences* 4. Elsevier ed., pp. 324–372.

Liu, K., and Fearn, M. L., (1993). Lake-sediment record of late Holocene hurricane activities from coastal Alabama. *Geology,* 21, 793-796.

Lui, K., and Fearn, M. L., (2000). Reconstruction of Prehistoric landfall frequencies of catastrophic hurricanes in Northwestern Florida from lake sediment records. *Quaternary Research*, 54, 238-245.

Liu, K., Shen, C. and Louie, K.A. (2001). 1000 year history of typhoon landfalls in Guangdong, southern China, reconstructed from Chinese historical documentary records. *Annals of the Association of American Geographers,* 91, 453–64.

Liu, Z., Colin, C., Trentesaux, A., Blamart, D., Bassinot, F., Siani, G. and Sicre, M.A. (2004). Erosional history of the eastern Tibetan Plateau over the past 190 kyr: Clay mineralogical and geochemical investigations from the southwestern South China Sea. *Marine Geology*, 209, 1–18.

Liu, Z., Colin C., Huang, W., Le, W.P., Tong, S., Chen, Z. and Trentesaux, A. (2007). Climatic and tectonic controls on weathering in south China and Indochina Peninsula: Clay mineralogical and geochemical investigations from the Pearl, Red, and Mekong drainage basins. *Geochemistry Geophysics and Geosystems,* 8, Q05005, doi:10.1029/2006GC001490.

Luterbacher, J., Xoplaki, E., Detrich, D., Jones, P.D., Davies, T.D., Portis, D., Gonzalez-Rouco, J.F., Von Storch, H., Gyalistras, D., Casty, C., and Wanner, H. (2002). Extending

North Atlantic Oscillation reconstructions back to 1500. *Atmosheric Science Letters*, doi:10.1006/asle.2001.0044.

Luterbacher, J., Dietrich, D., Xoplaki, E., Grosjean, M., and Wanner, H. (2004). European seasonal and annual temperature variability, trends, and extremes since 1500. *Science*, 303, 1499, doi: 10.1126/science.1093877.

Luterbacher, J. et al. (2006) Mediterranean climate variability over the last centuries: a review. In: P. Lionello, P. Malanotte-Rizzoli and R. Boscolo (Eds), Mediterranean Climate Variability, Amsterdam: Elsevier, pp. 27—148.

Luterbacher, J., Xoplaki, E., Casty, C., Wanner, H., Pauling, A., Küttel, M., Rutishauser, T., Brönnimann, S., Fischer, E., Fleitmann, D., González-Rouco, F.J., García-Herrera, R., Barriendos, M., Rodrigo, F., Gonzalez-Hidalgo, J.C., Saz, M.A., Gimeno, L., Ribera, P., Brunet, M., Paeth, H., Rimbu, N., Felis, T., Jacobeit, J., Dünkeloh, A., Zorita, E., Guiot, J., Türkes, M., Alcoforado, M.J., Trigo, R., Wheeler, D., Tett, S., Mann, M.E., Touchan, R., Shindell, D.T., Silenzi, S., Montagna, P., Camuffo, D., Mariotti, A., Nanni, T., Brunetti, M., Maugeri, M., Zerefos, C., De Zolt, S., Lionello, P., Nunes, M.F., Rath, V., Beltrami, H., Garnier, E. and Le Roy Ladurie, E. (2006). Mediterranean Climate Variability over the last Centuries: a Review. *In* P. Lionello, P. Malanotte-Rizzoliet R. Boscolo. Mediterranean climate variabilty. Elsevier. pp 27-148.

Magny, M., Miramont, C. and Sivan, O. (2002). Assessment of the impact of climate and anthropogenic factors on Holocene Mediterranean vegetation in Europe on the basis of palaeohydrological records. *Palaeogeography, Palaeoclimatology, Palaeoecology*, 186, 47-59.

Maheras, P., Flocas, H., Patrikas, I. and Anagnostopoulou, Ch. (2001). A 40 year objective climatology of surface cyclones in the Mediterranean region: spatial and temporal distribution. *International Journal of Climatology*, 21, 109–130.

Masson-Delmotte, V., Kageyama, M., Braconnot, P., Charbit, S., Krinner, G., Ritz, C., Guilyardi, E., Jouzel, J., Abe-Ouchi, A., Crucifix, M., Gladstone, R.M., Hewitt, C.D., Kitoh, A., LeGrande, A.N., Marti, O., Merkel, U., Motoi, T., Ohgaito, R., Otto-Bliesner, B., Peltier, W.R., Ross, I., Valdes, P.J., Vettoretti, G., Weber, S.L., Wolk, F. and Yu, Y. (2006). Past and future polar amplification of climate change: Climate model intercomparisons and ice-core constraints. *Climate Dynamics*, 26, 513-529.

Matias, A., Ferreira, O., Vila-Concejo, A., Garcia, T. and Dias J.A. (2008). Classification of washover dynamics in barrier islands. *Geomorphology*, 97, 3-4, 655-674.

Mayewski, P.A., Rohling, E.E., Stager, J.C., Karlen, W., Maasch, K.A., Meeker, L.D., Meyerson, E.A., Gasse, F., van Kreveld, S., Holmgren, K., Lee-Thorp, J., Rosqvist, G. Rack, F., Staubwasser, M., Schneider, R.R. and Steig, E.J. (2004). Holocene climate variability. *Quaternary Research*, 62, 243-255.

Mazzini, I., Anadon, P., Barbieri, M., Castorina, F., Ferreli, L., Gliozzi, E., Mola, M. and Vittori, E. (1999). Late Quaternary sea-level changes along the Tyrrhenian coast near Orbetello (Tuscany, central Italy): palaeoenvironmental reconstruction using ostracods. *Marine Micropaleontology*, 37, 289–311.

Molinaroli, E. (1996). Mineralogical characterisation of Saharan dust with a view to its final destination in Mediterranean sediments. *In :* S. Guerzoni, and R. Chester, *The impact of desert dust across the Mediterranean* (pp. 153–162). Kluwer Academic Publishers.

Miller, D. L., Mora, C. I., Grissino-Mayer, H. D., Uhle, M. E. and Sharp, Z. (2006). Tree-ring isotope records of tropical cyclone activity. *Proceedings of the National Academy of Sciences,* 103, 14294–14297.

Miramont, C., Jorda, M., Pichard, G., (1998). Evolution historique de la morphogénèse et de la dynamique £uviale d'une rivière méditerranéenne: l'exemple de la moyenne Durance (France du sud-est). *Géographie physique du Quaternaire,* 52, 381-392.

Mitchell, T. D. and Jones, P. D. (2005). An improved method of constructing a database of monthly climate observations and associated high-resolution grids. *International Journal of Climatology*, 25, 693.

Monna, F., Lancelot, J., Bernat, M., and Mercadier, H. (1995). Sedimentation rate in the Thau Basin based on geochronological, geochemical, and stratigraphic data. *Oceanologica Acta,* 20, 627–638.

Morhange, M., Laborel, J. and Hesnard, A. (2001). Changes of sea level during the past 5000 years in the ancient harbor of Marseille, Southern France. *Palaeogeogrphy Palaeoclimatology Palaeoecology,* 166, 319–329.

Morton, R.A., Gonzalez, J.L., Lopez, G.I. and Correa, I.D. (2000). Frequent Non-storm Washover of Barrier Islands, Pacific Coast of Colombia. *Journal of Coastal Research*, 16, 82–87.

Morton, R.A. and Sallenger, A.H. (2003) Morphological impacts of extreme storms on sandy beaches and barriers. *Journal of Coastal Research,* 19 (3), 560–573.

Nerem, R.S., Leuliette, E. and Cazenave, A. (2006). Present-day sea-level change: A review. *Compte Rendus Geoscience*, 338, 1077–1083.

Noller, J. S. (2000). *Lead-210 geochronology*, chapter Noller, J.S., and Sowers, J.M., and Lettis, W.R., pages 115–120. AGU Reference Shelf 4.

Nott, J. and Hayne, M. (2001). High frequency of 'super-cyclones' along the Great Barrier Reef over the past 5,000 years. *Nature,* 413, 508–12.

Nott, J. (2004). Palaeotempestology: The study of and implications of prehistoric tropical cyclones, a review for hazard assessment. *Environment International*, 30, 433-447.

Nott, J., Haig, J., Neil, H. and Gillieson, D. (2007). Greater frequency variability of landfalling tropical cyclones at centennial compared to seasonal and decadal scales. *Earth Planetary Science Letters*, 255, 367–372.

Nott, J., Smithers, S., Walsh, K. and Rhodes, E. (2009). Sand beach ridges record 6000 year history of extreme tropical cyclone activity in northeastern Australia. *Quaternary Science Reviews,* 28, 1511–1520.

Oldfield, F., Asioli, A., Accorsi, C.A., Mercuri, A.M., Juggins, S., Langone, L., Rolph, T., Trincardi, F., Wolff, G., Gibbs, Z., Vigliotti, L., Frignani, M., van der Post, K., and Branch, V. (2003). A high resolution late Holocene palaeo environmental record from the central Adriatic Sea. *Quaternary Science Reviews,* 22, 319–342.

Orford, J.D. and Carter, R.W.G. (1982). Crestal overtop and washover sedimentation on a fringing sandy gravel coast, Carnsore Point, Southeast Ireland. *Journal of Sedimentary Research*, 1, 265–278.

Pavan, V., Molteni, F. and Bankovic, C. (2000). Winter variability in the Euro-Atlantic region in observations and in ECMWF seasonal ensemble experiments. *Quarterly Journal of the Royal Meteorological Society*, 126, 2143–2173.

Pauling, A., Luterbacher, J., Casty, C., and Wanner, H. (2005). 500 years of gridded high resolution precipitation reconstructions over Europe and the connection to large-scale circulation. *Climate Dynam*ics, doi: 10.1007/S00382-005-0090-8.

Pe-Piper, G., Triantafyllidis, S. and Piper, D.J.W. (2008). Geochemical identification of clastic sediment provenance from known sources of similar geology; the Cretaceous Scotian Basin, Canada. *Journal of Sedimentary Research,* 78(9), 595-607.

Pennington, W., Cambray, R., Eakins, J., and Harkness, D. (1976). Radionuclide dating of the recent sediment in Blelham Tarn. *Freshwater Biology*, 6, 317–331.

Petschick, R. (2000). MacDiff 4.2.5 manual. Available at http://www.geologie.uni frankfurt.de/Staff/Homepages/Petschick/PDFs/MacDiff_Manual_E.pdf (verified 16 Apr. 2007).

Pichard, G., (1995). Les crues sur le bas Rhône de 1500 à nos jours. Pour une histoire hydro-climatique. Méditerranée 3-4, 105-116.

Pielke, R.A. and Landsea, C.W. (1999). La Niña, El Niño, and Atlantic Hurricane Damages in the United States. *Bulletin of American Meteorological Society*, 80, 2027-2033.

Pielke, Jr., R. A., Landsea, C. W., Mayfield, M., Laver J. and Pasch, R., (2005). Hurricanes and Global Warming. *Bulletin of American Meteorological Society*, 86, 1571-1575.

Pirazzoli, P.A. (1991). World Atlas of Holocene Sea-Level Changes. *Elsevier Oceanography Series*, Vol. 58, 300 p., Amsterdam.

Pittalwala, I. and Hameed, I. (1991). Simulation of the North Atlantic Oscillation in a general circulation model. *Geophysical Research Letters*, 18, 841-844.

Quadrelli, R., Pavan, V. and Molteni, F. (2001). Wintertime variability of Mediterranean precipitation and its links with large-scale circulation anomalies. *Climate Dynamics*, 17, 457–466.

Raible, C.C., Yoshimori, M., Stocker, T. F. and Casty, C. (2007). Extreme midlatitude cyclones and their implications to precipitation and wind speed extremes in simulations of the Maunder Minimum versus present day conditions. *Climate Dynamics*, 28, 409-423.

Rampino, M.R. and Sanders, J.E. (1981). Evolution of the barrier islands of southern Long Island, New York. *Sedimentology*, 28, 37-47.

Radakovitch, O., Charmasson, S., M., A., and Bouisset, P. (1999). 210Pb and Caesium Accumulation in the Rhône Delta Sediments. *Estuarine, Coastal and Shelf Science*, 48, 77–92.

Radakovitch, O., Sanchez-Cabeza, J.A., Abassi, A., Masqué, P. and Heussner, S. (2003). Meso and small-scale variations of 210Pb fluxes on the Northwestern Mediterranean continental margins. *Continental Shelf Research*, 23, 693–715.

Raynal, O. (2008). Architectures de depots et facteurs de contrôle d'un système côtier à faibles apports sédimentaires : le littoral languedocien (Golfe du Lion, Sud de la France). *Thèse de Doctorat, Université Montpellier 2, pages 187.*

Raynal, O., Bouchette, F., Certain, R., Séranne, M., Dezileau, L., Sabatier, P., Lofi, J., Bui Xuan Hy, A., Briqueu, L., Pezard, P. and Tessier, B. (2009). Control of alongshore-oriented sand spits on the dynamic of a wave-dominated coastal system (Holocene deposits, northern Gulf of Lions, France). *Marine Geology, 264, 242-257.*

Raynal, O., Bouchette, F., Certain, R., Sabatier, P., Séranne, M., Lofi, J., Dezileau, L., Briqueu, L., Pezard, P., Courp., P., Holocene evolution of Languedocian lagoonal environment controlled by inherited coastal morphology (Northern Gulf of Lions, France). Submitted to *Bulletin Societé Géologique Française*.

Reimer, PJ., Reimer, RW. (2001). A marine reservoir correction database and on-line interface. *Radiocarbon*, 43 (2A), 461–3.

Reimer, PJ., and McCormac, FG. (2002). Marine radiocarbon reservoir corrections for the Mediterranean and Aegean Seas. *Radiocarbon,* 44(1), 159–66.

Reimer, P. J., Baillie, M. G. L., Bard, E., Bayliss, A., Beck, J. W., Bertrand, C. J. H., Blackwell, P. G., Buck, C. E., Burr, G. S., Cutler, K. B., Damon, P. E., Edwards, R. L., Fairbanks, R. G., Friedrich, M., Guilderson, T. P., Hogg, A. G., Hughen, K. A., Kromer, B., McCormac, F. G., Manning, S. W., Ramsey, C. B., Reimer, R. W., Remmele, S., Southon, J. R., Stuiver, M., Talamo, S., Taylor, F. W., van der Plicht, J., and Weyhenmeyer, C. E. 2004. IntCal04 Terrestrial radiocarbon age calibration, 26 - 0 ka BP. *Radiocarbon*, 46, 1029-1058.

Ricci Lucchi, M., Fiorini, F., Colalongo, M.L. and Curzi, P.V. (2006). Late-Quaternary paleoenvironmental evolution of Lesina lagoon (southern Italy) from subsurface data. *Sedimentary Geology,* 183, 1 –13.

Richter, T.O., Van der Gaast, S.J., Koster, B., Vaars, A.J., Gieles, R., De Stigter, H.C., De Haas H. and Van Weering, T.C.E. (2006). The Avaatech XRF Core Scanner: technical description and applications to NE Atlantic sediments. In: R.G. Rothwell, Editor, *New*

Techniques in Sediment Core Analysis. Special Publications, Geological Society, London, pp. 39–50.

Robbins, J. and Edgington, D. (1975). Determination of recent sedimentation rates in Lake Michigan using Pb-210 and Cs-137. *Geochimica et Cosmochimica Acta*, 39, 285–304.

Robert, C., Gauthier, A. and Chamley, H. (1984). Origine autochtone et allochtone des argiles récentes de haute altitude en Corse. *Géologie de la Méditerranée XI*, 243–253.

Rodríguez, S., Querol, X., Alastuey, A., Kallos, G. and Kakaliagou, O. (2001). Saharan dust contributions to PM10 and TSP levels in Southern and Eastern Spain. *Atmospheric Environment*, 35, 2433–2447.

Rohling, E.J., Grant, K., Hemleben, C., Siddall, M., Hoogakker, B.A.A., Bolshaw, M. and Kucera, M. (2008). High rates of sea-level rise during the last interglacial period. *Nature Geoscience*, 1, 38–42.

Rothwell, R.G., Hoogakker, B., Thomson, J., Croudace I.W. and Frenz, M. (2006). Turbidite emplacement on the southern Balearic Abyssal Plain (western Mediterranean Sea) during Marine Isotope Stages 1–3: an application of ITRAX XRF scanning of sediment cores to lithostratigraphic analysis. In: R.G. Rothwell, Editor, *New Techniques in Sediment Core Analysis*, Geological Society, London, pp. 79–98.

Sabatier, P., Dezileau, L., Condomines, M., Briqueu, L., Colin, C., Bouchette, F., Le Duff, M. and Blanchemanche P., (2008). Reconstruction of paleostorm events in a coastal lagoon (Hérault, South of France). *Marine Geology*, 251, 224-232.

Sabatier, P., Dezileau, L., Barbier, M., Raynal, O., Briqueu, L., Bouchette, F., Condomines, M., Lofi, J., Certain, R., Van Grafenstein, U., Jorda, C. and Blanchemanche, P. (2010). Late-Holocene evolution of coastal lagoon in the Gulf of Lions (South of France). *Bulletin de la Société Géologique Française*, 1, 10p.

Sáenz, J., Rodrıíguez-Puebla, C., Fernández, J. and Zubillaga, J. (2001). Interpretation of interannual winter temperature variations over Southwestern Europe. *Journal of Geophysical Research*, 106, 20641–20651.

Schmidt, S., Jouanneau, J., Weber, O., Lecroart, P., Radakovitch, O., Gilbert, F., and Jézéquel, D. (2007). Sedimentary processes in the Thau Lagoon (France): from seasonal to century time scales. *Estuarine, Coastal and Shelf Science*, 72, 534-542.

Scileppi, E., and Donnelly J.P. (2007). Sedimentary evidence of hurricane strikes in western Long Island, NY. *Geochemistry Geophysics and Geosystems*, 8, Q06011, doi: 10.1029/2006GC001463.

Scott, D.B., Collins, E.S., Gayes, P.T., and Wright, E. (2003). Records of prehistoric hurricanes on the South Carolina coast based on micropaleontological and sedimentological evidence, with comparison to other Atlantic Coast records. *Bulletin of American Geological Society*, 115, 1027-1039.

Serra, L. (2004). L'épave d'un marchand d'huile. *Archeologia*, 415, 74–81.

Sharma, P., Gardner, L.R., Moore, W.S., and Bollinger, M.S., (1987). Sedimentation and bioturbation in a salt marsh as revealed by ^{210}Pb, ^{137}Cs, and ^{7}Be studies. *Limnology and Oceanography*, 32, 313-326.

Siani, G., Paterne, M., Arnold, M., Bard, E., Métivier, B., Tisnerat, N. and Bassinot, F. (2000). Radiocarbon reservoir ages in the Mediterranean sea and in Black sea. *Radiocarbon*, 42, 271-280

Siani, G, Paterne, M, Michel, E, Sulpizio, R, Sbrana, A, Arnold, M, Haddad, G. (2001). Mediterranean sea surface radiocarbon age changes since the last glacial maximum. *Science*, 294, 1917–20.

Smith, J. and Walton, A. (1980). Sediment accumulation rates and geochronologies measured in the Saguenay Flord using the Pb-210 dating method. *Geochimical et Cosmochimical Acta*, 44, 225–240.

Springer, J. (1993). Decompaction and backstripping with regard to erosion, salt movement, and interlayered bedding. *Computer Geosciences*, 19, 1115-1125.

Solomon, S., et al., (2007). Climate Change 2007. The physical science basis: contribution of Working Group I to the Fourth Assessment Report of the Intergovernmental Panel on Climate Change, viii. *Cambridge University Press*, Cambridge, New York, 996p.

Somot, S, Sevault, F., Déqué M. and Crépon, M. (2008). 21st century climate change scenario for the Mediterranean using a coupled atmosphere-ocean regional climate model. *Global and Planetary Change*, 63, 112–126.

Sorrel, P., Tessier, B., Demory, F., Delsinne, N. and Moazé, D. (2009). Evidence for millennial-scale climatic events in the sedimentary infilling of macrotidal estuarine system, the Seine estuary (NW France), *Quaternary Science Reviews*, 28 (5-6), 499-516.

Southon, J, Kashgarian, M, Fontugne, M, Metivier, B, Yim, WWS. (2002). Marine reservoir corrections for the Indian Ocean and Southeast Asia. *Radiocarbon*, 44(1), 167–80.

Spennemann, D.H.R. and Head, M J (1998). Tongan pottery chronology, ^{14}C dates and the hardwater effect. *Quaternary Geochronology*, 17, 1047-1056.

Stuiver, M. and Polach, H.A. (1977). Discussion: Reporting of 14C data. *Radiocarbon*, 19, 355-363.

Stuiver, M., Pearson, G. W., Braziunas, T. 1986. Radiocarbon age calibration of 700 marine samples back to 9000 cal yr BP. *Radiocarbon*, 28 (2), 980-1021.

Stuiver, M., and Reimer, P. J., 1993, Extended 14C database and revised CALIB radiocarbon calibration program, *Radiocarbon*, 35, 215-230.

Stuiver, M., and Braziunas, T. F. (1993). Modelling atmospheric 14C influences and 14C ages of marine samples to 10,000 BC. *Radiocarbon*, 35 (1), 137-189.

Switzer, A.D., Bristow, C.S. and Jones, B.G. (2006). Investigation of large-scale washover of a small barrier system on the southeast Australian coast using ground penetrating radar. *Sedimentary Geology*, 183, 145–156.

Tanner, W.F. (1992). Late Holocene sea-level changes from grain-size data: Evidence from the Gulf of Mexico. *The Holocene*, 2, 249-254.

Tessier, B., Certain, R., Barusseau, J-P., and Henriet, J-P. (2000). Evolution historique du prisme littoral du lido de l'étang de Thau (Sète, Sud-Est de la France). Mise en évidence par sismique réflexion très haute résolution. *Compte Rendus de l'Académie des Sciences Paris*, 331, 709-716.

Thiry, M. (2000). Palaeoclimatic interpretation of clay minerals in marine deposits: An outlook from the continental origin. *Earth Sciences Reviews*, 49, 201–221.

Tisnérat-Laborde, N., Poupeau, JJ., Tannau, JF., Paterne, M. (2001). Developpement of a semi-automated system for routine preparation of carbonate samples. *Radiocarbon*, 43 (2A), 299-304.

Tolosana-Delgado, R., Otero, N., Pawlowsky-Glahn, V. and Soler, A. (2005). Some basic concepts of compositional geometry. *Mathematical Geology*, 37, 681–702.

Trigo, I. F., Davies, T. D., and Bigg, G. R. (2000). Decline in Mediterranean rainfall caused by weakening of Mediterranean cyclones. *Geophysical Research Lett*ers, 27, 2913–2916.

Trigo R., Xoplaki, E. Zorita, E., Luterbacher, J., Krichak, S.O., Alpert, P., Jacobeit, J., Saenz, J., Fernandez, J., Gonzalez-Rouco, F., Garcia-Herrera, R., Rodo, X., Brunetti, M., Nanni, T., Maugeri, M., Turkes, M., Gimeno, L., Ribera, P., Brunet, M., Trigo, I.F., Crepon, M. and Mariotti, A. (2006). Relations Between Variability in the Mediterranean Region and Mid-Latitude Variability. In: Lionello, P., Malanotte-Rizzoli, P., Boscolo, R. (Eds.), Mediterranean Climate Variability, *Developments in Earth & Environmental Sciences* 4. Elsevier ed., pp. 179–226.

Turner, R., Baustian, J., Swenson, E., and Spicer, J. (2006). Wetland Sedimentation from Hurricanes Katrina and Rita. *Science*, 314, 449–452.

Ullmann, A., Pirazzoli, P.A. and Moron, V. (2008). Sea surges around Gulf of Lions and atmospheric conditions. *Global and Planetary Change*, 63, 203-214.

Van de Plassche, O., Van der Borg, K., and De Jong, A. (1998). Sea level climate correlation during the past 1400 yr. *Geology*, 26, 319- 322.

Van den Boogaart, K.G. and Tolosana-Delgado, R. (2008). "compositions": A unified R package to analyze compositional data. *Computers and Geosciences*, 34, 320-338.

Vella C. and Provansal M. (2000). Relative sea-level rise and neotectonic events during the last 6500 yr on the southern eastern Rhône delta, France. *Marine Geology*, 170, 27–39.

Wanner, H., Beer, J., Butikofer, J., Crowley, T.J., Cubasch, U., Fluckiger, J., Goosse, H., Grosjean, M., Joos, F., Kaplan, J.O., Kuttel, M., Muller, S.A., Prentice, I.C., Solomina, O.,

Stocker, T.F., Tarasov, P., Wagner, M. and Widmann, M. (2008). Mid- to Late Holocene climate change: an overview. *Quaternary Science Reviews*, 27, 1791-1828.

Webster, P. J., Holland, G. J., Curry, J. A., and Chang, H. R. (2005). Change in tropical cyclone number, duration, and intensity in a warming environment. *Science*, 309, 1844-1846.

Woodruff, J.D., Donnelly, J.P., Mohrig, D. and Geyer, W.R., (2008). Reconstructing relative flooding intensities responsible for hurricane-induced deposits from Laguna Playa Grande, Vieques, Puerto Rico. *Geology*, 36, 391-394.

Woodruff, J. D., Donnelly, J.P., Emanuel, K. and Lane, P. (2008). Assessing sedimentary records of paleohurricane activity using modeled hurricane climatology, *Geochemistry Geophysics Geosystems*, 9, Q09V10, doi:10.1029/2008GC002043.

Woodruff, J.D., Donnelly, J.P. and Okusu, A. (2009). Exploring typhoon variability over mid-to-late Holocene: evidence of extreme coastal flooding from Kamikoshiki, Japan. *Quaternary Sciences Reviews*, in press.

Xoplaki, E., González-Rouco, J. F., Luterbacher, J. and Wanner, H. (2004). Wet season Mediterranean precipitation variability: influence of large-scale dynamics and trends. *Climate Dynamics*, 23, 63, doi: 10.1007/s00382-004-0422-0.

Yum J.G., Takemura K., Tokuoka T. and Yu K.M. (2003). Holocene environmental changes of the Hwajinpo Lagoon on the eastern coast of Korea. *Journal of Paleolimnology*, 29, 155-166.

Zazo, C., Dabrio, C.J., Goy, J.L., Lario, J., Cabero, A., Silva, P.G., Bardají, T., Mercier, N., Borja, F. and Roquero, E. (2008). The coastal archives of the last 15 ka in the Atlantic-Mediterranean Spanish linkage area: Sea level and climate changes. *Quaternary International*, 181, 72–87.

Zoppi, U., Albani, A., Ammerman, A., Hua, Q., Lawson, E. and Serandrei Barbero, R. (2001). Preliminary estimate of the reservoir age in the lagoon of Venice. *Radiocarbon*, 43, 489-494.

Zuo, Z., Eisma, D., Gieles, R. and Beks, J. (1997). Accumulation rates and sediment deposition in the northwestern Mediterranean. *Deep-Sea Research II*, 44(3-4), 597-609.

Liste des figures

Liste des tableaux

8. Annexes

8.1 Article 7: Archives sédimentaires dans les lagunes du Golfe d'Aigues Mortes : Estimation de l'aléa de tempête depuis 2000 ans

Sabatier Pierre et Dezileau Laurent

Université Montpellier 2, Geosciences Montpellier, CNRS, UMR 5243.

Accepté et à paraître dans un numéro spécial de la revue Quaternaire: Littoraux, lagunes et basses plaines alluviales à l'Holocène, *Quaternaire*, 20, (3), 2009.

Résumé :

Avec l'augmentation récente de la population mondiale et des infrastructures en domaine littoral, les tempêtes et les cyclones sont devenues un des risques majeurs à l'échelle globale. La Méditerranée, et plus particulièrement le Golfe du Lion, ne sont pas épargnés par ces phénomènes. La tempête de 1982 par exemple, de catégorie 2 sur l'échelle de Saffir-Simpson est responsable du décès de 15 personnes et de plus de 400 millions d'euros de pertes économiques. La prévision de ces évènements à partir de modèles climatiques est devenue primordiale. Le problème majeur dans cette approche est le manque de recul dans le temps pour calibrer ces modèles. Notre approche a donc été de reconstituer ces tempêtes du passé à partir de l'étude d'archives sédimentaires (paléotempestologie).
Les lagunes du littoral Languedocien sont les réceptacles de matériels terrigènes provenant des bassins versants en période de crues, mais aussi de sables transportés par la mer en période de tempêtes. L'étude des archives sédimentaires dans l'étang de Pierre Blanche nous a permis d'identifier et de reconstituer l'alternance des événements les plus extrêmes au cours des 2000 dernières années. La fréquence de ces tempêtes semble varier dans le temps et une augmentation significative est constatée durant la fin du « Petit Age Glaciaire ».

Mots clés: Méditerranée, lagune, tempête, ^{210}Pb, C14, Petit Age Glaciaire.

Sedimentary record in Aigues Mortes Gulf lagoons: Storm risk estimation for the last 2000 yrs

Abstract :

Hurricane and cyclone, are one of the most alarming natural hazard due to the recent concentration of resources and population in coastal areas. Let us consider the last storm events having affected the south of France (Gulf of Lion, Mediterranean Sea) like in 1982, category 2 in Saffir–Simpson scale, this storm caused the death of 15 people and economic losses estimated at 400 million euros, it is necessary to examine the past decadal- to millennial-scale variability of storm activity. Nevertheless the lack of instrumental long time series does not allow to determine the frequency of the most extreme events, therefore we

have to resort to other methods. Paleotempestology was used, in this study, to record the past overwash in sediment cores.
To identify and characterize the record of environmental changes due to these hurricanes, this work focused on the wetland complex of the Aigues-Mortes gulf (central part of the Gulf of Lion). The filling of these coastal lagoons was due to riverine particulate input during floods and marine sediment input during storm events. Thus cores sediments study of this lagoon allows to characterize the record of these paleostorm events for the last 2000 yrs. Little Ice Age seems to affect the storm frequency with an increase of hurricanes landfall probabilities from 0.06% to 0.86% during this cold period.

Keys words: Mediterranean Sea, lagoon, storm, ^{210}Pb, C14, Little Ice Age.

1. Introduction

Le littoral, situé à l'interface entre la terre et la mer, est une zone très dynamique et directement soumise aux phénomènes marins, et donc particulièrement sensible aux aléas majeurs littoraux tels que l'érosion et la submersion marines. Ces aléas sont étroitement liés lors des événements de tempêtes, en effet la surélévation du plan d'eau et la plus grande énergie des houles accélèrent l'érosion. Le recul du littoral et la disparition des cordons dunaires rendent les aménagements plus vulnérables face à la submersion marine. L'étude de l'impact des tempêtes actuelles sur le littoral Méditerranéen a montré que ces événements extrêmes jouent un rôle fondamental quant à la morphologie et l'évolution du trait de côte actuel (Bruzzi, 1998 ; Moron et Sabatier, Projet IMPLIT 2007). Avec l'augmentation récente de la population mondiale et des infrastructures en domaine littoral, l'impact des tempêtes et des cyclones est donc un des risques majeurs à l'échelle mondiale (Sarewitz *et al.*, 2003; Pielke *et al*., 2005; Turner *et al.*, 2006). La Méditerranée, et plus particulièrement le Golfe du Lion, ne sont pas épargnés par ces phénomènes. La tempête de 1982 par exemple, de catégorie 2 sur l'échelle de Saffir-Simpson est responsable du décès de 15 personnes et de plus de 400 millions d'euros de pertes économiques. La prévision de ces évènements à partir de modèles climatiques est devenue primordiale. Le problème majeur dans cette approche est le manque de recul dans le temps pour calibrer ces modèles. Ce manque d'enregistrement historique quantitatif documentant ces évènements climatiques extrêmes au cours des derniers millénaires, ne permet pas d'évaluer de façon fiable cet aléa. C'est pourquoi d'autres méthodes doivent être employées pour estimer la fréquence de ces évènements sur le long terme (Goldenberg *et al.*, 2001; Webster *et al.*, 2005). Cette étude rentre dans le cadre du projet ECLICA (projet INSU/ACI FNS « Aléas et changements globaux », coordinateur L. Dezileau) qui vise à identifier et estimer la récurrence des évènements extrêmes (crues, tempêtes) qui ont affecté la partie occidentale du bassin méditerranéen au cours de l'Holocène à partir de l'étude d'archives sédimentaires prélevées par carottages dans les lagunes et deltas du Languedoc-Roussillon. L'identification des événements sédimentologiques brefs de fortes amplitudes associé aux paléotempêtes à l'échelle des derniers milliers d'années est une thématique relativement nouvelle dans cette région du pourtour méditerranéen.
Le littoral du Languedoc-Roussillon est caractérisé par des lagunes résultant de l'interaction entre un processus de régularisation du trait de côte par migration de barrières littorales et le lent comblement de ces zones par les apports fluviatiles (Certain *et al.*, 2004). Ces lagunes sont les réceptacles à la fois de matériels terrigènes provenant des bassins versants en période de crues mais aussi de sables venus de la mer en période de tempêtes. L'étude du complexe lagunaire de l'étang de Pierre Blanche, nous a permis de reconstituer l'alternance de ces événements catastrophiques de tempête au cours des derniers siècles à partir de l'analyse de

carottes sédimentaires (Sabatier *et al.*, 2008 ; Dezileau *et al.*, 2008). Notre démarche a pour but ici, d'évaluer le risque tempête au cours des deux derniers millénaires et d'évaluer l'évolution de ce risque au regard des changements climatiques passés.

2. Site d'étude

L'environnement laguno-littoral du Languedoc-Roussillon offre des systèmes sédimentaires dans lesquels les matériaux peuvent s'accumuler à des vitesses d'accumulation relativement élevées (Monna *et al.*, 1995; Sabatier *et al*., 2008), en particulier lors de dépôts de crues ou de tempêtes.

L'étang de Pierre Blanche fait partie du complexe lagunaire palavasien, c'est une lagune allongée de 267ha et de 55cm de profondeur moyenne (*Figure 8.1*). La bordure Sud-Est de cette lagune est constituée par un cordon littoral sur plus de 5 km. Cette lagune est soumise à une forte influence marine, surtout durant les événements de tempêtes. Il n'existe pas de connexions directes avec la mer et le maximum de marée « moyenne » est de l'ordre de 50 cm. Ces phénomènes hivernaux associant des vents de secteur S-E à S-W supérieur à 20 m/s, une forte houle et une surcôte importante, sont relativement rares (1 à 5 événements par an). Cependant certaines de ces tempêtes, comme celles du 6-8 Novembre 1982, peuvent atteindre des vents de 46 m/s (catégorie 2 sur l'échelle de Saffir-Simpson).
Sabatier *et al.*, (2008) montrent que les archives sédimentaires des lagunes palavasiennes enregistrent principalement les évènements de tempêtes les plus intenses, avec une faible période de retour, ces événements extrêmes sont identifiés jusqu'à 600 m à l'intérieur de la lagune. Les carottes sédimentaires étudiées ici, a été prélevée à 500 m du bord de la lagune (*Figure 8.1*).

3. Paléotempestologie

La paléotempestologie est une méthode décrite pour la première fois par Liu and Fearn, (1993). Cette méthode consiste à reconstituer les tempêtes et les cyclones du passé à partir d'archives sédimentaires, elle utilise des traceurs géologiques comme la granulométrie, la géochimie ou les bio-indicateurs. Cette méthode est en grande partie basée sur l'étude des « overwashs » en anglais ou « cônes de tempête » en français qui se forment à la suite d'un cyclone en arrière d'un cordon littoral sableux. Un cône de tempête est formé par l'activité de la houle, principalement liée aux vents, qui érodent le cordon dunaire et déposent un niveau de sable dans une lagune. L'épaisseur de cette couche de sable est importante sur le bord de la lagune et diminue avec l'éloignement. Les extensions horizontales de ces niveaux sableux sont soumises à différents facteurs comme l'intensité et la durée de la tempête, la hauteur des vagues, la direction du vent par rapport au lido, l'épaisseur du lido et la quantité de sable disponible, la configuration de la côte avec la présence ou non de passe, la morphologie de la lagune ainsi que la succession de plusieurs événements extrêmes. De nombreuses études se sont concentrées sur l'étude de la récurrence des cyclones en Amérique du nord, dans les Caraïbes (Liu et Fearn, 1993, 2000; Donnelly *et al.*, 2001; Scott *et al.*, 2003; Donnelly *et al*., 2004; Donnelly et Woodruff, 2007; Scileppi et Donnelly 2007) et dans le Pacifique (Goff *et al.*, 2000; Hayne et Chappell 2001; Nott, 2004). Peu d'études concernent les côtes Méditerranéennes (Blanc, 1985 ; Dezileau *et al.*, 2005 ; Sabatier *et al.*, 2008). La paléotempestologie permet de calculer la récurrence des tempêtes les plus extrêmes au cours du temps, souvent exprimée, en pourcentage, ou probabilité d'avoir un événement par an (Liu et Fearn, 2000).

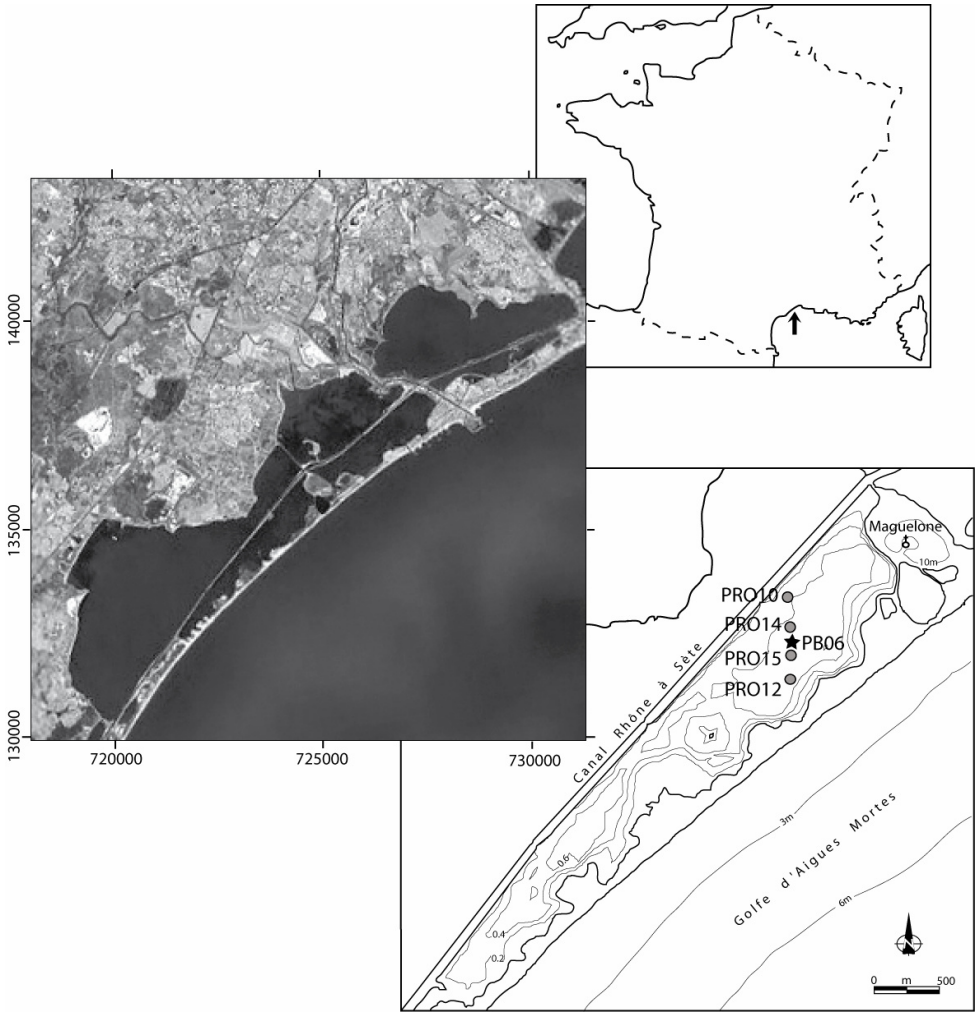

Figure 8.1 : Carte de l'étang de Pierre Blanche avec la localisation, en ronds gris des quatre carottes courtes selon un transect N-S (PRO 10, PRO 14, PRO 12 et PRO 15), et l'étoile noire de la carotte longue PB06.
Figure 8.1: Map of Pierre Blanche lagoon with localisation in grey circles of the four short cores along a N-S transect (PRO 10, PRO 14, PRO 12 and PRO 15) and the black star correspond to the long core PB06.

4. Méthodes d'analyse

Quatre carottes courtes (inférieures à 1m) ont été prélevées manuellement à l'aide de tubes en PVC selon un transect N-S (PRO 10, PRO 14, PRO 12 et PRO 15). Une carotte longue de 7,5 m a été extraite à partir de la plateforme de carottage UWITEC (PB06, *Figure 8.1*). Cette carotte prélevée en mars 2006 traverse l'intégralité du remplissage Holocène de la lagune. Ces différentes sections ont ensuite été radiographiées, photographiées et découpées tous les centimètres avant analyse. Dans la carotte PB06, le contenu malacologique a été étudié tous les deux centimètres (fraction supérieure à 1 mm) ainsi que la granulométrie laser (fraction inférieure à 150 µm, Beckman Coulter LS 13 320). Le ^{210}Pb et le ^{137}Cs ont été mesurés sur les archives sédimentaires à partir d'un spectrométre gamma CANBERRA BEGe 3825 pour

obtenir une chronologie des 100 dernières années. La méthode de datation par le ^{210}Pb a été établi pour la première fois en 1963 par Goldberg, depuis cette étude plusieurs modèles ont été définis et sont résumés par Appleby and Oldfield, (1992). Le modèle le plus simple suppose un flux de ^{210}Pb en excès et un taux de sédimentation constant, ce qui signifie que la concentration initiale en (^{210}Pbex) reste constante sur la période de temps étudiée (Goldberg, 1963; Krishnaswami *et al.*, 1971). La méthode de datation basée sur le ^{137}Cs (Robbins et Edgington, 1975) suppose que la profondeur présentant l'activité maximale en ^{137}Cs dans le sédiment, correspond à la date de 1958, pic de production atmosphérique du ^{137}Cs dans la région étudiée (Radakovitch *et al.*, 1999). Pour les périodes plus anciennes, des analyses ^{14}C ont été réalisées au LMC14 sur des échantillons de coquilles lagunaires (Laboratoire de Mesure ^{14}C, ARTEMIS) à l'institut du CEA à Saclay (Commisariat de l'Energie Atomique, projets ECLICA et INTEMPERIES, coordinateur L. Dezileau). Les âges ^{14}C ont été convertis en âges calibrés AD grâce au programme de calibration Calib 5.0.2 à deux sigma (Hughen *et al.*, 2004).

5. Résultats

5.1 Stratigraphie sédimentaire

Les carottes sédimentaires prélevées dans la lagune de Pierre Blanche présentent un matériel sédimentaire relativement fin. Elles sont principalement constituées d'argile et de limons fins de couleur gris contenant des coquilles lagunaires de types *Hydrobia acuta*, *Abra ovata*, *Cerastoderma glaucum*. Ces sédiments sont en majeures parties formés de smectite et de kaolinite, on note aussi la présence de cristaux de gypse néoformés. Certains niveaux présentent une forte abondance en débris végétaux ainsi que des graines de *Ruppia maritima,* la matière organique peut atteindre des concentrations de 4% (en moyenne 2%) tandis que la perte en eau est d'environ 50%. Intercalés au milieu de ces sédiments fins, on note la présence de niveaux gris foncés plus grossiers, silt à sable fin d'épaisseur variant entre 1 et plus de 10 cm. Ces couches sont constituées de grains de quartz, feldspath, biotite ainsi que quelques minéraux lourds comme le zircon et l'apatite, ces passées sableuses contiennent également de l'illite et de la chlorite. Dans ces niveaux de sable on retrouve une faune supportant des conditions environnementales plus marine avec par exemple *Bittium recticulatum* et *Rissoa ventricosa.* La corrélation des ces niveaux de sable entre les différentes carottes (Figure 2) permet de mettre en évidence la continuité latérale de ces cortèges sableux sur des distances pouvant atteindre plus de 800m. Les niveaux sableux décrits par Sabatier *et al.*, (2008) dans le premier mètre sont retrouvés dans la carotte longue PB06.

5.2 Chronologie

Sabatier et al. (2008) ont démontré qu'il est possible d'utiliser le modèle CFCS sur les intervalles sédimentaires strictement lagunaires au cours des 100 dernières années. Les données ^{210}Pb donnent des taux de sédimentation qui varient entre 4.2 ± 0.7 et 3.0 ± 0.4 mm.an^{-1} entre le centre (carotte PRO15) et le bord (carotte PRO12) de la lagune. Le ^{137}Cs, malgré sa haute mobilité dans les eaux interstitielles des sédiments marins (Charmasson *et al.*, 1998; Radakovitch *et al.*, 1999), peut être utilisé pour obtenir un taux de sédimentation fiable dans ce type d'environnement (Sabatier *et al.*, 2008). Ces vitesses de sédimentation sont respectivement de 4.4 à 2.8 mm.an^{-1} pour les carottes PRO15 et PRO12, ce qui est en accord avec les données obtenues par le ^{210}Pb.

Pour cette étude sept âges radiocarbone ont été réalisés sur l'espèce *Cerastoderma glaucum*, trois sur la carotte PRO15 et 4 sur la carotte PB06, ces données sont reportées dans le *Tableau 8-1* et la *Figure 8.2*. Siani *et al.*, (2000) a montré que les âges réservoirs en Méditerranée occidentale étaient plus importants que l'âge réservoir marin global (Hughen *et al.*, 2004). Cette différence est expliquée par d'importants apports en eau douce provenant de petits fleuves côtiers possédant un bassin versant presque exclusivement constitué de calcaire Mésozoïque contenant donc de faibles teneurs en ^{14}C. Les lagunes, zone réceptacle de ces eaux continentales, ont donc logiquement des âges réservoirs encore plus importants que l'océan ouvert (Siani *et al.*, 2000; Zoppi *et al.*, 2001; Sabatier *et al.*, 2008). Les lagunes Palavasiennes quand à elles, présentent des âges réservoirs de 953 ± 25 ^{14}C ans, cette estimation est basée sur la corrélation entre différentes méthodes de datation comme le ^{210}Pb et ^{137}Cs, les événements historiques, ou des coquilles de niveaux archéologiques (Sabatier *et al.*, accepté). Dans cette étude les datations ^{14}C sont donc calibrées en tenant compte de cet âge réservoir (*Tableau 8-1*).

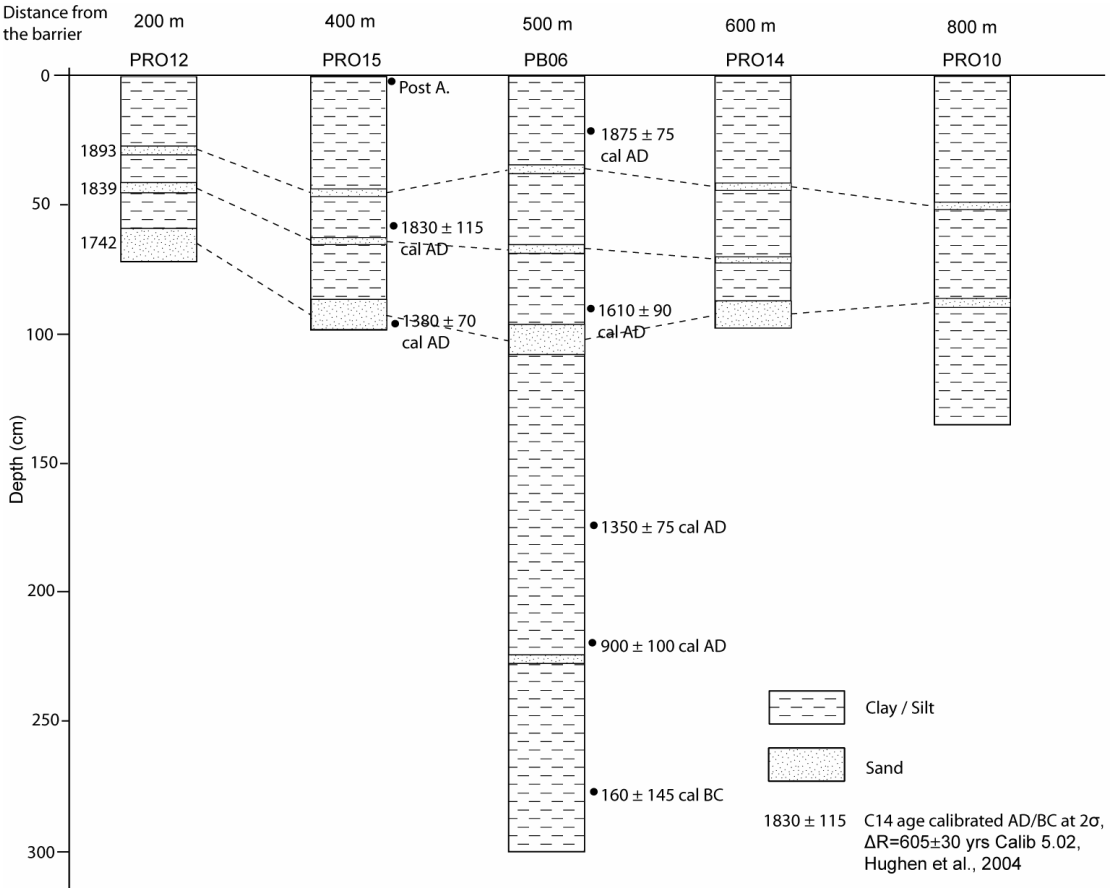

Figure 8.2 : Stratigraphie sédimentaire des carottes PRO12, PRO15, PB06, PRO14 et PRO10, classé de gauche à droite en fonction de l'éloignement du cordon littoral. Les traits en pointillés représentent les liens entre les différents niveaux de sable observés. Les âges radiocarbones sont calibrés à 2σ avec Calib. 5.02 (Hughen et al., 2004) et exprimés en année B.P.

Figure 8.2: Sediment stratigraphy for cores PRO12, PRO15, PB06, PRO14 and PRO10, arranged from left to right according to increasing distance from the sandy barrier. Dashed lines display the link between sand layers. Radiocarbon dates are calibrated at 2σ with Calib. 5.02 (Hughen et al., 2004), and express in years before present (yr cal B.P.).

6 Discussion

A partir du croisement entre les archives sédimentaires et les archives textuelles historiques, Sabatier *et al.*, (2008) ont mis en évidence trois événements de tempêtes majeures qui ont pu être datés à 1742, 1839 et 1893 dans le Golfe d'Aigue Mortes. La tempête de 1982 (catégorie 2 sur l'échelle de Saffir-Simpson) qui a causé d'énorme dégâts humains et matériels sur le littoral (Blanc, 1985), n'est pas enregistrée dans ces archives sédimentaires. L'étude de photos de terrain montre très clairement que les sables du lido n'ont pas été déplacés sur de longues distances au cours de l'événement (com. Pers. Michel Séranne). Il est donc fortement probable que ces évènements anciens étaient beaucoup plus puissants que la tempête de 1982.

Cores	Depth (cm)	C14 Age BP	C14 Age cal AD/BC, 2σ, R(t)=953±25yrs
PRO15	3	145 ± 30	post A.
	60	1095 ± 30	1835 ± 115 cal A.D.
	95	1580 ± 30	1380 ± 70 cal A.D.
PB06	20	1055 ± 30	1875 ± 75 cal A.D.
	83	1285 ± 30	1610 ± 90 cal A.D.
	173	1645 ± 30	1350 ± 75 cal A.D.
	225	2100 ± 30	900 ± 100 cal A.D.
	278	3050 ± 30	160 ± 145 cal B.C.

Tableau 8-1 : Age radiocarbone sur les carottes PRO15 et PB06. Calibration marine à l'aide de Calib 5.02 à 2σ (Hughens et al, 2004), avec un age réservoir de 953±30 ^{14}C ans (Sabatier et al., 2008; Sabatier et al., accepté).
Tableau 8-1 : Radiocarbon ages from PRO15 and PB06 cores. Marine calibration with R(t)=953±30 ^{14}C yrs (Sabatier et al., 2008; Sabatier et al., accepted) with Calib 5.0.2 program at 2σ (Hughens et al, 2004).

Ces tempêtes sont identifiées par une séquence sédimentaire typique avec la succession d'un niveau de sable (cône de tempête), la présence d'espèces marines puis d'espèces lagunaires. Toutefois, le système lagunaire devait être différent dans le passé. Sabatier *et al.*, (2010) estiment qu'il y a eu un changement paléo-environemental majeur autour de 1000 yr cal B.P. Cette date représente le passage d'un système lagunaire plus ouvert sur la mer, avec des passes permanentes coupant le lido, vers un système plus protégé comme nous le connaissons actuellement. Ce changement s'observe dans les archives sédimentaires (*Figure 8.3*) à une profondeur de l'ordre de 220 cm, avec une prédominance des espèces lagunaires qui augmentent au détriment des espèces marines.
Les différents dépôts de sable ou de tempête se retrouvent sur l'ensemble des archives sédimentaires avec une extension latérale importante pouvant atteindre 600 m de distance. Deux informations peuvent être déduites de ce résultat : (1) Les tempêtes étaient de fortes intensités et (2) la bonne préservation du signal sédimentaire sur de grandes distances signifie que des reconstitutions paléoclimatiques sont réalisables dans ce type de milieu lagunaire. L'étude de la carotte longue PB06 met en évidence 4 événements extrêmes de tempête. La datation des ces événements (*Figure 8.3*) met en évidence que parmi les 4 tempêtes, 3 sont déjà décrites par Sabatier *et al.*, (2008) et sont datées à 1742, 1839, 1893. Le dernier événement date de 800 ans cal AD. Il est possible de calculer la probabilité d'avoir un événement extrême par an, même si la rareté de ces tempêtes ne permet pas d'obtenir des données statistiquement significatives. Si nous considérons l'ensemble des données d'une

façon homogène, la probabilité d'avoir une tempête, suffisamment puissante pour être enregistrée sur toute la lagune, est non plus de 1% par an (3 tempêtes durant les 300 dernières années, Sabatier *et al.*, 2008) mais de 0.2% par an (4 tempêtes en 2000 ans). Cependant, nous savons que depuis le début de notre ère le climat mondial et surtout européen a été perturbé par une période chaude s'étalant de 850-1250 AD nommée l'Optimum Médiéval, et une période froide de 1550-1900 AD appelée le Petit Age Glaciaire (PAG), reportées dans la figure 3 (Esper *et al.*, 2005). Si nous prenons en compte ces périodes climatiques pour calculer la période de retour des tempêtes depuis 2000 ans, on s'aperçoit qu'il n'y a pas d'événements extrêmes durant l'Optimum Médiéval alors que l'on identifie 3 tempêtes majeures au cours du PAG. La probabilité d'avoir un événement de tempête durant le PAG est de 0.86% alors qu'elle n'ait que de 0.06% pour le reste des 2000 dernière années. Il existe donc clairement une augmentation de la fréquence des événements intenses de tempête pendant le PAG, c'est à dire pendant une période climatique à configuration froide.

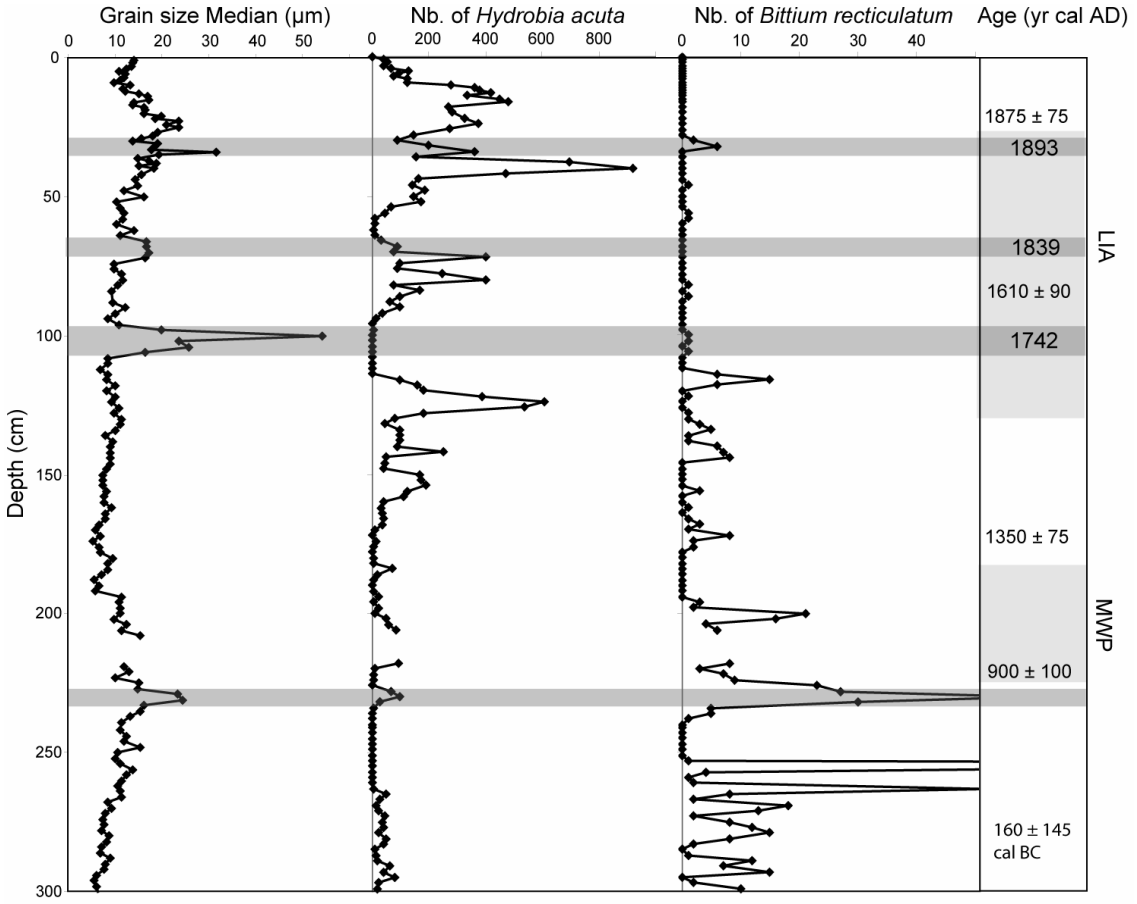

Figure 8.3 : Caractérisation des événements de tempêtes dans la carotte PB06 représentée en gris foncé. De gauche à droite : médiane granulométrique exprimée en micromètre, nombre d'individus de l'espèce lagunaire Hydrobia acuta, nombre d'individus de l'espèce marine Bittium recticulatum, chronologie ^{14}C et événements de tempêtes historiquement connus 1742, 1839 et 1893 (Sabatier et al., 2008). De plus, à droite du graphique l'Optimum Médiéval (MWP : 850-1250 AD) et le Petit Age Glaciaire (LIA : 1550-1900 AD) sont représentés en gris clair.

Figure 8.3 : Storm event characterization in core PB06 display in dark grey bands. From left to right: grain size median, lagoonal species (Hydrobia acuta), marine species (Bittium recticulatum), ^{14}C dates and historical storm events (Sabatier et al., 2008). Medieval Warm

Period (MWP : 850-1250 AD) and Little Ice Age (LIA : 1550-1900 AD) were represented in light grey on the right part of the figure.

7. Conclusion

La paléotempestologie, associant des données sédimentologiques, malacologiques et différentes méthodes de datation, permet de mettre en évidence 4 événements extrêmes de tempêtes (au moins de catégorie 3 sur l'échelle de Saffir-Simpson avec des vents pouvant dépasser les 200 km/h) au cours des 2000 dernières années. La chronologie de ces tempêtes obtenues grâce au ^{210}Pb, ^{137}Cs pour des échelles de temps courtes et au ^{14}C pour des périodes plus anciennes, permet de dater ces 4 événements en 1893, 1839, 1742 et autour de 800 ans de notre ère. La répartition de ces tempêtes dans le temps n'est pas homogène. En effet, il y a une augmentation de la probabilité d'avoir un événement extrême par an d'un facteur supérieur à 10 durant le « Petit Age Glaciaire », avec 0.86% alors qu'elle n'est que de 0.06% sur les 2000 dernières années.

Remerciements

Cette recherche a été supportée par le programme ECLICA financé par l'INSU (ACIFNS "Aleas et Changement Globaux", L. Dezileau). Les auteurs remercient IFREMER Palavas d'avoir permis le stockage des carottes dans leur chambre froide, ainsi le docteur A. Bengana et son équipe pour avoir réalisé la radiographie X au département de "la Clinique du Milénaire". Merci aussi au LMC14 d'avoir réalisé les mesures ^{14}C et au SARM pour les analyses en éléments traces et majeurs. Et enfin à M. Barbier et à tout les membres du programme ECLICA pour leurs investissements et leurs discussions constructives au cour de cette étude.

Bibliographie

Andrade, C., Freitas, M., Moreno, J., and Craveiro, S. (2004). Stratigraphical evidence of Late Holocene barrier breaching and extreme storms in lagoonal sediments of Ria Formosa, Algarve, Portugal. *Marine Geology*, 210, 339–362.

Appleby, P. and Oldfield, F. (1992). *Uranium Series Disequilibrium, Application to Earth, Marine and Environmental Sciences.*, chapter Application of lead-210 to sedimentation studies, 731–778. Clarendon Press, Oxford.

Blanc, J.J. (1985). Ruptures d'équilibre au littoral de Provence occidentale : l'action des tempêtes, relations avec les aménagements, *Tethys*, 11, 3-4, 350-359.

Bruzzi, C., (1998). Les tempêtes et l'évolution morphosédimentaire des plages orientales du delta du Rhône, *Thèse de doctorat de Géograpgie physique, Université d'Aix-Marseille 1*, 403 pp.

Certain, R., Tessier, B., Courp, T., Barusseau, J., and Pauc, H. (2004). Reconnaissance par sismique tres haute resolution du remplissage sedimentaire de la lagune de Leucate (Aude et Pyrénées-Orientales - SE France). *Bulletin de la Société Géologique Française*, 175, 35–48.

Charmasson, S., Radakovitch, O., Arnaud, M., Bouisset, P., and Pruchon, A., (1998). Long-cores profiles of 137Cs, 134Cs, 60Co and 210Pb in sediment near the Rhône river (Northwestern Mediterranean sea). *Estuaries*, 21–3, 367–378.

Dezileau, L., Bordelais, S., Condomines, M., Bouchette, F., and Briqueu, L. (2005). Evolution des lagunes du Golfe d'Aigues-Mortes à partir de l'étude de carottes sédimentaires courtes (étude géochronologique, sédimentologique et géochimique des sédiments récents). In Publications ASF, Paris, 51, p. 91.

Dezileau, L., Sabatier P and Blanchemanche P. (2008). Increase of storm activity during the Little Ice Age in the French Mediterranean coast. *Hymex, Ecole Polytechnique, Paris, p. 34*.

Donnelly, J. P., Smith Bryant, S., Butler, J., Dowling, J., Fan, L., Hausmann, N., Newby, P., Shuman, B., Stern, J., Westover, K., and Webb, T. III (2001). 700 yr sedimentary record of intense hurricane landfalls in southern New England. *Geological Society of America Bulletin*, 113, 714–727.

Donnelly, J. P., Butler, J., Roll, S., Wengren, M., and Webb, T. III (2004), A backbarrier overwash record of intense storms from Brigantine, New Jersey, *Marine Geology*, 210, 107–121.

Donnelly, J. P., and Woodruff, J.D. (2007). Intense hurricane activity over the past 5,000 years controlled by El Nino and the West African monsoon. *Nature*, 447, 465-468.

Esper, J., Wilson, R.J.S., Frank, D.C., Moberg, A., Wanner, H., and Luterbacher, J., (2005). Climate: past ranges and future changes, *Quaternary Science Reviews*, 24, 2164–2166.

Goff, J., Rouse, H., Jones, S., Hayward, B., Cochran, U., a. M. W., Dickinson, W., and Morley, M. (2000). Evidence for an earthquake and tsunami about 3100-3400 yr ago, and other catastrophic saltwater inundations recorded in a coastal lagoon, New Zealand. *Marine Geology*, 170, 231–249.

Goldberg, E. (1963). *Geochronology with lead-210*, chapter radioactive dating, 121–131. International Atomic Energy Agency.

Goldenberg, S. B., Landsea, C. W., Mestas-Nunez, A.M., and Gray, W.M., (2001). The recent increase in Atlantic hurricane activity : Causes and implications. *Science*, 293, 474-479.

Hayne, M., and Chappell, J., (2001). Cyclone frequency during the last 5000 yrs from Curacoa Island Queensland. *Palaeogeography Palaeoclimatology Palaeoecol*ogy, 168, 201–219.

Hughen, K., Baillie, M., Bard, E., Beck, J., Bertrand, C., Blackwell, P., Buck, C., Burr, G., Cutler, K., Damon, P., Edwards, R., Fairbanks, R., Friedrich, M., Guilderson, T., Kromer, B., McCormac, G., Manning, S., Bronk Ramsey, C., Reimer, P., Reimer, R., Remmele, S., Southon, J., Stuvier, M., Talamo, S., Taylor, F., Van der Plicht, J. and Weyhenmeyer, C. (2004). Marine04: Marine radiocarbon age calibration, 0-26 cal kyr BP. *Radiocarbon*, 46, 1059-1086.

Krishnaswami, S., Lal, D., Martin, J.M., and Meybeck M. (1971). Geochronology of lake sediments. *Earth and Planetary Science Letters*, 11, 407–414.

Liu, K., and Fearn, M. L., (1993). Lake-sediment record of late Holocene hurricane activities from coastal Alabama: *Geology*, 21, 793-796.

Liu, K., and Fearn, M.L., (2000). Reconstruction of prehistoric landfall frequencies of catastrophic hurricanes in NW Florida from lake sediment records. *Quaternary Research*, 54, 238– 245.

Monna, F., Lancelot, J., Bernat, M., and Mercadier, H. (1995). Sedimentation rate in the Thau Basin based on geochronological, geochemical, and stratigraphic data. *Oceanologica Acta*, 20, 4, 627–638.

Moron, V., & Sabatier, F. (2007). IMPLIT – Impact des évènements extrêmes (tempêtes et surcotes) sur les hydrosystèmes du littoral méditerranéen dans le cadre du changement climatique. Rapport final. 173 p.

Nott, J., (2004) Palaeotempestology: The study of and implications of prehistoric tropical cyclones - A review for hazard assessment. *Environment International*, 30, 433–447.

Pielke, Jr., R. A., Landsea, C. W., Mayfield, M., Laver J. and Pasch, R., (2005). Hurricanes and Global Warming. *Bulletin of the American Meteorology Society*, 86, 1571-1575.

Radakovitch, O., Charmasson, S., M., A., and Bouisset, P., (1999). 210Pb and caesium accumulation in the Rhône Delta sediments. *Estuaries and Coastal Shelf Sciences*, 48, 77–92.

Raynal, O., Bouchette, F., Certain, R., Séranne, M., Dezileau, L., Sabatier, P., Lofi, J., Bui Xuan Hy, A., Briqueu, L., Pezard, P., and Teissier, B. Control of alongshore-oriented sand spits on the dynamic of a wave-dominated coastal system (Holocene deposits, northern Gulf of Lion, France). *Marine Geology*, 264, 242-257.

Robbins, J., & Edgington, D., (1975). Determination of recent sedimentation rates in Lake Michigan using Pb-210 and Cs-137. *Geochimica Cosmochimca Acta*, 39, 285–304.

Sabatier, P., Dezileau, L., Condomines, M., Briqueu, L., Colin, C., Bouchette, F., Le Duff, M. and Blanchemanche, P. (2008). Reconstruction of paleostorm events in a coastal lagoon (Herault, South of France). *Marine Geology*, 251, 224-232.

Sabatier, P., Dezileau, L., Barbier, M., Raynal, O., Briqueu, L., Bouchette, F., Condomines, M., Lofi, J., Certain, R., Van Grafenstein, U., Jorda, C. and Blanchemanche, P. (2010). Late-Holocene evolution of coastal lagoon in the Gulf of Lions (South of France). *Bulletin de la Société Géologique Française*, 1, 10p.

Sabatier, P., Dezileau, L., Blanchemanche, P., Siani, G., Condomines, M., Bentaleb, I., Piquès, G. Estimation of reservoir effect in coastal area in relation to paleoenvironmental change. *Radiocarbon, accepté*

Sarewitz, D., Pielke, Jr. R. A., and Keykyah, M. (2003). Vulnerability and risk: Some thoughts from a political and policy perspective. *Risk Analysis*, 23**,** 805–810.

Scileppi, E., & J. P. Donnelly (2007), Sedimentary evidence of hurricane strikes in western Long Island, NY. *Geochemistry Geophysics Geosystems*, 8, Q06011, doi: 10.1029/2006GC001463.

Scott, D.B., Collins, E.S., Gayes, P.T., and Wright, E. (2003). Records of prehistoric hurricanes on the South Carolina coast based on micropaleontological and sedimentological evidence, with comparison to other Atlantic Coast records. *Geological Society of American Bulletin*, 115, 1027-1039.

Siani, G., Paterne, M., Arnold, M., Bard, E., Métivier, B., Tisnerat, N., and Bassinot, F., (2000). Radiocarbon reservoir ages in the Mediterranean sea and in Black sea. *Radiocarbon*, 42, 271–280.

Turner, R., Baustian, J., Swenson, E., and Spicer, J. (2006). Wetland Sedimentation from Hurricanes Katrina and Rita. *Science*, 314, 449–452.

Webster, P. J., Holland, G. J., Curry, J. A., and Chang, H. R. (2005). Change in tropical cyclone number, duration, and intensity in a warming environment. *Science*, 309, 1844-1846.

Zoppi, U., Albani, A., Ammerman, A., Hua, Q., Lawson, E., and Serandrei Barbero, R., (2001). Preliminary estimate of the reservoir age in the lagoon of Venice. *Radiocarbon*, 43, 489–494.

8.2 Article 8: Control of alongshore-oriented sand spits on the dynamic of a wave-dominated coastal system (Holocene deposits, northern Gulf of Lions, France)

Olivier Raynal[1], Frédéric Bouchette[1], Raphaël Certain[2], Michel Séranne[1], Laurent Dezileau[1], Pierre Sabatier[1], Johanna Lofi[1], Anna Bui Xuan Hy[3], Louis Briqueu[1], Philippe Pezard[1] and Bernadette Tessier[4]

1 Geosciences Montpellier, CNRS, UMR 5243, Université Montpellier 2
2 IMAGES, Université de Perpignan.
3 Schlumberger, Le palatin 1 - 1, cours du Triangle, 92 936 La Défence cedex, France.
4 M2C, UMR CNRS 6143, Université de Caen.

Received 19 September 2008; revised 4 June 2009; accepted 12 June 2009. Available online 21 June 2009.

Abstract

The Maguelone shore extends along the northern coast of the Gulf of Lions, west of the Rhône Delta and east of high gradient coastal streams that have provided most of the clastic sediments to the Gulf of Lions margin since early Miocene. This 10 kilometres wide area is constituted by a small coastal watershed (15 km long) in low-lying carbonate hills, a kilometre-wide marsh, a sandy beach barrier and a shoreface experiencing local low sedimentation rates. This onshore-offshore transition zone is a key area to understand the relationships between erosion, by-pass, deposition and preservation processes. Unlike the neighbouring Rhône deposits that display numerous thick deltaic sequences related to a continuous sediment flux, the Maguelone shore exhibits peculiar sedimentary bodies. The analysis of about 250 km of new VHR seismic profiles acquired over the study area, 9 short cores and outcrops data allowed us to determine the three-dimensional high-resolution geometry of the coastal system tracts from Quaternary to present-day. This revealed dominant denudation processes in the upstream catchments associated with the formation of incised valleys during Quaternary lowstands. In addition, this study investigates the erosion and deposition mechanisms controlled by littoral hydrodynamics that have been taken place on this shore since the last transgression. In particular, metre-high and hundreds of metre-long sandy bodies constructed by alongshore hydrodynamics were identified and their effect on the morphodynamics of the whole littoral system is discussed. The Maguelone shore can be used as an experimental study for onshore/offshore dynamics under the influence of microtidal wave/current hydrodynamics and very low river-derived sediment flux during a eustatic cycle. Geometry of system tracts across flood plain to shoreface is usually considered to be controlled by relative sea-level changes, and is successfully analysed with 2D sequence stratigraphy cross-shore models. It is observed that in areas like the Maguelone shore, traditional sequence stratigraphy methods might not be fully relevant and need to integrate alongshore hydrodynamical processes.

Keywords: sand spit; transgression; deglacial deposits; Gulf of Lions; alongshore drift; coastal tract

8.3 Article 9: Holocene evolution of languedocian lagoonal environment controlled by inherited coastal morphology (Northern Gulf of Lions, France)

Olivier Raynal[1], Frédéric Bouchette[1,3], Raphaël Certain[2], Pierre Sabatier[1], Michel Séranne[1], Johanna Lofi[1], Laurent Dezileau[1], Louis Briqueu[1], Pierre Ferrer[2], Thierry Courp[2]

1 Geosciences Montpellier, CNRS, UMR 5243, Université Montpellier 2
2 IMAGES, Université de Perpignan.
3 Institute of Applied Mathematics and modelling, Université Montpellier 2

Abstract

The Maguelone shore extends along the northern coast of the Gulf of Lions margin, West of the Rhône delta and East of some high gradient coastal streams that have been providing most of the clastic sediments to the Gulf of Lions margin since early Miocene. This 10 km wide area comprises an onshore small coastal watershed (15 km long) in low-lying carbonate hills, km-wide marsh, sandy beach and shoreface featuring local low sedimentation. This coastal zone exhibits evolution of incised valleys under the influence of rivers and microtidal wave/current hydrodynamics during an eustatic cycle.
Analysis of about 250 km of VHR seismic profiles, tens of cores and outcrops data allowed us to determine the evolution of the Maguelone coastal system from Late-Quaternary to presentday. This paper highlights dominant denudation processes in the upstream catchments associated to the formation of incised valley seaward during Quaternary. Combination of this inherited morphology and hydrodynamics control the lagoonal environment evolution since the last transgression. In particular, the Maguelone shore is characterized by the formation of "lagoonal rias" and records an evolution from partially protected lagoon to isolated lagoon environment. These two stages of lagoon evolution correspond to distinct deposit environments. Study of coastal system tract evolution shows the balance between sea-level rise and hydrodynamics.

Keywords: lagoonal environment; wave-driven littoral; transgression; post-glacial deposits; Gulf of Lions; Holocene; incised valley.

8.4 Article 10: Dynamiques fluviales et lagunaires en basse vallée du Vidourle au cours des 6 derniers siècles: confrontation des données pédosédimentaires à haute résolution temporelle à l'analyse fréquentielle des crues historiques

Jean-François Berger[1], Philippe Blanchemanche[2], Christelle Reynès[3] et Pierre Sabatier[4]

1 CEPAM, CNRS UMR 6130, Valbonne.
2 Archéologie des sociétés méditerranéennes, CNRS UMR 5140, Lattes.
3 Laboratoire de Physique industrielle et traitement de l'information, EA2415 faculté de Pharmacie, UM1, Montpellier.
4 Geosciences Montpellier, CNRS, UMR 5243, Université Montpellier 2

Accepté et à paraître dans un numéro spécial de la revue Quaternaire: Littoraux, lagunes et basses plaines alluviales à l'Holocène, *Quaternaire*, 20, (3), 2009.

Résumé

L'histoire paléohydrologique du delta du Vidourle au cours du dernier millénaire est examinée par l'étude comparative de deux types de proxies : les archives sédimentaires et les séries temporelles de crues historiques. L'analyse de la rythmicité des crues du Vidourle repose sur une étude micromorphologique à haute résolution des 3m supérieurs de la carotte du Lièvre, localisée dans l'axe de l'embouchure moderne du Vidourle dans l'étang de Mauguio (Hérault). La vitesse de sédimentation est établie par 7 datations au carbone 14. Le modèle âge-profondeur illustre une rupture dans le taux de sédimentation un peu après l'An Mil et une nette accélération de la sédimentation à partir du XVIIe s. Les tests de stationnarité réalisés montrent que la série de crues toute classes confondues n'obéit pas à une distribution homogène. Aussi bien pour le Vidourle que pour l'ensemble des fleuves côtiers du bas Languedoc oriental pris en compte, une phase très active d'un siècle environ de 1680 à 1780 est caractérisée par la recrudescence des épisodes « extraordinaires » et « catastrophiques ». Elle met en évidence la variabilité cyclique de la composante hydro-climatique. Même si le forçage sédimentaire lié à la proximité du carottage par rapport au front du delta perturbe le signal, il est possible pour le dernier millénaire de restituer des phases d'hydrologie abondante responsables de crues de haute énergie et de les replacer dans le contexte des mises en valeur et des variations climatiques dans le Nord Ouest du bassin méditerranéen au cours du dernier millénaire.

Mots-Clés : bas Languedoc, Vidourle, Petit Âge Glaciaire, sédimentation, micromorphologie, paléohydrologie, crue, analyse fréquentielle

Fluvial dynamics in Vidourle low flood plain during the last six centuries : comparison of high temporal resolution pedosedimentary data with stationarity analysis of historical floods

Abstract

The palaeohydrological history of the lower floodplain of the Vidourle River during the Little Ice Age has been carried out by comparing two kinds of proxies: sedimentary archives and attested historical floods. The Vidourle flood frequency has been established after the micromorphological study, at a high resolution, of the upper three meters of the Lièvre core, sampled near the Vidourle River mouth, in the Mauguio coastal lagoon. Seven ^{14}C dates enabled us to estimate the velocity of fluvial deposition. The age-deep modeling shows a change in the deposition rate after 1000 AD and its increase since the seventeenth century. Stationary analysis exhibits a non-homogeneous behavior for all classes of floods. For the Vidourle River, like for all coastal rivers of the eastern Languedoc, « extraordinary » and catastrophic floods increased from 1680 to 1780 A.D. They reveal a cyclic variability of hydroclimatic factors, even the proximity of the delta front can disturb the signal. It is possible to identify numerous hydrological periods responsible of high energy floods and replace them in the context of human activity and climatic fluctuations of the North-Western Mediterranean basin during the last millennium.

Keywords : lower Languedoc, Vidourle, Little Ice Age, fluvial deposits, micromorphology, palaeohydrology, flood, stationary analysis

8.5 Calcul de barres d'erreurs pour les données radiocarbones

Soit deux âges ^{14}C : X et Y avec des erreurs respectives x et y :

X +/- x et Y +/- y

- Addition / Soustraction :

Age : X + Y ou X - Y

Erreur ajouté en quadrature : racine($x^2 + y^2$)

- Moyenne :

Moyenne(X ; Y)

Erreur : moyenne(x ; y) / racine(2).

8.6 Données malacologiques de la carotte PB06

Prof.	Hydrobie	Loripies	Abra o.	Cerast. g.	Gibbule	Bittium r.	Rissoa v.	Cyclope	Moule
0	41	0	4	21	0	0	0	1	0
1	53	0	11	51	0	0	0	1	0
2	41	0	9	35	0	0	0	2	0
3	64	0	3	29	0	0	0	0	0
4	128	0	13	45	0	0	0	0	0
5	92	0	9	29	0	0	0	0	0
6	74	0	20	37	0	0	0	0	0
7	125	0	21	59	0	0	0	1	0
8	123	0	13	35	0	0	0	1	0
9	278	0	27	72	0	0	2	6	0
10	362	0	35	54	0	0	0	3	0
11	377	0	169	31	0	0	0	0	2
12	420	0	23	40	0	0	0	1	0
13	337	0	4	55	0	0	1	2	0
14	450	0	17	87	0	0	2	0	0
15	480	0	24	53	0	0	0	0	3
16	268	1	12	14	0	0	1	0	0
18	282	0	11	20	0	0	0	0	0
20	327	0	12	19	0	0	0	0	0
22	376	0	11	19	0	0	0	0	1
24	273	0	7	3	0	0	0	0	1
26	147	0	7	7	0	0	0	0	0
28	89	0	3	5	0	0	0	0	0
30	200	1	30	25	0	2	0	1	2
32	362	1	21	22	2	6	1	0	1
34	156	0	4	11	0	0	0	0	1
36	694	0	21	16	4	0	1	3	6
38	921	1	5	11	8	0	0	1	1
40	471	0	3	3	2	0	0	0	8
42	164	0	1	1	0	0	0	0	2
44	140	0	1	7	0	0	0	0	4
46	187	0	2	6	2	1	0	0	1
48	144	0	9	6	3	0	1	0	1
50	173	1	3	6	0	0	2	0	3
52	67	0	2	1	2	0	0	0	1
54	42	2	13	0	3	0	2	1	1
56	7	0	2	0	3	1	0	0	0
58	11	1	1	0	10	1	0	0	2
60	3	0	1	2	0	0	1	0	1
62	7	0	0	1	0	0	0	0	0
64	30	0	0	0	0	0	1	1	0
66	88	0	0	15	0	0	0	0	0
68	77	2	2	30	1	0	1	0	1
70	399	0	15	4	0	0	0	2	34
72	97	0	2	1	0	0	2	0	21
74	88	0	12	1	0	0	2	0	0
76	248	0	13	26	0	0	7	2	2
78	401	0	6	32	0	0	2	0	0
80	73	0	0	0	0	0	0	0	2

82	166	3	7	8	15	1	1	1	0
84	98	2	13	2	2	0	4	0	0
86	61	11	12	3	7	1	10	0	0
88	96	0	21	4	19	0	16	2	1
90	34	2	8	2	0	0	2	0	1
92	13	0	1	1	1	0	0	0	0
94	2	0	1	2	0	0	0	0	0
96	3	0	2	0	0	0	0	0	0
98	2	0	0	0	0	0	1	0	0
100	0	1	0	0	0	1	1	0	0
102	1	0	0	0	0	1	1	0	0
104	0	2	0	2	0	0	0	0	0
106	0	0	0	2	1	1	3	0	0
108	0	0	1	0	0	0	0	0	0
110	0	0	0	1	0	0	0	0	0
112	0	0	7	2	0	0	0	0	0
114	96	1	23	69	38	6	18	1	0
116	158	3	45	57	58	15	10	1	2
118	182	4	14	22	10	6	8	0	2
120	389	3	33	14	1	0	7	0	7
122	608	6	66	40	0	1	22	0	16
124	536	7	52	7	0	0	9	1	15
126	180	2	24	21	0	0	5	0	13
128	79	9	10	12	0	1	7	1	1
130	42	10	19	5	0	1	4	0	0
132	96	4	4	8	0	3	6	0	0
134	95	4	25	7	0	5	4	1	2
136	99	1	9	5	0	1	3	0	0
138	86	0	16	4	0	1	0	0	5
140	250	3	52	15	0	6	5	0	9
142	50	0	6	1	0	7	1	0	0
144	43	0	3	1	0	8	0	1	2
146	39	1	2	1	0	0	0	0	0
148	168	1	13	15	0	0	1	1	3
150	174	1	16	13	0	0	4	0	5
152	189	2	12	11	1	0	4	1	5
154	124	2	13	15	0	0	1	0	5
156	108	3	17	23	0	3	8	3	3
158	40	0	5	6	0	0	5	0	3
160	29	1	8	2	0	0	3	0	1
162	37	3	24	28	0	1	5	0	2
164	40	2	14	20	0	0	9	0	9
166	36	1	18	9	0	1	3	1	2
168	7	0	4	6	0	3	2	0	2
170	2	1	5	6	0	1	1	0	2
172	14	9	15	34	0	8	12	1	6
174	3	0	2	7	0	2	8	0	0
176	2	0	3	4	0	2	5	0	1
178	3	0	4	10	0	0	2	0	2
180	4	0	5	15	0	0	3	0	14
182	69	0	6	8	0	0	7	0	8
184	19	2	7	10	0	0	26	0	27
186	3	0	0	0	0	0	0	0	0
188	0	0	0	1	0	0	0	0	18

190	6	0	1	2	0	0	0	0	1
192	24	4	17	38	0	0	4	1	9
194	4	8	17	22	0	0	12	0	6
196	21	15	26	55	2	3	22	0	6
198	11	8	12	26	3	2	11	0	3
200	47	9	17	47	2	21	28	2	6
202	58	2	16	24	1	16	23	3	5
204	85	2	15	10	0	4	14	0	3
206	94	1	9	19	0	6	29	0	5
218	8	0	17	14	0	8	10	2	1
220	4	5	33	8	0	3	5	2	1
222	3	3	16	19	0	7	8	1	3
224	1	0	6	8	0	9	6	1	1
226	65	14	13	48	1	23	30	6	2
228	95	15	29	62	4	27	26	2	3
230	25	11	22	65	12	60	13	3	5
232	6	13	5	19	15	30	8	1	2
234	0	2	0	5	1	5	2	0	0
236	0	6	2	1	5	5	2	0	1
238	1	2	1	11	2	1	0	0	0
240	0	0	0	0	0	0	0	0	0
241	0	1	0	1	0	0	0	0	0
243	0	0	1	0	0	0	0	0	0
245	0	0	0	1	0	0	0	0	0
247	0	0	0	0	0	0	0	0	0
249	0	0	0	0	0	0	0	0	0
251	0	0	0	0	0	0	0	0	0
253	0	0	0	1	0	1	0	0	0
255	1	21	8	24	32	151	8	0	0
257	0	0	0	1	1	4	0	0	0
259	1	0	0	12	0	1	0	0	0
261	5	0	0	24	0	2	1	0	1
263	49	0	0	81	0	52	38	0	4
265	25	0	0	37	0	8	15	0	7
267	15	16	4	12	0	2	5	0	3
269	22	0	0	13	0	18	13	0	10
271	44	0	0	59	0	13	12	0	14
273	36	5	22	25	0	2	3	0	8
275	38	5	29	28	0	8	9	0	8
277	21	1	11	22	0	12	7	0	3
279	50	3	17	37	0	15	21	0	7
281	40	3	52	28	0	8	25	0	7
283	8	0	11	9	0	2	7	0	2
285	14	2	22	5	0	0	12	0	6
287	19	6	17	13	0	1	17	0	6
289	61	6	24	15	0	12	33	0	9
291	39	5	44	11	0	7	14	0	21
293	81	1	13	28	0	15	15	0	5
295	20	0	7	22	0	0	4	0	2
297	17	0	11	10	0	2	2	0	5
299	56	4	30	44	0	10	14	0	10
301	7	0	10	8	0	2	3	0	4
303	2	2	7	6	0	2	2	0	2
305	1	0	0	3	0	0	0	0	0

307	0	0	0	6	0	0	0	0	0
309	0	0	0	1	0	1	0	0	0
311	16	0	13	26	0	3	11	0	1
313	2	0	1	6	0	1	4	0	0
315	3	0	2	11	0	5	8	0	2
317	14	8	20	29	0	34	59	0	1
319	2	9	10	7	0	39	40	0	0
321	1	3	6	5	0	6	1	0	0
323	15	19	28	49	0	35	29	0	2
325	15	0	5	47	0	10	13	0	1
327	56	1	16	47	0	2	39	0	2
329	36	1	15	44	0	2	15	0	3
331	16	0	16	28	0	2	3	0	3
333	29	0	10	25	0	7	9	0	3
335	20	7	12	27	0	16	21	0	0
337	3	0	5	1	0	4	1	0	0
339	3	2	5	11	0	6	6	0	0
341	2	0	2	9	0	6	6	0	1
343	10	5	19	26	0	15	20	0	4
345	22	8	12	31	0	27	27	0	5
347	9	0	5	10	0	5	8	0	1
349	9	0	5	7	0	3	9	0	1
351	3	0	1	4	0	2	7	0	0
353	9	2	1	12	0	17	42	0	0
355	1	0	0	1	0	2	11	0	1
357	5	5	5	25	0	15	80	0	4
359	1	4	5	5	0	11	20	0	2
361	1	5	3	1	0	11	7	0	0
363	1	5	5	5	0	20	19	0	1
365	1	0	2	5	0	2	1	0	1
367	1	3	2	9	0	17	25	0	1
369	1	0	0	0	0	0	0	0	0
371	1	1	0	0	0	1	0	0	0
373	1	0	0	0	0	1	0	0	0
375	1	9	4	24	0	6	8	0	2
377	1	3	3	6	0	2	0	0	1
379	10	3	15	28	0	9	16	0	2
381	90	13	15	135	3	85	49	0	7
383	129	9	27	97	0	45	37	0	6
385	160	9	30	66	0	18	36	0	6
387	145	2	56	66	0	20	35	0	6
389	69	1	12	27	0	6	10	0	2
391	47	0	10	34	0	5	10	0	1
393	95	1	19	112	0	9	53	0	2
395	53	0	11	47	0	3	16	0	0
397	10	0	3	15	0	0	2	0	0
399	141	2	23	88	0	5	31	0	1
401	41	0	8	14	0	43	12	0	0
403	6	0	2	4	0	1	7	0	0
405	11	1	1	8	0	1	13	0	0
407	14	0	4	19	0	0	10	0	0
409	7	0	3	9	0	0	3	0	0
411	54	3	21	30	0	10	12	1	2
413	71	4	21	34	1	5	12	1	6

415	43	1	17	29	1	5	12	2	3
417	29	1	21	23	0	8	14	0	4
419	217	2	27	46	0	19	45	0	6
421	26	3	9	50	0	10	19	0	7
423	9	2	14	48	0	15	29	0	1
425	8	4	5	35	0	7	21	0	1
427	1	4	9	13	0	4	13	0	2
429	12	22	23	79	0	54	74	0	7
431	4	6	8	32	0	23	12	0	1
433	21	6	6	87	0	10	39	0	1
435	21	1	11	90	0	4	19	0	1
437	10	0	8	19	0	2	11	0	2
439	25	0	4	19	0	1	12	0	1
441	19	0	17	33	0	0	6	0	2
443	29	0	38	12	0	0	5	0	4
445	14	0	3	10	0	0	2	0	1
447	18	0	4	19	0	0	1	0	1
449	675	0	62	102	0	1	25	0	73
451	437	0	61	105	0	3	35	0	10
453	4	0	5	8	0	1	2	0	1
455	1	0	6	3	0	0	1	0	2
457	55	0	11	22	0	1	7	0	10
459	29	0	8	9	0	0	5	0	1
461	5	0	1	6	0	0	0	0	1
463	80	0	7	13	0	0	8	0	14
465	37	0	16	21	0	2	4	0	6
467	5	0	2	5	0	0	1	0	9
469	10	0	3	20	0	0	6	0	9
471	1	0	1	1	0	0	0	0	3
473	2	0	0	6	0	0	0	0	1
475	2	0	2	8	0	2	2	0	0
477	7	0	3	15	0	1	5	0	5
479	1	0	1	5	0	1	1	0	0
481	1	2	2	8	0	4	21	0	0
483	1	1	0	6	0	4	9	0	3
485	1	3	2	14	0	31	22	0	0
487	1	6	2	2	0	10	7	0	0
489	1	2	2	2	0	3	1	0	0
491	1	4	4	8	0	15	4	0	0
493	1	4	1	1	0	1	1	0	0
495	1	3	1	5	0	2	1	0	0
497	1	1	1	3	0	3	1	0	0
499	1	0	4	4	0	8	1	0	0
501	1	4	1	1	0	1	0	0	0
503	1	7	2	12	0	23	19	0	1
505	1	6	5	6	0	37	47	0	0
507	1	0	2	3	0	1	0	0	0
509	1	2	2	1	0	20	7	0	0
511	1	5	6	7	0	49	18	0	0
513	1	2	1	3	0	4	1	0	1
515	1	0	0	0	0	2	0	0	0
517	1	0	0	0	0	4	0	0	0
519	1	4	2	3	0	17	10	0	2
521	1	6	5	32	0	133	146	0	4

523	1	1	0	2	0	16	19	0	0
525	1	0	1	1	0	12	1	0	0
527	1	3	1	9	0	12	2	0	0
529	3	0	3	19	0	8	14	0	1
531	21	1	11	21	0	28	40	0	1
533	10	0	7	23	0	8	27	0	0
535	9	3	7	24	0	5	23	0	2
537	9	6	7	49	0	9	22	0	1
539	11	1	6	24	0	19	27	0	2
541	5	1	8	29	0	11	23	0	3
543	14	1	5	38	0	12	32	0	2
545	7	1	5	28	0	1	18	0	0
547	4	0	2	22	0	4	10	0	1
549	34	1	13	35	0	9	133	0	38
551	5	0	1	3	0	0	14	0	5
553	19	1	8	7	0	4	77	0	8
555	10	0	1	3	0	2	57	0	3
557	46	0	3	19	0	3	161	0	6
559	11	0	2	13	0	2	40	0	2
561	16	0	3	14	0	1	18	0	2
563	26	0	10	31	0	5	23	0	1
565	7	0	1	7	0	4	8	0	1
567	21	1	3	11	0	19	19	0	1
569	8	0	1	20	0	7	15	0	0
571	5	0	0	7	0	0	8	0	0
573	2	0	1	2	0	0	2	0	0
575	5	0	1	5	0	0	2	0	0
577	5	0	4	3	0	7	10	0	0
579	10	4	21	27	0	33	59	0	3
581	20	4	15	23	0	33	110	0	1
583	18	4	20	15	0	33	86	0	4
585	34	4	6	19	0	24	98	0	4
587	29	0	4	5	0	8	70	0	1
589	22	0	8	12	0	15	42	0	4
591	75	0	33	30	0	5	84	0	19
593	49	2	18	26	0	8	48	0	10
595	51	3	23	16	0	3	42	1	4
597	59	1	17	26	0	7	53	0	4
599	157	7	45	49	0	52	236	0	22
601	90	7	8	18	1	16	84	0	23
603	86	4	23	22	0	17	86	0	16
605	54	1	9	11	0	12	44	0	5
607	64	6	17	10	1	21	57	0	7
609	49	5	10	8	0	22	84	0	8
611	65	0	16	13	2	16	72	0	8
613	15	3	8	11	0	7	50	0	2
615	15	1	11	15	0	7	56	0	4
617	11	0	1	3	0	1	4	0	2
619	6	0	0	1	0	1	3	0	1
621	3	4	1	1	0	0	1	0	1
623	7	0	4	3	0	1	0	0	0
625	6	0	2	1	0	0	0	1	0
627	4	1	4	2	0	1	1	0	0
629	6	4	2	6	0	6	9	0	0

631	1	3	2	1	0	1	5	0	0
633	0	0	4	2	0	7	28	0	0
635	4	8	7	9	0	18	52	0	1
637	4	1	2	4	0	7	50	0	1
639	1	4	8	12	0	8	99	0	1
641	2	2	4	5	0	3	38	0	1
643	1	6	6	8	0	11	88	0	4
645	1	2	3	7	0	3	31	0	1
647	0	2	2	5	0	3	29	0	1
649	1	2	5	2	0	3	47	0	2
651	0	0	2	1	0	0	28	0	3
653	1	0	1	1	0	2	20	0	2
655	0	2	1	3	0	5	20	0	0
657	0	1	1	1	0	1	5	0	0
659	0	1	1	0	0	1	4	0	0
661	3	2	5	4	0	1	25	0	0
663	0	0	3	4	0	3	21	0	1
665	1	6	7	4	0	7	10	0	2
667	0	3	5	1	0	4	12	0	0
669	0	2	1	1	0	4	3	0	2
671	0	2	1	1	0	2	1	0	2
673	0	3	11	3	0	10	9	0	1
675	0	6	4	3	0	3	9	0	1
677	0	0	1	3	0	1	8	0	0
679	0	0	2	2	0	1	4	0	0
681	0	3	5	5	0	5	9	0	1
683	0	7	6	4	0	8	27	0	2
685	0	43	17	52	0	52	80	0	7
687	0	9	6	2	0	5	5	0	0
689	0	8	3	4	0	2	3	0	1
691	0	7	2	3	0	2	11	0	1
693	0	5	5	6	0	7	17	0	0
695	0	37	12	15	0	40	51	0	2
697	0	3	2	5	0	9	7	0	1
699	0	7	3	3	0	16	38	0	4
701	0	4	3	7	0	8	4	0	1
703	0	2	2	8	0	3	4	0	1
705	1	4	3	1	0	8	9	0	3
707	0	8	2	4	0	16	19	0	3
709	0	4	4	1	0	3	9	0	0
711	0	1	4	2	0	1	8	0	3
713	0	6	1	0	0	1	6	0	1
715	0	8	5	1	0	14	10	0	1
717	0	6	8	3	0	3	29	0	2
719	0	9	3	4	0	4	23	0	2
721	0	5	0	1	0	4	9	0	2
723	0	2	4	5	0	4	35	0	2
725	0	7	3	8	0	8	33	0	3
735	15	43	13	36	0	99	329	0	32
745	35	58	25	29	0	146	720	0	112

Tableau 8-2 : Données de Malacofaune sur la carotte PB06.

8.7 Données des minéraux argileux du bassin versant et de la carotte PB06

Site	Ech.	Smectite	Illite	Kaolinite	Chlorite	Sm/(Ill+Chl)
Mosson	VIT	69	5	22	5	7.12
	BV-1	72	6	17	4	7.04
	BV-2	68	10	18	3	4.93
	BV-9	71	11	14	4	4.91
	BV-6	58	14	22	6	2.91
	BV-7	68	13	14	5	3.90
	BV-5	51	24	18	7	1.64
	BV-8	47	30	14	8	1.22
Crue Mosson	Mpail	76.7	7.8	3.0	12.6	3.77
	MA2	72.7	13.8	3.2	10.3	3.01
	PM	81.5	9.1	1.7	7.6	4.86
Cordon	E1	8	57	9	26	0.10
	E2	24	45	13	19	0.37
	E3	14	52	16	18	0.21
	E4	13	51	14	23	0.18
	E4B	18	48	13	21	0.26
	CT0	20	54	6	21	0.27
	CT21	28	46	8	17	0.45
	CT20	14	59	8	19	0.19
	CT6	20	53	6	21	0.27
	B6	33.0	42.5	6.8	17.6	0.55
PB06	0	55.0	23.2	13.6	8.1	1.75
	2	54.2	24.9	12.5	8.4	1.63
	4	52.8	25.8	15.4	6.0	1.66
	6	56.0	24.6	11.8	7.6	1.74
	8	56.9	22.7	13.5	7.0	1.92
	10	54.7	23.9	14.7	6.7	1.79
	12	49.8	28.2	15.6	6.4	1.44
	14	54.2	25.9	11.0	9.0	1.56
	16	60.1	21.5	13.1	5.4	2.24
	18	60.0	20.8	13.4	5.9	2.25
	20	54.4	26.4	11.7	7.6	1.60
	22	59.2	21.0	12.4	7.4	2.09
	24	53.3	25.7	13.4	7.7	1.59
	26	55.0	22.3	16.6	6.1	1.93
	28	56.8	23.3	12.9	7.0	1.87
	30	59.1	19.9	15.7	5.4	2.34
	32	53.6	26.3	10.7	9.4	1.50
	34	47.9	29.0	11.7	11.4	1.19
	36	45.1	28.7	14.3	11.8	1.11
	38	54.7	25.8	11.1	8.4	1.60
	40	54.0	25.4	10.9	9.7	1.54
	42	53.3	26.2	11.2	9.4	1.50
	44	28.9	41.3	10.6	19.2	0.48
	46	49.6	26.5	12.3	11.6	1.30
	48	43.4	31.3	12.5	12.7	0.98
	50	43.8	31.5	10.4	14.2	0.96
	52	30.3	38.3	12.0	19.4	0.52
	54	31.1	41.6	9.7	17.6	0.53
	56	38.8	37.2	8.9	15.2	0.74
	58	19.9	42.4	13.4	24.3	0.30
	60	37.9	36.2	11.2	14.8	0.74

62	37.4	34.2	9.8	18.6	0.71
64	25.5	49.6	8.1	16.8	0.38
66	43.1	34.4	8.5	14.0	0.89
68	49.0	29.4	10.6	10.9	1.22
70	49.3	29.1	10.6	11.0	1.23
72	59.3	22.1	13.0	5.7	2.14
74	53.4	25.8	13.1	7.7	1.59
76	52.1	26.3	12.4	9.2	1.47
78	53.7	26.9	10.2	9.2	1.49
80	50.9	25.8	13.3	10.0	1.42
82	55.2	25.5	10.8	8.5	1.62
84	50.2	27.1	12.3	10.5	1.34
86	60.0	22.2	11.2	6.7	2.08
88	60.4	21.9	11.1	6.5	2.12
90	54.5	26.7	11.2	7.6	1.59
92	54.4	27.4	10.0	8.1	1.53
94	47.2	29.7	12.7	10.4	1.18
96	41.3	33.1	11.1	14.6	0.87
98	43.7	31.9	11.7	12.8	0.98
100	44.8	34.3	9.1	11.8	0.97
102	33.3	37.1	11.3	18.4	0.60
104	40.6	35.6	9.0	14.7	0.81
106	43.9	31.7	10.9	13.4	0.97
108	33.2	39.7	11.4	15.7	0.60
110	50.1	26.3	14.8	8.8	1.43
112	53.6	24.3	15.6	6.5	1.74
114	55.9	23.3	16.1	4.7	2.00
116	54.6	26.2	10.5	8.6	1.57
118	54.2	24.4	13.0	8.4	1.65
120	42.1	31.0	13.8	13.1	0.96
122	61.7	20.9	11.5	5.8	2.31
124	61.7	19.5	14.2	4.7	2.56
126	64.2	18.9	11.5	5.3	2.65
128	58.5	21.9	12.7	6.9	2.03
130	53.1	24.3	14.8	7.7	1.66
132	51.8	25.9	14.1	8.2	1.52
134	60.6	21.4	11.8	6.2	2.19
136	57.3	24.6	10.7	7.4	1.79
138	58.2	22.8	13.2	5.8	2.03
140	61.6	20.5	12.3	5.6	2.36
142	60.2	22.2	10.1	7.5	2.03
144	55.5	23.7	13.5	7.3	1.79
146	53.9	25.7	14.7	5.7	1.71
148	60.0	21.1	12.0	7.0	2.14
150	62.2	19.3	13.0	5.5	2.51
152	67.0	18.2	10.2	4.6	2.94
154	69.6	16.0	10.6	3.9	3.51
156	60.8	20.0	13.8	5.3	2.40
158	65.6	18.9	11.2	4.3	2.83
160	67.0	18.7	10.8	3.6	3.01
162	57.7	23.1	10.8	8.3	1.84
164	63.6	20.2	11.2	5.0	2.52
166	59.1	21.8	13.4	5.7	2.14
168	56.6	23.4	12.6	7.5	1.84
170	55.7	24.4	11.1	8.8	1.68
172	56.2	24.3	10.9	8.6	1.71
174	63.1	19.2	12.1	5.6	2.54
176	61.1	21.2	12.7	5.0	2.33
178	61.7	20.6	12.2	5.5	2.36
180	52.9	23.2	15.3	8.5	1.67
182	61.4	20.3	13.5	4.8	2.45
184	59.9	21.4	12.5	6.2	2.17

186	66.2	17.7	10.9	5.2	2.89
188	58.8	20.7	13.9	6.5	2.16
190	61.9	21.0	12.0	5.1	2.37
192	67.4	18.1	10.3	4.2	3.03
194	54.5	24.9	11.8	8.7	1.62
196	57.3	23.9	9.4	9.3	1.72
198	53.8	27.3	9.6	9.2	1.47
200	49.7	29.4	9.7	11.3	1.22
202	58.4	23.4	10.6	7.6	1.88
204	48.7	29.1	11.7	10.5	1.23
206	50.9	29.1	10.3	9.7	1.31
208	44.1	32.8	12.1	11.0	1.01
219	46.1	31.4	11.0	11.6	1.07
221	47.4	30.8	10.8	11.0	1.13
223	41.1	34.7	11.4	12.9	0.86
225	38.9	35.4	12.6	13.1	0.80
227	44.5	32.4	11.3	11.8	1.01
229	37.1	36.4	11.3	15.3	0.72
231	32.7	38.5	10.6	18.1	0.58
233	34.5	38.9	10.4	16.2	0.63
235	31.4	42.8	9.1	16.7	0.53
237	31.4	41.0	10.6	17.0	0.54
239	38.7	38.6	9.9	12.9	0.75
242	47.7	31.6	9.8	10.9	1.12
244	42.8	35.2	10.2	11.9	0.91
246	33.0	39.5	11.0	16.5	0.59
248	23.1	45.3	12.5	19.1	0.36
250	29.2	44.4	13.6	12.8	0.51
252	36.4	37.5	12.7	13.5	0.71
254	36.6	36.6	12.5	14.3	0.72
256	32.4	40.1	10.2	17.4	0.56
258	38.3	38.6	9.3	13.8	0.73
260	46.9	30.7	12.2	10.2	1.15
260	49.2	28.9	13.2	8.7	1.31
262	52.8	28.0	12.0	7.3	1.50
264	54.7	25.3	12.1	7.9	1.65
266	55.4	23.9	14.4	6.4	1.83
268	56.5	24.3	12.1	7.1	1.80
270	61.8	21.4	10.9	5.9	2.26
272	65.4	19.2	11.3	4.1	2.80
276	59.6	23.1	10.7	6.7	2.00
278	56.4	23.7	13.2	6.7	1.86
280	59.1	22.8	10.9	7.2	1.97
282	62.0	21.9	10.5	5.6	2.26
284	61.9	21.7	11.1	5.3	2.29
286	62.1	22.2	9.2	6.5	2.16
288	53.7	25.4	14.4	6.5	1.68
290	61.5	23.0	9.8	5.7	2.14
292	55.6	24.9	11.4	8.0	1.69
294	64.7	21.1	8.8	5.3	2.44
296	60.5	22.4	9.8	7.3	2.04
298	67.0	18.3	11.2	3.5	3.08
300	64.3	20.7	10.6	4.4	2.57
302	53.2	28.2	11.3	7.3	1.50
304	60.0	23.9	10.2	5.9	2.01
306	61.2	22.3	12.3	4.3	2.30
308	63.9	21.6	9.5	5.1	2.40
310	54.7	22.4	16.6	6.4	1.90
312	56.8	26.4	9.7	7.2	1.69
314	60.2	23.7	9.7	6.4	2.00
316	49.0	29.1	10.6	11.2	1.21
318	50.9	29.4	9.6	10.1	1.29

318	44.9	32.9	10.7	11.5	1.01
322	47.7	30.1	11.1	11.1	1.16
324	39.7	34.5	12.7	13.0	0.84
326	50.1	30.1	11.2	8.6	1.30
328	41.8	33.4	12.4	12.5	0.91
330	41.2	33.2	11.3	14.3	0.87
332	36.7	37.7	11.8	13.9	0.71
334	33.1	39.0	12.0	15.9	0.60
336	41.8	37.1	8.5	12.6	0.84
338	37.1	36.6	11.6	14.7	0.72
340	38.4	35.9	11.9	13.8	0.77
342	40.7	33.7	13.1	12.6	0.88
344	44.9	32.0	11.8	11.3	1.04
346	41.8	33.1	11.9	13.2	0.90
348	43.6	33.4	13.3	9.6	1.01
350	42.1	32.9	11.6	13.3	0.91
352	44.7	32.6	12.3	10.4	1.04
354	46.1	30.3	11.3	12.4	1.08
356	46.8	30.5	12.6	10.1	1.15
358	45.5	31.2	11.3	12.0	1.05
360	41.3	33.2	12.6	13.0	0.89
362	50.6	27.2	11.4	10.9	1.33
364	52.9	25.4	11.0	10.8	1.46
366	55.9	25.9	10.3	7.9	1.65
368	50.3	26.3	11.9	11.6	1.33
370	51.5	27.4	10.3	10.8	1.35
372	50.4	24.9	16.6	8.1	1.52
374	58.8	23.5	10.3	7.4	1.90
374	40.4	37.5	10.0	12.2	0.81
376	46.6	31.0	9.5	12.8	1.06
378	41.9	32.9	9.7	15.6	0.86
380	47.9	29.8	10.5	11.7	1.16
382	25.4	44.9	11.8	17.8	0.41
384	30.8	41.6	10.4	17.2	0.52
386	26.2	42.8	10.3	20.7	0.41
388	37.1	38.9	9.9	14.1	0.70
390	29.5	42.2	9.2	19.1	0.48
392	36.8	39.5	9.5	14.2	0.68
394	37.9	37.2	9.5	15.4	0.72
396	44.7	34.7	10.5	10.2	1.00
398	41.2	35.9	9.3	13.5	0.83
400	36.2	39.0	9.1	15.8	0.66
402	34.1	41.4	9.0	15.5	0.60
404	34.3	38.1	10.6	17.0	0.62
406	33.5	38.9	9.8	17.7	0.59
408	35.1	37.9	10.4	16.6	0.64
410	46.4	31.3	11.3	11.0	1.10
410	32.1	42.0	10.3	15.6	0.56
412	53.6	26.7	10.6	9.1	1.50
414	40.0	34.7	10.0	15.3	0.80
416	36.1	37.6	10.0	16.3	0.67
418	30.0	41.1	9.5	19.4	0.50
420	25.6	44.1	10.7	19.5	0.40
422	29.2	42.5	10.4	17.9	0.48
424	29.1	42.9	11.6	16.5	0.49
426	29.1	42.0	10.4	18.5	0.48
428	31.1	40.1	11.0	17.8	0.54
430	30.3	41.6	10.9	17.2	0.52
432	36.6	37.4	10.5	15.5	0.69
434	41.0	35.5	11.1	12.4	0.86
436	38.2	35.1	12.4	14.3	0.77
438	39.2	35.4	12.1	13.3	0.80

440	37.1	37.0	11.7	14.2	0.72
442	40.7	35.6	11.0	12.6	0.84
444	41.8	34.2	11.6	12.5	0.90
446	42.4	34.1	10.5	13.0	0.90
448	38.4	35.4	11.1	15.1	0.76
452	46.5	31.0	11.0	11.5	1.10
454	41.2	32.3	13.8	12.7	0.92
456	43.1	33.5	11.8	11.6	0.95
458	33.2	36.9	15.5	14.4	0.65
460	44.5	32.4	13.1	10.1	1.05
462	49.9	29.4	12.2	8.4	1.32
464	44.7	31.5	14.3	9.6	1.09
466	44.7	32.3	14.3	8.7	1.09
468	48.8	27.9	14.5	8.8	1.33
470	47.6	30.0	12.5	10.0	1.19
472	44.5	31.4	14.0	10.1	1.07
474	45.1	31.0	13.0	11.0	1.07
476	41.7	33.2	12.8	12.2	0.92
478	45.9	31.6	12.6	9.9	1.11
480	37.3	37.6	10.6	14.4	0.72
482	33.0	40.1	10.3	16.6	0.58
484	25.0	45.6	11.8	17.5	0.40
486	27.2	45.7	11.6	15.6	0.44
488	30.0	41.9	10.5	17.5	0.51
490	29.5	42.1	10.7	17.7	0.49
492	34.9	39.4	9.5	16.2	0.63
494	37.7	37.5	9.7	15.1	0.72
496	28.4	43.2	9.2	19.2	0.46
498	36.4	38.2	8.9	16.4	0.67
500	39.5	35.2	9.7	15.6	0.78
502	43.2	33.9	9.2	13.6	0.91
504	41.2	34.8	9.4	14.6	0.84
506	47.5	31.5	10.4	10.6	1.13
508	42.6	32.3	9.8	15.4	0.89
510	38.4	36.4	9.2	16.0	0.73
512	35.4	37.6	9.6	17.5	0.64
514	30.0	42.8	10.6	16.7	0.50
516	21.7	47.7	9.5	21.1	0.32
518	22.5	46.9	9.1	21.4	0.33
520	17.8	50.4	9.3	22.6	0.24
522	28.6	43.5	9.4	18.4	0.46
524	30.8	41.6	11.2	16.4	0.53
526	34.1	39.0	10.0	16.8	0.61
528	40.4	35.8	12.2	11.6	0.85
530	45.9	33.9	11.7	8.5	1.08
532	41.3	34.7	13.1	10.9	0.91
534	41.8	33.2	11.6	13.4	0.90
536	40.8	34.0	11.8	13.3	0.86
538	44.4	31.4	12.6	11.5	1.03
540	54.6	26.1	10.9	8.3	1.59
542	50.1	29.2	11.7	9.0	1.31
544	53.8	26.0	11.7	8.5	1.56
546	48.8	28.9	11.9	10.3	1.24
548	49.3	27.2	12.6	10.9	1.29
550	53.0	25.4	13.9	7.6	1.61
552	49.3	28.1	13.5	9.1	1.32
554	47.9	28.6	12.3	11.2	1.20
556	47.4	28.9	13.1	10.6	1.20
558	48.9	28.3	11.8	11.0	1.25
560	48.6	28.7	12.1	10.6	1.24
562	49.3	28.0	12.3	10.4	1.28
564	46.3	29.6	12.3	11.8	1.12

566	49.4	28.5	11.6	10.5	1.27
568	48.4	28.0	13.2	10.4	1.26
570	45.3	30.8	12.2	11.7	1.07
572	40.8	34.1	11.0	14.2	0.85
574	45.7	31.0	11.8	11.5	1.07
576	49.1	30.1	10.4	10.4	1.21
578	46.4	29.7	11.4	12.5	1.10
580	46.7	28.8	12.6	11.8	1.15
582	49.3	28.1	11.5	11.1	1.26
584	47.1	29.8	12.0	11.1	1.15
586	53.2	28.0	10.6	8.2	1.47
586	52.4	26.9	9.4	11.3	1.37
588	57.4	25.2	10.4	7.1	1.78
588	45.1	31.7	12.8	10.5	1.07
590	54.5	26.7	10.5	8.4	1.55
592	47.3	31.5	10.4	10.8	1.12
592	50.9	29.6	10.9	8.5	1.33
592	48.7	27.7	13.6	9.9	1.29
594	50.3	30.0	10.2	9.5	1.27
594	49.3	30.3	11.1	9.4	1.24
594	46.3	30.2	12.8	10.7	1.13
596	47.7	32.1	11.3	9.0	1.16
596	45.4	30.8	11.8	12.0	1.06
602	47.1	29.5	10.2	13.2	1.10
604	45.3	31.5	10.5	12.7	1.03
606	38.2	36.1	9.2	16.5	0.73
608	32.7	37.7	12.8	16.7	0.60
608	36.9	37.6	9.2	16.4	0.68
612	38.5	36.5	9.2	15.9	0.73
614	36.9	37.1	9.6	16.4	0.69
616	34.9	38.7	8.7	17.7	0.62
618	38.0	36.2	9.8	16.0	0.73
620	34.3	39.6	9.0	17.0	0.61
622	37.9	37.5	9.2	15.4	0.72
624	39.3	36.7	8.9	15.1	0.76
626	59.7	22.3	10.7	7.4	2.01
628	40.4	37.4	7.3	14.9	0.77
630	41.5	36.6	10.1	11.7	0.86
632	35.0	41.0	8.1	15.9	0.62
634	35.7	40.0	9.5	14.7	0.65
636	41.7	34.6	8.4	15.4	0.83
638	44.6	34.2	11.1	10.1	1.01
640	50.2	31.1	9.9	8.7	1.26
642	38.7	34.7	10.7	16.0	0.76
644	48.4	31.1	10.4	10.1	1.17
646	46.8	32.5	8.5	12.2	1.05
648	43.6	32.0	9.2	15.2	0.92
650	46.6	31.2	9.6	12.6	1.06
652	48.9	30.0	9.0	12.1	1.16
654	50.2	29.2	9.7	10.8	1.25
656	42.5	34.5	9.4	13.6	0.88
658	42.3	33.8	8.8	15.1	0.86
660	46.4	31.8	9.5	12.3	1.05
662	38.9	37.0	9.3	14.8	0.75
664	47.7	34.4	8.9	9.0	1.10
664	41.9	34.9	9.2	14.0	0.86
666	36.5	39.1	9.1	15.4	0.67
668	35.1	38.9	9.6	16.4	0.63
670	38.2	37.5	8.3	15.9	0.71
672	40.2	36.5	8.5	14.8	0.78
674	38.8	36.8	8.7	15.7	0.74
676	35.5	38.9	9.2	16.4	0.64

678	42.6	35.2	11.1	11.1	0.92
680	40.3	34.7	9.7	15.2	0.81
682	34.4	39.3	9.4	16.8	0.61
684	30.7	41.4	10.0	17.8	0.52
686	20.7	49.8	9.0	20.5	0.30
688	24.0	47.6	7.7	20.6	0.35
690	28.8	44.2	9.1	17.9	0.46
692	29.4	43.5	8.9	18.1	0.48
694	26.0	46.4	8.5	19.0	0.40
696	20.6	50.3	7.8	21.3	0.29
698	15.3	52.8	7.9	24.0	0.20
700	18.7	51.4	7.7	22.2	0.25
702	17.2	55.0	7.2	20.7	0.23
704	15.8	52.9	6.2	25.0	0.20
706	19.9	52.1	7.6	20.4	0.27
708	18.8	50.6	8.7	21.9	0.26
710	22.4	48.2	7.8	21.6	0.32
712	20.5	50.5	7.3	21.7	0.28
714	16.5	52.7	7.7	23.2	0.22
716	19.9	51.5	7.4	21.2	0.27
718	17.5	52.6	8.2	21.8	0.23
720	17.2	53.1	8.1	21.6	0.23
722	17.7	53.6	8.2	20.5	0.24
722	16.7	51.8	8.8	22.8	0.22
724	17.6	53.2	8.0	21.2	0.24
726	31.0	47.3	8.0	13.8	0.51
728	34.7	42.4	9.3	13.7	0.62
730	29.1	44.3	9.0	17.5	0.47
730	28.2	45.3	8.4	18.2	0.44
732	36.3	42.7	6.6	14.3	0.64
734	35.6	42.6	8.1	13.8	0.63
736	29.8	45.6	7.7	16.9	0.48
738	39.5	39.1	7.9	13.5	0.75
740	34.7	40.8	10.7	13.8	0.64
742	38.5	39.2	8.8	13.6	0.73
744	26.5	47.0	9.9	16.6	0.42
746	30.8	43.3	10.1	15.7	0.52
748	28.8	46.4	7.0	17.8	0.45
750	19.4	53.3	9.6	17.8	0.27
752	18.0	54.3	8.5	19.2	0.25
754	21.6	49.5	8.7	20.2	0.31
756	23.1	52.1	8.4	16.4	0.34
758	27.2	47.7	10.5	14.7	0.44
760	41.8	37.0	15.4	5.8	0.98

Tableau 8-3 : Données de minéraux argileux du bassin versant et de la carotte PB06.

8.8 Données géochimiques du basin versant (Article 2)

Location	Sample	SiO2	Al2O3	Fe2O3	MnO	MgO	CaO	Na2O	K2O	TiO2	P2O5	PF	Ba	Cd	Cu	Hf	La	Nb	Ni	Pb	Rb	Sr	Ta	Th	Zr
		%	%	%	%	%	%	%	%	%	%	%	ppm	ppm	ppm	ppm	ppm	ppm	ppm	ppm	ppm	ppm	ppm	ppm	ppm
Mosson	BV 1	41.6	2.4	1.2	0.0	0.4	28.6	0.1	0.3	0.2	0.1	25.3	57.4	< L.D.	35.7	2.4	14.1	3.6	12.1	16.3	15.3	116	0.3	2.9	98.4
channel deposit	BV 2	39.7	1.4	1.0	0.0	0.4	32.0	< L.D.	0.2	0.1	0.1	26.0	53.9	< L.D.	15.9	0.8	10.6	2.3	9.5	12.9	9.2	117	0.2	1.8	32.5
	BV 3	32.0	2.2	1.4	0.0	0.7	34.9	0.1	0.3	0.1	0.1	28.8	49.5	< L.D.	19.4	0.9	14.1	2.6	14.0	20.0	13.2	115	0.2	2.2	36.9
	BV 4	44.0	1.6	2.0	0.1	0.4	28.8	< L.D.	0.3	0.1	0.0	23.6	70.9	< L.D.	9.9	0.8	14.9	2.2	16.4	15.8	11.4	93	0.2	1.7	30.3
	BV 5	38.9	1.5	1.8	0.0	0.4	31.3	0.1	0.3	0.1	0.2	24.9	50.9	< L.D.	71.2	0.7	13.9	1.8	14.8	15.6	13.3	139	0.2	1.7	28.2
	BV 6	41.1	2.1	1.1	0.0	0.7	29.9	0.1	0.4	0.2	0.1	25.0	80.1	< L.D.	17.3	1.6	12.2	3.3	25.4	25.6	18.7	140	0.3	2.2	61.9
	BV 7	44.0	2.4	0.9	0.0	0.3	27.6	0.1	0.7	0.1	0.1	23.6	105.3	< L.D.	19.4	1.3	11.5	2.2	11.0	19.5	27.9	119	0.2	2.0	49.2
	BV 8	51.6	3.7	2.2	0.0	0.6	21.2	0.2	0.9	0.2	0.2	19.0	120.4	0.5	46.1	2.0	14.7	3.8	21.4	103.4	36.2	268	0.3	3.0	76.2
	BV 9	39.5	2.7	1.3	0.0	0.5	29.0	0.1	0.5	0.2	0.1	26.1	92.6	< L.D.	43.8	2.2	13.4	3.7	13.5	131.9	23.3	123	0.3	2.9	88.8
Mosson	Mau1	36.7	7.2	2.8	0.1	1.0	22.8	0.3	1.1	0.4	0.3	27.3	160.1	0.5	63.0	3.5	23.1	8.4	27.1	35.6	56.1	144	0.7	6.4	138.2
suspended sed.	Mau2	35.3	11.6	4.4	0.1	1.2	20.4	0.2	1.3	0.6	0.2	25.4	180.2	0.5	82.4	3.2	31.3	12.3	40.6	40.1	76.5	123	1.1	8.9	119.9
	Cou	36.5	10.5	4.1	0.1	1.1	20.0	0.1	1.2	0.6	0.2	26.5	170.1	0.6	94.9	3.8	35.2	13.2	39.8	38.2	69.3	105	1.2	8.9	144.3
	Mpail	33.8	10.5	4.0	0.1	1.0	22.9	0.1	1.1	0.6	0.1	26.4	158.6	0.5	92.0	3.1	29.4	12.1	35.0	33.7	63.7	109	1.0	8.3	117.3
Sandy barrier	E 4	65.1	4.6	0.9	0.0	0.6	15.0	1.1	1.3	0.2	0.1	11.4	226.3	< L.D.	< L.D.	1.1	10.4	3.1	7.2	7.7	44.9	350	0.4	2.6	38.2
	EO	40.2	3.2	1.1	0.1	0.7	28.8	0.8	0.7	0.5	0.1	23.4	131.9	< L.D.	< L.D.	4.2	26.1	8.3	11.2	6.6	27.9	738	1.0	5.7	164.4
	HP	57.8	3.3	0.5	0.0	0.3	19.5	0.9	1.2	0.1	0.0	16.2	194.2	< L.D.	< L.D.	0.7	5.5	1.6	6.7	7.5	37.7	546	0.1	1.6	26.5
PB06	0	33.8	9.3	3.6	0.0	1.6	20.8	0.4	1.4	0.5	0.2	27.0	154.5	0.6	71.6	2.7	24.7	10.0	35.5	81.4	84.3	491	0.8	7.3	97.7
	3	33.7	9.1	3.6	0.0	1.6	21.8	0.4	1.5	0.5	0.2	26.4	147.6	0.5	62.5	2.3	22.6	9.2	33.7	48.9	72.1	396	0.7	6.6	93.7
	6	33.9	9.8	3.9	0.1	1.6	22.2	0.4	1.5	0.5	0.2	26.3	157.9	0.8	83.9	2.5	25.0	9.9	35.8	68.4	85.5	416	0.9	7.4	92.6
	9	31.6	9.5	3.7	0.0	1.6	22.9	0.3	1.4	0.5	0.2	27.3	152.3	0.8	102.2	2.4	24.2	9.8	35.1	79.1	84.1	501	0.8	7.1	91.2
	12	29.4	9.0	3.5	0.0	1.7	24.9	0.4	1.3	0.4	0.2	28.6	142.9	0.7	103.2	2.1	22.9	9.1	34.8	75.2	81.0	709	0.8	6.8	81.6
	15	29.8	9.1	3.5	0.0	1.7	24.2	0.4	1.4	0.4	0.2	28.6	143.7	0.6	98.6	2.2	23.1	9.4	34.4	72.9	81.8	724	0.8	6.9	84.0
	18	30.3	9.3	3.6	0.0	1.6	23.9	0.3	1.4	0.4	0.2	28.1	140.5	0.6	80.7	2.3	24.0	9.8	35.1	72.4	81.4	558	0.8	7.1	86.7
	21	30.5	9.6	3.7	0.0	1.7	22.6	0.3	1.5	0.4	0.2	28.7	132.9	0.5	68.5	2.0	23.6	9.6	36.0	62.5	79.8	562	0.8	6.8	78.5
	24	29.4	8.9	3.5	0.0	1.6	24.0	0.3	1.4	0.4	0.2	29.0	129.5	0.4	55.4	1.9	22.9	9.3	37.8	59.8	76.5	785	0.7	7.1	81.0
	27	27.5	7.8	3.1	0.1	1.5	27.2	0.3	1.2	0.4	0.1	29.7	112.0	0.3	29.2	2.1	19.2	7.5	29.2	41.5	61.2	876	0.6	5.6	77.5
	30	32.2	9.3	3.5	0.1	1.6	23.6	0.4	1.5	0.4	0.1	26.7	151.1	0.3	25.8	2.6	24.4	9.5	35.9	40.4	80.7	551	0.8	7.1	98.2
	32	33.6	8.4	3.2	0.1	1.5	23.8	0.5	1.4	0.4	0.1	25.7	160.7	0.3	19.6	2.6	22.5	8.6	33.7	31.1	75.1	730	0.7	6.7	100.7
	34	36.6	8.3	3.1	0.1	1.5	23.3	0.7	1.4	0.4	0.1	23.9	186.0	0.3	16.1	3.4	22.9	8.5	32.7	26.3	76.4	759	0.8	6.7	129.5
	36	34.7	8.7	3.2	0.1	1.6	23.6	0.6	1.5	0.4	0.1	25.0	175.7	0.3	18.0	2.9	23.8	8.9	33.1	28.0	78.9	739	0.8	7.0	107.2

38	32.8	8.9	3.4	0.1	1.7	23.7	0.5	1.4	0.4	0.1	25.7	167.7	0.3	18.6	2.7	24.8	9.2	34.7	27.9	79.2	721	0.8	7.1	101.0
40	32.4	9.4	3.5	0.1	1.7	22.8	0.5	1.5	0.4	0.1	26.1	160.7	0.3	20.0	2.6	24.2	9.2	36.8	28.7	81.5	649	0.8	7.2	97.8
42	32.4	10.0	3.7	0.1	1.8	22.2	0.5	1.5	0.5	0.1	27.2	161.2	0.3	21.3	2.3	24.8	9.6	38.8	29.5	85.7	607	0.8	7.3	87.7
46	33.3	10.4	3.8	0.1	1.8	19.5	0.4	1.7	0.5	0.1	27.3	175.0	0.3	25.8	2.8	28.0	10.9	43.3	33.3	97.1	502	1.0	8.0	99.2
50	35.5	10.4	4.0	0.1	1.9	20.5	0.5	1.7	0.5	0.1	25.8	179.2	0.2	20.9	2.7	25.4	10.0	38.8	27.5	88.9	488	0.9	8.2	100.5
54	37.5	10.0	3.9	0.1	1.8	19.8	0.6	1.7	0.5	0.1	23.2	193.4	0.2	19.6	2.8	24.5	9.6	36.6	26.2	84.9	518	0.8	7.6	106.2
58	36.0	10.1	3.9	0.1	1.8	20.5	0.6	1.7	0.5	0.1	23.6	195.2	0.3	20.4	2.7	24.8	9.8	37.8	24.7	88.9	625	0.8	7.6	105.0
62	37.4	10.0	3.9	0.1	1.8	19.2	0.6	1.8	0.5	0.1	23.4	192.4	0.2	22.5	2.8	23.8	9.6	39.0	24.3	87.9	496	0.9	7.7	106.5
64	38.3	9.7	3.7	0.1	1.8	19.2	0.6	1.7	0.5	0.1	23.1	203.5	0.3	21.1	3.0	25.4	9.8	40.6	25.3	90.2	505	0.9	7.6	112.5
66	31.8	9.5	3.6	0.1	1.9	20.5	0.4	1.6	0.4	0.1	28.9	170.6	0.3	22.7	2.4	24.1	9.9	40.7	27.9	89.3	589	0.8	7.1	89.8
68	30.5	9.3	3.5	0.1	1.9	21.3	0.4	1.5	0.4	0.1	30.9	155.8	0.3	22.4	2.3	23.3	9.5	38.7	26.5	84.3	560	0.8	6.7	86.9
70	31.7	10.0	3.8	0.1	1.9	21.0	0.4	1.6	0.5	0.1	29.2	165.9	0.4	23.0	2.5	25.2	10.4	39.6	32.4	92.7	498	0.9	7.4	88.9
72	33.2	10.7	4.0	0.1	1.9	20.0	0.4	1.7	0.5	0.1	27.5	167.8	0.3	23.7	2.4	25.9	11.0	41.9	29.2	98.0	420	0.9	7.7	85.9
74	33.1	10.9	4.0	0.1	1.9	19.7	0.4	1.8	0.5	0.1	27.4	171.5	0.3	24.8	2.4	26.4	11.2	42.7	32.2	101.0	409	1.0	7.9	84.8
78	33.5	10.6	3.9	0.1	1.8	20.1	0.4	1.7	0.5	0.1	26.6	171.1	0.3	23.0	2.5	25.5	11.0	41.7	29.9	97.4	388	0.9	7.6	85.8
82	34.4	10.0	3.9	0.1	1.8	21.2	0.5	1.6	0.5	0.1	25.0	168.7	0.3	22.2	2.7	25.7	10.3	38.4	33.5	89.1	429	0.9	7.7	99.8
85	33.9	10.2	4.0	0.1	1.6	20.9	0.4	1.6	0.5	0.1	25.5	164.8	0.3	21.0	2.6	26.6	10.5	38.6	28.4	92.3	411	0.9	8.2	98.6
89	36.9	10.4	4.0	0.1	1.7	19.8	0.4	1.7	0.5	0.1	23.2	180.0	0.3	22.5	2.9	27.3	10.9	40.2	28.8	93.8	388	0.9	8.4	108.3
93	40.4	11.1	4.2	0.1	1.7	16.6	0.5	1.9	0.5	0.1	21.9	211.1	0.3	22.6	3.3	28.0	11.0	40.9	27.6	104.4	330	1.0	8.9	121.0
97	42.9	10.4	4.1	0.1	1.7	17.1	0.7	1.9	0.5	0.1	19.3	237.0	0.3	19.9	3.5	26.7	10.5	39.1	23.7	95.3	351	0.9	8.9	133.1
99	44.0	9.8	3.7	0.1	1.6	17.1	0.7	1.8	0.5	0.1	19.4	230.1	0.2	16.5	3.8	25.8	9.8	39.6	21.1	87.7	361	0.9	8.2	139.4
101	45.4	9.7	3.7	0.1	1.6	17.3	0.8	1.8	0.5	0.1	18.7	223.5	0.2	15.0	4.2	25.0	9.6	37.8	19.3	87.5	365	0.9	7.8	161.3
103	44.3	9.9	3.8	0.1	1.7	17.6	0.8	1.9	0.5	0.1	18.5	212.1	0.2	13.3	2.9	21.3	8.8	33.8	16.7	77.2	344	0.8	7.2	115.6
105	44.7	9.2	3.6	0.1	1.5	17.9	0.8	1.8	0.4	0.1	18.4	262.0	0.3	16.5	3.5	25.2	10.1	42.3	21.1	87.0	408	0.9	8.3	128.6
107	40.8	10.4	4.1	0.1	1.7	18.0	0.6	1.8	0.5	0.1	20.9	226.2	0.2	17.6	3.3	26.6	10.6	39.6	23.7	95.1	365	0.9	8.7	123.5
109	40.5	11.0	4.3	0.1	1.7	18.2	0.6	1.9	0.5	0.1	22.0	203.7	0.2	18.9	3.2	26.5	10.5	40.3	24.6	98.7	338	0.9	8.5	118.2
111	38.0	11.6	4.4	0.1	1.7	18.1	0.4	1.9	0.5	0.1	23.5	184.9	0.3	20.0	2.8	27.2	10.8	40.1	28.5	104.7	304	0.9	8.5	97.9
115	35.4	10.9	4.2	0.1	1.7	19.5	0.4	1.8	0.5	0.1	25.7	188.9	0.3	19.6	2.5	26.0	10.6	40.2	28.2	101.2	430	0.9	8.8	97.8
119	33.2	10.3	4.0	0.1	1.7	22.1	0.4	1.6	0.5	0.1	25.2	164.8	0.3	18.2	2.7	25.1	10.1	36.7	28.5	92.2	466	0.9	7.7	96.7
123	28.6	9.4	3.6	0.1	1.7	25.8	0.3	1.4	0.4	0.1	28.3	140.8	0.3	17.8	2.1	22.9	9.1	34.1	26.5	81.3	604	0.8	6.9	77.6

Tableau 8-4 Mosson drainage basin (channel deposits, suspended sediment), sandy barrier and PB06 concentration of major and selected trace elements.

Résumé
Les effets du changement climatique sur les événements extrêmes sont difficiles à estimer car ces phénomènes présentent une large variabilité, et par conséquent il est délicat d'identifier des tendances significatives compte tenu de l'absence de longues séries de données instrumentales. Dans cette étude, nous présentons un enregistrement de ces tempêtes extrêmes sur la côte Méditerranéenne française au cours des 7000 dernières années à partir de carottes sédimentaires prélevées dans un système lagunaire du Golfe du Lion. L'utilisation d'une approche multi-traceur à haute résolution avec des analyses granulométriques, faunistiques, géochimiques (XRF), en minéraux argileux associées à des données chronologiques de radiocarbone et de ^{210}Pb, ^{137}Cs ; nous a permis de reconstruire l'histoire, au cours de l'Holocène, des dépôts lagunaires en relation avec l'activité des tempêtes.
Bien que les paramètres morphologiques de cet environnement lagunaire aient changé durant l'Holocène, ne permettant pas de comparer ces événements au cours du temps en terme d'intensité, nous enregistrons six périodes d'augmentation de l'activité des tempêtes datées à 6200, 5500, 4400, 3200, 1500 an cal B.P. et durant le Petit Age Glaciaire (de 450 à 100 an cal B.P.). Ces changements de l'activité hydrodynamique côtière, en antiphase avec les périodes d'aridifications en Méditerranée de l'Ouest, sont corrélées avec celles observées dans le bassin Nord Atlantique et correspondent aux événements de refroidissement Holocène. L'augmentation de l'activité des tempêtes dans la cette région de la Méditerranée durant les périodes froides, associée à une diminution des températures au pôle Nord, est probablement liée à l'augmentation du gradient thermique qui, par interaction barocline, favorise les cycles d'évolution des tempêtes dans toute l'Europe et la Méditerranée de l'Ouest. Cette étude démontre ainsi que la température dans la région Nord Atlantique influence l'activité des tempêtes extrêmes et donc du climat Méditerranéen à l'échelle de l'Holocène.

Mots clés : paléotempêtes, lagune, Climat Méditerranéen, radiocarbone, Holocène

Abstract
The effects of climate change on extreme events are difficult to assess because extremes present large variability and consequently, it is difficult to identify significant trends in relation to the lack of instrumental long time series. Here we present a record of these extreme storm events in the French Mediterrannean coast over the past 7000 years based on a long sediment core from lagoonal environment in Gulf of Lions. Using a high resolution multi-proxies approach on core associating grain size, faunal to reconstruct Mid to Late Holocene history of backbarrier deposits in relation to landfalling activity.
Even if change in lagoon geomorphological setting over the Holocene does not allow to compare storm events in terms of intensity trough time, we have recorded six periods of increase in storm activity at 6200, 5500, 4400, 3200, 1500 yr cal B.P. and over the LIA (450 and 100 yr cal B.P.). These evidences of changes in coastal hydrodynamic, inversely correlated to periods of aridification in Western Mediterranean region, are in phase with those observed over the North Atlantic and correspond to Holocene cooling events. This increase in storm activity during Holocene cold events over Mediterranean region was probably due to thermal gradient increase leading to enhanced lower tropospheric baroclinicity over a large Central Atlantic-European domain. This study demonstrates that temperatures in North Atlantic region influence the severe storm activity and therefore the Mediterranean climate at Holocene timescale.

Keywords: paleostrom, lagoon, Mediterranean climate, radiocarbon, Holocene